The Dissertation Committee for Talal Mohammad AL-Bazali Certifies that this is the approved version of the following dissertation:

EXPERIMENTAL STUDY OF THE MEMBRANE BEHAVIOR OF SHALE DURING INTERACTION WITH WATER-BASED AND OIL-BASED MUDS

Committee:

Martin E. Chenevert, Supervisor

Mukul M. Sharma, Co-Supervisor

Steven L. Bryant

Jon E. Olson

Lynn E. Katz

EXPERIMENTAL STUDY OF THE MEMBRANE BEHAVIOR OF SHALE DURING INTERACTION WITH WATER-BASED AND OIL-BASED MUDS

by

Talal Mohammad AL-Bazali, B.S., M.S.

Dissertation

Presented to the Faculty of the Graduate School of

The University of Texas at Austin

in Partial Fulfillment

of the Requirements

for the Degree of

DOCTOR OF PHILOSOPHY

The University of Texas at Austin

May, 2005

Dedication

This dissertation is gratefully dedicated to my family. A special dedication goes to my mentor, best friend and brother, Saif. A warm dedication goes to my idol, my mother. An extended dedication goes to my lovely wife and beautiful children, Rakan, Mohamad and Sara

Acknowledgements

This dissertation could not have been completed without the help of those people who have encouraged and inspired me through out this research. I would like to extend my gratitude to Dr. Martin Chenevert and Dr. Mukul Sharma. Thank you for your consistent technical and moral support throughout. Also, thank you for trusting my decisions and giving me the opportunity to express my ideas and thoughts. Your endless help and constant encouragement and enthusiasm made this work a reality.

A special thank goes to my committee members, Dr. Steven L. Bryant, Dr. Jon E. Olson and Dr. Lynn E. Katz. Thank you for your willingness to share your time and knowledge. My sincere gratitude goes to Glen Baum and Bob Savicki for their technical support. Your help and friendship will not be forgotten. The author deeply appreciates the help and support offered by Dr. Russ Ewy and the rest of the drilling research group. I would also like to extend my thanks to my colleagues for their support and friendship.

To all the above recognized persons, I would like to reiterate my gratitude and thanks. Lady and Gentlemen, it has been an honor and a privilege knowing and working with you.

EXPERIMENTAL STUDY OF THE MEMBRANE BEHAVIOR OF SHALE DURING INTERACTION WITH WATER-BASED AND OIL-BASED MUDS

Publication No._____

Talal Mohammad AL-Bazali, Ph.D

The University of Texas at Austin, 2005

Supervisors: Martin E. Chenevert and Mukul M. Sharma

Three integrated experimental studies were carried out in order to study the membrane behavior of shale when interacting with water-based and oil-based muds. Results confirmed the belief that shales act as leaky semi-permeable membranes. Measured membrane efficiencies were low and ranged from 0.18 % to 4.23 % when shales interacted with water-based muds. Independently, measured ion selectivities (modified diffusion potentials) indicated that shales behaved as ion-selective membranes that restrict the flow of anions. In addition, results showed that both the membrane efficiency and the ion selectivity of shales increase with decreasing shale permeability and increasing cation exchange capacity. Our results also showed a good correlation between the membrane efficiency and the ion selectivity of shales.

A gravimetric test was developed that allows us to measure the flux of water and ions into or out of a shale. Results from this test show that the flux of ions depends on the ionic radii and the shale permeability and CEC. These results are consistent with the ion exclusion and membrane potential measured for the shale.

The membrane efficiency of oil-based muds was high compared to that obtained for water-based muds. However, the measured membrane efficiency was not 100 %. Results obtained from immersion tests also showed that the oil-based mud was not a perfect ionic barrier since it allowed ions to exchange. A capillary threshold pressure was measured which must be overcome before oil-based mud flows through a shale. Results showed that this capillary entry pressure increases as the shale permeability decreases and the interfacial tension between non-wetting fluid and shale pore fluid increases.

Table of Contents

List of Tables

List of Figures

CHAPTER 1

Introduction

1.1 BACKGROUND

Shales are low permeability sedimentary rocks that have distinct laminated layers and moderate to high clay content. These characteristics make them vulnerable to phenomena such as hydration, swelling, shrinking, strength reduction and ultimately failure. Manohar (1999) notes that the distinguishing features of shales are its clay content and low permeability due to poor pore connectivity through narrow pore throats (typical pore diameters range from 3nm to100nm). The ability of shales to adsorb water depends on the amount and type of clay minerals present. For example, shales that mainly contain smectite (surface area – 750 m^2/gm) have more affinity for water than shales that mainly contain illite (surface area –80 m^2/gm) or kaolinite (surface area –25 m^2/gm).

Shales are considered to be the most challenging formation to drill. According to Dzialowski et al (1993), over 90% of the formations drilled worldwide are classified as shale formations and about 75% of drilling operations' problems are related to shales. Wellbore instability, hole enlargement, stuck pipe, high torque and drag, and side tracking are some of the most challenging drilling problems related to shale formations. Shale problems have often been approached on a trial and error basis. This kind of solution results in higher overall well-costs and rig-time losses.

The most costly and troublesome problem in shale drilling is wellbore instability especially in deviated wells. van Oort et al (1996) states that wellbore instability problems cost the petroleum industry an estimated $500 million a year.

Wellbore instability in shales is attributed to many factors. The most common ones are mechanical effects and physico-chemical effects. Mechanical failure takes place when the stresses acting on the wellbore exceed the shale strength. This occurs when the mud weight is either too low (compressive failure) or too high (tensile failure). Shale failure due to mechanical effects is outside the scope of this work.

Unlike shale failure due to mechanical effects, physico-chemical effects are poorly investigated and understood. Fundamentally speaking, the flux of water and ions in or out of the shale is considered to be the primary reason for shale instability. The flux of water and ions could alter the shale stress state through pore pressure and shale strength alterations. Furthermore, hydration or dehydration of the shale matrix could lead to the development of swelling stresses, which ultimately could lead to wellbore instability.

When drilling shale under an overbalance condition without an effective barrier present at the wellbore wall, mud pressure would penetrate progressively into the shale formation. Due to the low permeability of shales, the mud pressure penetration would result in an increase in pore pressure near the wellbore wall. According to van Oort (1997), the rate and magnitude of the pore pressure increase depends strongly on the mud filtrate and pore fluid properties (viscosity and adhesion) and the petrophysical properties of the rock material (permeability, pore size distribution and porosity). This flux of water into the shale could increase the pore pressure and thus decrease the effective stress, which may destabilize the wellbore. Ghassemi et al (2001) argues that shale deterioration and borehole instability are significantly influenced by the amount and distribution of

water within the shale and that the influx of mud filtrate into a shale formation increases water content and pore pressure near the borehole, alters the solid structure, and reduces shale strength. Also, it has long been argued that rock strength is inversely related to the moisture content. Chenevert (1970) showed that adsorption of water by confined shales samples generated internal stresses that led to hydraional spalling, vertical fracturing and compressive strength reduction.

In addition to pore pressure increase and shale strength reduction, the unfavorable flux of water leads to shale swelling which could lead to borehole failure if the shale is not allowed to expand freely into the wellbore. According to Edwin et al (1982), shales and clays swell by two mechanisms; crystalline and osmotic. Osmotic swelling occurs in shales when the chemical potential of the shale pore fluid is less than that of the drilling fluid. Shale swelling reduces the shale permeability and pore space which further increase the pore pressure since fluid dissipation into the far field is impaired by the further reduced permeability and this in turn aggravates the stress state acting on the shale. Santarelli et al (1992) argues that there exists a strong relationship between shale swelling and shale permeability as clay mineral expansion impairs permeability by at least one or two orders of magnitude.

Besides the adverse effect of the flux of water into shale, the flux of ions into the shale changes the ionic concentration of pore fluid, which could affect the shale matrix mechanical properties and could result in cohesion degradation and cementing bonds weakening and thus reduces the overall rock strength. Ghassemi et al (2001) states that ions transfer into the rock adversely impacts hole stability by inducing tensile stresses. According to Fam and Dusseault (1998), changes in the ionic concentration of the pore fluid may influence some of the engineering properties of shales through changes in the double layer thickness and if the thickness of this layer is substantially altered, the

volume of structured water in the shale changes which affects both the mechanical properties (stiffness, strength) and the fluid phase transport properties (permeability, diffusivity).

Until recently, the oil industry combated the flux of water and ions into shale by the use of oil-based muds, which showed great success in preventing borehole instability in shale formations. The restriction of water flow due to the existence of a threshold capillary entry pressure between oil-based muds and low permeability shale is considered to be the one of main factors in preventing shale failure. This capillary entry pressure is translated into a net compressive radial stress on the borehole wall, which promotes hole stability if this pressure does not exceed the shale compressive strength and fracture it, (Hale et al 1993). Furthermore, oil-based muds are assumed to act as semi-permeable membranes therefore sustaining osmotic flow. Fundamentally speaking, osmosis is the flow of water from a dilute solution (or pure water) to a more concentrated solution in the presence of a semi-permeable membrane. Therefore, osmosis depends on the existence of a semi-permeable membrane, which only allows the water (solvent) molecules to pass through while restricting the solutes and other unwanted particles. The osmotic pressure difference across a semi-permeable membrane can be calculated using:

$$\Pi = \frac{RT}{V} \ln \frac{a_{w2}}{a_{w1}} \quad \text{..... (1.1)}$$

where Π is the osmotic potential, R is the gas constant, T is the absolute temperature, V is the partial molar volume of water and aw is the water activity. Early work by Chenevert (1970) confirmed the belief that the oil-based muds emulsifier surrounding discrete water droplets provides the characteristics of a semi-permeable membrane that allows the osmotic transport of water to or from the shale. The oil-based mud's water phase activity

(molar free energy) is manipulated to ensure water is transported from the shale. van Oort (2003) states that oil-based muds have been presumed to provide the characteristics of the semi-permeable membrane required in an osmotic mechanism for water transport to and from the shale and that the difference in the molar free energy of water in the oil-based mud and the shale is the driving mechanisms for hydration or dehydration of the shale.

Although oil-based muds provide a definite solution to wellbore instability problems, the use of oil-based muds is not only environmentally hazardous but also expensive. Therefore, oil companies have turned their attention to using water-based muds since they are much more environmentally benign and affordable. However, water-based muds success does not match that of oil-based muds. Due to the absence of interfacial tension forces between water-wet shales and water-based muds, the hydraulic pressure-pore pressure difference becomes direct. Therefore, drilling fluid filtrate (containing water and ions) is free to move in or out the shale depending on the direction of the hydraulic gradient. Moreover, unlike oil-based muds, water-based muds do not behave as perfect semi-permeable membranes and thus ions will be free to exchange between the shale and the drilling fluid.

Since the use of water-based muds became a necessity, a great deal of effort and resources has been devoted to finding ways to improve the performance of water-based muds. Some of these attempts deal with incorporating polymers in drilling fluid design to increase the filtrate viscosity and thus decrease its invasion into shale. Other methods focus on reducing shale permeability by depositing plugging material into shale pore throats. By far, the most used method for enhancing the performance of water-based muds is osmotically extracting water out of the shale. In order to invoke osmosis as a means for water transport during shale and water-based muds interaction, the shale itself

will have to act as a semi-permeable membrane. The literature supports the contention that clays and shales exhibit membrane characteristics due to their narrow pore throats and negative surface charge.

In order to fully utilize osmosis for shale stability purposes, the membrane behavior of shale need to be fully understood. In addition, the factors that control the membrane behavior of shale need to be studied. Moreover, the water and ions movement during shale and water-based muds interactions need to be fully mapped and analyzed. A successful water-based mud design hinges upon the complete understanding of its mechanical and physico-chemical effects on shales. We believe that a good understanding of shale and water-based muds physcio-chemcial interactions will help avoid wellbore instability and lead to safe and financially sound drilling programs.

1.2 FORMULATION OF THE PROBLEM

It is widely believed that dehydration of shales could lead to an increase in shales strength and thus avoid wellbore failure. Ideally, stimulating the water flow out of the shale and into the wellbore can strengthen the shale, (Chenevert, 1970). This idea has spurred much research and interest on the so-called osmotic pressure gradient and shale membrane efficiency concepts. In order to build an effective osmotic pressure gradient into the wellbore, shale and drilling fluid system must produce a high osmotic pressure gradient and exhibit high membrane efficiency. Although we can produce a high osmotic pressure gradient through the manipulation of the water activity of the drilling fluid, the membrane efficiency of shale is more difficult to predict and control. The membrane efficiency is a function of both the shale and the drilling fluid properties. Therefore, it is

very important to know the membrane efficiency and pore fluid composition of shale in order to design a drilling fluid that would produce a highly effective osmotic pressure gradient when interacting with the shale formation.

Early membrane efficiency studies, which were carried out in the laboratory, did not truly tell the whole story and could have lead to inaccurate conclusions. These studies ignored many factors, which are extremely important to the complete understanding of shale membrane behavior. Although these studies simulated the high pressure condition downhole, they did not consider the effect of high temperature on the membrane efficiency of shale. The high temperature that exists downhole could have a profound effect on the membrane efficiency of shale and ignoring it could lead to serious errors. Furthermore, these studies did not clearly present the dependence of membrane efficiency on the properties of shale and water-based muds. We believe that an understanding of the relationship between the membrane efficiency of shale and these properties is very important to the proper design of water-based muds. In addition, in these studies, ions flow into shales was not investigated thoroughly. Its effect was accounted for indirectly by a lesser membrane efficiency coefficient. This non-ideality is expressed as a membrane efficiency (also referred to as reflection coefficient) using the following equation:

$$\sigma = \Delta P / \Delta \pi \quad \text{..... (1.2)}$$

where σ is the membrane efficiency, ΔP is an experimentally measured pressure drop and $\Delta \pi$ is the osmotic potential of the system. An ideal semi-permeable membrane will have a reflection coefficient of 1, which indicates that all solutes are reflected (rejected) by the membrane. A non-ideal membrane has a reflection coefficient of less than 1 depending on the severity of solutes passage through the membrane. We believe that a good

understanding of water and ions uptake during shale and water-based mud interaction is essential to understanding shale membrane behavior.

Besides the need to fully investigate the fundamental concept of membrane efficiency of shales, there exists a need for employing quick tests at the rig floor to evaluate the compatibility of water-based mud and shale. Today, there does not exist any test that would quickly and reliably evaluate shale and water-based mud compatibility at the rig floor. Most tests used today for such purpose are time and space consuming, which makes them impractical.

1.3 SCOPE OF RESEARCH

The accurate estimation of the membrane efficiency of shale is an integral part to the complete understanding of the physico-chemical interactions between shale and water-based muds. Shale failure could be prevented if such interactions are fully understood and favorably utilized. The main objectives of our study are summarized as follows:

1. To investigate the membrane efficiency and ion selectivity behavior of shales when exposed to water-based and oil-based muds using pressure transmission and electrochemical potential tests.
2. To investigate the effects of ion type and concentration on the membrane efficiency and ion selectivity behavior of shales.
3. To verify osmosis as a means to strengthen shales by extracting water from the shale when exposed to water-based and oil based muds.
4. To investigate and verify the phenomenon of ion diffusion into shale through

the use of a newly developed immersion test and gravimetric swelling technique. Also to investigate the effects of ion type and concentration on the rate and magnitude of ions diffusion.

5. To analyze the competing effects of osmosis and ion diffusion on shale swelling and strength behavior when exposed to water-based and oil-based muds. Also, to measure the amount of water and ions, which is exchanged during shale and drilling fluid interaction using a gravimetric swelling technique.
6. To analyze the relationship between the membrane efficiency and the ion selectivity of shales.
7. To analyze the relationship between water and ions uptake , during shale and drilling fluid interactions, and the membrane efficiency and ion selectivity of shales.
8. To investigate the effect of temperature on the membrane efficiency of shales. In addition, to investigate thermal osmosis impact on water transport during shale and drilling fluid interactions.
9. To study and quantify the minimum capillary entry pressure of non-wetting fluids through shales. Also, to analyze the factors on which the capillary entry pressure depends.
10. To propose two quick tests that can be reliably used to study the membrane efficiency of shale and the compatibility of shale with water-based muds. These tests are the electrochemical test and the immersion test.

We believe that there is a great need for understanding the membrane behaviour of shale. A proper estimate of the shale membrane efficiency will help us greatly in designing our mud chemistry necessary for generating maximum osmotic pressure gradients into the wellbore. We believe that investigating ion diffusion along with

osmosis in shales is essential to understanding shale failure and wellbore instability. A better understanding of shales and drilling fluid system interactions will significantly minimize shale instability problems.

This dissertation is organized as follows. Chapter 2 describes the properties of shales used in this study. It also discusses the techniques used to measure these properties. In Chapter 3, a complete description of the membrane efficiency test and results is given. Chapter 4 discusses the evaluation of the ion selectivity of shales through electrochemical tests. The ion selectivity of shale should correlate well with the membrane efficiency of shale since they are both a measure of ion movement in shales. Chapter 5 explains a newly developed immersion test to evaluate shale and drilling fluid compatibility. It also introduces a gravimetric technique that is used for measuring water and ions uptake during shale and water-based muds interactions. In Chapter 6, the effect of temperature of the membrane efficiency of shale is investigated and explained. Chapter 7 discusses the experimental procedure and results for measuring the capillary entry "threshold" pressure through shales. This pressure is responsible for the success of oil-based muds. Finally, conclusions and recommendations are outlined in Chapter 8.

CHAPTER 2

Properties of Shales Studied

2.1 INTRODUCTION

The physical, chemical, petrophysical and geological properties of shales control wellbore instability. Laboratory testing is, for the most part, used for determining shale properties and many laboratory tests have been standardized for this purpose. Shale properties can be affected by poor preservation and handling. Chenevert and Amanullah (1997) showed that shales must be preserved at their native water content if accurate physical measurements are to be made. Shale exposure to air produces capillary effects, which could change the shale properties significantly, and this will ultimately lead to a poor estimation of their properties. Forsans and Schmitt (1994) stated that capillary effects could greatly alter the shale samples being tested, which in turn lead to misleading data, and possibly wrong interpretations.

The following text discusses the description and properties of the shales that were studied in our research. It also describes the laboratory procedures that were used to preserve and measure the shales properties.

2.2 DESCRIPTION OF SHALES

Four different shales obtained from different locations were used in our work.

1. Pierre shale was donated by OGS. It is an outcrop shale.
2. Arco-China shale was also donated by Arco. It was cored from 12,500 feet of depth.

3. C1-shale was donated by Chevron-Texaco. It was taken from 6966.50 feet.
4. C2 shale was also donated by Chevron-Texaco. It was taken from 8927.6 feet.

Upon arrival at The University of Texas at Austin, all shales were coated and wrapped in thick polyethylene bags and housed inside sealed barrels or heavy-duty plastic covering. This was done in order to lessen shale exposure and interaction with the atmosphere. The exposure of shales to air could lead to changes in the shale properties, especially the native water activity (Chenevert and Amanullah, 1997).

2.3 SHALES SAMPLE PREPARATION

For testing purposes, different shale sizes were used for different tests. For pressure transmission and electrochemical tests, we used circular shale samples of 2.5" diameter and 0.25" thickness. Cubic shale samples of dimensions 0.5" x 0.5" x 0.5" were used for immersion and linear swelling tests.

We have developed a satisfactory method by which we can obtain circular shale samples of desired diameters. First, we open the shale wrapping and place the shale cores in oil cans in order to prevent exposure to air. Shale core-plugs are then cored with a 2" coring machine into 2" x 4" long cylindrical cores using a low toxicity mineral oil. The 2" x 4" cores were then sliced into 0.25" thick samples, as shown in figure 2-1, as follows:

- Prepare an epoxy by mixing the epoxy resin and hardener at a 1:1 ratio by weight. Make sure that it is mixed thoroughly. This epoxy was used to bind the shale sample to the interior of a plastic tubing.
- Pour the epoxy inside the plastic tubing that has a base plate at the bottom. The plastic tubing has an outside diameter of 2.5", an inside diameter of 2.125 " and length of 8".

The plastic tubing is made up of heat-resistance materials (Acrylic or Polycarbonate).

- Place the shale core inside the tubing and use 4 plastic rods (1/16") to centralize the core.
- Leave the epoxy to cure for 24 hours.
- Heat the whole assembly in the oven to 212 F for 1 hour. This is done in order to test the plastic and epoxy mixture integrity. Figure 2-2 shows a photo of the plastic tubing with the epoxy and the shale inside.
- Slice the shale core into circular discs of 0.25" thickness, as shown in figure 2-3, using a circular saw, which uses a low-toxicity mineral oil for lubrication purposes.
- After the shale core is sliced into circular discs, the discs are placed in sealed cans full of mineral oil so as to prevent exposure to air and moisture.

During the course of this research, we were having problems using the coring machine to obtain cylindrical core plugs from the softer shales, especially Pierre shale. Therefore, we made a slight procedural change to deal with softer shales. Instead of using the coring machine to obtain cylindrical core plugs, we used a circular saw, which uses synthetic oil as a cooling fluid, to cut long cubical plugs with square cross-sectional areas. These plugs have dimensions of 2" x 2" x 8". These cubical plugs are then encapsulated into the plastic tubing using the above-mentioned procedure in order to obtain shale discs with square cross-sectional areas for testing as shown in figure 2-4. Figures 2-5 and 2-6 show photographs of shale samples with circular and square cross-sectional areas prepared from cylindrical and cubical shale plugs respectively.

The immersion and linear swelling test sample preparation procedure is much simpler. We used a smaller circular saw to cut 0.5" x 0.5" x 0.5" cubic samples as shown in figure 2-7. This circular saw uses Escaid synthetic oil for cooling purposes.

The prepared shale samples were then put in sealed cans full of Escaid oil in order to prevent damage due to exposure to air. Once we knew the native water activity of the shale, we placed the shale samples in desiccators for humidity control prior to testing. It was found later that this practice often dehydrated the shale samples when water activities were unbalanced. Also, it introduced surface hydration and capillary effects. After realizing this, we started testing shales straight out of the oil cans without placing them in desiccators.

2.4 SHALE PROPERTIES

To study the interaction of shales with different drilling fluids, we must first determined the pertinent properties of our shale samples. The following discussion explains the properties of the shales used in our work and the testing conducted to obtain such properties.

2.4.1 Mineralogy and Clay Content

When shales interact with drilling fluids, it is extremely important to know the mineralogical make up of the shales in order to draw logical conclusions and make recommendations. The clay minerals present in the shales play an important role in the physcio-chemical behavior of these shales especially when exposed to aqueous solutions. X-ray diffraction analysis is the most widely used technique for the identification of fine-grained minerals especially clays which are present in the shale. OGS labs provided us with the mineralogy of both Pierre and Arco-China shales while Chevron-Texaco provided us with the mineralogical make up of C1 and C2 shales. Table 2-1, 2-2, 2-3 and 2-4 show the mineralogy and clay content of Pierre, Arco-China, C1 and C2 shales respectively.

2.4.2 Native Moisture Content and Water Activity

The native moisture content is the amount of water the shale contains within its pores. It is very important to measure this parameter once the preserved shale is removed out of its wrapping in order to get the closest estimate of the in-situ shale moisture content. The native moisture content, otherwise known as water content, is used in conjunction with adsorption isotherm curves to determine the shale native water activity. The following discussion presents the method used to obtain the native moisture content and water activity of the shales used in our study.

We obtained 6 cubical shale samples of dimension 0.5 “x 0.5” x 0.5” for each shale type. The initial weight of each shale sample was designated (w_i). The shale samples were dried by placing them in an oven at 200 F for 24 hours, then the weight of each dry shale sample was measured (w_d). The native moisture content for each shale sample was calculated as follows:

$$\text{Native Moisture Content } \% = [(w_i - w_d) / w_d]*100 \quad \ldots\ldots\ldots\ldots\ldots\ldots\ldots\ldots\ldots\ldots (3.1)$$

The native moisture content of all 6 shale samples was averaged and used as the average native moisture content for that shale type. Table 2-5 shows the native moisture content for Pierre, Arco-China, C1 and C2 shales respectively. The native moisture content is used in conjunction with adsorption isotherm curves to determine the shale native water activity as shown below.

Adsorption isotherm tests were used to determine the shale native water activity. The adsorption isotherm curve is a plot of the amount of water absorbed by the shale when placed in various desiccators versus the desiccator’s water activity. Figure 2-8 shows the type of desiccator used in our research for humidity control purposes. To prepare these desiccators, various kinds of saturated salt solutions were used to provide

and maintain different relative humidity environments. Table 2-6 shows the different saturated salts that were used to achieve the different relative humidities in the desiccators. The adsorption isotherm tests were conducted as follows:

- Shale samples are placed in several desiccators with different relative humilities.
- A vacuum is pulled on the desiccators in order to remove the air and accelerate the test towards equilibrium.
- As the shale adsorbs water, a weight gain is observed.
- Each shale sample is weighted daily until there is no further weight gain observed. The shale sample is in equilibrium with the atmosphere inside the desiccators when the shale sample weight becomes constant.
- The final weight of each sample is taken.
- The amount of water absorbed by the shale sample is calculated as the difference between the final weight and the dried weight.

$$\text{Water absorbed \%} = [(w_f - w_i) / w_i]*100 \quad \text{.....(3.2)}$$

- The adsorption isotherm curve is constructed by plotting the % water-absorbed by the shale against the respective relative humidity (water activity) of the desiccator in which the shale was placed.
- The shale water activity is determined by matching the native moisture content of the shale with its respective water activity value from the adsorption isotherm curve.

Figures 2-9, 2-10, 2-11 and 2-12 show the adsorption isotherm curves for Pierre, Arco-China, C1 and C2 shales respectively. Table 2-7 shows the native water activity obtained from the adsorption isotherms for all shales.

2.4.3 Shales Permeability

Shale permeability is an important parameter to measure since it describes the shale's ability to conduct fluid and ions through it. The relative ion size to shale pore throat size controls the ions ability to flow through shale and this in turn affects both the membrane efficiency and ion selectivity of shales. Therefore, it is very important to measure the shale permeability and correlate it with its membrane efficiency and ion selectivity.

In this dissertation, pressure transmission tests were conducted to estimate the shale permeability. To measure the shale sample permeability, we need to eliminate any osmotic flow across the shale sample; therefore, we flowed a simulated pore fluid upstream and downstream of the shale. Under such conditions, the only flow that will occur will be due to a hydraulic potential gradient. Knowing the pressure differential across the shale sample as a function of time, pore fluid viscosity, shale geometry and flow rate (volume of pore fluid entering the downstream chamber), we calculated the shales permeability using a transient pressure model. A complete description of the transient pressure model can be found in the appendix. Figures 2-13, 2-14, 2-15 and 2-16 show the pressure transmission tests for Pierre, Arco-China, C1 and C2 shales respectively. Using the model, we estimated the shales permeability from these graphs. Table 2-8 shows the estimated permeabilities for all shales.

2.4.4 Cation Exchange Capacity of Shales

The ability of shales to act as semi-permeable membranes is attributed to two factors: the presence of negative charges on the shale surface due to the presence of reactive clay minerals as part of its matrix make up and the small pore throat sizes due to shale compaction and burial. The ability of shales to act as semi-permeable membranes arises from the presence of the diffuse double layers on the clay surfaces (Keijzer et al, 1999). The diffuse double layer creates an environment with a higher concentration of cations and lower concentration of anions in the pore fluid. The cation exchange capacity is a direct measure of the strength of the electrical double layer. Therefore, the cation exchange capacity should influence the shale membrane efficiency and ion selectivity. Cation exchange capacities are either estimated analytically or measured in the lab using dye adsorption methods. Table 2-9 shows the cation exchange capacity of our shales.

Table 2-1: The mineralogical composition of Pierre shale

X-Ray Diffraction	% by weight
Quartz	19.0
Feldspar	4.0
Calcite	3.0
Dolomite	7.0
Pyrite	2.0
Siderite	1.0
Total Clay	64.0
Chlorite	4.0
Kaolinite	11.0
Illite	19.0
Smectite	17.0
Mixed Layer	49.0

Table 2-2: The mineralogical composition of Arco-China shale

X-Ray Diffraction	% by weight
Quartz	51.0
Feldspar	12.0
Calcite	3.0
Dolomite	1.0
Halite	2.0
Siderite	0.0
Total Clay	31.0
Chlorite	10.0
Kaolinite	14.0
Illite	44.0
Smectite	13.0
Mixed Layer	20.0

Table 2-3: The mineralogical composition of C1 shale

X-Ray Diffraction	% by weight
Quartz	14.0
Feldspar	2.0
Calcite	0.0
Dolomite	0.0
Pyrite	0.5
Siderite	0.0
Total Clay	76.0
Chlorite	N/A
Kaolinite	39.0
Illite	N/A
Smectite	N/A
Mixed Layer	N/A

Table 2-4: The mineralogical composition of C2 shale

X-Ray Diffraction	% by weight
Quartz	18.0
Feldspar	3.0
Calcite	0.0
Dolomite	0.0
Pyrite	0.7
Siderite	0.0
Total Clay	70.0
Chlorite	N/A
Kaolinite	26.0
Illite	N/A
Smectite	N/A
Mixed Layer	N/A

Table 2-5: Native moisture contents for all shales

Shale Type	**Native Moisture Content %**
Pierre Shale	13.03
Arco-China Shale	9.88
C1 Shale	14.45
C2 Shale	5.53

Table 2-6: Saturated salt solutions and their relative humidity %

Saturated Salt Type	***Relative Humidity %***
K_2SO_4	98
KNO_3	94
KCl	86
NaCl	76
$Ca(NO_3)_2$	50
$CaCl_2$	30
$ZnCl_2$	10

Table 2-7: Native water activity for all shales

Shale Type	**Native Water Activity**
Pierre Shale	0.98
Arco-China Shale	0.85
C1 Shale	0.98
C2 Shale	0.94

Table 2-8: The permeability shales studied

Shale Type	**Permeability, nD**
Pierre Shale	6.48
Arco-China Shale	0.45
C1 Shale	2.96
C2 Shale	0.83

Table 2-9: Cation exchange capacity shales studied

Shale Type	**Cation Exchange Capacity, mleq/100 gm**
Pierre Shale	10.5
Arco-China Shale	24.5
C1 Shale	21
C2 Shale	23

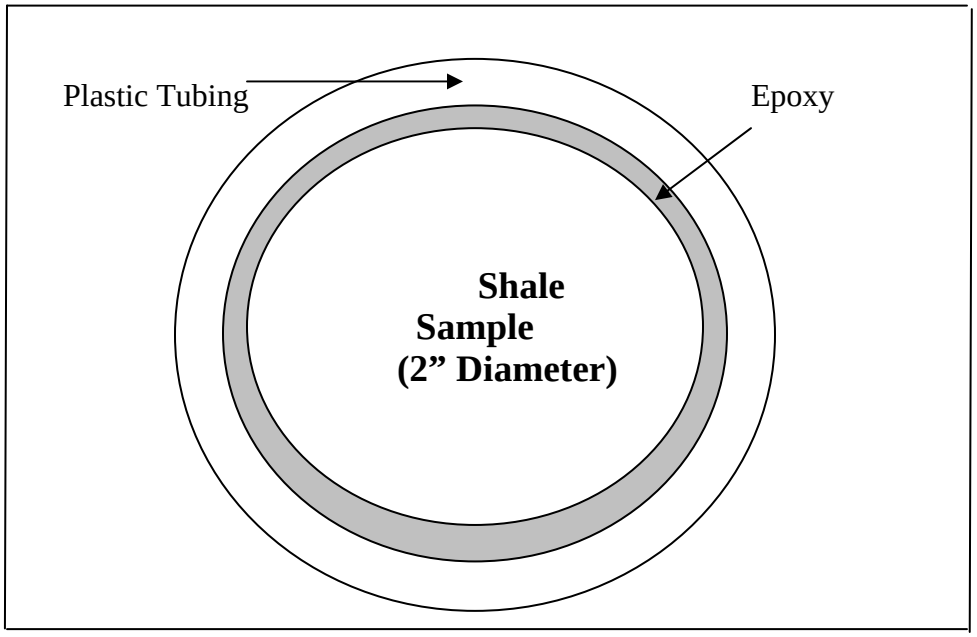

Figure 2-1: Circular shale sample

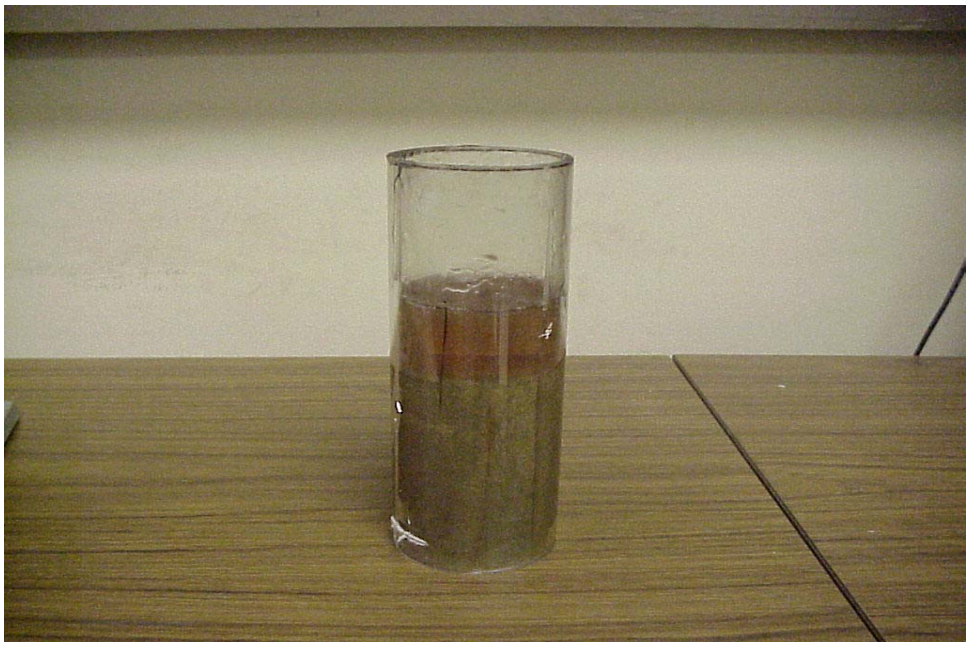

Figure 2-2: A photo of a shale plug encapsulated in plastic tubing filled with epoxy which binds the shale to the tubing surface.

Figure 2-3: A photo of a shale sample that was sliced from a shale plug that was encapsulated in a plastic tubing

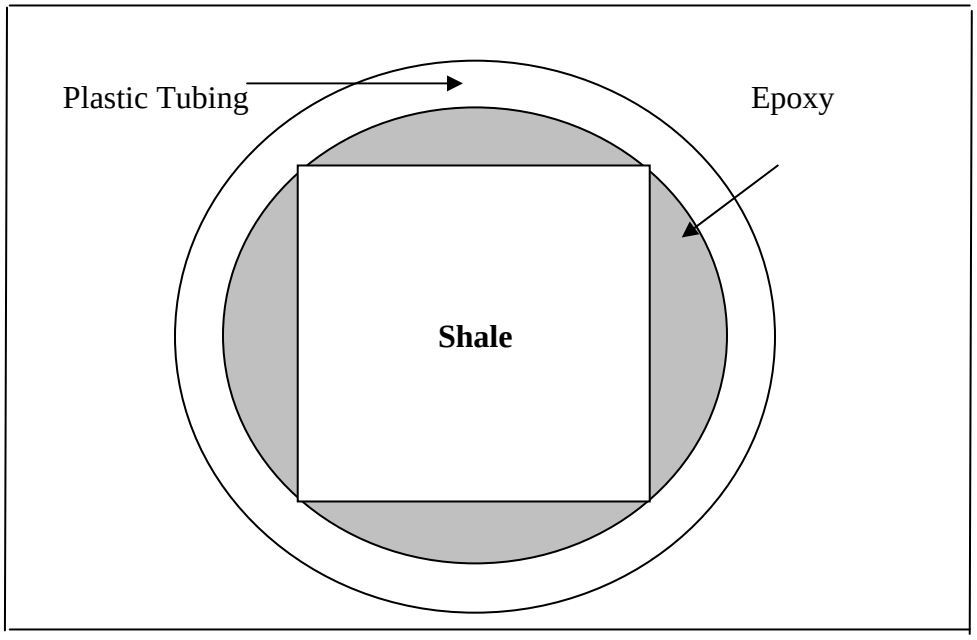

Figure 2-4: Cubical shale sample

Figure 2-5: A photo of a shale sample prepared from a cylindrical shale plug Notice the circular cross-sectional area of the shale.

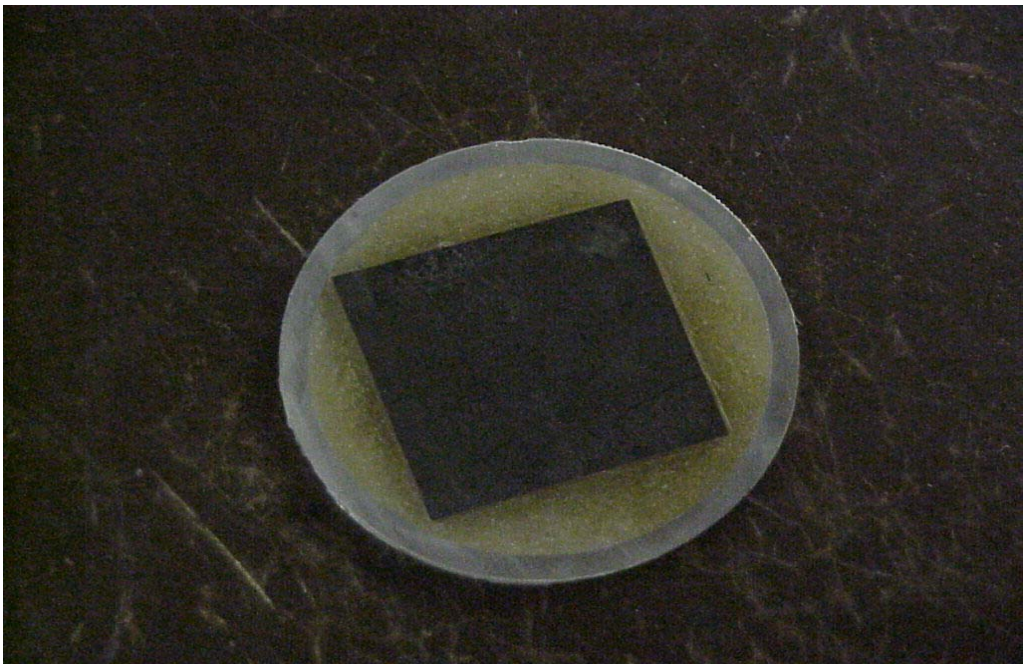

Figure 2-6: A photo of a shale sample prepared from a cubical shale plug. Notice the square cross-sectional area of the shale.

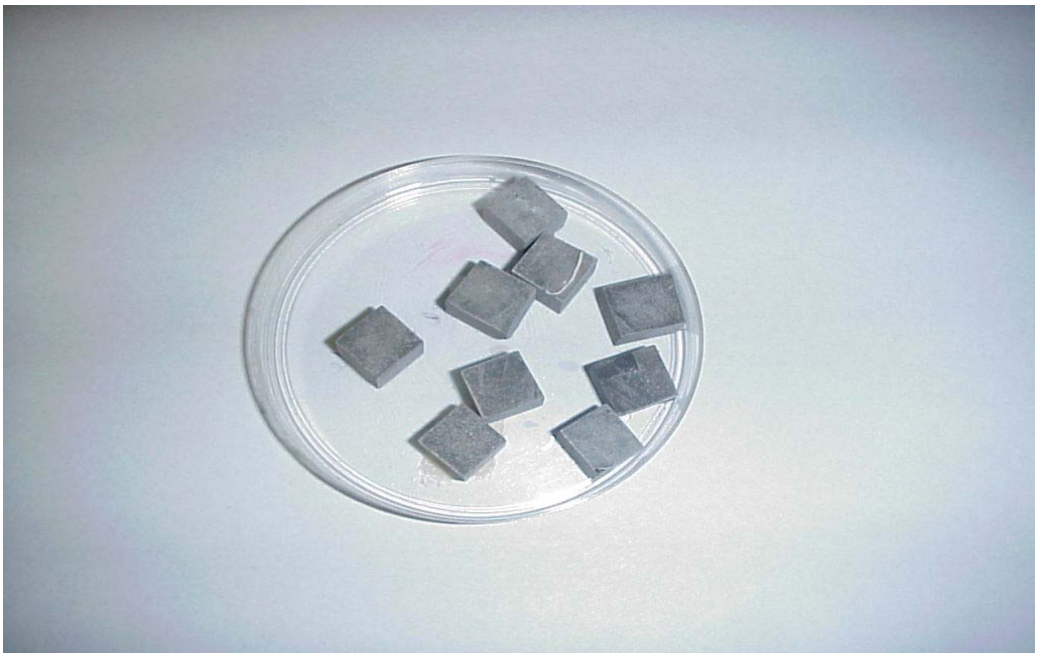

Figure 2-7: Cubical shale samples made especially for the immersion and linear swelling tests.

Figure 2-8: Desiccator's type used for humidity control purposes

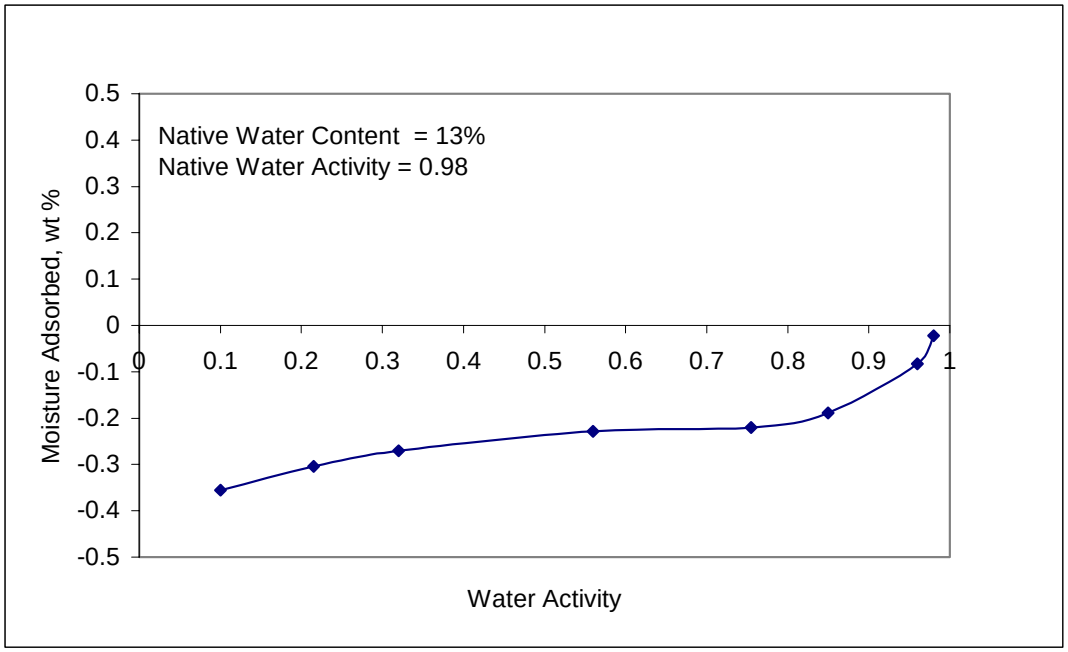

Figure 2-9: Adsorption isotherm curve for Pierre shale

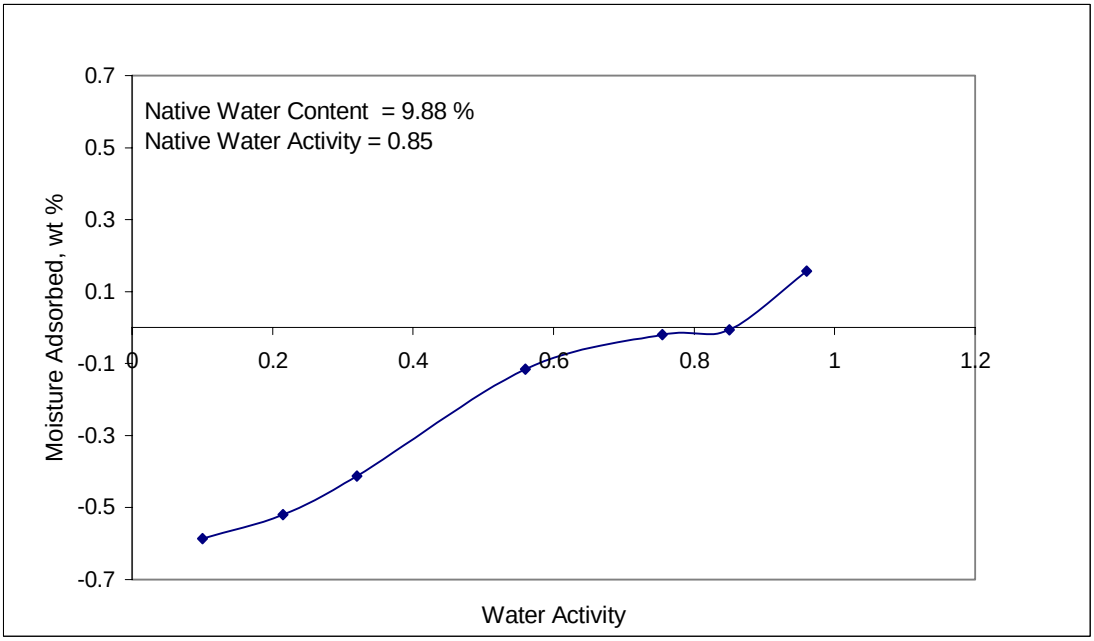

Figure 2-10: Adsorption isotherm curve for Arco-China shale

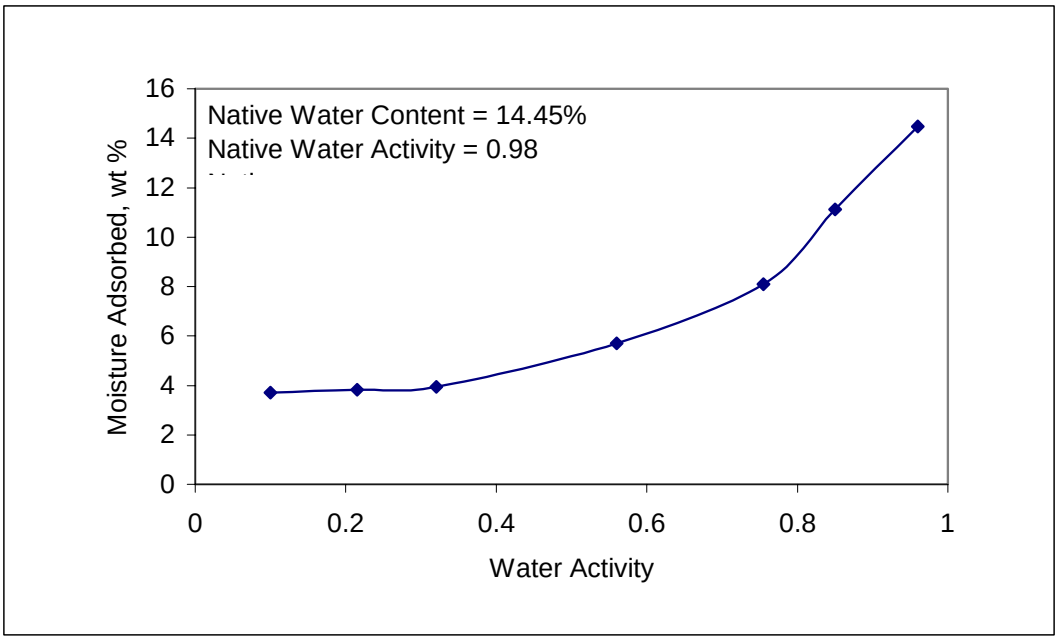

Figure 2-11: Adsorption isotherm curve for C1 shale

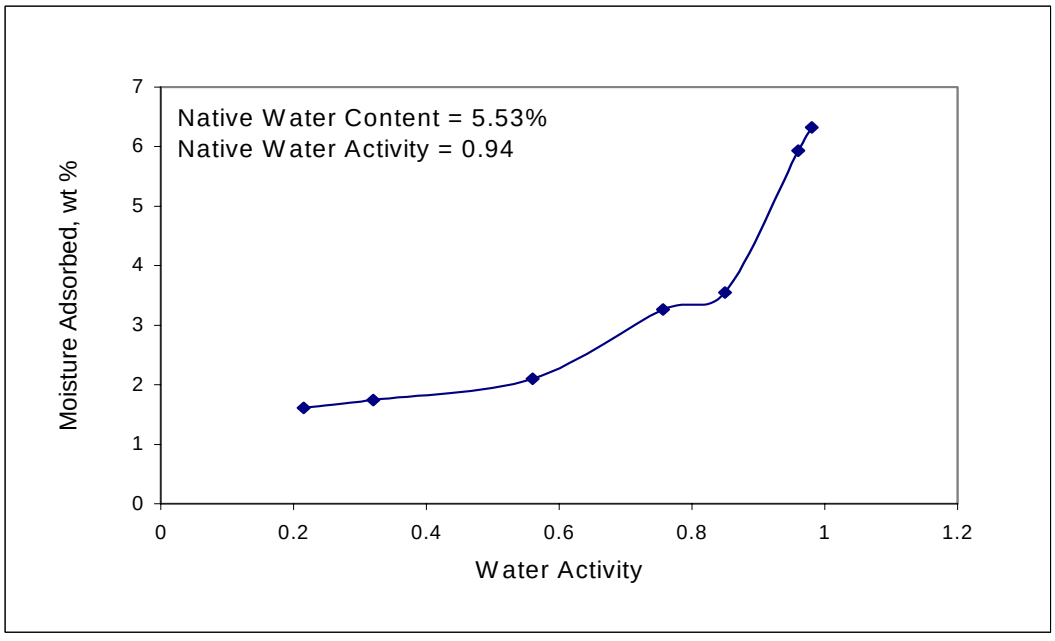

Figure 2-12: Adsorption isotherm curve for C2 shale

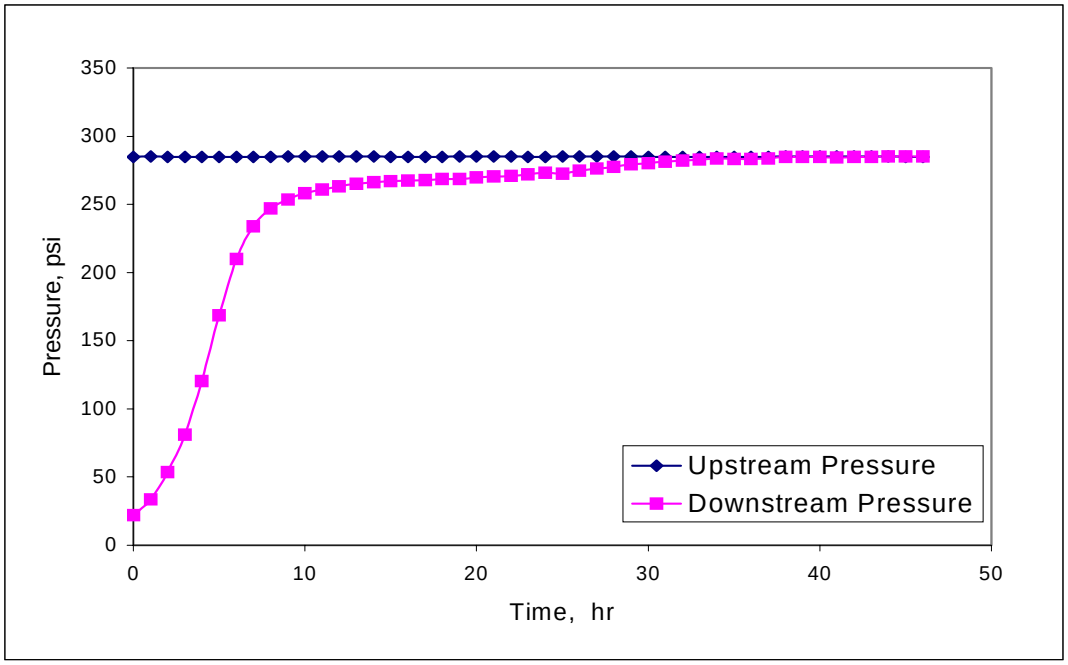

Figure 2-13: Permeability test for Pierre shale

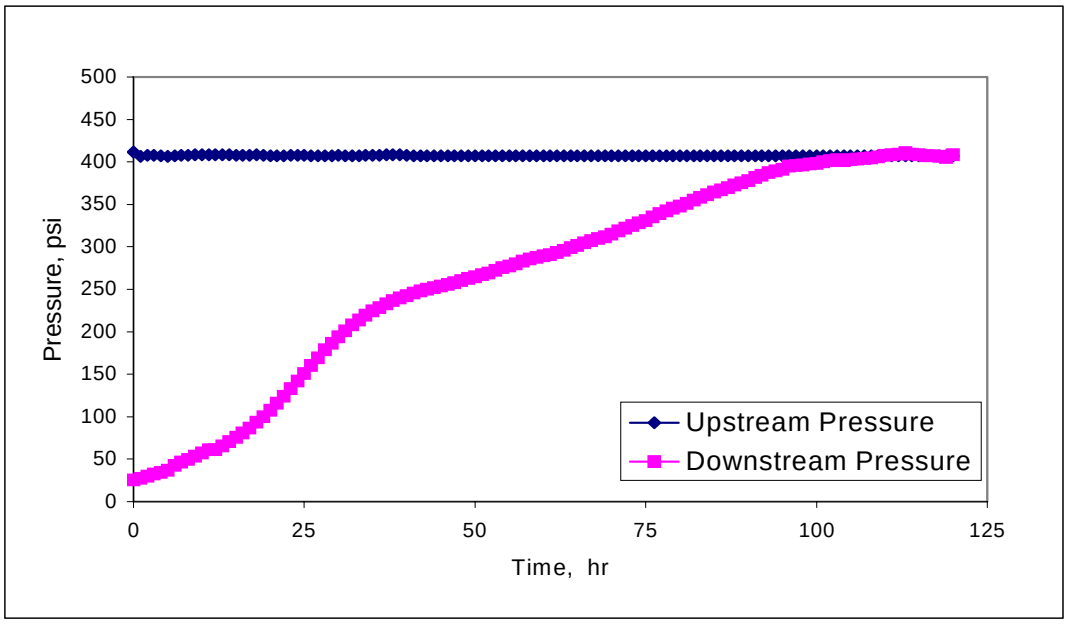

Figure 2-14: Permeability test for Arco-China shale

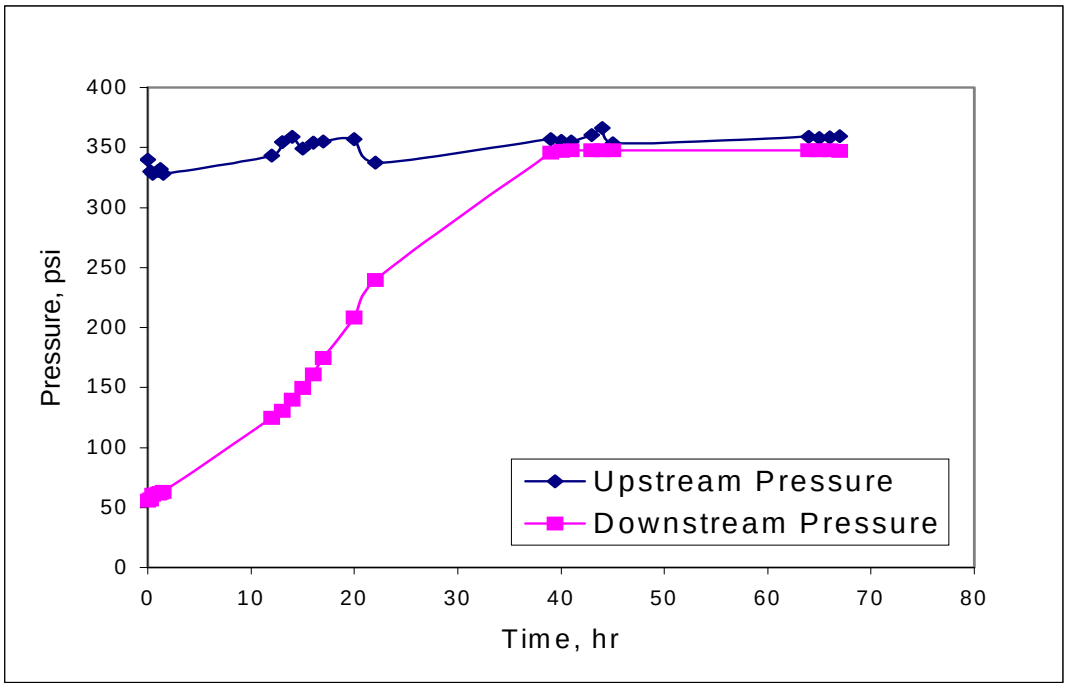

Figure 2-15: Permeability test for C1 shale

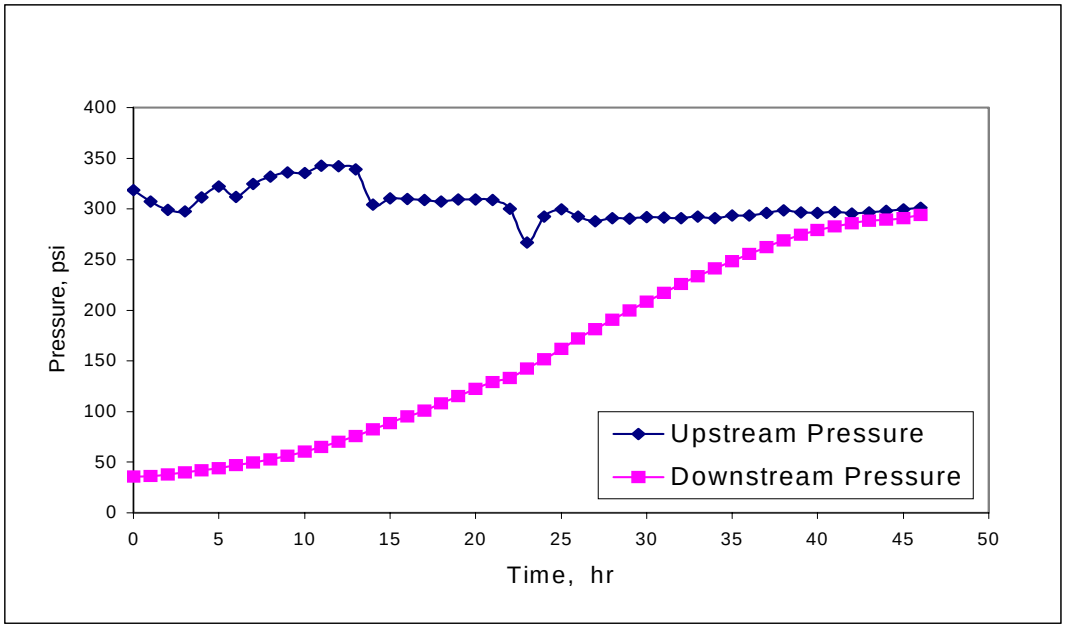

Figure 2-16: Permeability test for C2 shale

CHAPTER 3

Evaluation of Membrane Behavior of Shales Using Pressure Transmission Tests

3.1 INTRODUCTION

Osmosis has long been recognized as a means to extract water out of a shale when the water activity of the shale is higher than that of the drilling fluid. In the absence of a hydraulic pressure gradient, the movement of mud filtrate into shale is mainly governed by the chemical potential difference between the pore fluid and the mud and this results in the osmotic transport of water, (Ewy and Stankovich 2000). However, it has been recently shown that the osmotic potential generated between shale and drilling fluid is greatly influenced by the flow of ions into or out of shale due to ionic concentration imbalances (Zhang et al, 2004). Therefore, the actual osmotic effect is often less than the osmotic potential. This has spurred much interest to quantify the impact of ionic flow on the osmotic potential and that in turn has lead to introducing the concept of shale membrane efficiency. The membrane efficiency describes the ability of a shale to hinder ion movement when interacting with drilling fluids. If the shale completely stops ionic flow, the shale is said to act as a perfect semi-permeable membrane with a membrane efficiency of unity. If the shale lets ions flow freely, the shale is said to act as a non-selective membrane with a membrane efficiency of zero.

This chapter addresses the evaluation of the membrane efficiency of shales when interacting with drilling fluids (water-based and oil-based muds) using a pressure transmission technique. Section 3.2 discusses the background and presents a literature

review of shale membrane efficiency. In Section 3.3, a full description of the membrane efficiency test is given. More specifically, the test definition, objectives, experimental procedure and test matrix are addressed. Section 3.4 analyzes the experimental results for shale interaction with both water-based and oil-based muds. Finally, Section 3.5 draws conclusions and makes recommendations based on the experimental results.

3.2 BACKGROUND AND LITERATURE REVIEW

Numerous studies in soil mechanics showed that clays could act as semi-permeable membranes and, therefore, could sustain osmosis, because they allow only water to enter their pore space and restrict solutes (ions), (van Oort et al, 1994). This sparked much interest on the ability of shale to effectively sustain osmotic flow when interacting with water-based muds. Over the last fifty years, much effort and resources have been devoted to verify and quantify the membrane efficiency of shales.

Staverman (1952) presented a model to estimate the reflection coefficient (i.e. the membrane efficiency) of shale membranes. He showed that the measured osmotic pressure obtained using a non-ideal membrane is different from the thermodynamically predicted value. Furthermore, this measured osmotic pressure is highly dependent on the permeability of the membrane to the solutes. Following Staverman, Low and Anderson (1958) presented a theory that suggests osmosis as a mechanism for swelling pressures generated by shales. This theory is based on the principle that the shale itself acts as a semi-permeable membrane, which allows for the generation of osmotic pressure between the shale and the drilling fluid. Fritz and Marine (1983) supported the osmotic theory as a basis to explain water and ion transport in shales. They reported that clay membranes

were not ideal and that the degree of ideality was a function of the membrane's cation exchange capacity, porosity, and concentration of pore fluid. To better clarify the non-ideal behavior of shale, Ballard et al (1992) used radioactive traces of ^{36}Cl, ^{22}Na and ^{45}Ca to trace the movement of the respective ions through shales. He showed that the ionic species traced are capable of passing through the shale and concluded that shales behave only as leaky membranes that permit the transport of ions to some extent. He further concluded that osmosis is only a transient phenomenon and there will be no osmotic pressure at all when thermodynamic equilibrium is established. While many agreed that shales are leaky membranes, Bol et al (1992) experimentally showed that osmosis was not observed in shales and concluded that shales do not act as semi-permeable membranes. It is important to note that Bol performed his tests on high permeability shales, which in fact do not represent low permeability shales encountered in highly stressed environments.

All the above studies focused on verifying osmotic transport in shales and gave a qualitative measure of the membrane efficiency of shale. However, the need to actually quantitatively measure the membrane efficiency has gained much interest in the last decade especially since the membrane efficiency is an important input parameter for wellbore stability models. Therefore, the next phase of experimental work by various researchers focused solely on quantitatively estimating the membrane efficiency of shale. van Oort et al (1996) conducted pressure transmission tests to measure the membrane efficiency of shales. In addition, they studied the transport of water and ions in shales and its impact on shale stability in order to facilitate the improvement of water-based muds as shale drilling fluids. Their results showed that low permeability shales could act as semi-permeable membranes that sustain osmotic flow of water. Also, they showed that the membrane efficiency of shales was low and ranged from 1-10%. They argued

that shale cation exchange capacity could be responsible for the membrane behavior of shales. Based on their results, they concluded that the ability of shale to act as osmotic membranes could provide a powerful new means for stabilizing shale rocks when exposed to water-based drilling fluids. Building on van Oort's work, Ewy and Stankovich (2000*)* developed a technique for measuring shale pore pressure caused by hydraulic and chemical forces with the shales under stress, fully saturated, and not contacted by simulated pore fluid. They wanted to mirror downhole-drilling conditions as best as possible. They concluded that chemical (osmotic) forces could offset hydraulic forces. Moreover, they concluded that the chemically induced pressure difference was a function of the fluid activity and the shale and not of the salt type. More importantly, their wok showed that membrane efficiencies of shales in contact with salt solutions were low and ranged between 2% to 4%. Equally important was the conclusion that shales with low clay content and high permeability exhibited zero membrane efficiency. Schlemmer et al (2003*)* followed the same idea used by van Oort et al (1996) and Ewy *and* Stankovich (2000) to measure shale membrane efficiencies. They used a refined pressure transmission technique to study osmotic behavior. Conventional invert emulsion fluids, silicate-based fluids and water-based fluids were used in his study. Their data were used to better understand the concepts of osmotic pressure and membrane efficiency of shales and how they related to shale stability. This study concluded that the produced osmotic pressure and membrane efficiency of water-based fluids is low and did not exceed 10% for most cases. In addition, they observed that membrane efficiency of water-based fluids is different than that of invert emulsion fluids and silicate drilling fluids. Mody et al (2002) expanded on his previous work (1993) in the area of membrane efficiency measurements. He conducted a series of experiments with two objectives in mind. The first objective was the identification and evaluation of

compounds for use in water-based drilling fluids that generate high efficiency membranes at the wellbore wall. Secondly, they wanted to use these compounds to formulate a drilling fluid that exhibits high membrane efficiency characteristics. There results showed that membrane efficiencies of shales when interacting with water-based muds were low and seldom exceed 10%. In addition they showed that a membrane efficiency of up to 80% could be obtained using some compounds in the drilling fluid. They concluded that shale borehole stability can be achieved through shale pore pressure reduction that can occur because of the development of osmotic forces between the shale and the drilling fluid.

While all these studies gave a general idea of the low membrane efficiency of shale when interacting with drilling fluids, none of these studies presented a clear picture on the relationship between the membrane efficiency of shales and the properties of shale and drilling fluids. In this work, the membrane efficiency of shales, when interacting with water-based and oil-based muds, has been estimated using pressure transmission tests. The dependence of the membrane efficiency of shales on ion type and concentration in the drilling fluid is fully explored using different cations and different anions at different concentrations. The influence of the shale's permeability and cation exchange capacity on the membrane efficiency is also investigated using four different shales.

3.3 MEMBRANE EFFICIENCY TEST DESCRIPTION

3.3.1 Test Definition and Objectives

The membrane efficiency test used in our study made use of a pressure transmission technique where shale samples were subjected to both hydraulic and osmotic gradients during exposure to drilling fluids (water-based and oil-based muds). The pressure drop (resultant osmotic pressure) across the shale sample was measured in response to both hydraulic and osmotic pressure gradients. The pressure drop was then converted to membrane efficiency. For water-based muds, the membrane efficiency of the shale was measured since the shale is assumed to act as a semi-permeable membrane. However, for oil-based muds, it is presumed that the oil-based mud provides the characteristics of a semi-permeable membrane and the measured membrane efficiency corresponds to the oil-based mud membrane efficiency. The objectives of the test are as follows:

1. Measure the membrane efficiency of shales and oil-based muds during interaction of shales with water-based muds and oil-based muds.
2. Verify the ability of shales and oil-based muds to sustain osmotic flow.
3. Study the impact of salt type and concentration on the membrane efficiency of shale and the resultant osmotic pressure.
4. Study the influence of different cations and anions on the membrane efficiency of shales and the resultant osmotic pressure.
5. Study the impact of shale permeability and cation exchange capacity on the membrane efficiency and resultant osmotic pressure.

3.3.2 Test Equipment

Figure 3-1 shows the experimental set-up and equipment components that were used to evaluate the membrane efficiency of shale during interaction with water-based muds. Figures 3-2 and 3-3 show actual photos of the equipment during a test. The following section describes the test equipment components used and their functions.

Main Cell

The main cell (Figure 3-4) hosted the shale sample to be tested. The shale sample holder contains the shale sample (about 0.27" thick) imbedded in a plastic ring around its circumference. An epoxy bonds the plastic ring to the shale piece. The purpose of the plastic ring is to seal against any leakage that might occur around the shale.

The top cap is a steel piece that is 1.25" in thickness and 3.86" in diameter. This part contains an O-ring groove. The O-ring is used for sealing purposes, and seals on the plastic part of the shale sample. Two 1/16" holes are drilled in the top cap to allow communication between the flowing test fluids and the shale sample. The top cap and the base are held together with bolts and nuts.

The base part has the same dimensions as the top cap. The base part has a 0.25" recess to host the shale sample. A 1/8" tubing is silver solder to the bottom of the base. The purpose of this tubing is to allow communication between the shale sample and the simulated pore fluid. The reader is referred to Figure 3-4 for more details on dimensions.

Vacuum Pump

A vacuum pump was used to ensure that the upstream flow lines are air free. The presence of air will compromise the data and, therefore, the study analysis and conclusions.

Downstream Syringe Pump

The downstream syringe pump was used to manually pressurize the downstream chamber, which contains a simulated pore fluid. The downstream chamber is pressurized to compress any air bubbles in the chamber and thereby speed up the pressure build up in the downstream chamber. Furthermore, pressurizing the downstream chamber allowed us to perform our experiments under non-atmospheric pressure conditions. In other words, we were able to perform our experiments at different downstream pressures.

Upstream Injection Pump

The upstream pump was used to host and circulate the test fluids and thereby subject the sample to a constant fluid saturation.

Backpressure Regulator

The backpressure regulator was used to ensure a specific pressure upstream. In our experiment we flowed the test fluids at 350 to 500 psi. With the backpressure regulator, the test fluids flowed on top of the shale sample at the desired pressure.

Nitrogen Cylinder

The nitrogen cylinder was used to supply the back pressure regulator with the nitrogen at the desired pressure.

Simulated Pore Fluid Reservoir

This reservoir contained a simulated pore fluid. The water activity and ion concentrations of this simulated pore fluid matched the water activity and primary ions of the in-situ pore fluid of the shale sample. This prevented any water and ions transfer between the shale and the simulated pore fluid.

Pressure Gauges

The pressure gauges were placed strategically to monitor the pressures of interest in the system. The downstream pressure gauge recorded the pressure changes in the

downstream chamber while the pressure gauge upstream monitored the pressure of the flowing test fluids.

Valves

Different valves were placed strategically to regulate and control the flow and pressures of both upstream and downstream fluids.

For oil-based mud testing, Figure 3-5 shows the experimental set-up and equipment components that were used in this test. Figure 3-6 shows the experimental equipment during a test run. The same equipment that was used for shale and water-based muds, was utilized to run this test with some modification. Instead of having an injection pump and a back pressure regulator to circulate the oil-based mud at constant pressure, we added a pressure vessel upstream that contained the oil-based mud. The inside of pressure vessel holds two compartments separated by a floating piston. The top compartment was filled with pressurized nitrogen gas while the bottom compartment was filled with the oil-based mud to be tested. The pressurized nitrogen gas pushed against the floating piston supplying the oil-based mud with the desired pressure and forcing to come in contact with the shale.

3.3.3 Test procedure

The following describes the experimental steps taken to conduct the membrane efficiency test for shale and water-based muds. In our experiments, we maintained a higher water activity solution downstream and flowed a solution of lower water activity upstream across the shale. The solution upstream flowed under a constant pressure between 350 and 500 psi. Since we were imposing a pressure gradient across the shale, the upstream pressure was transmitted to the downstream pressure given enough time. Therefore, we expected to see the downstream pressure increase until it reached the

upstream pressure. However, since we had a higher water activity solution downstream, an osmotic backflow took place. Namely, water flowed out of the downstream chamber across the shale sample and into the upstream flow lines. Therefore, the hydraulic flow caused by the pressure gradient was offset by the backflow caused by the development of osmosis. If the shale acts as a membrane, its membrane efficiency can be estimated using equation (1.5). If the shale acts as a perfect semi-permeable membrane, its membrane efficiency will equal one. A reduction from a membrane efficiency of unity will indicate that the shale acts as a leaky membrane. In other words, the shale has allowed ions to pass through.

Our experimental set up allowed us to run our experiments under dynamic conditions since we continuously circulated the upstream fluid on top of the shale sample at the desired pressure. The continuous flow prevented ions from precipitating on top of the shale sample. Before starting our experiments, we needed to prepare our simulated pore fluid properly. The water activity and ion concentrations of the simulated pore fluid were made to match the water activity and ion concentrations of the real pore fluid in the shale sample to avoid any interaction between the shale pore fluid and the simulated pore fluid. After preparing the simulated pore fluid properly, we then proceeded to run our experiments. The following procedure was adopted to run our experiments.

- Close V2, V3, V4, V5
- Open V1
- Fill the syringe pump with the simulated pore fluid.
- Using the syringe pump, evacuate the downstream chamber. It is very important that the chamber is as air free as possible. The presence of air would extend the time duration greatly. Next, pressurize the downstream reservoir with the simulated pore

fluid using the syringe pump.

- Close V1
- Connect a vacuum pump to V3 and evacuate the upstream flow line and main cell. The presence of air in the upstream flow lines and main cell could distort the test outcome.
- Close V3
- Open V5 and bring up the backpressure regulator to the desired flowing pressure.
- Close V5 after the desired flowing pressure is achieved.
- Open V2 & V3 and turn on the upstream injection pump at 0.2 cc/hr flow rate.
- The upstream injection pump will withdraw the test fluid from the test fluid cylinder located inside the pump and deliver it at 0.2 cc/hr flow rate. The test fluid will flow upstream through the tubings and on top of the shale sample. The flowing pressure for the test fluid will increase until it equals the backpressure regulator pressure, which is the desired flowing pressure.
- The test fluid will circulate upstream at the desired pressure and exist the backpressure regulator into a waste cup, which is open to the atmosphere.
- The injection pump keeps circulating the test fluid across the shale sample. The test fluid flowing pressure will be maintained at the desired level by the backpressure regulator.
- The pressure gauge upstream is used to monitor the test fluid pressure to make sure that it is maintained at the desired level.
- The simulated pore fluid pressure in the downstream chamber is monitored and recorded with time.

For the oil-based mud tests, a slight change in procedure was adopted to accommodate the slightly different set-up. The following describes the experimental procedure for evaluating the membrane efficiency of oil-based muds.

- Close V2, V3
- Open V1 (a two-way valve)
- Using a vacuum pump, evacuate the downstream chamber. It is very important that the chamber is as air free as possible. The presence of air will extend the time duration greatly.
- Next, fill the injection pump with the simulated pore fluid. Using the injection pump, pressurize the downstream reservoir with the simulated pore fluid. The applied pressure should be the same as that of the upstream pressure which is 1000 psi.
- Close V1
- Connect the vacuum pump to V2 and evacuate the upstream flow line and main cell. The presence of air in the upstream flow lines and main cell could distort the test outcome.
- Close V2
- Fill the bottom compartment of the pressure vessel with the oil-based mud to be tested.
- Open V3 and pressurize the top compartment of the pressure vessel using nitrogen gas supplied by the gas cylinder. Normally, this pressure will be at 1000 psi. The constant flow of nitrogen gas will ensure that pressure upstream stays constant at 1000 psi while the floating piston will help in maintaining the upstream pressure at 1000 psi by pushing against the gas contained in the top compartment whenever the pressure in the bottom compartment becomes greater than 1000 psi.

- The pressure gauge upstream is used to monitor the test fluid pressure to make sure that it is maintained at the desired level.
- The simulated pore fluid pressure in the downstream chamber is monitored and recorded with time.

3.3.4 Test Matrix

In our research, we evaluated the membrane efficiency of four different shale samples as a result of their interaction with water-based and oil-based muds. The effects of shale permeability and cation exchange capacity on shale membrane efficiency were investigated using four different shales. In addition, this study aimed to investigate the effects that different cations and anions have on the membrane efficiency. We also aimed at studying the influence of various concentrations (water activity changes) of these cations and anions on shale's membrane efficiency. Table 3-1 shows the test matrix designed to study the effects of cation type and concentration on shale membrane efficiency. Table 3-2 shows the test matrix designed to study the effects of anion type and concentration on shale membrane efficiency. The effects of shale permeability and cation exchange capacity were incorporated in Tables 1 and 2 by using different shales. In addition, Table 3-3 shows the test matrix designed to study the effects of shale type and permeability on oil-based mud membrane efficiency.

3.4 RESULTS & DISCUSSION

3.4.1 Membrane Efficiency of Shales during Interaction with Water-Based Muds

Our experimental results showed that all measured shale membrane efficiencies were low, ranging from 0.18% to 4.23%. This is not unusual when shales interact with

water-based muds (salt solutions). Researchers have recently reported that salt solutions and shale systems yielded low membrane efficiencies which ranged from 0% to 10 %, (van Oort, 2003). Moreover, it was found that the induced osmotic pressure was generally low compared to the applied theoretical osmotic potential.

Tables 3-4, 3-5, 3-6 and 3-7 show the experimentally measured membrane efficiency for shales C1, C2, Pierre and Arco-China during interactions with NaCl, KCl, $CaCl_2$ and KCOOH solutions of different water activities. To get a better sense of these values, we need to understand the experiments that lead to these measured values. Figures 3-7 and 3-8 show the downstream reservoir pressure build up during the interaction of C1 shale with NaCl solutions of 0.93 and 0.85 water activity. Figures 3-9, 3-10 and 3-11 show the downstream reservoir pressure build up during the interactions of C1 shale with KCl, $CaCl_2$ and KCOOH solutions of 0.93 and 0.85 water activity.

I will explain Figure 3-9 in detail to give a sense of what is actually happening during a typical test. Similar explanations can be provided for the other tests. Figure 3-9 shows the downstream reservoir pressure build up in response to flowing a KCl solution (a_w = 0.93) until equilibrium is reached (about 71 hours later) and then switching the upstream flowing solution to KCl solution (a_w = 0.85). The downstream reservoir, which was in contact with the shale sample, initially had a KCl solution (a_w = 0.98) and an average pressure of 53 psi. As shown, when the KCl solution (a_w = 0.93) was flowed across the top of the shale at a pressure of 360 psi; the downstream pressure reached equilibrium after 71 hours and the downstream pressure was 354 psi at that time. This means that the difference between the upstream flowing pressure and the downstream pressure was 6 psi. The theoretical osmotic potential due to the different water activity was calculated using equation (1.4) to be 1028 psi. The membrane efficiency was estimated using equation (1.5) to be 0.58%. When the KCl solution (a_w = 0.85) was

flowed across the top of the shale at a pressure of 362 psi; the downstream pressure reached equilibrium and equilibrium value of 348 psi after 66 hours. This means that the difference between the upstream flowing pressure and the downstream pressure was 14 psi. The theoretical osmotic potential due to the different water activity was calculated using equation (1.4) to be 2794 psi. The membrane efficiency was estimated using equation (1.5) to be 0.5%.

Figure 3-12 shows the downstream reservoir pressure build up during the interaction of C1 shale with KCOOH solution of 0.4 water activity. This test was conducted in order to study the behavior of C1 shale when exposed to very concentrated salt solution. Figures 3-13, 3-14, 3-15 and 3-16 show the downstream reservoir pressure build up during the interactions of C2 shale with NaCl, KCl, $CaCl_2$ and KCOOH solutions of 0.93 and 0.85 water activity respectively. Figures 3-17, 3-18, 3-19 and 3-20 show the downstream reservoir pressure build up during the interactions of Pierre shale with NaCl, KCl, $CaCl_2$ and KCOOH solutions of 0.93 and 0.85 water activity respectively. Figures 3-21, 3-22, 3-23 and 3-24 show the downstream reservoir pressure build up during the interactions of Arco-China shale with NaCl, KCl, $CaCl_2$ and KCOOH solutions of 0.93 water activity respectively. Since the Arco-China shale's water activity was 0.85 and the upstream flowing salt solutions water activities were 0.93, the downstream reservoir pressure increased above that of the upstream because of the combined flux of water due to hydraulic and osmotic effects. In all the other tests, the osmotic effect was offsetting some of the hydraulic effect, which lead to the downstream reservoir pressure being always less than the flowing upstream pressure.

While the membrane efficiency and induced osmotic pressure of shales when interacting with salt solutions are generally low, the membrane efficiency and induced osmotic pressure trend seem to correlate well with drilling fluid properties and shale

properties. The drilling fluids studied in this work contain solutes (ions) of different concentration and type (cations and anions). In addition, shale permeability and cation exchange capacity were the main shale properties, which were investigated in this research.

3.4.2 Effect of Ion Concentration on Membrane Efficiency of Shale

Our experimental results showed a consistent correlation between the water activity gradient imposed across the shale and the measured membrane efficiency of the shale. The higher the imposed water activity gradient (chemical potential), the higher the induced osmotic pressure. It is important to state that the induced osmotic pressure was not high. Tables 3-4, 3-5, 3-6 and 3-7 show the results of the induced osmotic pressure in response to water activity gradients for all shales. It is clearly shown that the induced osmotic pressure increased when the water activity gradient (chemical potential) imposed across the shale increased. This is expected since the higher the water activity gradient across the shale is, the higher the force that extracts the water out of the shale (higher water activity) becomes.

3.4.3 Effect of Shale Permeability on Membrane Efficiency of Shale

It is argued that shales exhibit membrane behavior partially due to their small pore size. Therefore, shale permeability which is a function of pore size should influence the shale membrane efficiency and induced osmotic pressure. Figures 3-25, 3-26, 3-27, 3-28 show the membrane efficiency dependence on shale permeability when shales with different permeabilities interacted with salt solutions of different water activities. The general trends shown in these graphs are the same; the membrane efficiency of shales increases when the shale permeability decreases. As the shale permeability (pore size) decreases due to burial and compaction, their ability to restrict solutes increases and their

membrane efficiency increases. In other words, it is the ratio of solute size to pore size that determine their ability to restrict solutes from entering their pore space and thus gives them the ability to behave as semi-permeable membranes.

It can also be seen that the induced osmotic pressure increased as the shale permeability decreased. This is expected since the osmotic pressure is a measure of the shale membrane efficiency. Figures 3-29, 3-30, 3-31, 3-32 show the induced osmotic pressure dependence on shale permeability.

3.4.4 Effect of Shale Cation Exchange Capacity on Membrane Efficiency of Shale

Another important factor affecting shale membrane behavior is their cation exchange capacity. The ability of shales to act as semi-permeable membranes based on electrical exclusion of co-ions (anions) arises from the presence of diffuse double layers on the clay surfaces (Keijzer et al, 1999). The cation exchange capacity of shales is a measure of the intensity of the negative charge environment between clay platelets and hence co-ions electrical exclusion property of shales. High cation exchange capacity indicates strong electrical repulsion of anions. Therefore, the cation exchange capacity should influence the shale membrane efficiency and induced osmotic pressure. Figures 3-33, 3-34, 3-35, 3-36 show the membrane efficiency dependence on shale cation exchange capacity when shales with different cation exchange capacities interacted with salt solutions of different water activities. These Figures show clearly that the membrane efficiency of shale is directly related to the shale's cation exchange capacity. In other words, the membrane efficiency of shale increases when the cation exchange capacity increases.

It can also be seen that the induced osmotic pressure increased as the shale cation capacity increases. This is expected since the osmotic pressure is a measure of the shale membrane efficiency. Figures 3-37, 3-38, 3-39, 3-40 show the induced osmotic pressure

dependence on shale cation exchange capacity when shales with different cation exchange capacities interacted with salt solutions of different water activities.

3.4.5 Effect of Ion Type on Membrane Efficiency of Shale

3.4.5.1 Cation Type

Our experimental results show that membrane efficiency and induced osmotic pressure obtained by calcium chloride solutions were higher than those obtained by sodium chloride or potassium chloride solutions at the same concentrations. In addition, sodium chloride solutions yielded higher membrane efficiencies than potassium chloride solutions at the same concentrations. This can be explained be the different hydrated diameters of these ions. Due to their complex and narrow pore throats, shales have a natural ability to screen out ions based on their size relative to the shale's pore throat size. Therefore, hydrated ion diameters can be used to rank an ion's ability to invade shale pores. Table 3-8 shows the hydrated diameter of different cations. According to this Table, the hydrated diameter for calcium is bigger than that for sodium which in turn is bigger than potassium. Figure 3-41 shows the membrane efficiency dependence on cation-hydrated radius when different cations (calcium, sodium and potassium) at different concentrations interact with C1, C2 and Pierre shales.

3.4.5.2 Anion Type

Just like cations, anions are screened out by shales on the basis of their size relative to the shale's pore throat size. Therefore, anion hydrated diameters can be used to rank their ability to invade shale pores. Since the hydrated diameter of formate is larger than that for chloride, one expects the invasion of formate anions into shales to be less than for chloride anions. Our experimental results generally follow the same hydrated diameter trend where membrane efficiencies and induced osmotic pressure obtained by

formate solutions were higher than those obtained by chloride solutions at the same concentrations. Figure 3-42 and Figure 3-43 shows the membrane efficiencies dependence on anion type when formate and chloride solutions of 0.93 water activity and 0.85 water activity interacted with C1- shale, C2-shale and Pierre shale respectively. From these Figures one can see that formate solutions yielded higher membrane efficiencies than chloride solutions owing to their bigger hydrated diameter and thus lower mobility.

3.4.6 Effect of Cation Exchange Capacity (CEC) and Shale Permeability (k) Ratio on Membrane Efficiency of Shale

In order to show the combined effect of both the cation exchange capacity and permeability of shales on the measured membrane efficiency of shales, the ratio of the cation exchange capacity to permeability of shales versus the measured membrane efficiency of shales was plotted. Figures 3-44, 3-45, 3-46, 3-47 show the membrane efficiency dependence on the ratio of cation exchange capacity and permeability (CEC/k) when shales interacted with solutions (NaCl, KCl, $CaCl_2$ and KCOOH) at different water activities (0.93 and 0.85). It is clearly shown from these graphs that the membrane efficiency is directly proportional to the ratio of the cation exchange capacity and permeability of shales. Higher cation exchange capacity and permeability (CEC/k) ratio correlates very well with higher membrane efficiency. The same argument and conclusion applies to the dependence of induced osmotic pressure on the ratio of the cation exchange capacity and permeability of shales. Figures 3-48, 3-49, 3-50, 3-51 show the induced osmotic pressure dependence on the ratio of cation exchange capacity and permeability (CEC/k) when different shales interacted with different solutions (NaCl, KCl, $CaCl_2$ and KCOOH) at different water activities (0.93 and 0.85). From these

graphs, one can see that, with a few exceptions, the induced osmotic pressure increases as the ratio of the cation exchange capacity and permeability (CEC/k) increases.

3.4.7 Implications for Design of Water-Based Muds

It is believed that extracting water out the shale strengthens the shale and avoids shale collapse. This is due to the fact that water flow out the shale reduced the shale pore pressure and that in turn leads to strength enhancement, (Mody and Hale, 1993). This concept has been utilized to osmotically induce water flow out of a shale through manipulation of the water activity of the drilling fluid. Following this observation, salts such as KCl, NaCl and $CaCl_2$ were used in the formulation of water-based muds to achieve low water activity water-based muds. To fully benefit from this idea, the shale must act as a perfect semi-permeable membrane where it only allows water to move and completely restricts the flow of ions. The flow of ions tends to reduce the difference in water chemical potential and thus destroys the osmotic mechanism that is responsible for water transport out of the shale. The flux of ions into the shale reduces the water activity in the shale and decreases the osmotic driving potential. This reduces any osmotic flow from the shale but also increases the near wellbore pore pressure which contributes to shale strength reduction. Furthermore, the ions can interact adversely with the shale constituents (cementing material, shale matrix and pore fluid) and that could lead to cohesive strength reduction and ultimately failure, (Hale and Mody, 1992).

In this work, we have shown that shales are not ideal semi-permeable membranes especially during interaction with salt solutions. In fact, they are very leaky membranes since the measured membrane efficiencies were very low. The higher the permeability of the shale, the lower the membrane efficiency. This presents a very interesting question; should concentrated salt solutions be used to osmotically stabilize reactive shales? Our results suggest that osmosis will not work in high permeability, low CEC, shales since the

ions will pass through unrestricted. This was clearly shown in Figures 3-25, 3-26, 3-27, 3-28 where the measured membrane efficiency correlated inversely with the permeability of shales. For low permeability shales, the measured membrane efficiencies and induced osmotic pressure were low. The induced osmotic pressure averaged about 35 psi which is not much compared to the typical hydraulic difference required for drilling. However, we have shown that the membrane efficiency is a function of the ratio of the hydrated diameter of the ion to the shale pore throat size. Generally speaking, the hydrated diameter of the K^+, Na^+ and Ca^{+2} are much smaller than the average shale pore throat radius. Therefore, using salts to achieve very low water activity water-based muds mud might not be of great benefit since this will increase the flux of ions and their associated water shells into the shale. It is, therefore, recommended that ions with large hydrated radii be used in water-based muds. These big ions lower the water activity of the mud and will not flow into the shale due to size restrictions. Simpson et al (1995) used an experimental approach in order to identify an environmentally acceptable water-based mud that can act as an oil-based mud. His results showed that a water soluble organic monomer with multiple hydroxyl groups on a two-tiered cyclic structure (methylglucoside) provides a mud that can prevent hydration, pore pressure increase and shale weakening. Therefore, the ratio of ion-hydrated diameter to the shale pore throat size may play a major role in cation selection for drilling fluid formulation.

It has been reported that, on occasion, improved wellbore stability was achieved using high salinity potassium chloride based muds. It is possible that shale strength was affected by high K^+ ion flow into the shale and that this altered the basic composition and properties of the shale. The potassium ion can exchange easily with other interlayer cations in the crystal lattice, thereby reducing the spacing between the layers, increasing

shale strength and promoting stability (Mondshine, 1972). Testing of such altered shales is beyond the scope of this work.

3.4.8 Membrane Efficiency of Oil-Based Muds

The measured membrane efficiencies of oil-based muds were high compared to those of shales. The membrane efficiencies of oil-based muds obtained from our experiments were 51.18 %, 48.62 % and 17.05 % during interactions with C1 shale, Arco-China shale and Pierre shale respectively. Figures 3-52, 3-53 and 3-54 shows the pressure transmission test when C1, Pierre and Arco-China shales were exposed to oil-based muds with water activities of 0.93, 0.93 and 0.8 respectively. The high membrane efficiency of oil-based muds can partly explain their ability to stabilize reactive shales through osmotic backflow especially when the water activity of the oil-based mud is lower than that of the shale. While the membrane efficiencies of oil-based muds were high compared to those for water-based muds, they are not 100% as is commonly assumed.

3.4.9 Implications for Design of Oil-Based Muds

While oil-based muds exhibited high membrane efficiency, which is certainly beneficial to shale stabilization and strength enhancement through pore pressure reduction, these membrane efficiencies were not 100% as postulated by many researchers. This means that some ions can still exchange between shale and oil-based muds and that in turn could affect shale cohesive strength through unfavorable interaction between ions and the shale cementing material. In addition, the flow of ions reduces the osmotic potential.

It is important to note that we have used the same oil-based mud in all our experiments. Therefore, the different membrane efficiencies of the oil-based muds must

be caused by the interaction between the emulsified water phase and the shale. If the emulsion, which contains the $CaCl_2$ solution, is perfectly stable and the EZ-MUL emulsifier used in the oil-based mud formulation is a perfect semi-preamble membrane, then one would expect the membrane efficiency of the oil-based mud to be 100% for all shales. However, if the emulsion is not stable and or the emulsifier is not exactly a perfect semi-permeable membrane, then one would expect that the ions contained in the $CaCl_2$ solution to be less restricted and thus diffuse in or out of the oil-based mud. When this happens, it comes directly in contact with the shale and the shale becomes the regulator of ion flow between the oil-based mud and the shale pore fluid. In other words, the oil-based mud may lose its ability to restrict ion flow due to emulsion instability. This is why it is very important to keep a very tight and stable emulsion when formulating oil-based muds for wellbore stability. While we made sure that our emulsion is stable by following standard procedures where the oil-based-mud and the brine are mixed to 200 F, the oil-based muds sat on the shelf for about two weeks before testing. It was noted that some of the EZ-MUL emulsifier precipitated to the bottom. Therefore, we believe that the emulsion was not 100% stable at the beginning of the test and that lead to differences in the membrane efficiency of oil-based muds and deviations from perfect 100% values.

When designing oil-based muds for wellbore stability purposes, it is always a good idea to periodically check the emulsion stability of the mud. A stable emulsion is required for the effective osmotic transport of water. Furthermore, having excess emulsifier in the oil-based mud formulation is recommended to satisfy any water influx from the formation.

3.5 CONCLUSIONS

The experimental results in this chapter show the membrane efficiency for shales during interactions with salt solutions and oil-based muds. The following conclusions were drawn from these results.

3.5.1 Interaction of Shales with Water-Based Muds

- All measured membrane efficiencies of salt solutions in contact with shales were low, ranging from 0.18% to 4.23%.
- The induced osmotic pressure was generally low compared to the theoretical osmotic potential.
- The membrane efficiency and induced osmotic pressure correlate well with the water activity gradient (chemical potential) imposed across the shale.
- The induced osmotic pressure increased when the water activity gradient (chemical potential) imposed across the shale increased.
- The membrane efficiency of shales increases when the shale permeability decreases. Therefore, as the shale permeability (pore size) decreases due to burial compaction, their ability to restrict solutes increases and their membrane efficiency increases.
- The ratio of solute size to shale pore throat determines shales ability to restrict solutes from entering their pore space and thus gives shales the ability to behave as semi-permeable membranes.

- The membrane efficiency of shales increases when the shale cation exchange capacity increases.
- The membrane efficiency is proportional to the ratio of the cation exchange capacity and permeability of shales. Higher cation exchange capacity and permeability (CEC/k) ratio correlates very well with higher membrane efficiency.
- Cations with big hydrated diameters yielded higher membrane efficiencies, when interacting with shales, than cations with small hydrated diameters. Thus, the ratio of cation-hydrated diameter to the shale pore throat size should play a major role in cation selection for drilling fluid formulations.
- Anions with big hydrated diameters yielded higher membrane efficiencies, when interacting with shales, than anions with small hydrated diameters. Thus, the ratio of anion-hydrated diameter to the shale pore throat size should play a major role in anion selection for drilling fluid formulations.

3.5.2 Interaction of Shales with Oil-Based Muds

- The membrane efficiency of oil-based muds was high compared to those obtained with shales and salt solutions. However, these membrane efficiencies were not 100 % as postulated by many earlier researchers.
- The membrane efficiency observed with oil-based muds is likely due to emulsion instability that causes the brine to come into direct contact with the shale (without an intervening oil film).

Table 3-1: Test matrix to study the effects cation type and concentration on the membrane efficiency of shales.

Salt Solution (Test Fluid)	Water Activity	Shales tested	Temperature
NaCl	**0.93**	**C1, C2, Pierre & Arco-China Shales**	**70 F**
	0.85	**C1, C2, Pierre & Shales**	**70 F**
KCl	**0.93**	**C1, C2, Pierre & Arco-China Shales**	**70 F**
	0.85	**C1, C2, Pierre & Shales**	**70 F**
CaCl2	**0.93**	**C1, C2, Pierre & Arco-China Shales**	**70 F**
	0.85	**C1, C2, Pierre & Shales**	**70 F**

Table 3-2: Test matrix to study the effects of anion type and concentration on the membrane efficiency of shales.

Salt Solution (Test Fluid)	Water Activity	Shales tested	Temperature
KCOOH	**0.93**	**C1, C2, Pierre & Arco-China Shales**	**70 F**
	0.85	**C1, C2, Pierre & Shales**	**70 F**
KCl	**0.93**	**C1, C2, Pierre & Arco-China Shales**	**70 F**
	0.85	**C1, C2, Pierre & Shales**	**70 F**

Table 3-3: Test matrix to study the membrane efficiency of oil-based muds during their interaction with different shales.

Shale Type	Shale Permeability	Downstream Fluid	Test Fluid "Upstream"	Temp
C1-Shale	2.96 nD	NaCl (aw = 0.98)	OBM (aw = 0.93)	70
Pierre Shale	6.48 nD	NaCl (aw = 0.98)	OBM (aw = 0.93)	70
Arco-China Shale	0.45 nD	NaCl (aw = 0.85)	OBM (aw = 0.80)	70

Table 3-4: The membrane efficiency experimental results for C1- shale during interaction with different salt solutions of different water activities.

Salt Solution (Test Fluid)	**Water Activity**	**Measured Osmotic Pressure (psi)**	**σ %**
NaCl	0.93	23	2.24
	0.85	30	1.1
KCl	0.93	6	0.58
	0.85	14	0.50
CaCl2	0.93	10	0.97
	0.85	28	1.0
KCOOH	0.93	24.5	2.38
	0.85	26	0.9
	0.4	60.5	0.34

Table 3-5: The membrane efficiency experimental results for C2- shale during interaction with different salt solutions of different water activities**.**

Salt Solution (Test Fluid)	**Water Activity**	**Measured Osmotic Pressure (psi)**	**σ %**
NaCl	0.93	31.9	3.1
	0.85	48	1.72
KCl	0.93	18.5	1.8
	0.85	15.3	0.55
CaCl2	0.93	36.6	3.56
	0.85	96	3.44
KCOOH	0.93	21.7	2.11
	0.85	75.2	2.69

Table 3-6: The membrane efficiency experimental results for Pierre shale during interaction with different salt solutions of different water activities.

Salt Solution (Test Fluid)	**Water Activity**	**Measured Osmotic Pressure (psi)**	**σ %**
NaCl	0.93	12.4	1.21
	0.85	25.6	0.92
KCl	0.93	2.9	0.28
	0.85	5	0.18
CaCl2	0.93	11.9	1.16
	0.85	49.8	1.78
KCOOH	0.93	4	0.39
	0.85	6.2	0.22

Table 3-7: The membrane efficiency experimental results for Arco-China shale during interaction with different salt solutions of 0.93 water activities

Salt Type	**Water Activity**	**Measure Osmotic Pressure, psi**	**σ %**
NaCl	0.93	69.75	3.95
KCl	0.93	34.6	1.96
CaCl2	0.93	74.7	4.23
KCOOH	0.93	48.56	2.75

Table 3-8: Hydrated and dehydrated cations diameter

	Dehydrated Diameter (Angstrom)	Hydrated Diameter (Angstrom)	Average Hydrated Diameter (Angstrom)
Sodium	**1.9**	**5.5-11.2**	**8.35**
Potassium	**2.66**	**4.64-7.6**	**6.12**
Cesium	**3.34**	**4.6-7.2**	**5.9**
Magnesium	**1.3**	**21.6**	**21.6**
Calcium	**1.9**	**19**	**19**

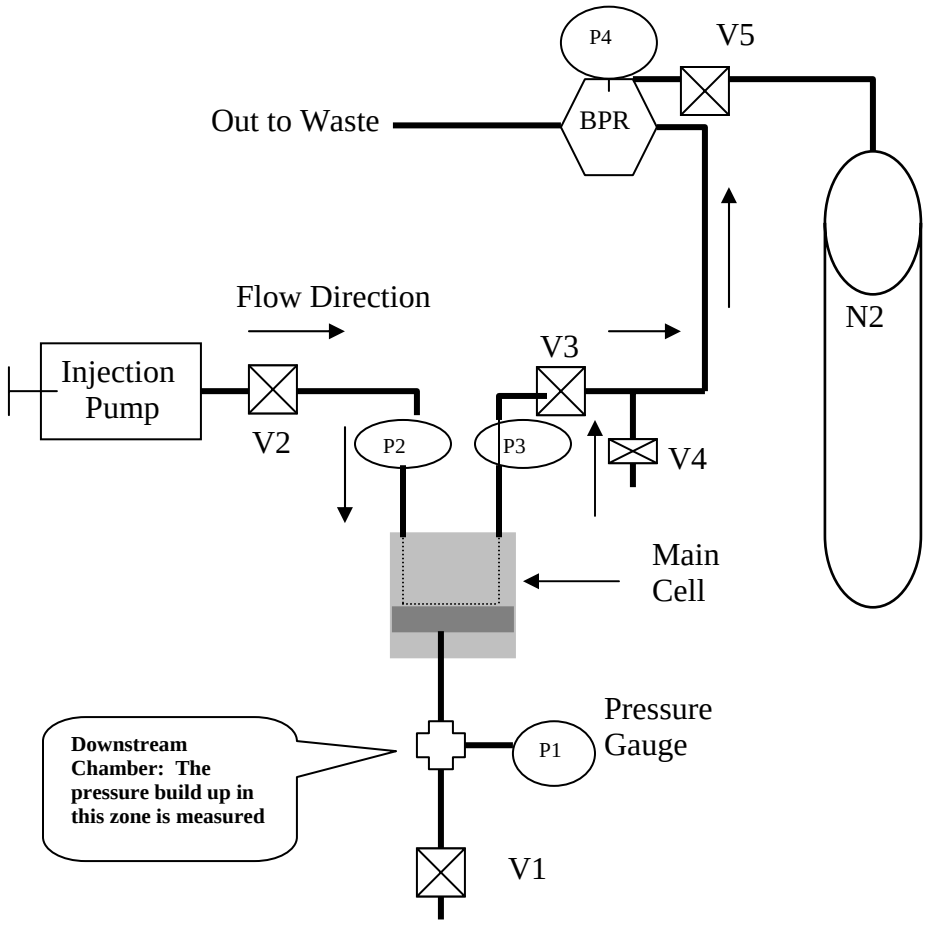

Figure 3-1: The experimental equipment & set-up for membrane efficiency measurements during shales and water-based muds (aqueous solutions) interaction.

Figure 3-2: The pressure transmission cell which was used for testing the membrane efficiency of shales during interaction with water based muds.

.

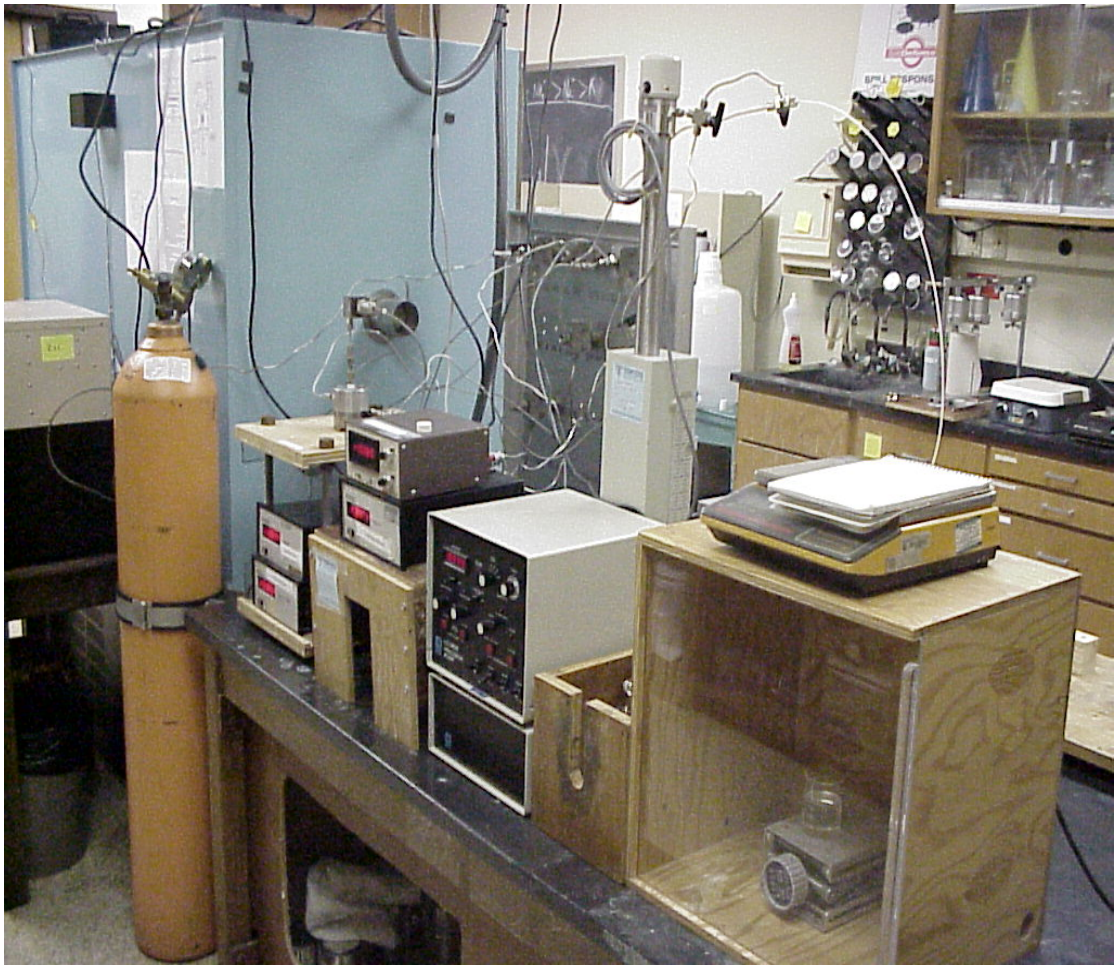

Figure 3-3: The rest of the experimental components that was used for testing the membrane efficiency of shales.

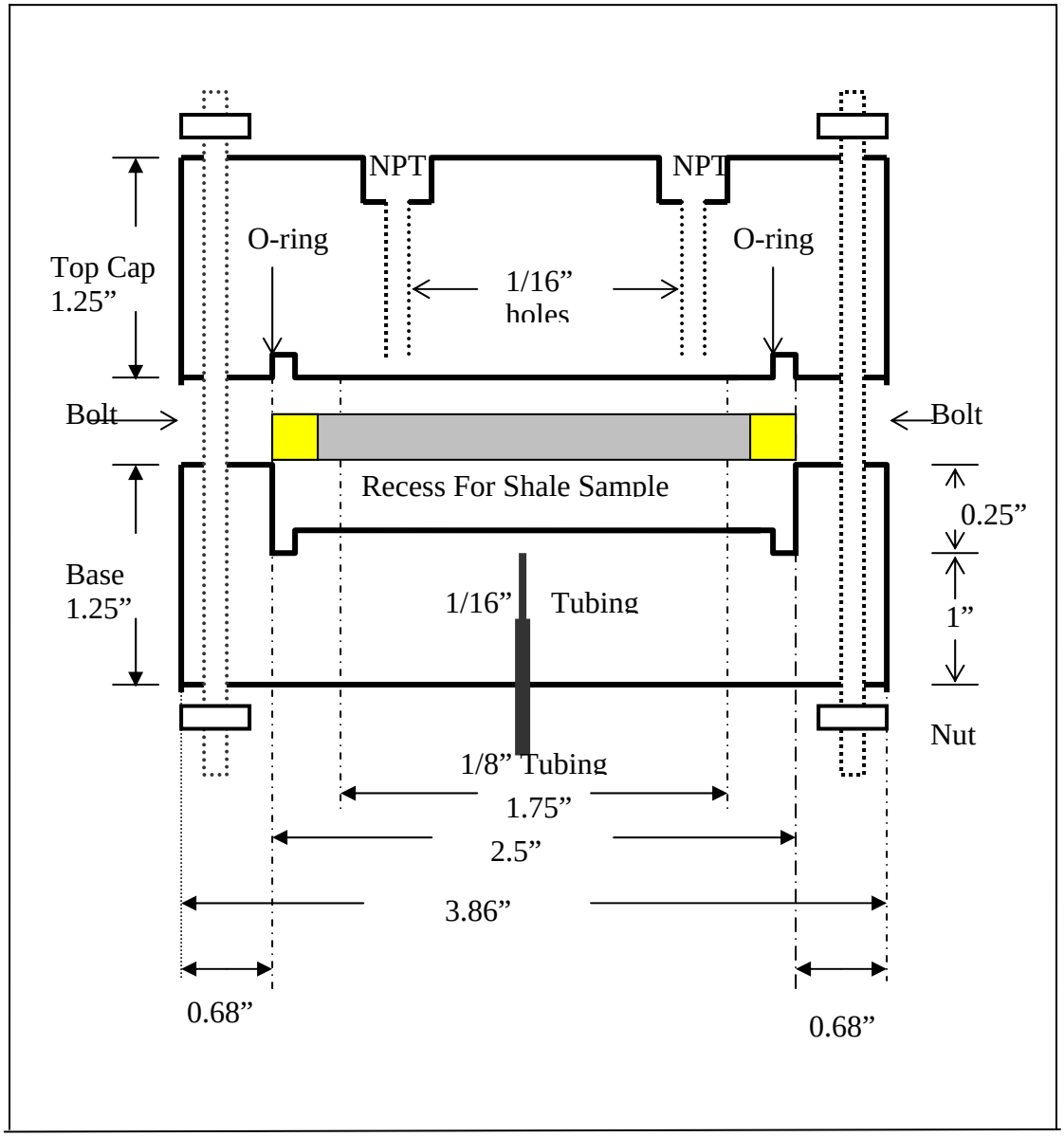

Figure 3-4: The membrane efficiency main cell assembly

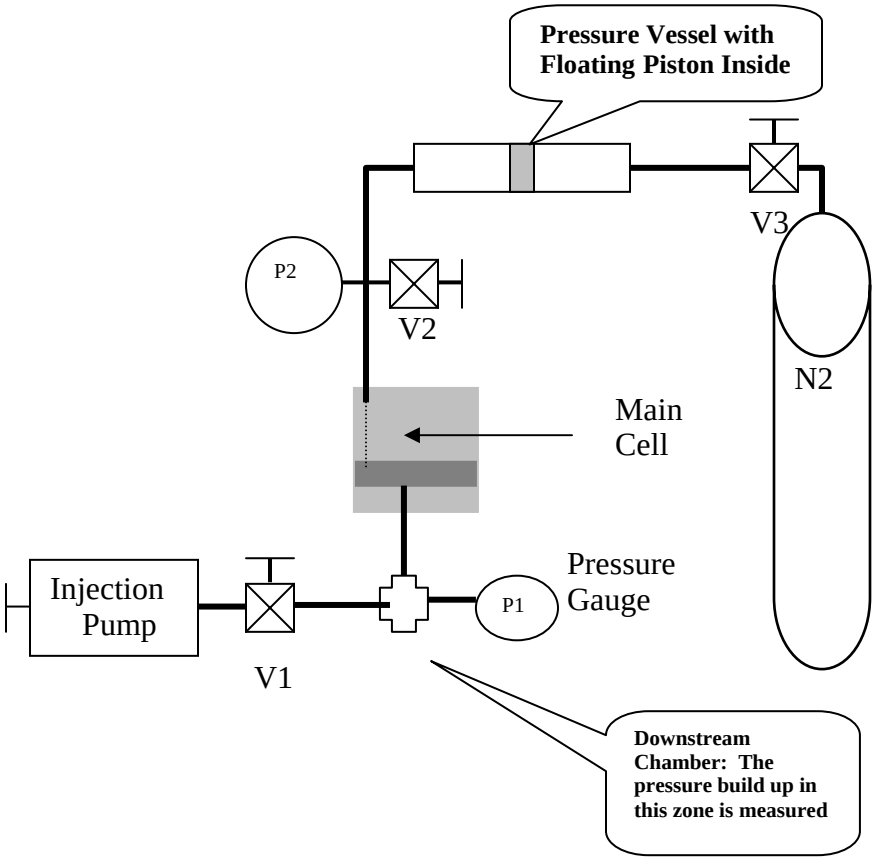

Figure 3-5: The experimental equipment & set-up for membrane efficiency measurements during shales and oil- based muds interaction.

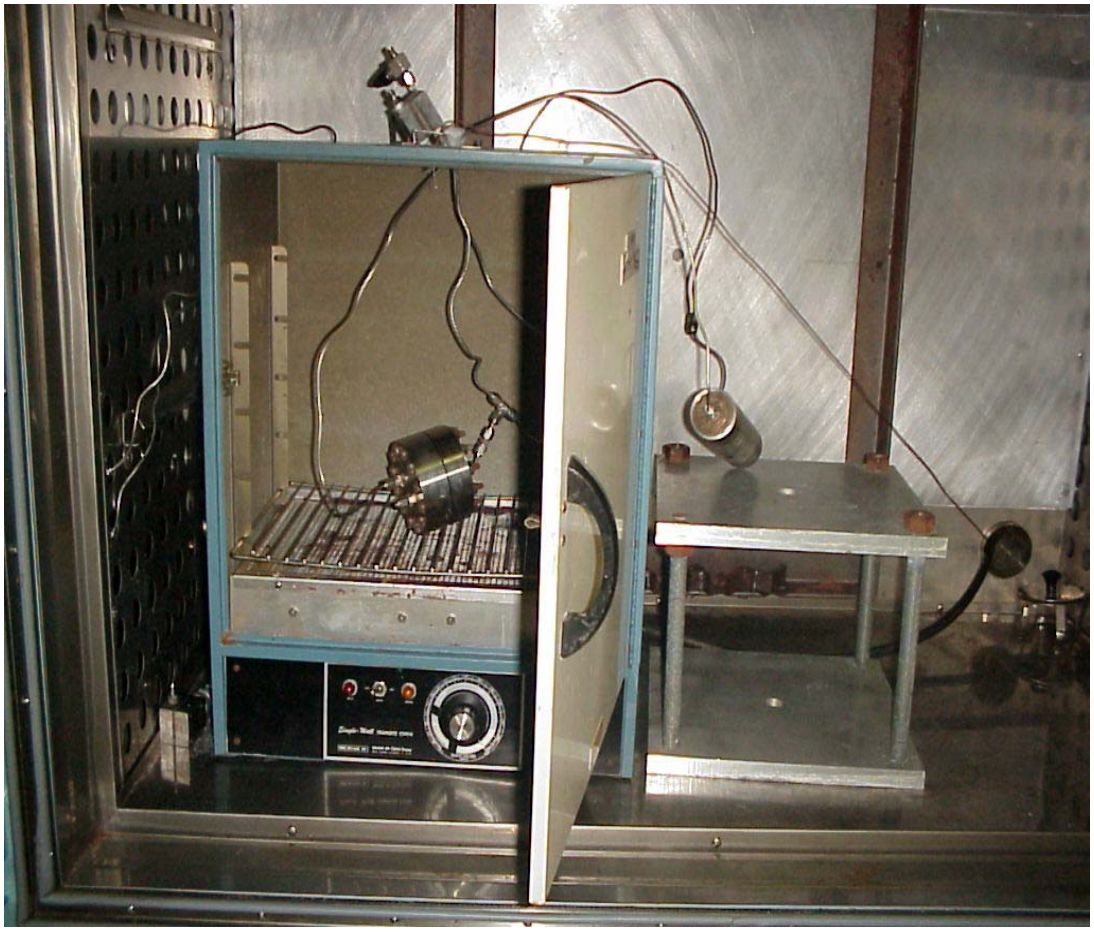

Figure 3-6: The pressure transmission cell which was used for testing the membrane efficiency of shales during interaction with oil-based muds.

Test Details

Upstream Fluid	NaCl (aw = 0.93)
Downstream Fluid	NaCl (aw = 0.98)
Shale Tested	C1 Shale (aw = 0.98)
Flow Rate	0.2 cc/hr
Shale Permeability	2.96 nD
Resultant Shale σ	2.24 %

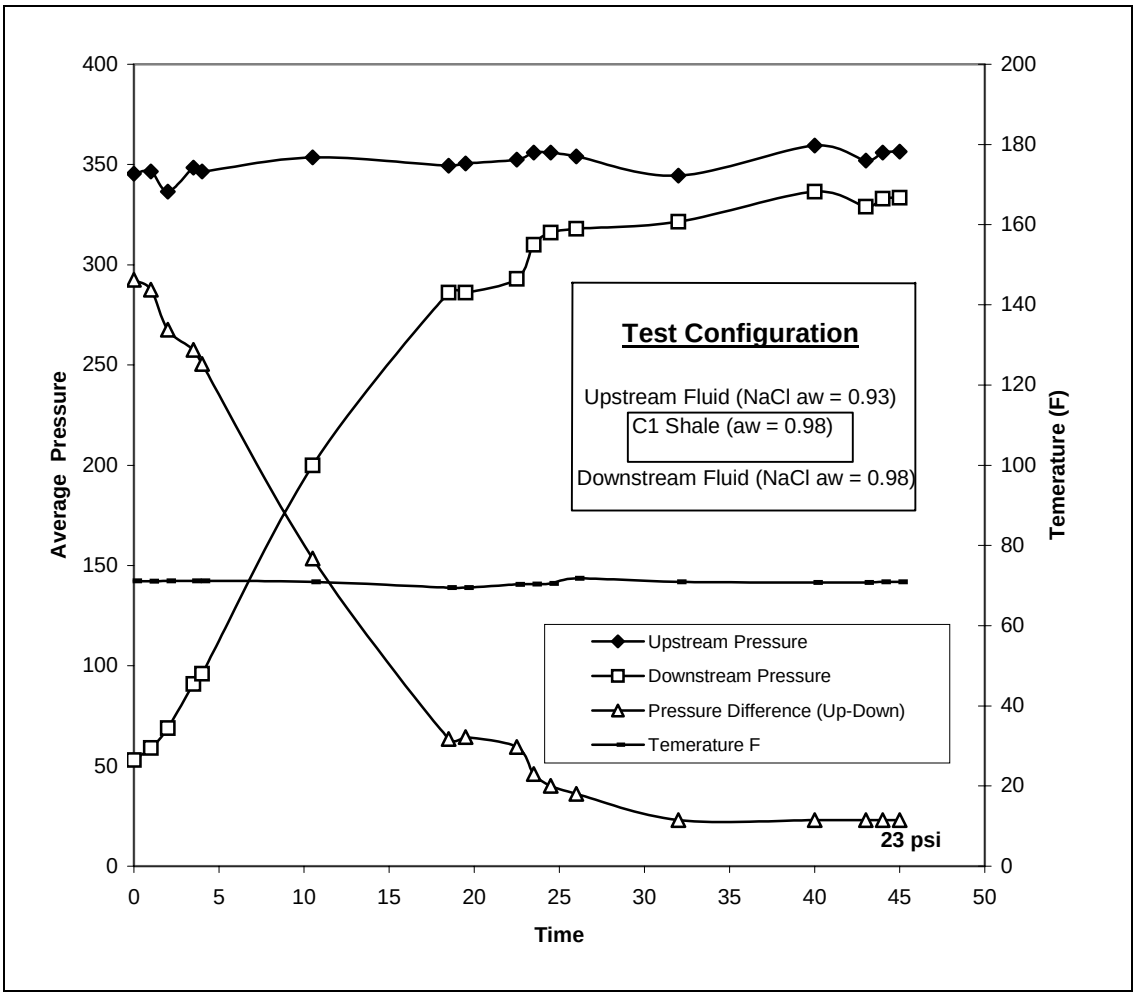

Figure 3-7: Downstream pressure build up when NaCl solution (a_w = 0.93) was flowing across the top of C1-shale sample (a_w = 0.98)

Test Details

Upstream Fluid	NaCl (aw = 0.85)
Downstream Fluid	NaCl (aw = 0.98)
Shale Tested	C1 Shale (aw = 0.98)
Flow Rate	0.2 cc/hr
Shale Permeability	2.96 nD
Resultant Shale σ	1.1 %

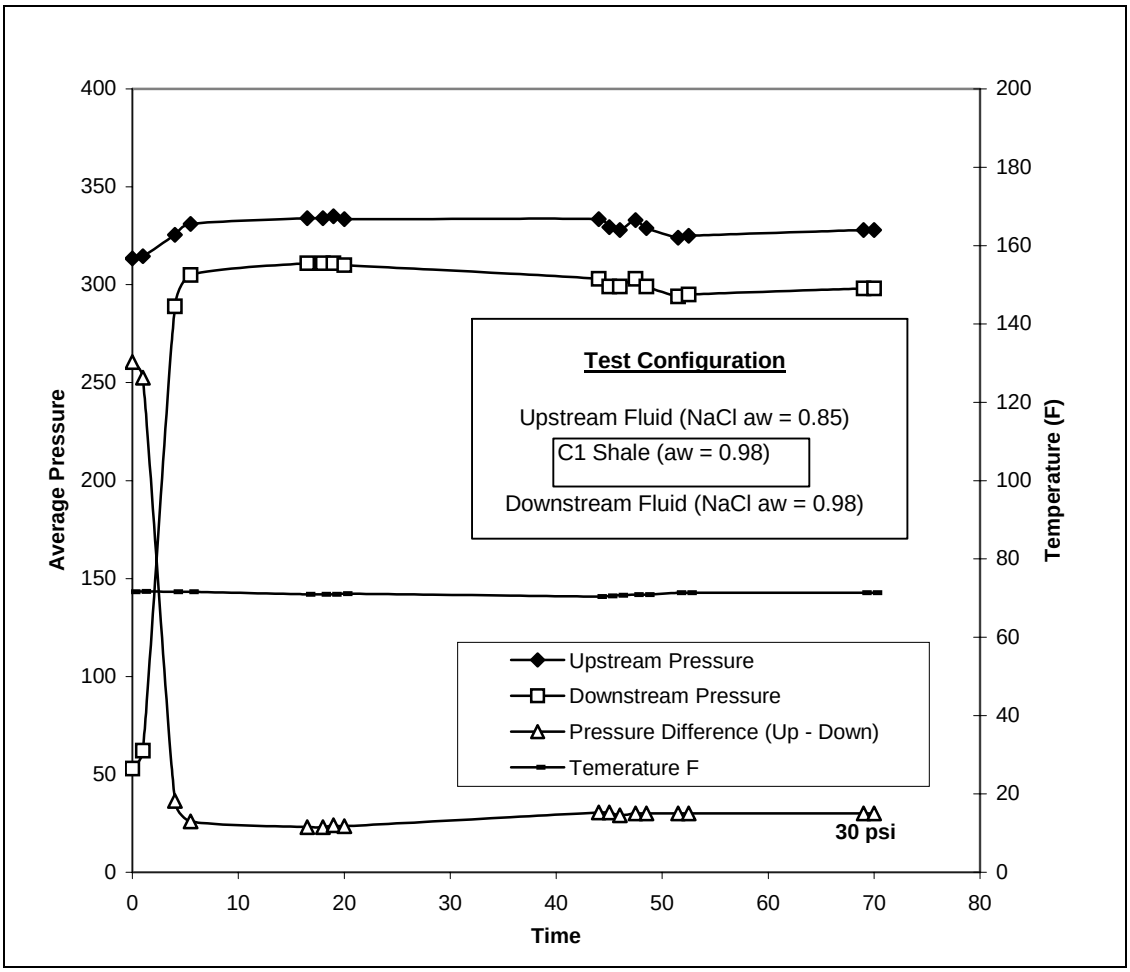

Figure 3-8: Downstream pressure build up when NaCl solution (a_w = 0.85) was flowing across the top of C1-shale sample (a_w = 0.98)

Test Details

Upstream Fluid	KCl (aw = 0.93) then KCl (aw = 0.85)
Downstream Fluid	KCl (aw = 0.98)
Shale Tested	C1 Shale (aw = 0.98)
Flow Rate	0.2 cc/hr
Shale Permeability	2.96 nD
Resultant Shale σ	σ 1 = 0.58 %, σ 2 = 0.50 %

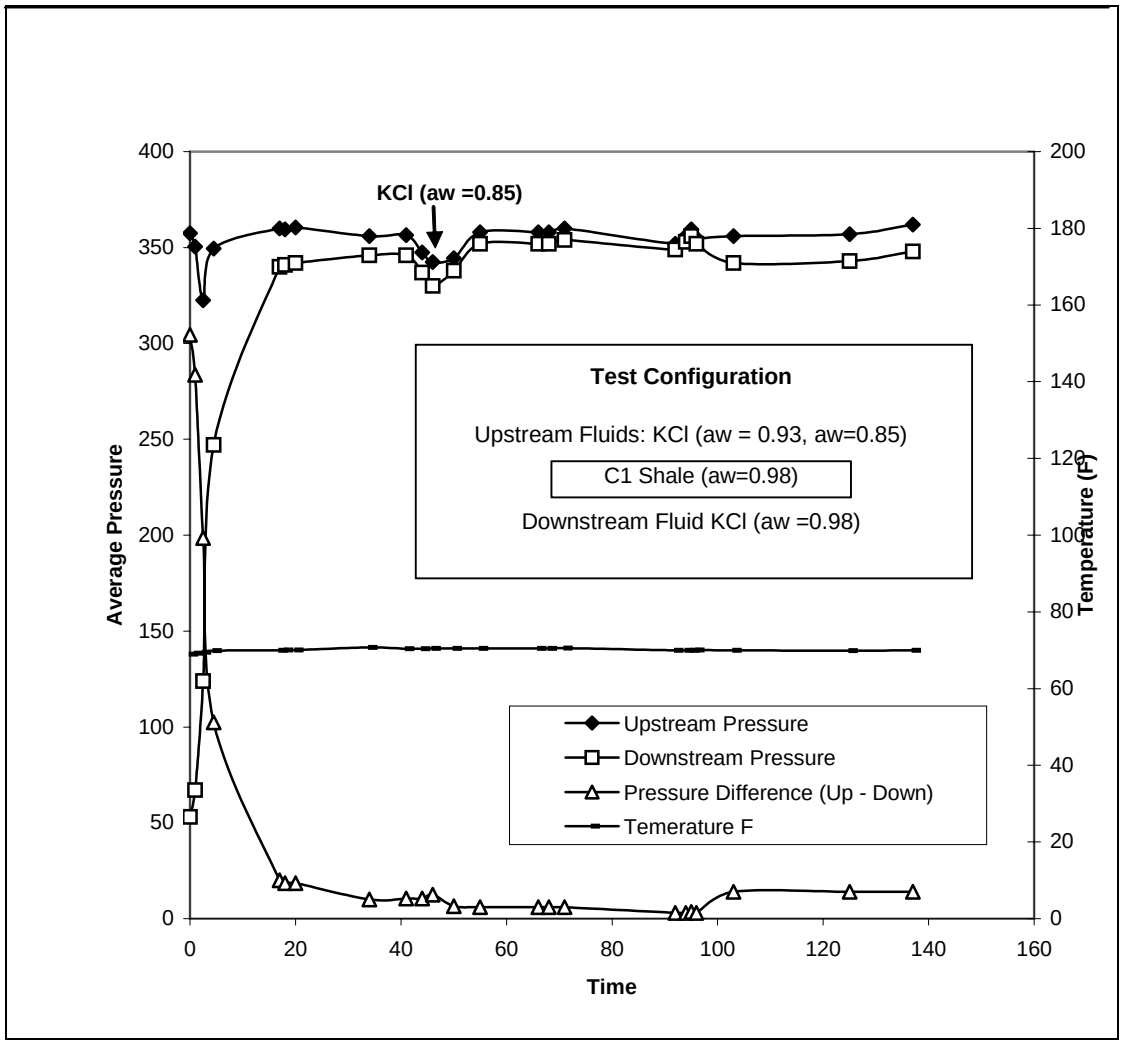

Figure 3-9: Downstream pressure build up when KCl solutions of different water activities were flowing across the top of C1-shale sample (a_w = 0.98)

Test Details

Upstream Fluid	CaCl2 (aw = 0.93) then CaCl2 (aw =0.85)
Downstream Fluid	CaCl2 (aw = 0.98)
Shale Tested	C1 Shale (aw = 0.98)
Flow Rate	0.2 cc/hr
Shale Permeability	2.96 nD
Resultant Shale σ	σ 1 = 0.97 %, σ 2 = 1 %

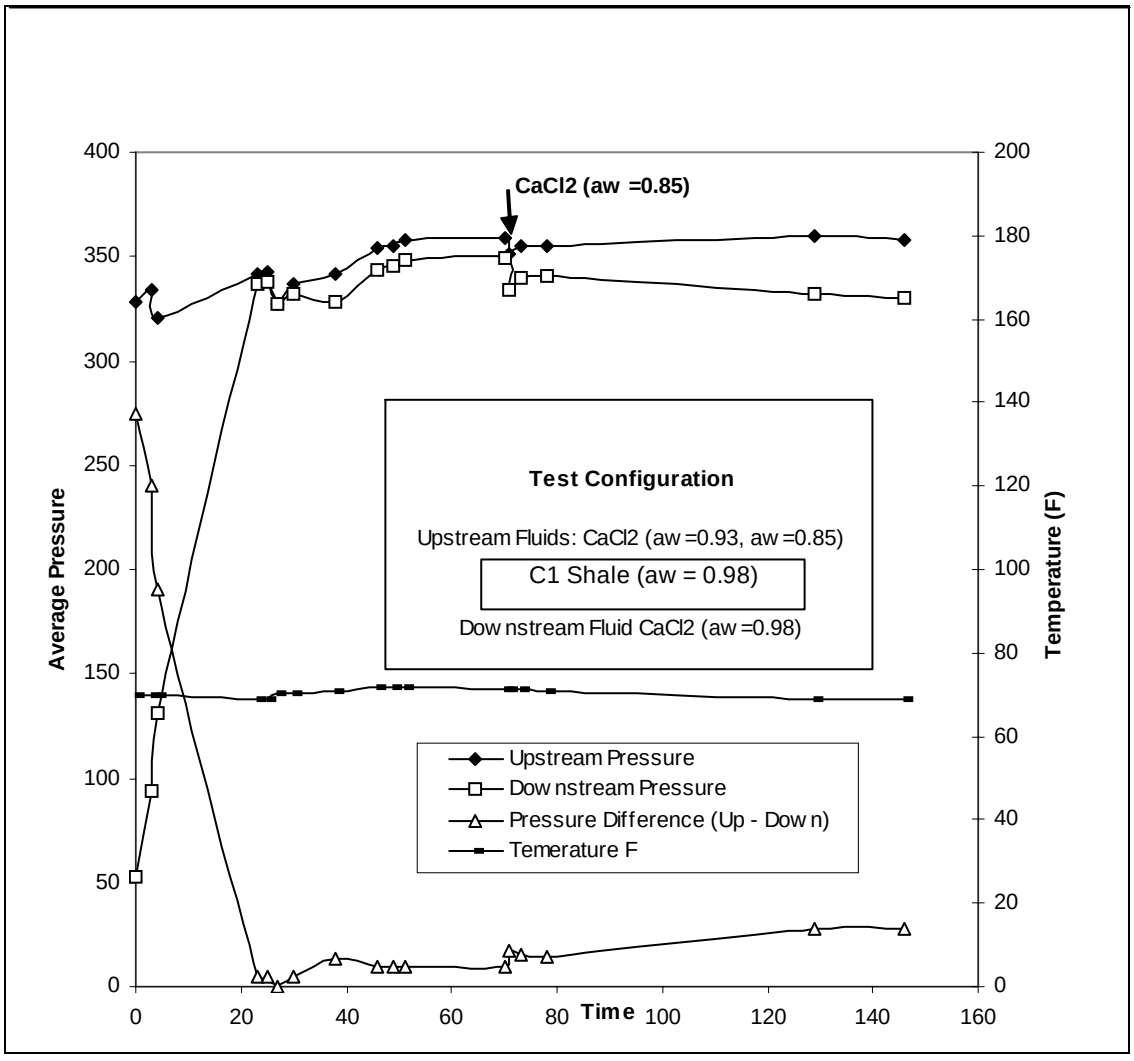

Figure 3-10: Downstream pressure build up when $CaCl_2$ solutions were flowing across the top of C1-shale sample (a_w = 0.98)

Test Details

Upstream Fluid	KCOOH (aw = 0.93) then KCOOH (aw =0.85)
Downstream Fluid	KCOOH (aw = 0.98)
Shale Tested	C1 Shale (aw = 0.98)
Flow Rate	0.2 cc/hr
Shale Permeability	2.96 nD
Resultant Shale σ	σ 1 = 2.38 %, σ 2 = 0.9 %

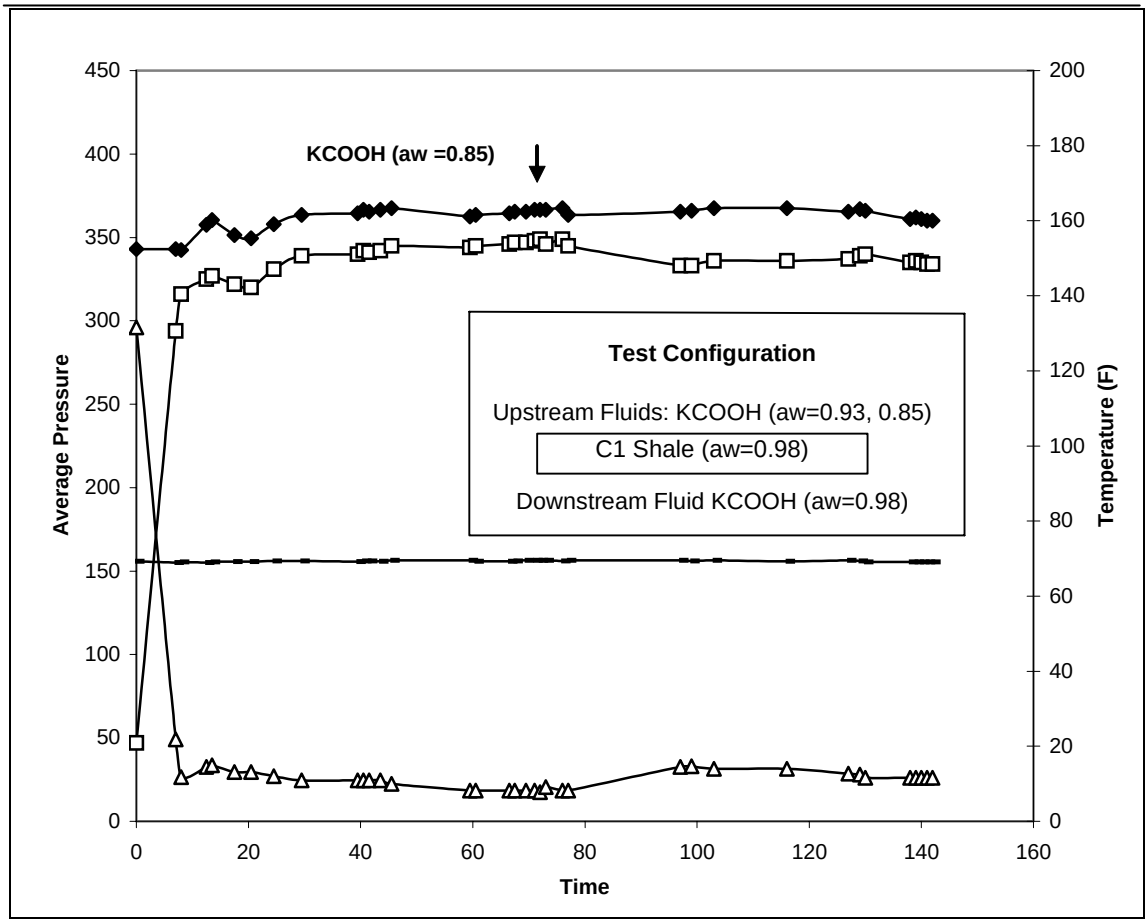

Figure 3-11: Downstream pressure build up when KCOOH solutions were flowing across the top of C1-shale sample (a_w = 0.98)

Test Details

Upstream Fluid	KCOOH (aw = 0.4)
Downstream Fluid	KCOOH (aw = 0.98)
Shale Tested	C1 Shale (aw = 0.98)
Flow Rate	0.2 cc/hr
Shale Permeability	2.96 nD
Resultant Shale σ	σ = 0.34 %

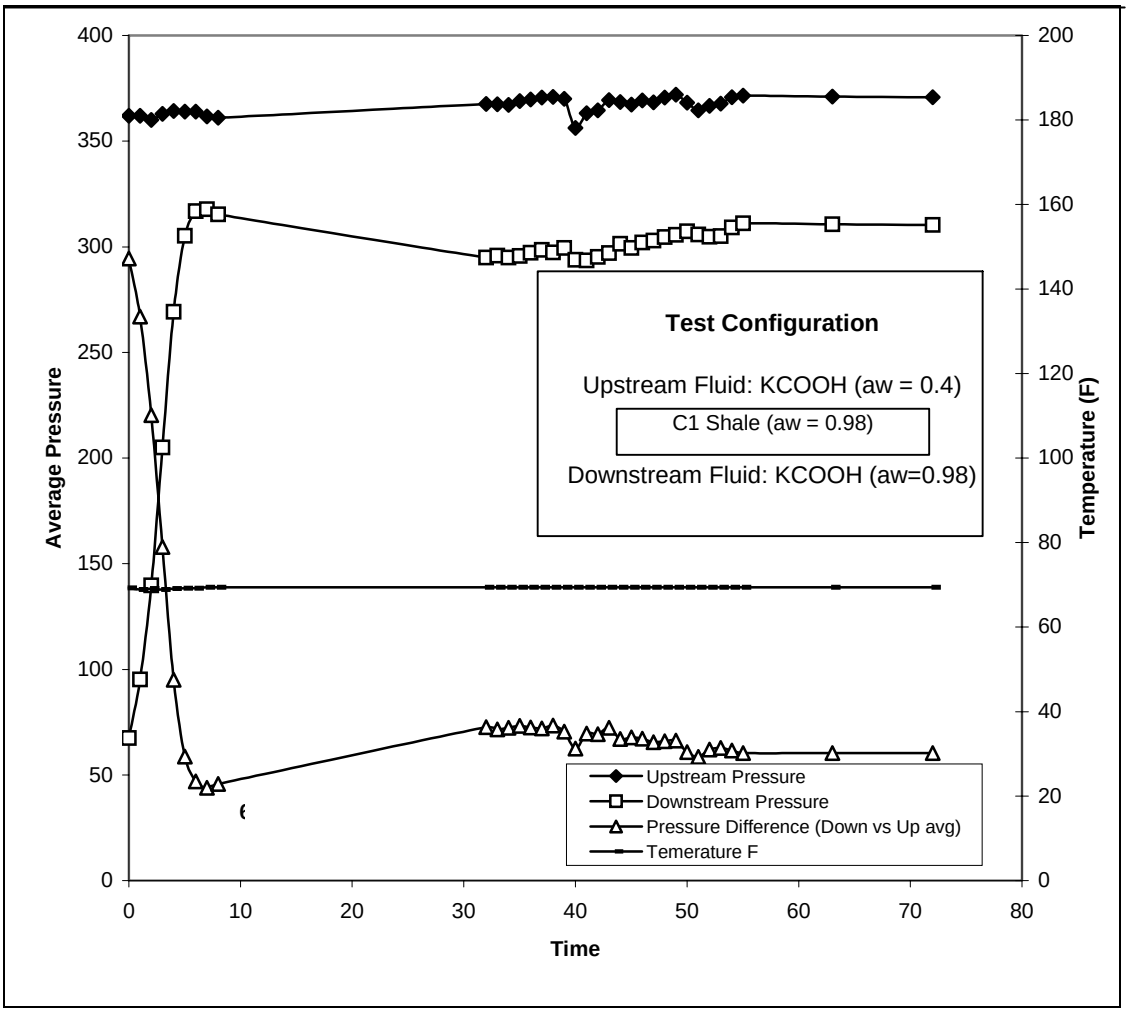

Figure 3-12: Downstream pressure build up when KCOOH (a_w =0.4) solution was flowing across the top of C1-shale sample (a_w = 0.98)

Test Details

Upstream Fluid	NaCl (aw = 0.93) then NaCl (aw=0.85)
Downstream Fluid	NaCl (aw = 0.98)
Shale Tested	C2 Shale (aw = 0.98)
Flow Rate	0.2 cc/hr
Shale Permeability	0.83 nD
Resultant Shale σ	σ 1 = 3.1 %, σ 2 = 1.72 %

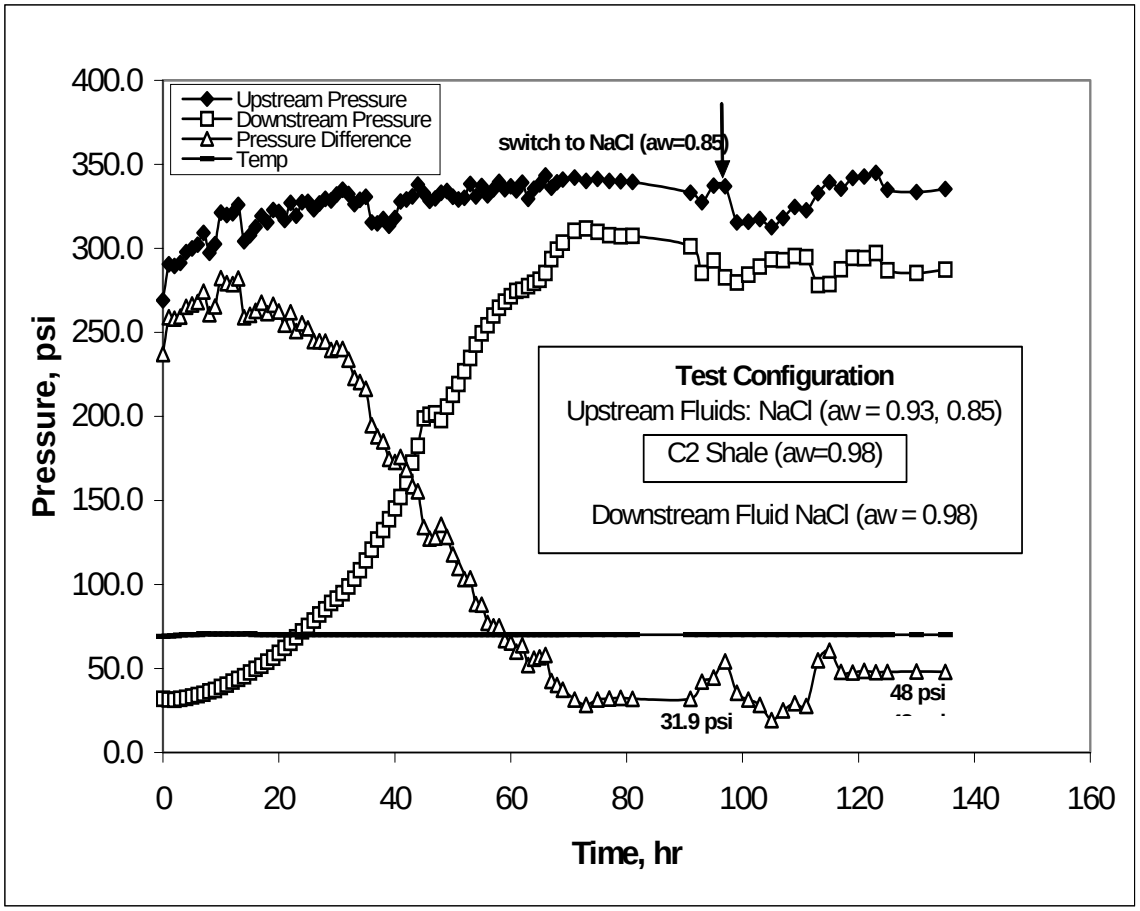

Figure 3-13: Downstream pressure build up when NaCl solutions were flowing across the top of C2-shale sample (a_w = 0.98)

Test Details

Upstream Fluid	KCl (aw = 0.93) then KCl (aw=0.85)
Downstream Fluid	KCl (aw = 0.98)
Shale Tested	C2 Shale (aw = 0.98)
Flow Rate	0.2 cc/hr
Shale Permeability	0.83 nD
Resultant Shale σ	σ 1 = 1.8 %, σ 2 = 0.55 %

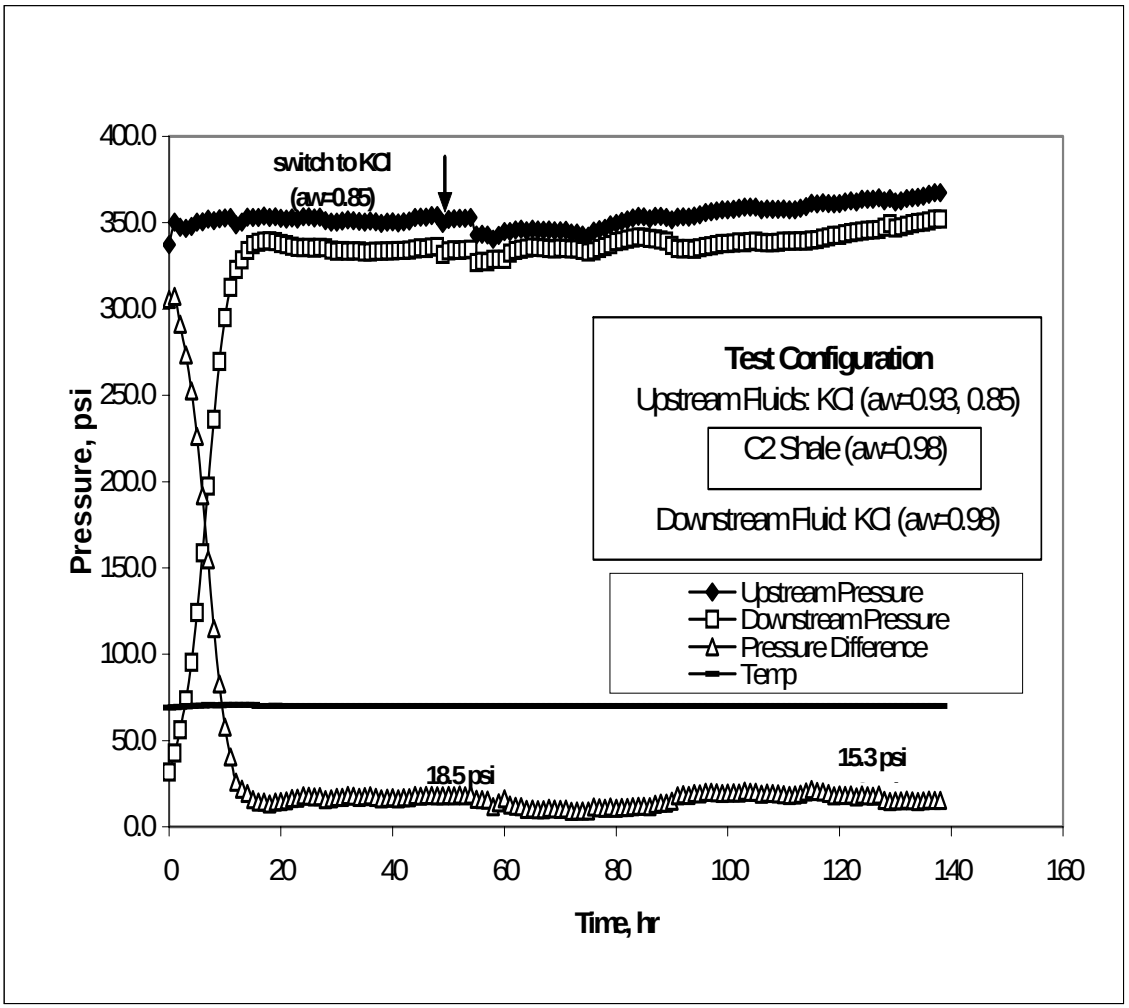

Figure 3-14: Downstream pressure build up when KCl solutions were flowing across the top of C2-shale sample (a_w = 0.98)

Test Details

Upstream Fluid	CaCl2 (aw = 0.93) then CaCl2 (aw=0.85)
Downstream Fluid	CaCl2 (aw = 0.98)
Shale Tested	C2 Shale (aw = 0.98)
Flow Rate	0.2 cc/hr
Shale Permeability	0.83 nD
Resultant Shale σ	σ 1 = 3.56 %, σ 2 = 3.44 %

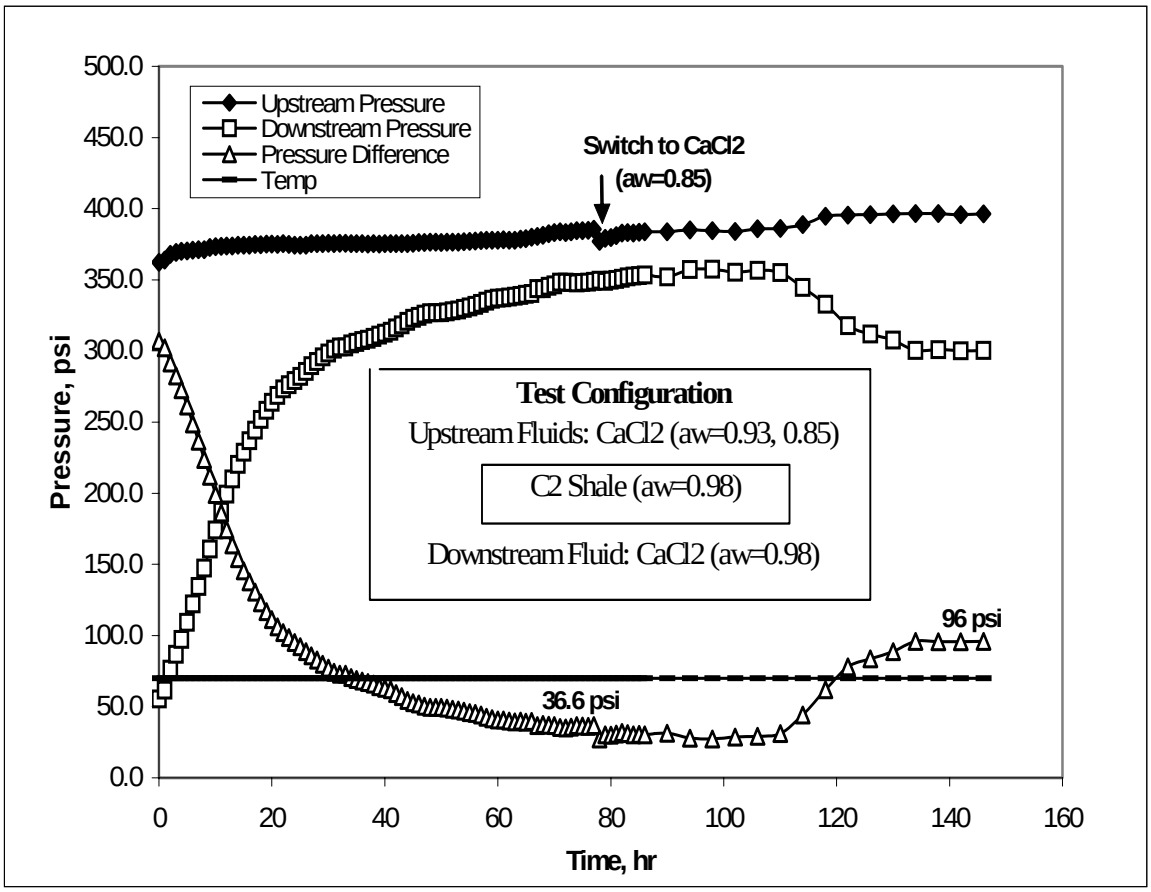

Figure 3-15: Downstream pressure build up when CaCl2 solutions were flowing across the top of C2-shale sample (a_w = 0.98)

Test Details

Upstream Fluid	KCOOH (aw = 0.93) then KCOOH (aw=0.85)
Downstream Fluid	KCOOH (aw = 0.98)
Shale Tested	C2 Shale (aw = 0.98)
Flow Rate	0.2 cc/hr
Shale Permeability	0.83 nD
Resultant Shale σ	σ 1 = 2.11 %, σ 2 = 2.69 %

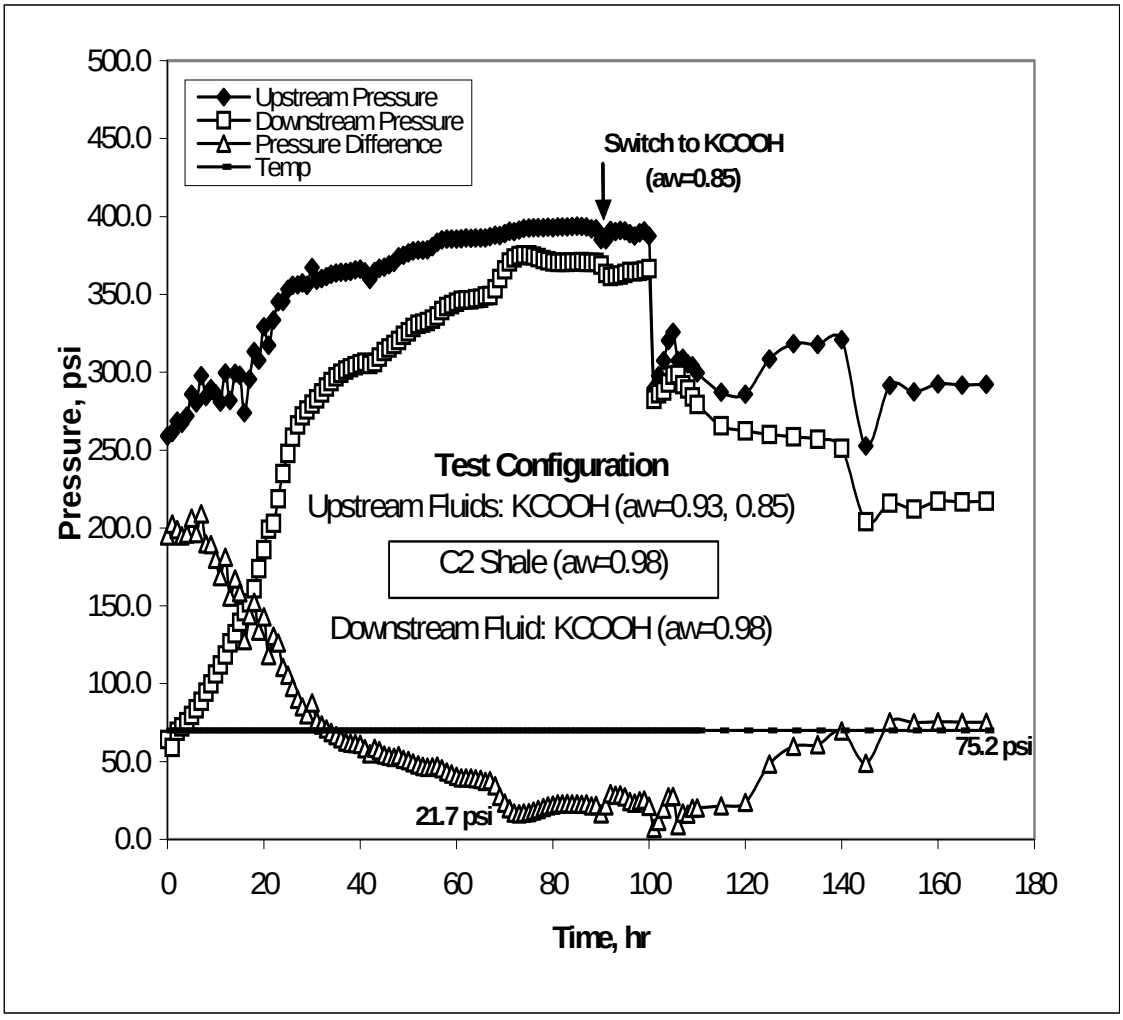

Figure 3-16: Downstream pressure build up when KCOOH solutions were flowing across the top of C2-shale sample (a_w = 0.98)

Test Details

Upstream Fluid	NaCl (aw = 0.93) then NaCl (aw=0.85)
Downstream Fluid	NaCl (aw = 0.98)
Shale Tested	Pierre Shale (aw = 0.98)
Flow Rate	0.2 cc/hr
Shale Permeability	6.48 nD
Resultant Shale σ	σ 1 = 1.21 %, σ 2 = 0.92 %

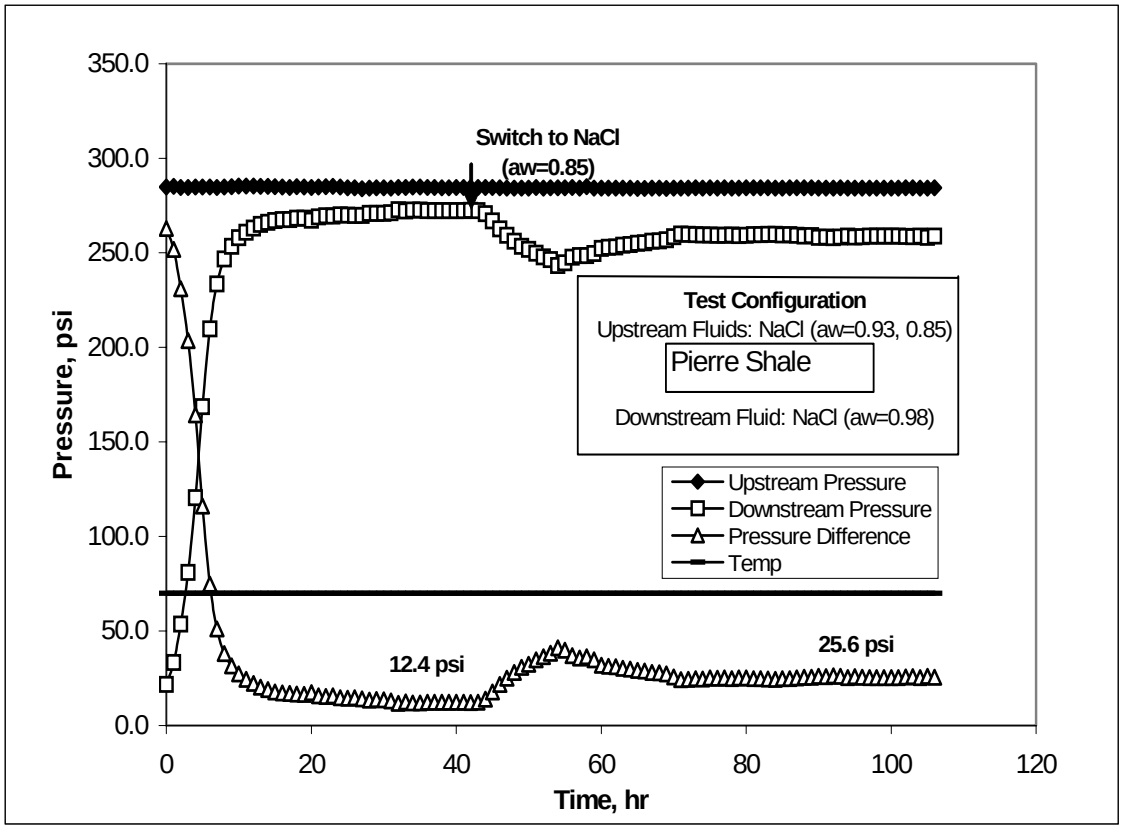

Figure 3-17: Downstream pressure build up when NaCl solutions were flowing across the top of Pierre shale sample (a_w = 0.98)

Test Details

Upstream Fluid	KCl (aw = 0.93) then KCl (aw=0.85)
Downstream Fluid	KCl (aw = 0.98)
Shale Tested	Pierre Shale (aw = 0.98)
Flow Rate	0.2 cc/hr
Shale Permeability	6.48 nD
Resultant Shale σ	σ 1 = 0.28 %, σ 2 = 0.18 %

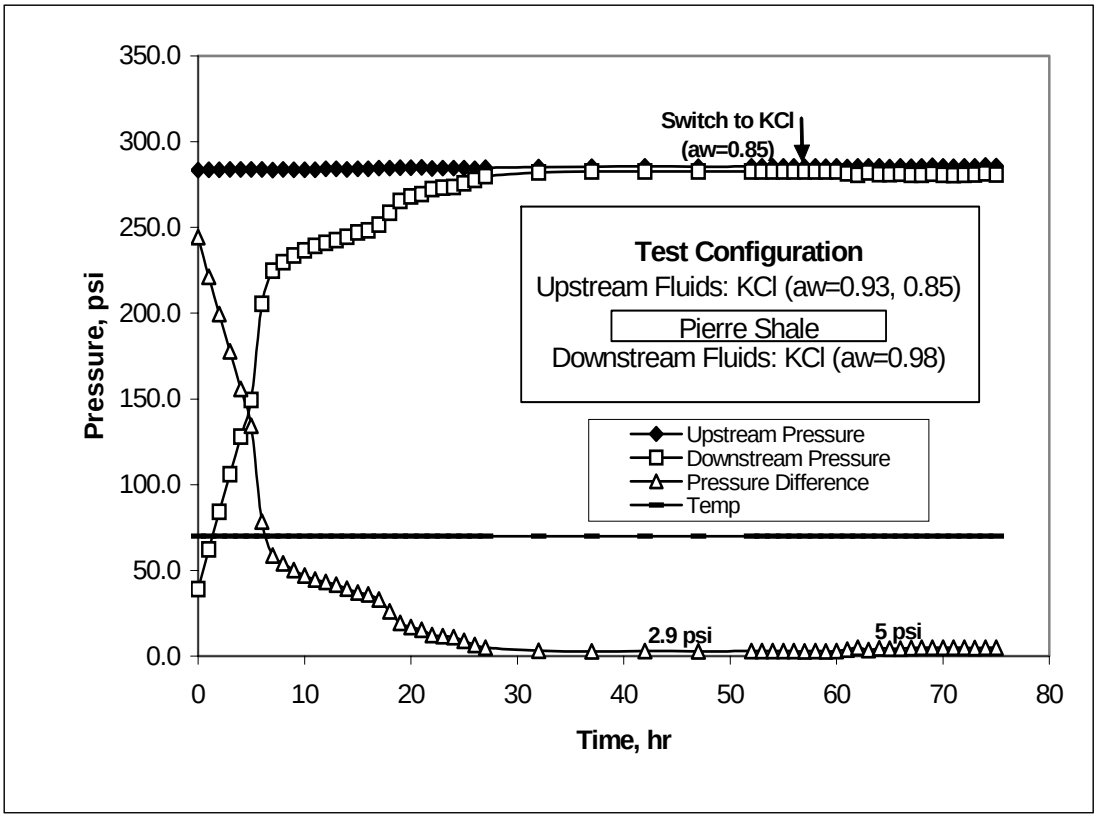

Figure 3-18: Downstream pressure build up when KCl solutions were flowing across the top of Pierre shale sample (a_w = 0.98)

Test Details

Upstream Fluid	CaCl2 (aw = 0.93) then CaCl2 (aw=0.85)
Downstream Fluid	CaCl2 (aw = 0.98)
Shale Tested	Pierre Shale (aw = 0.98)
Flow Rate	0.2 cc/hr
Shale Permeability	6.48 nD
Resultant Shale σ	σ 1 = 1.16 %, σ 2 = 1.78 %

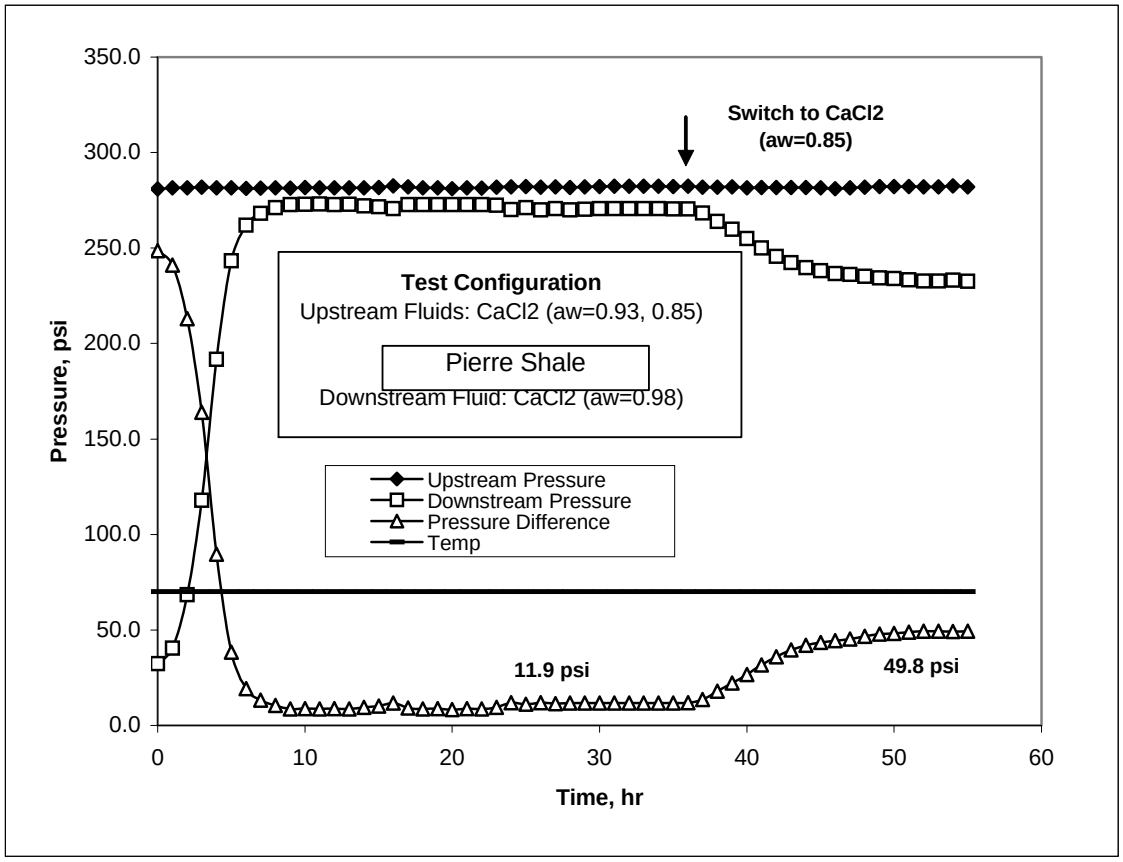

Figure 3-19: Downstream pressure build up when CaCl2 solutions were flowing across the top of Pierre shale sample (a_w = 0.98)

Test Details

Upstream Fluid	KCOOH (aw = 0.93) then KCOOH (aw=0.85)
Downstream Fluid	KCOOH (aw = 0.98)
Shale Tested	Pierre Shale (aw = 0.98)
Flow Rate	0.2 cc/hr
Shale Permeability	6.48 nD
Resultant Shale σ	σ 1 = 0.39 %, σ 2 = 0.22 %

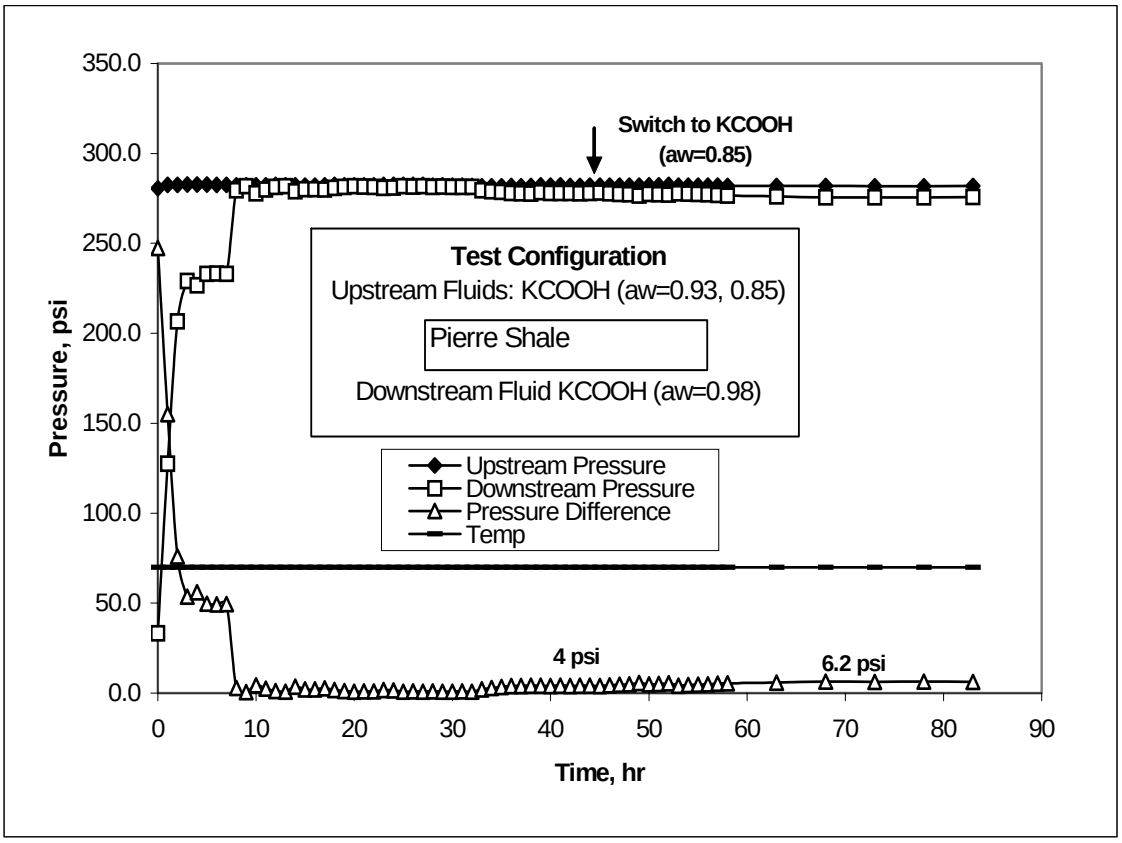

Figure 3-20: Downstream pressure build up when KCOOH solutions were flowing across the top of Pierre shale sample (a_w = 0.98)

Test Details

Upstream Fluid	NaCl (aw = 0.93)
Downstream Fluid	NaCl (aw = 0.85)
Shale Tested	Arco-China Shale (aw = 0.85)
Flow Rate	0.2 cc/hr
Shale Permeability	0.45 nD
Resultant Shale σ	σ = 3.95

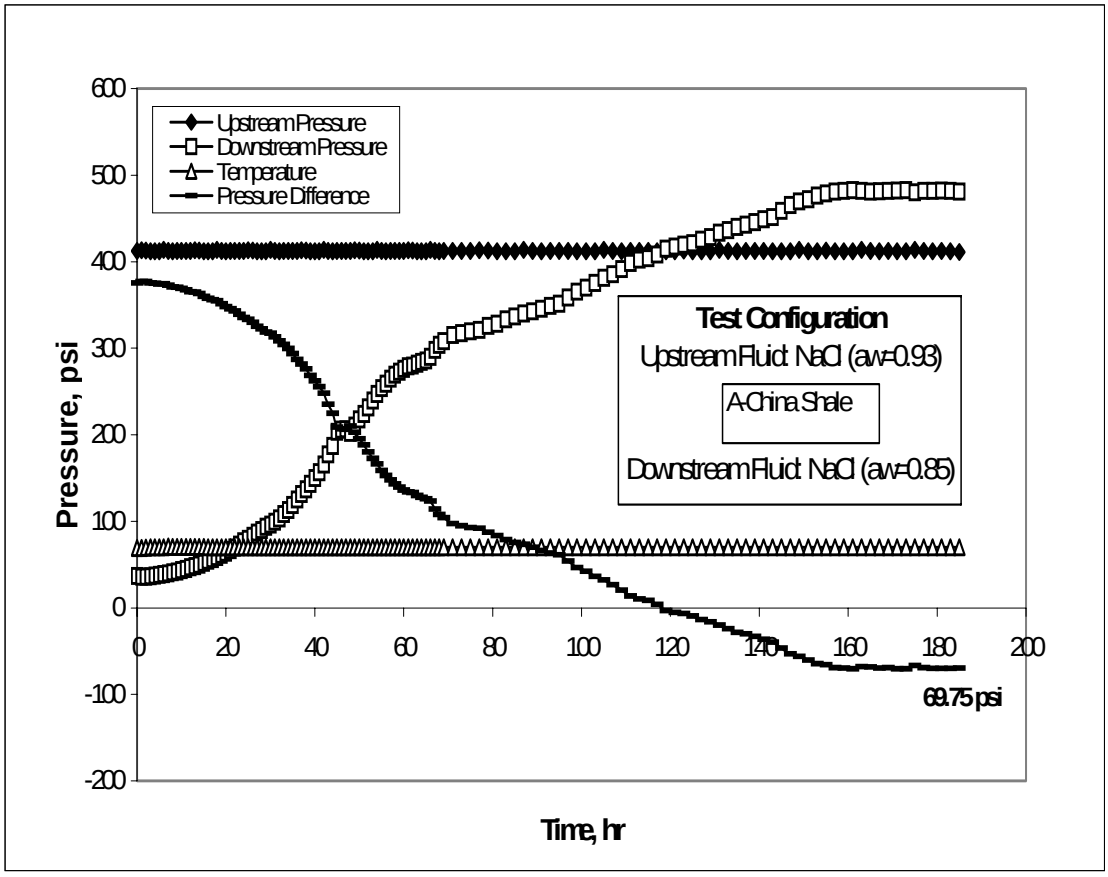

Figure 3-21: Downstream pressure build up when NaCl (a_w = 0.93) solution was flowing across the top of Arco-China shale sample (a_w = 0.85)

Test Details

Upstream Fluid	KCl (aw = 0.93)
Downstream Fluid	KCl (aw = 0.85)
Shale Tested	Arco-China Shale (aw = 0.85)
Flow Rate	0.2 cc/hr
Shale Permeability	0.45 nD
Resultant Shale σ	σ = 1.96

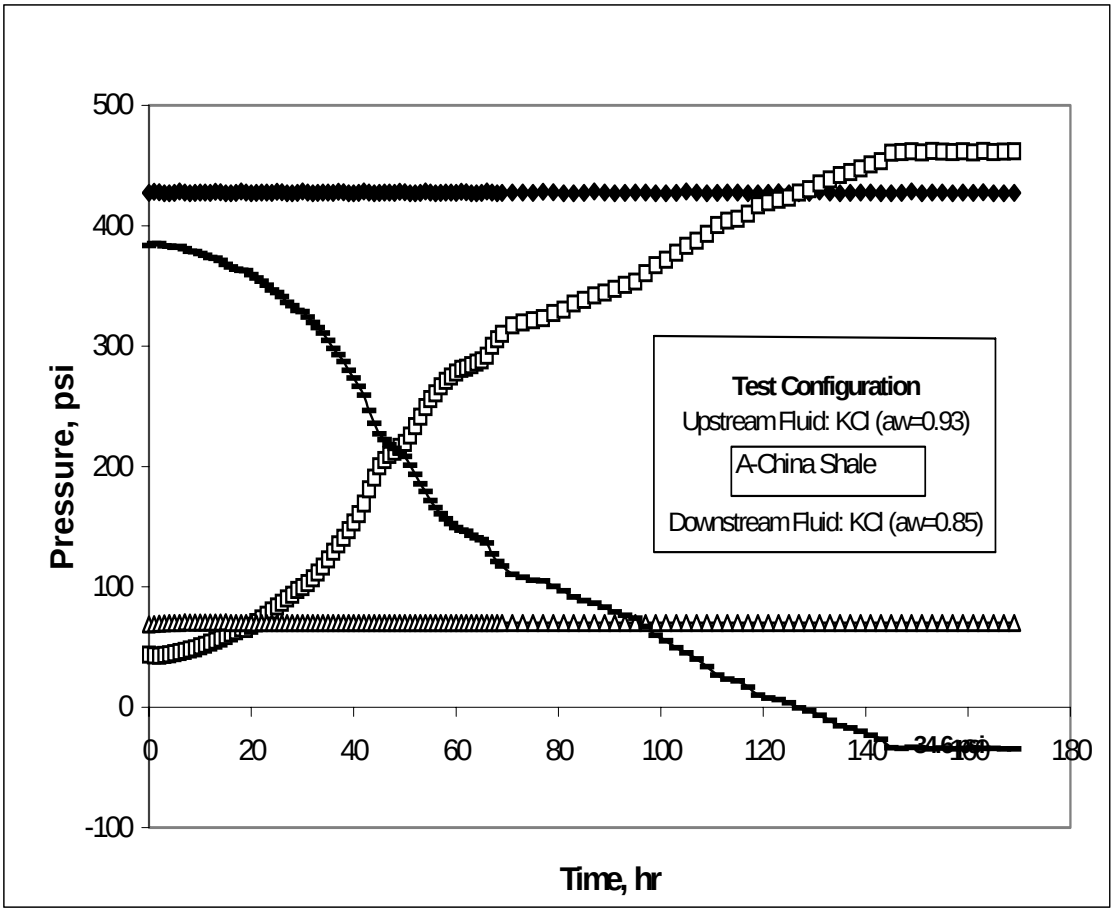

Figure 3-22: Downstream pressure build up when KCl (a_w = 0.93) solution was flowing across the top of Arco-China shale sample (a_w = 0.85)

Test Details

Upstream Fluid	CaCl2 (aw = 0.93)
Downstream Fluid	CaCl2 (aw = 0.85)
Shale Tested	Arco-China Shale (aw = 0.85)
Flow Rate	0.2 cc/hr
Shale Permeability	0.45 nD
Resultant Shale σ	σ = 4.23

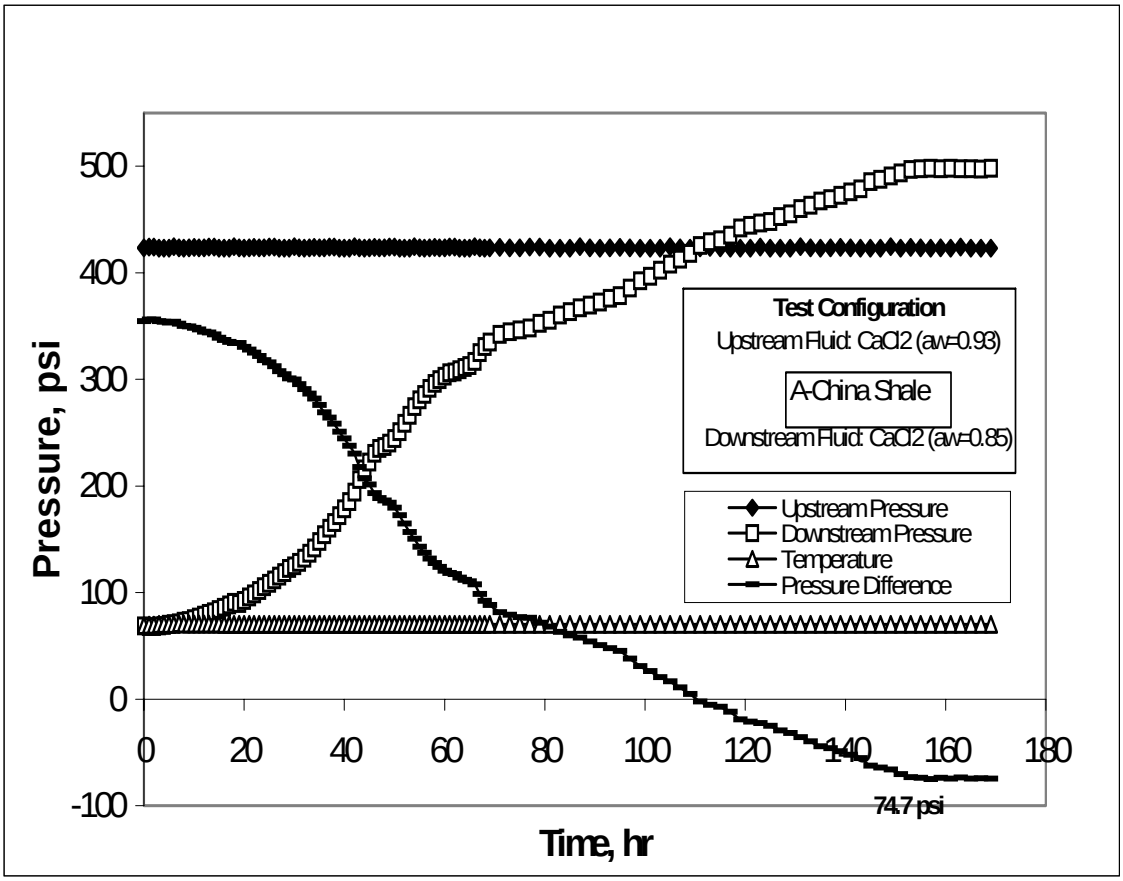

Figure 3-23: Downstream pressure build up when $CaCl_2$ (a_w = 0.93) solution was flowing across the top of Arco-China shale sample (a_w = 0.85)

Test Details

Upstream Fluid	KCOOH (aw = 0.93)
Downstream Fluid	KCOOH (aw = 0.85)
Shale Tested	Arco-China Shale (aw = 0.85)
Flow Rate	0.2 cc/hr
Shale Permeability	0.45 nD
Resultant Shale σ	σ = 2.75

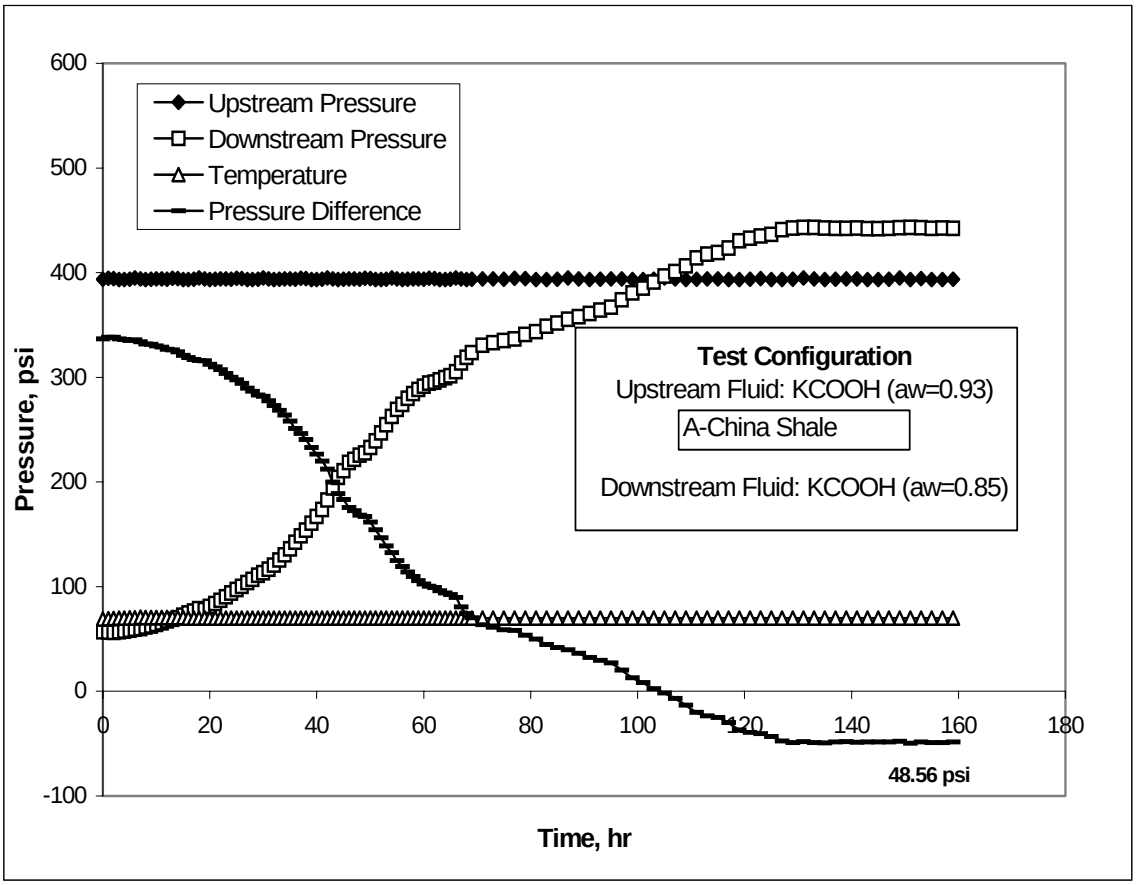

Figure 3-24: Downstream pressure build up when KCOOH (a_w = 0.93) solution was flowing across the top of Arco-China shale sample (a_w = 0.85)

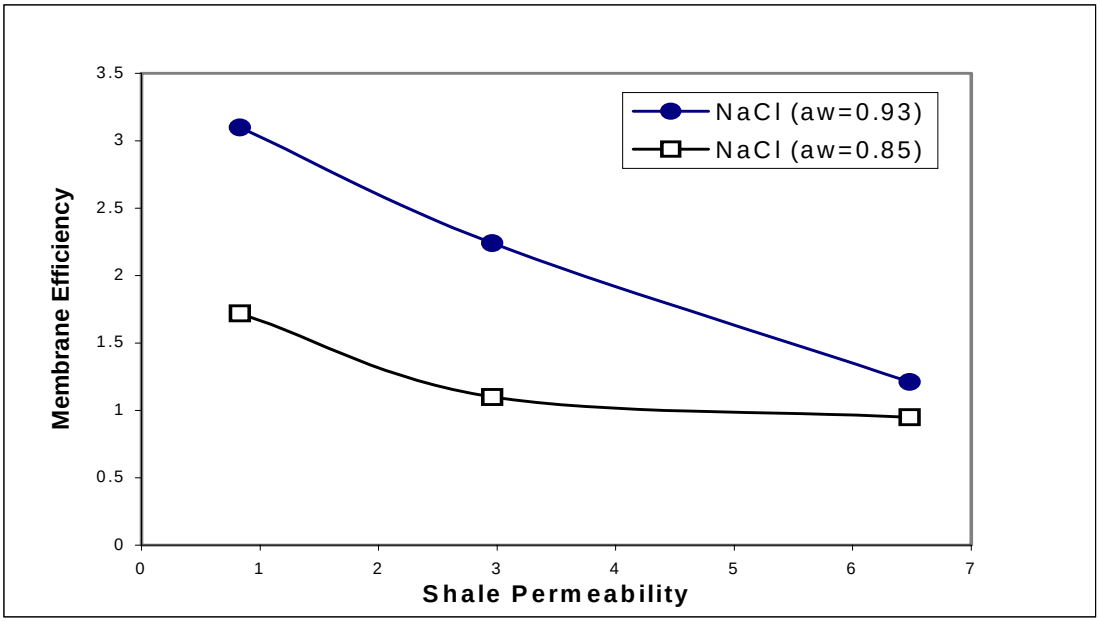

Figure 3-25: Membrane efficiency dependence on shale permeability during shales and NaCl solutions interaction.

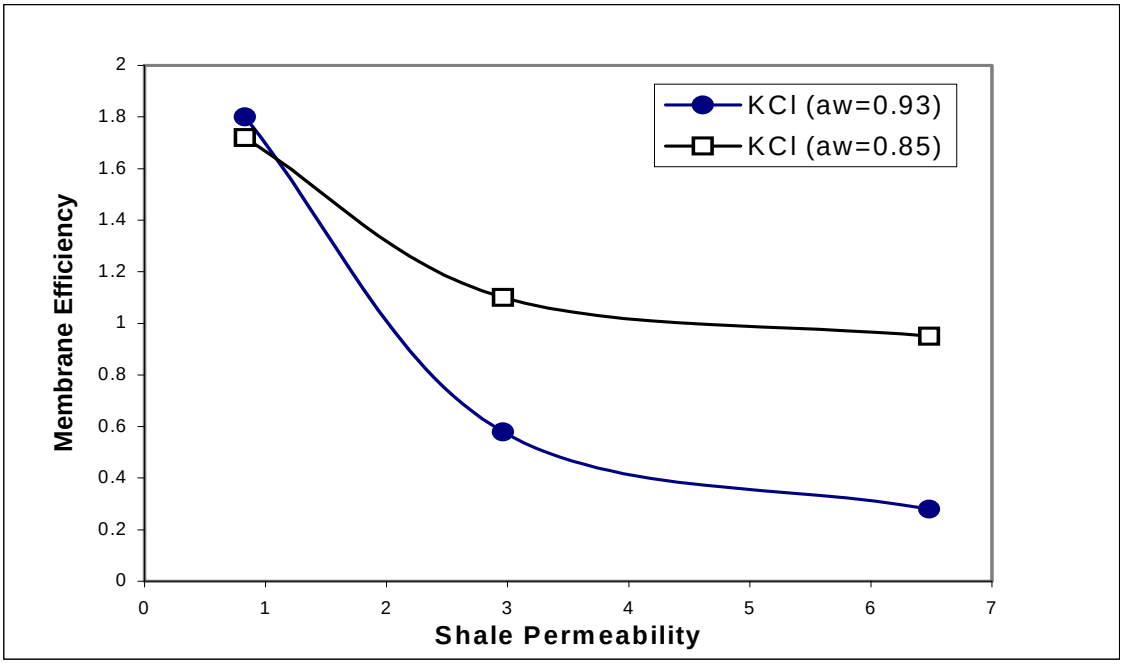

Figure 3-26: Membrane efficiency dependence on shale permeability during shales and KCl solutions interaction.

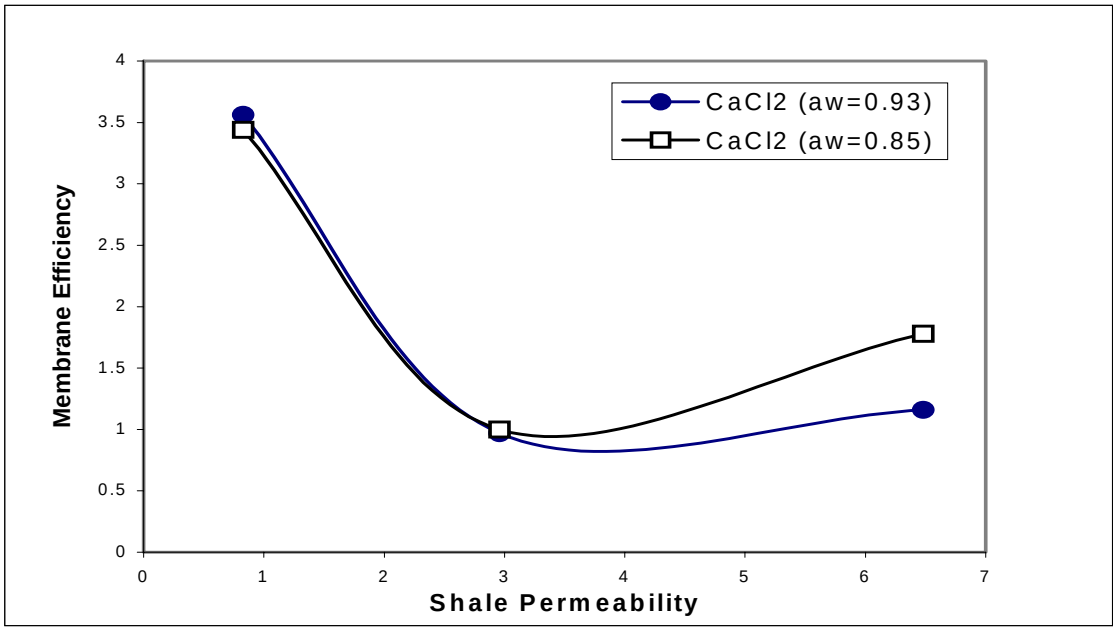

Figure 3-27: Membrane efficiency dependence on shale permeability during shales and CaCl2 solutions interaction.

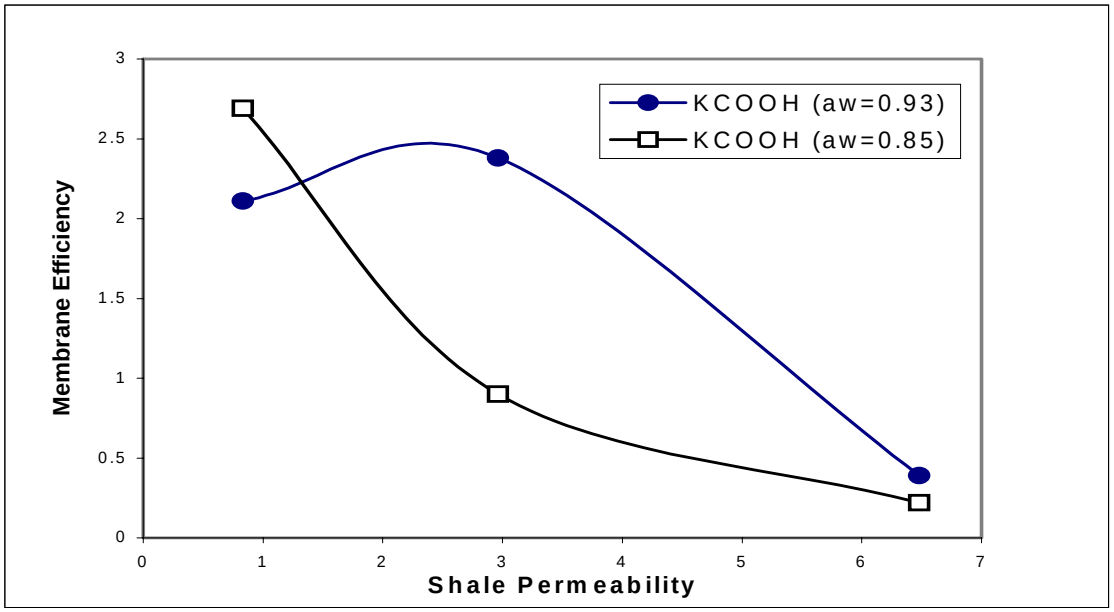

Figure 3-28: Membrane efficiency dependence on shale permeability during shales and KCOOH solutions interaction.

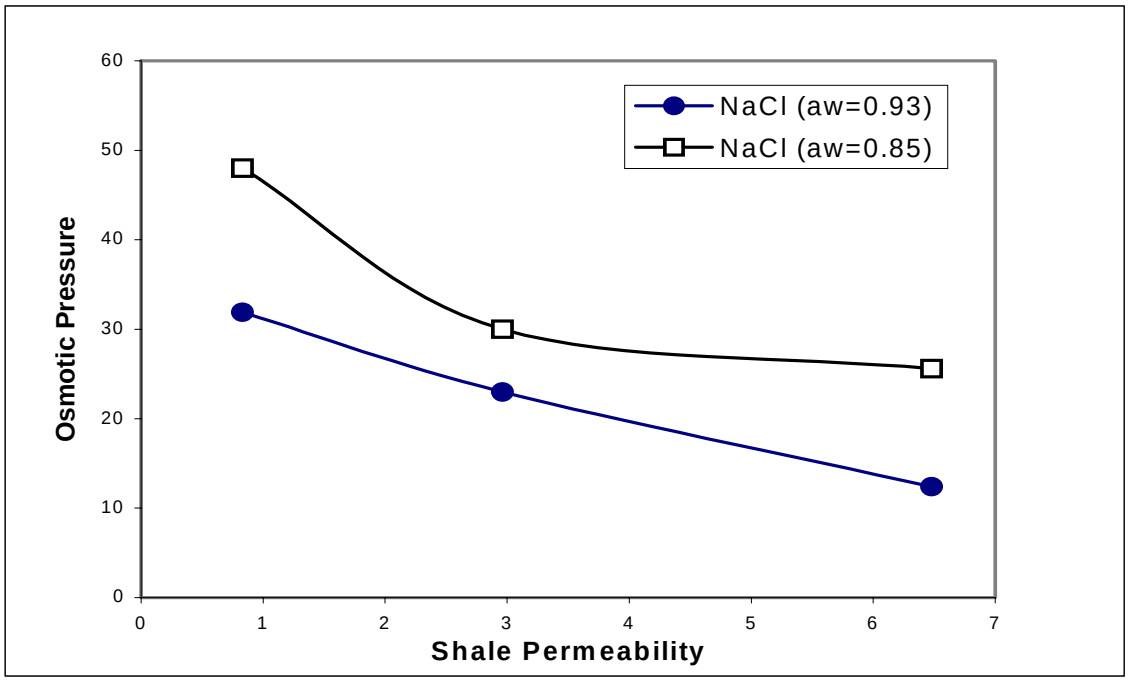

Figure 3-29: Induced osmotic pressure dependence on shale permeability during shales and NaCl solutions interaction.

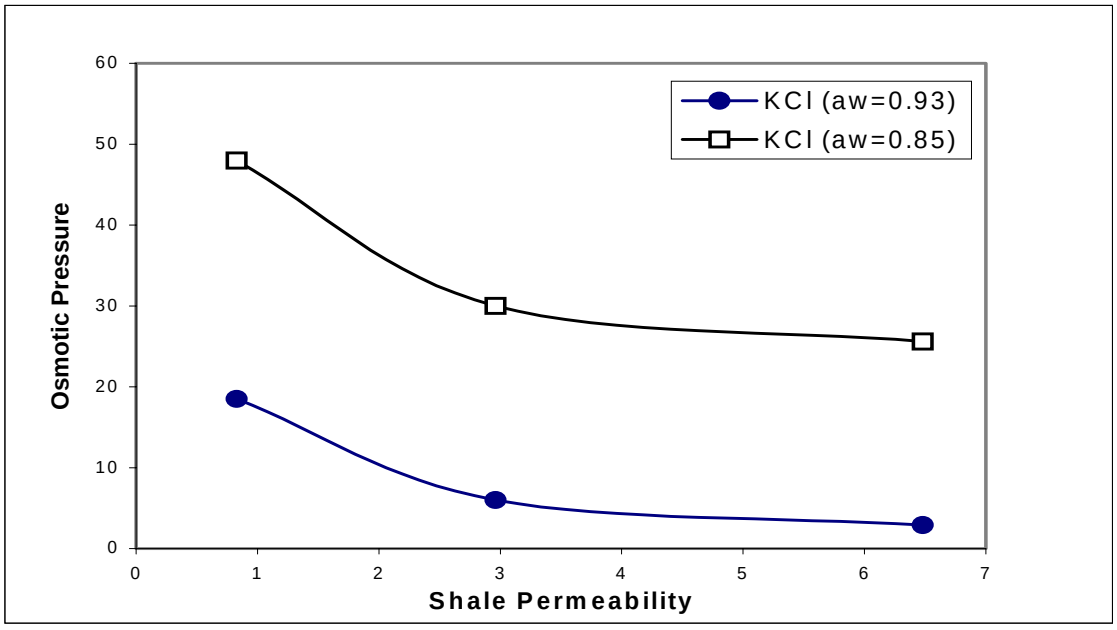

Figure 3-30: Induced osmotic pressure dependence on shale permeability during shales and KCl solutions interaction.

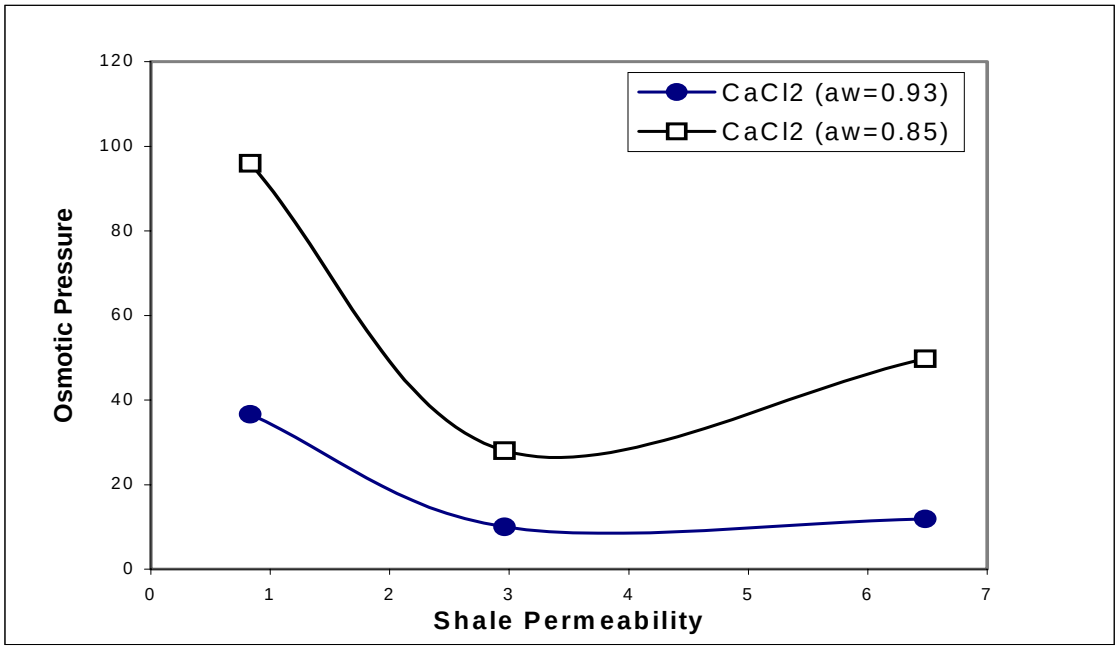

Figure 3-31: Induced osmotic pressure dependence on shale permeability during shales and CaCl2 solutions interaction.

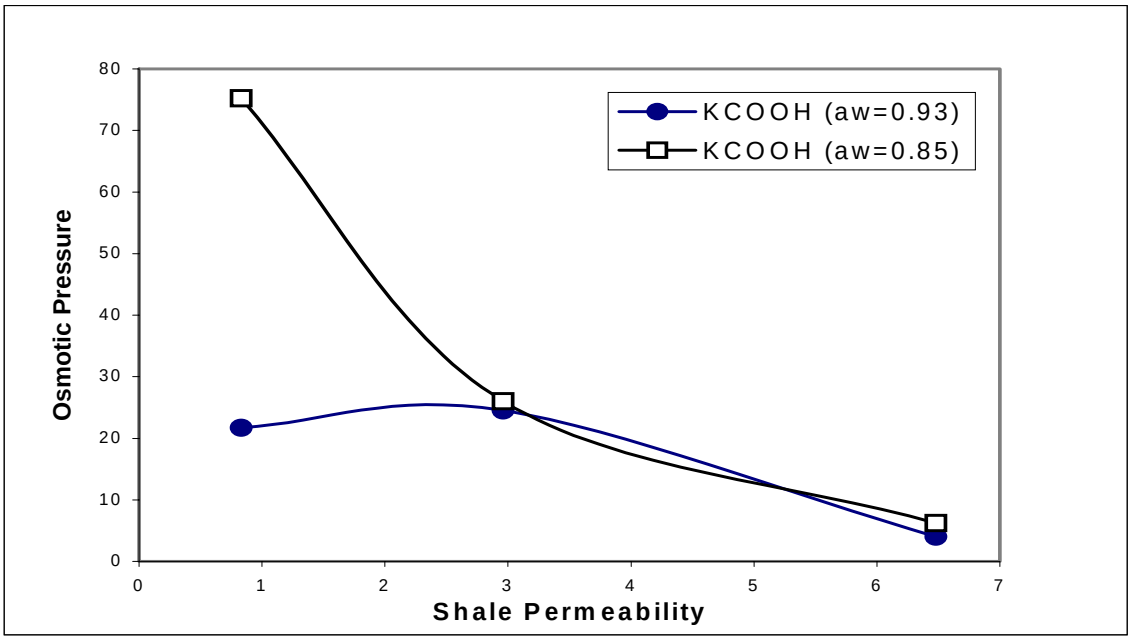

Figure 3-32: Induced osmotic pressure dependence on shale permeability during shales and KCOOH solutions interaction.

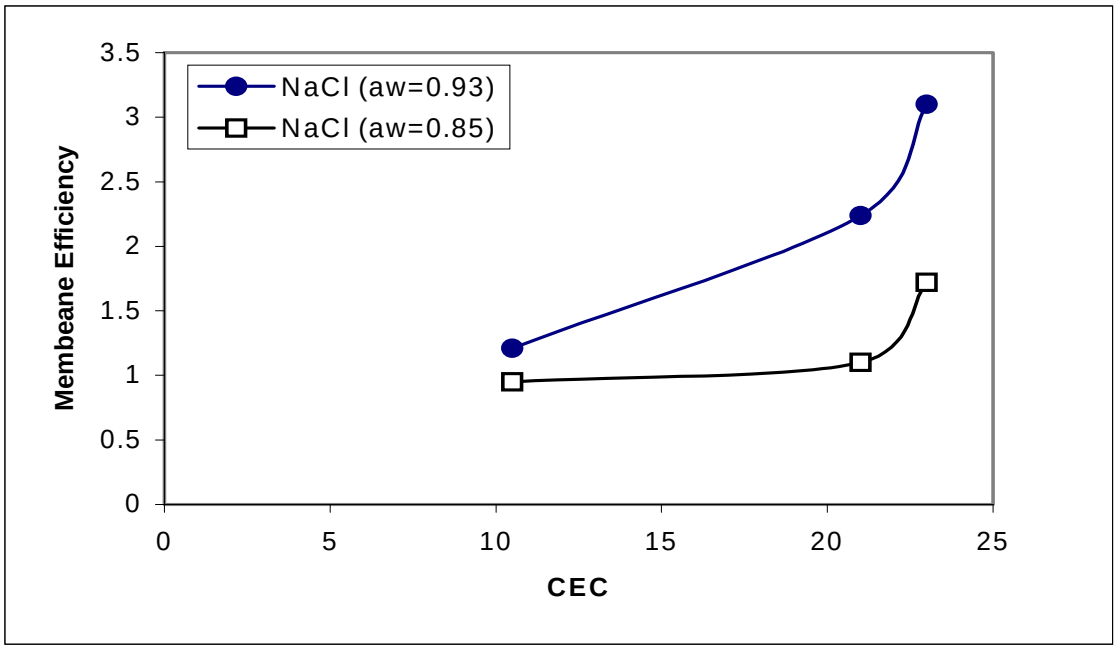

Figure 3-33: Membrane efficiency dependence on shale cation exchange capacity (CEC) during shales and NaCl solutions interaction.

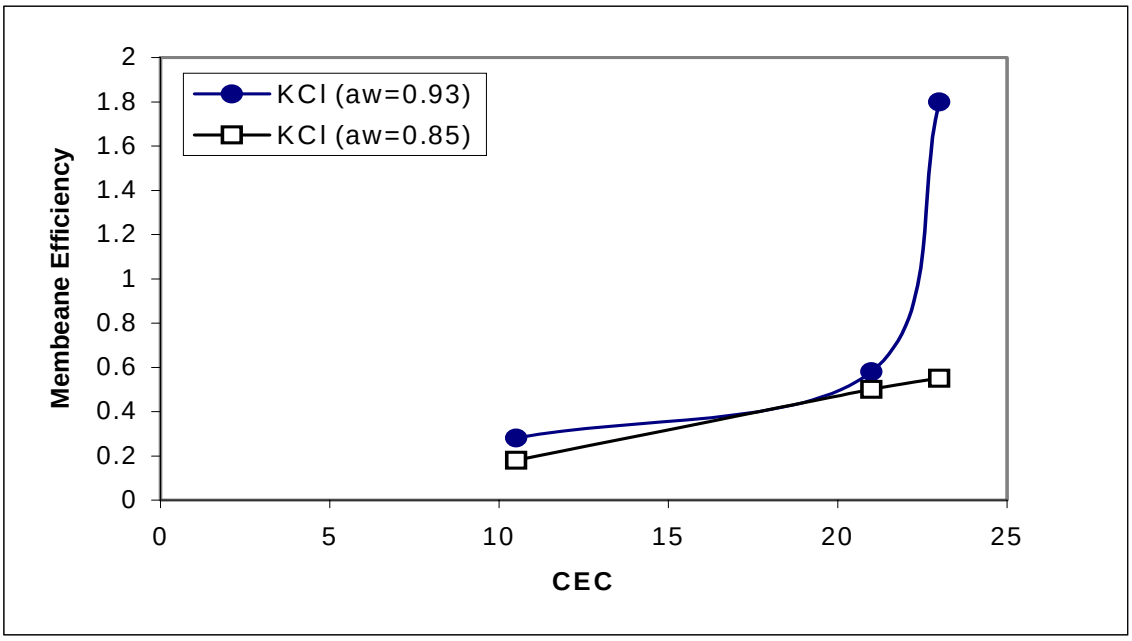

Figure 3-34: Membrane efficiency dependence on shale cation exchange capacity (CEC) during shales and KCl solutions interaction.

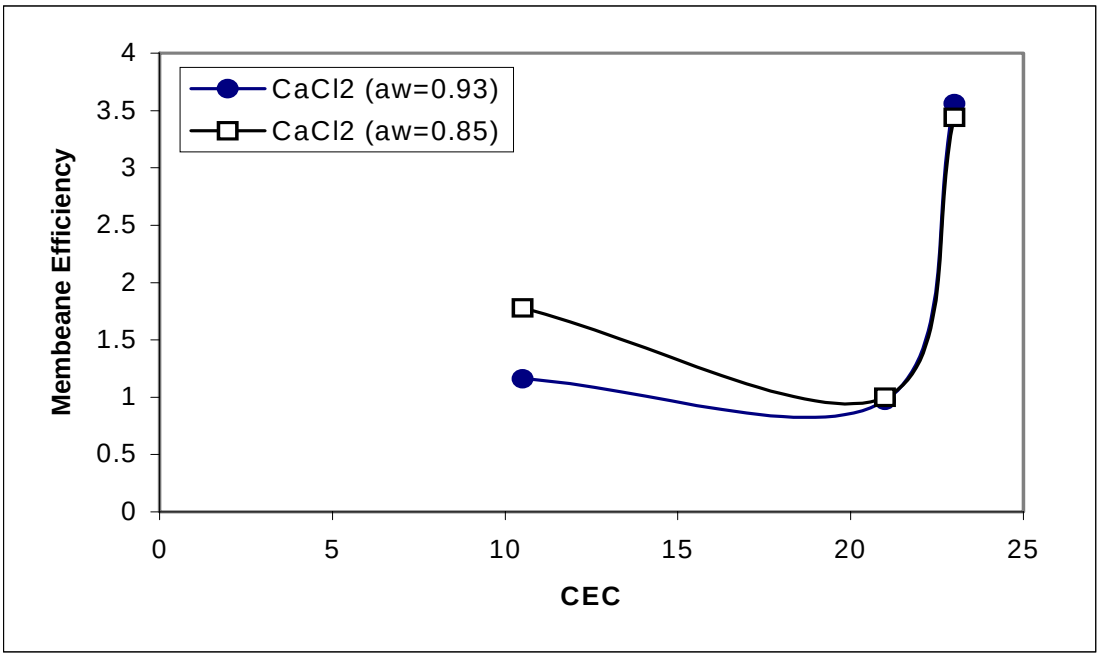

Figure 3-35: Membrane efficiency dependence on shale cation exchange capacity (CEC) during shales and CaCl2 solutions interaction.

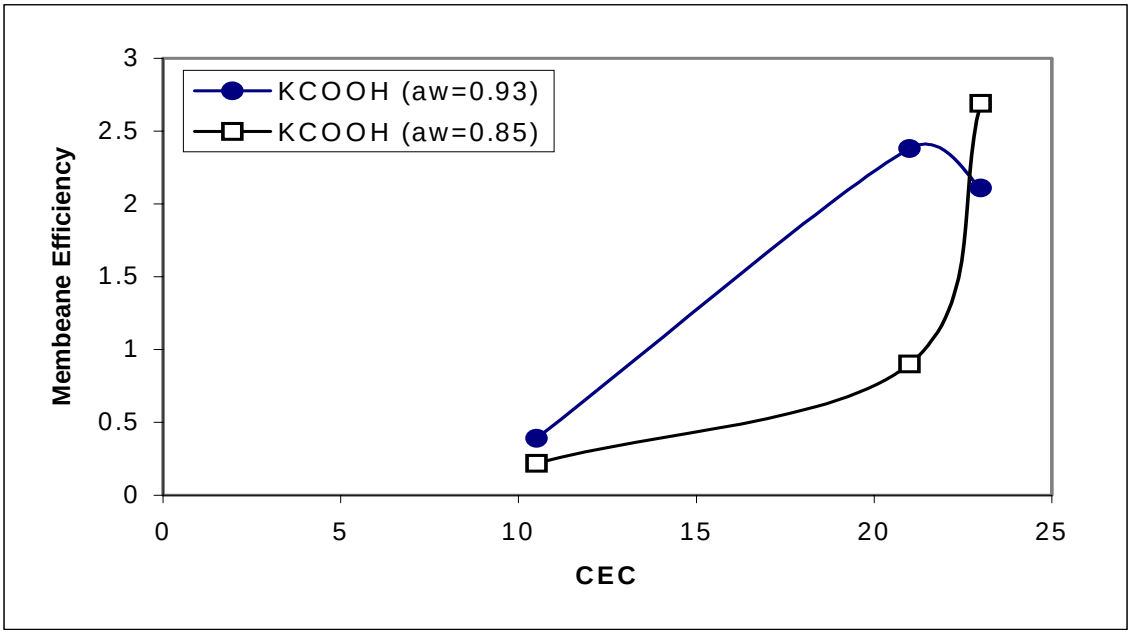

Figure 3-36: Membrane efficiency dependence on shale cation exchange capacity (CEC) during shales and KCOOH solutions interaction.

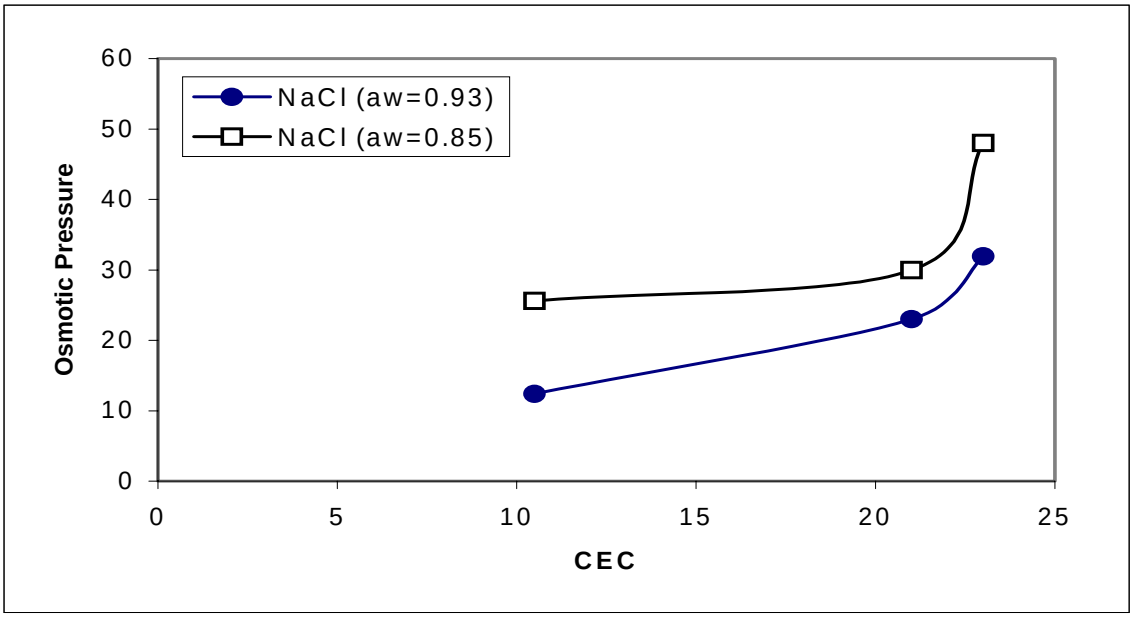

Figure 3-37: Induced osmotic pressure dependence on shale cation exchange capacity (CEC) during shales and NaCl solutions interaction.

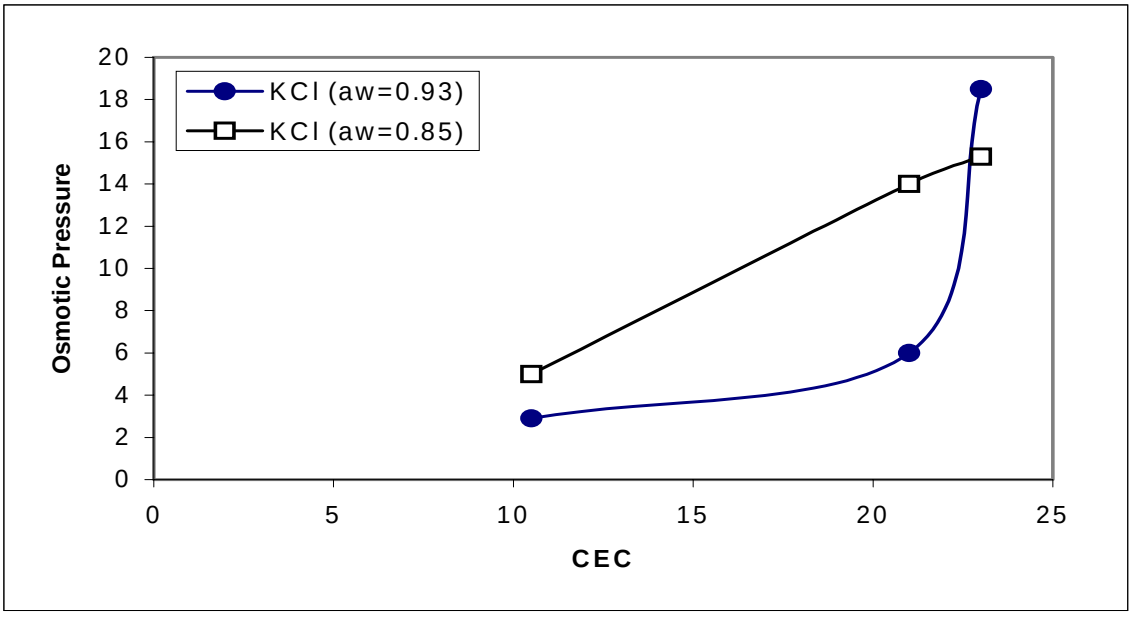

Figure 3-38: Induced osmotic pressure dependence on shale cation exchange capacity (CEC) during shales and KCl solutions interaction.

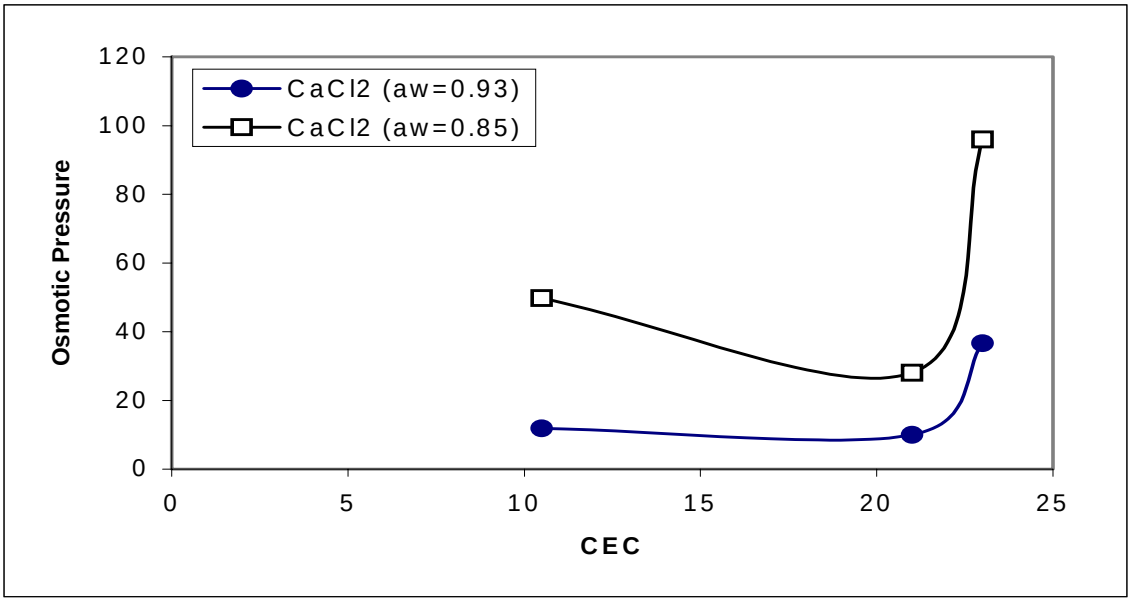

Figure 3-39: Induced osmotic pressure dependence on shale cation exchange capacity (CEC) during shales and CaCl2 solutions interaction.

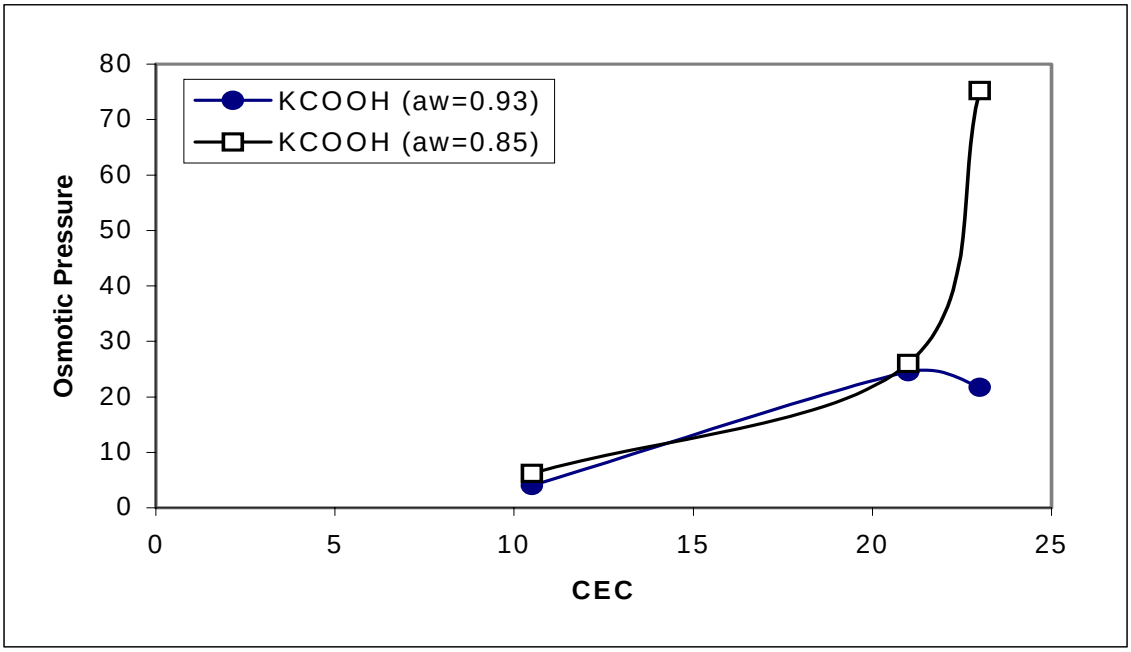

Figure 3-40: Induced osmotic pressure dependence on shale cation exchange capacity (CEC) during shales and KCOOH solutions interaction.

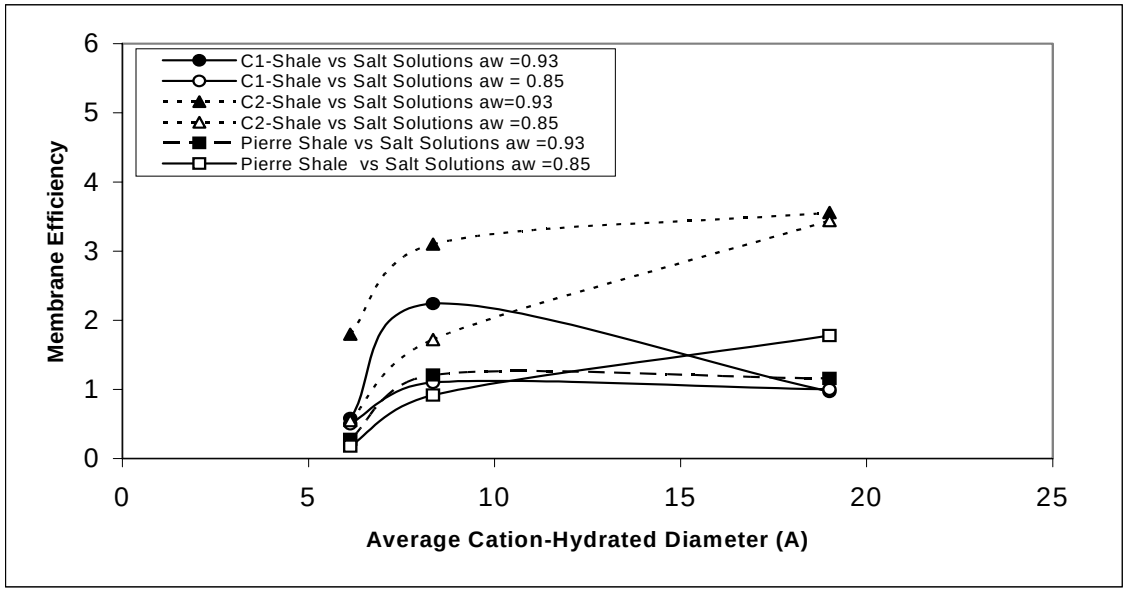

Figure 3-41: The membrane efficiencies dependence on cation-hydrated radius when different cations (calcium, sodium and potassium) of different concentrations interacted with C1- shale, C2-shale and Pierre shale.

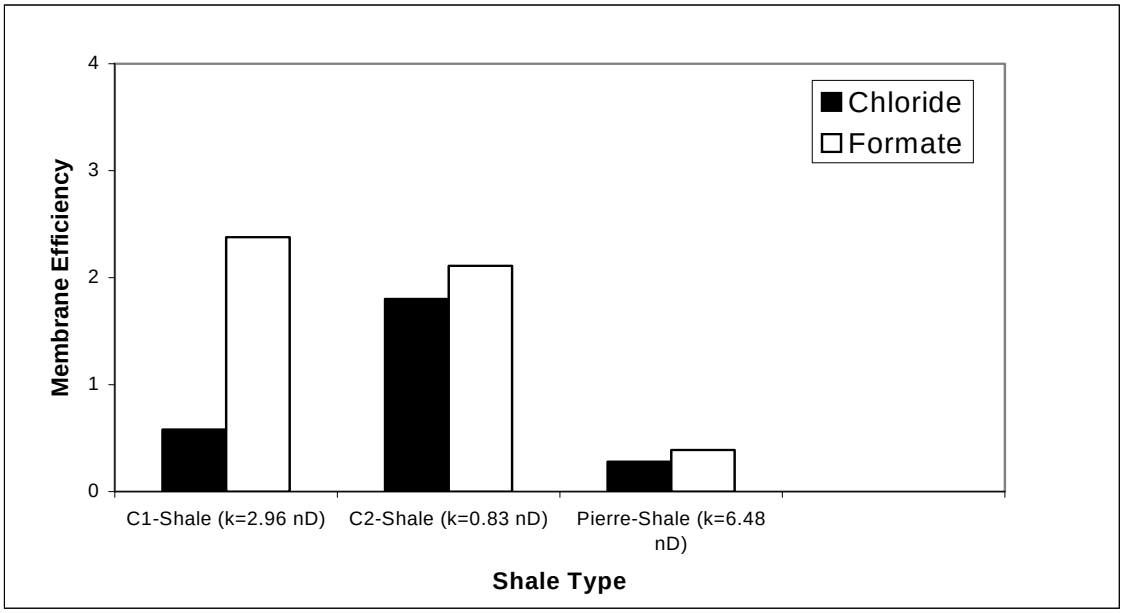

Figure 3-42: The membrane efficiencies dependence on anion type when formate and chloride solutions of 0.93 water activity interacted with C1- shale, C2-shale and Pierre shale.

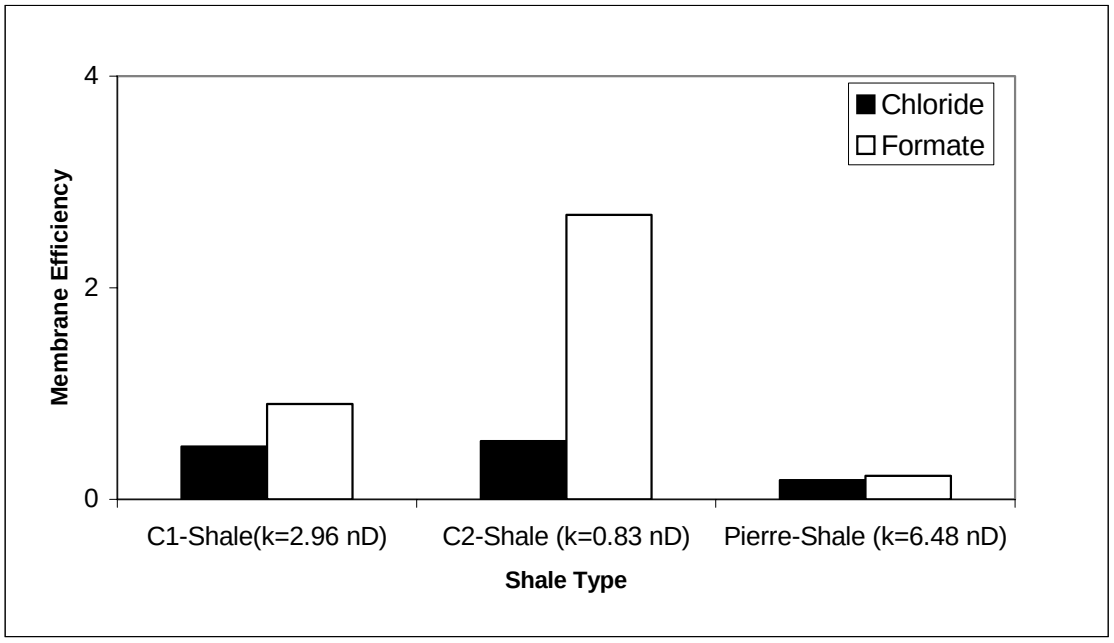

Figure 3-43: The membrane efficiencies dependence on anion type when formate and chloride solutions of 0.85 water activity interacted with C1- shale, C2-shale and Pierre shale.

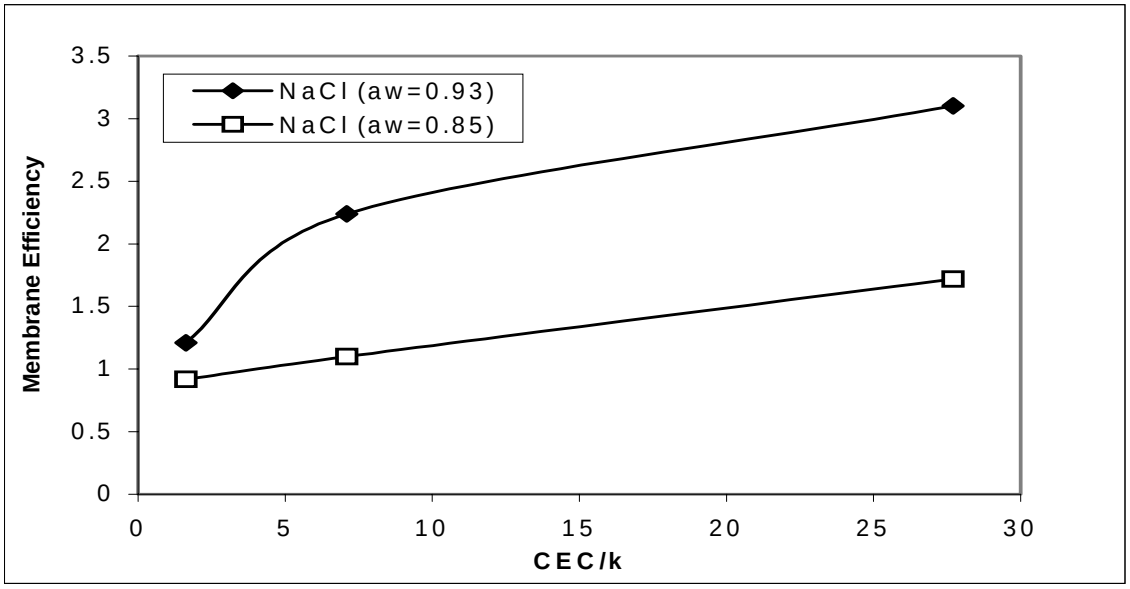

Figure 3-44: The membrane efficiency dependence on (CEC/k) of shales during NaCl solutions and shales interactions.

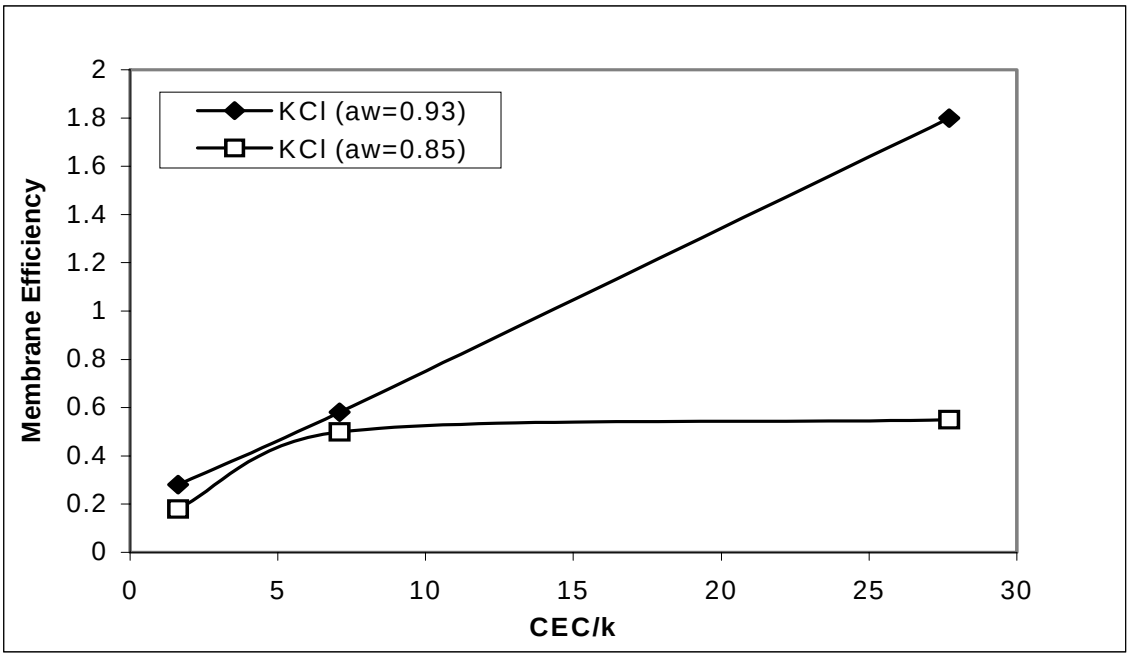

Figure 3-45: The membrane efficiency dependence on (CEC/k) of shales during KCl solutions and shales interactions.

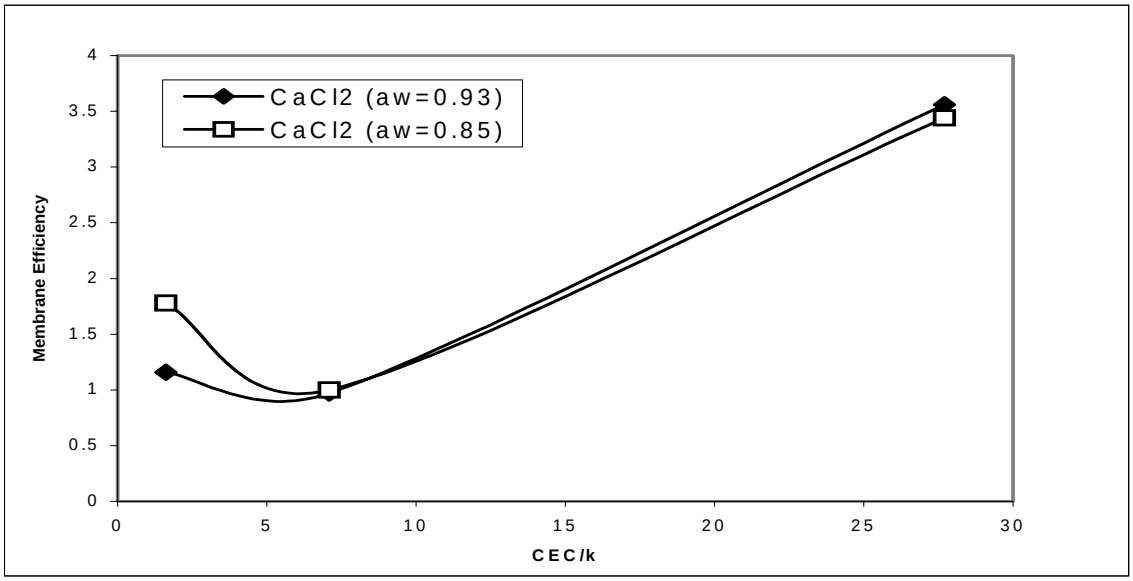

Figure 3-46: The membrane efficiency dependence on (CEC/k) of shales during $CaCl_2$ solutions and shales interactions.

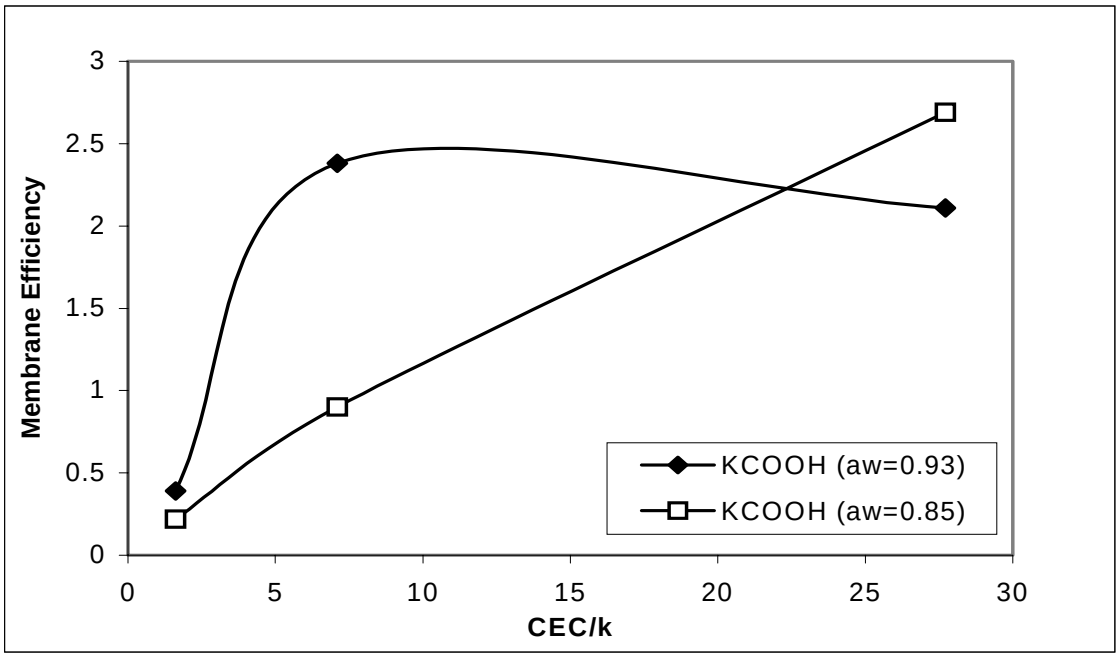

Figure 3-47: The membrane efficiency dependence on (CEC/k) of shales during KCOOH solutions and shales interactions.

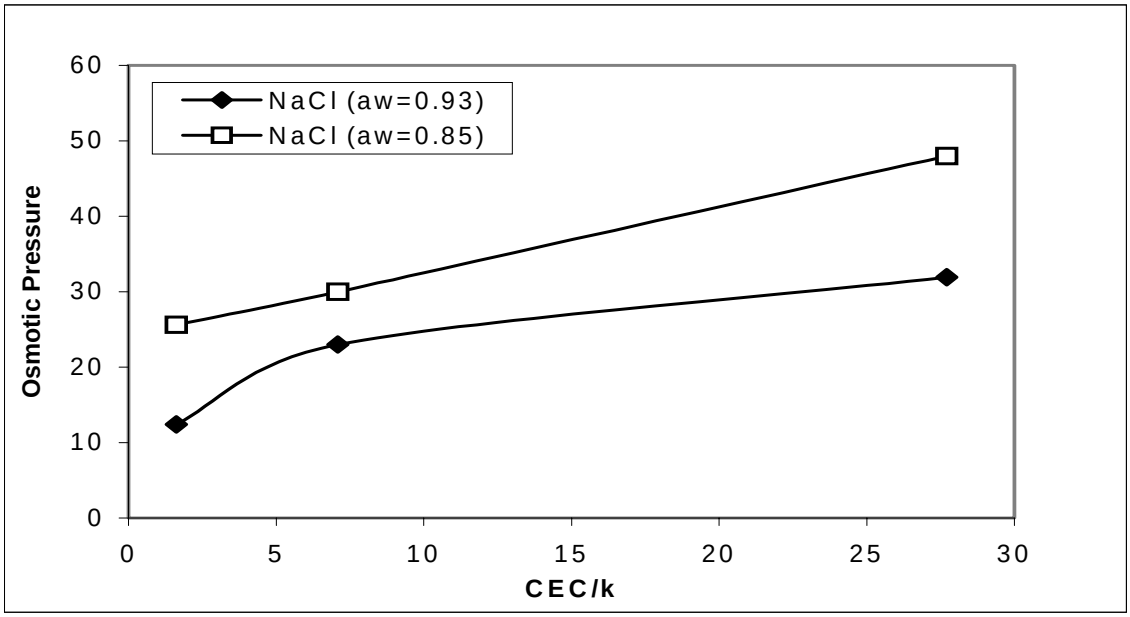

Figure 3-48: The induced osmotic pressure dependence on (CEC/k) of shales during NaCl solutions and shales interactions.

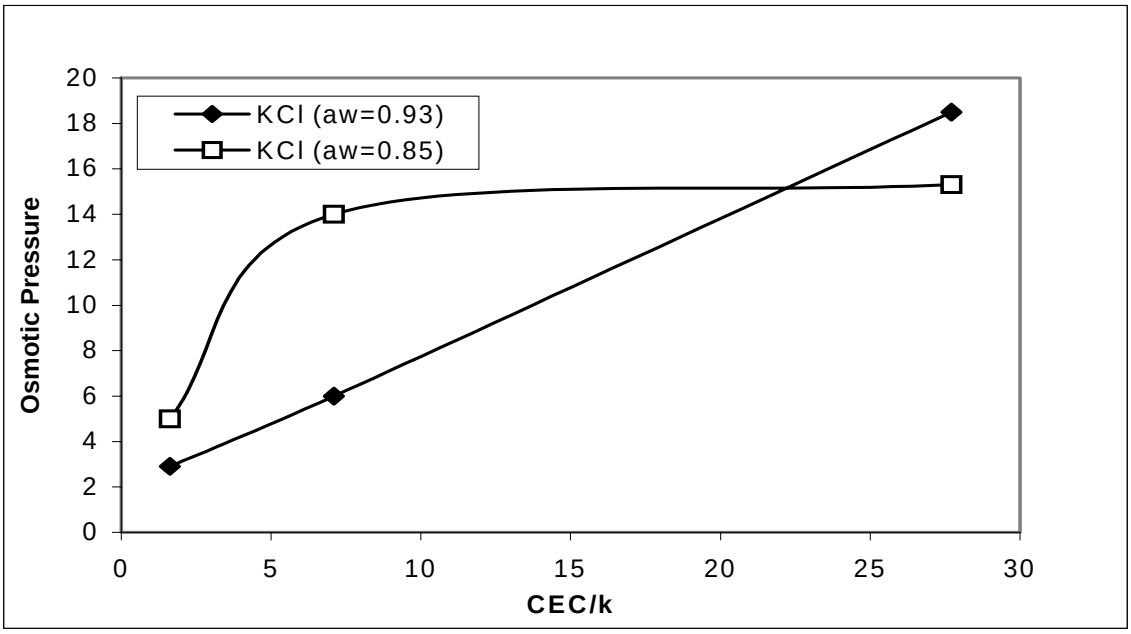

Figure 3-49: The induced osmotic pressure dependence on (CEC/k) of shales during KCl solutions and shales interactions.

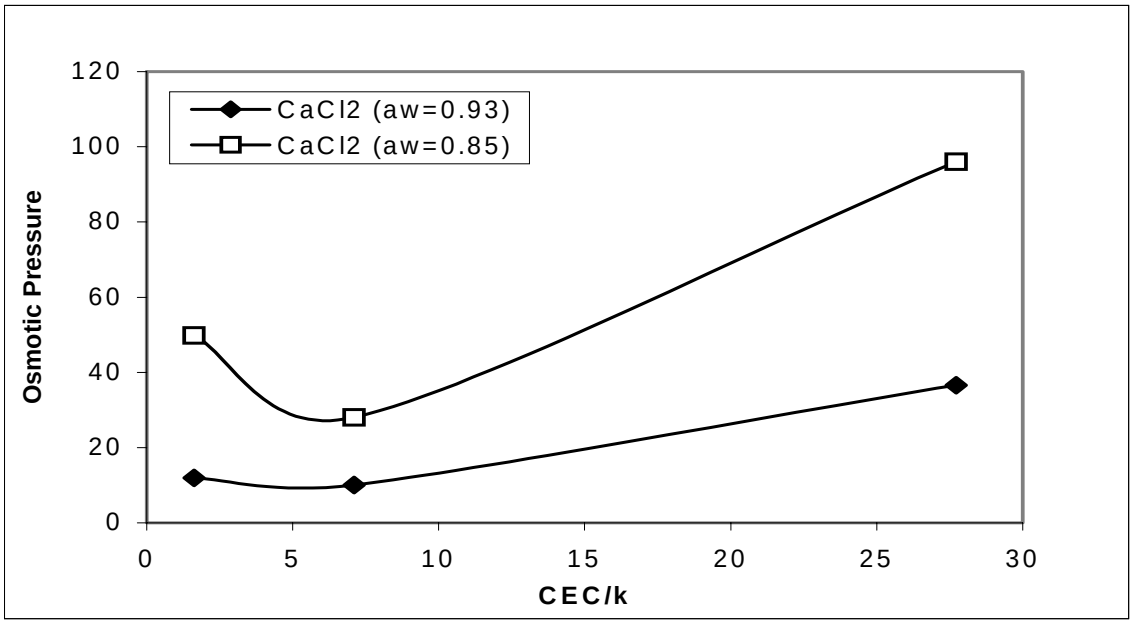

Figure 3-50: The induced osmotic pressure dependence on (CEC/k) of shales during $CaCl_2$ solutions and shales interactions.

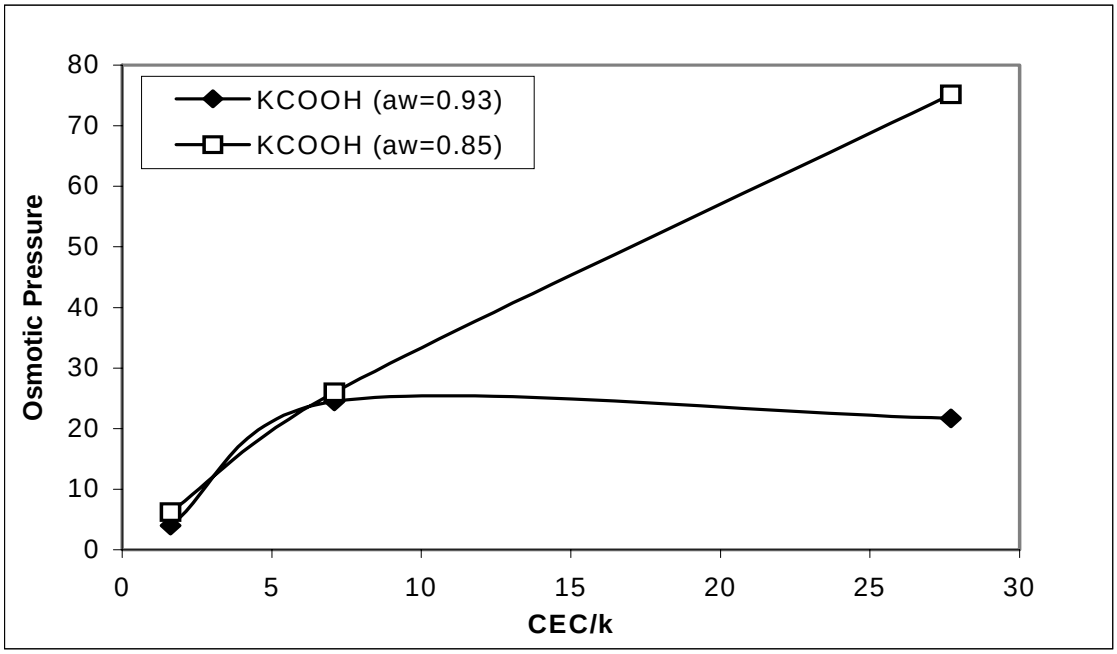

Figure 3-51: The induced osmotic pressure dependence on (CEC/k) of shales during KCOOH solutions and shales interactions.

Test Details

Upstream Fluid	Oil-Based Mud (aw = 0.93)
Downstream Fluid	NaCl (aw = 0.98)
Shale Tested	C1 Shale (aw = 0.98)
Shale Permeability	2.96 nD
Resultant Shale σ	σ = 51.18 %

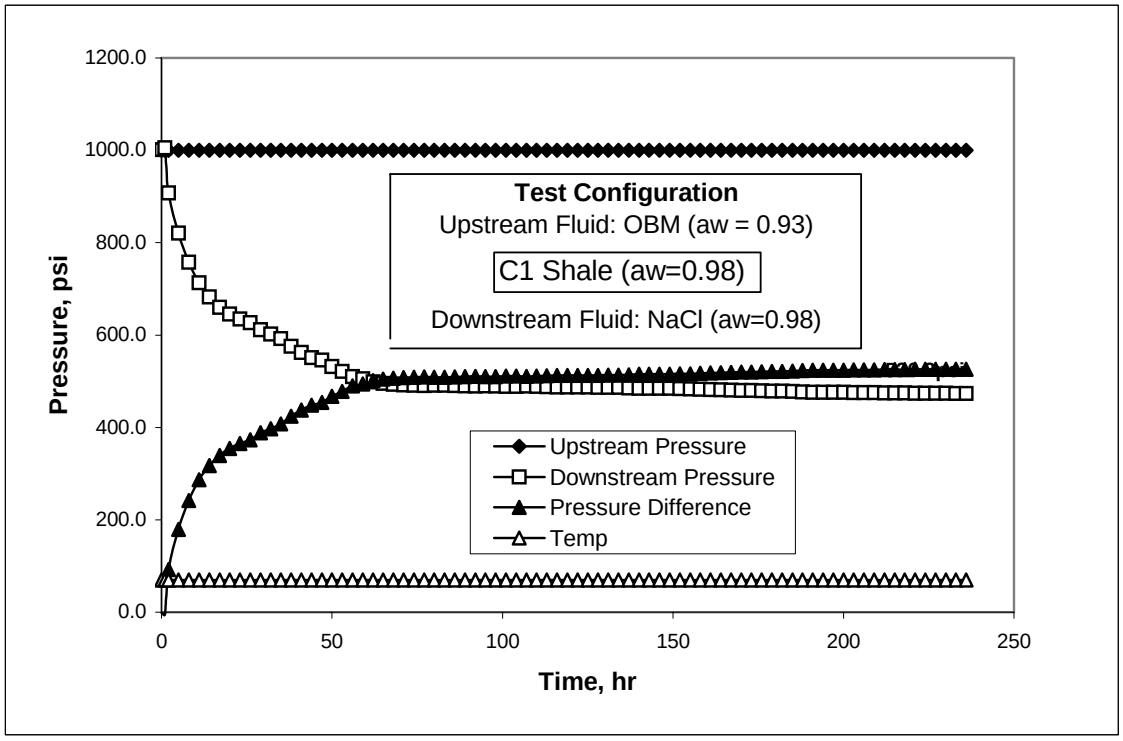

Figure 3-52: Oil-based mud membrane efficiency test where C1-shale interacted with oil-based mud of water activity of 0.93

Test Details

Upstream Fluid	Oil-Based Mud (aw = 0.93)
Downstream Fluid	NaCl (aw = 0.98)
Shale Tested	Pierre Shale (aw = 0.98)
Shale Permeability	6.48 nD
Resultant Shale σ	σ = 17.05 %

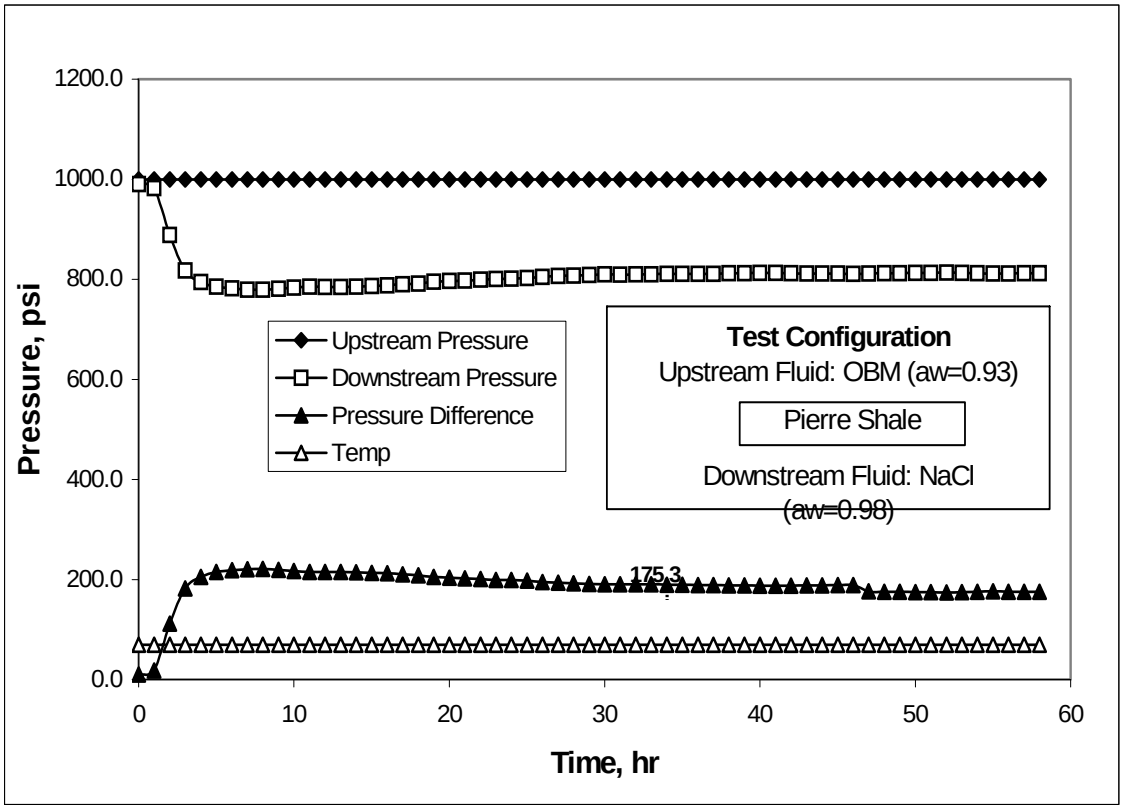

Figure 3-53: Oil-based mud membrane efficiency test where Pierre shale interacted with oil-based mud of water activity of 0.93

Test Details

Upstream Fluid	Oil-Based Mud (aw = 0.93)
Downstream Fluid	NaCl (aw = 0.85)
Shale Tested	Arco-China Shale (aw = 0.85)
Shale Permeability	0.45 nD
Resultant Shale σ	σ = 48.62 %

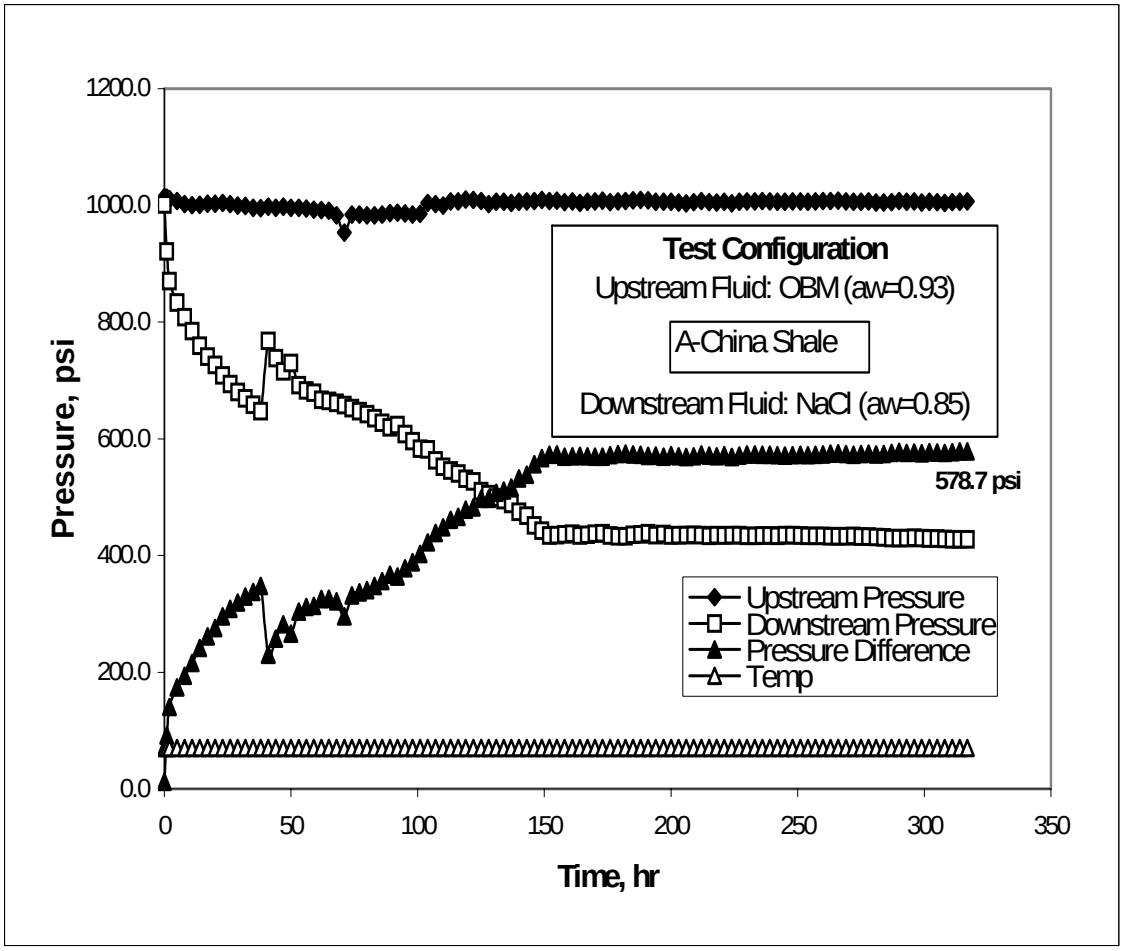

Figure 3-54: Oil-based mud membrane efficiency test where Arco-China shale interacted with oil-based mud of water activity of 0.80

CHAPTER 4

Evaluation of Ion Selectivity of Shales Using Electrochemical Potential Tests

4.1 INTRODUCTION

When two aqueous solutions of different concentrations are separated by a membrane that is permeable to cations and anions, an electrical potential develops. This is due to the separation of negative and positives charges across the membrane owing to the different ionic mobility (diffusion rate). Generally, smaller ions have higher mobilities than larger ones and multivalent ions have a lower mobility than mono-valent ions of the same size. Differences in ionic mobility can be attributed to the hydration shell for each type of ion. Sodium ions have a larger hydrated ion size than chloride ions. Thus chloride ions move faster than sodium ions and, as a result, a diffusion potential develops.

The magnitude of this diffusion potential depends on the difference between the transport number of cations and anions and the ratio of the ionic activities on both sides of the membrane as follows,

$$E_{LJ} = (t^+ - t^-)\,(RT/F)\,\ln\,(a_2/a_1) \quad \text{.....(4-1)}$$

where t^+ and t^- are the transport numbers of the cation and anion respectively, R is the universal gas constant, T is the absolute temperature, F is the Faraday constant, and a_1, a_2 are the ionic activities.

When two solutions of different concentrations are separated by shale, a modified diffusion potential develops because the shale allows cations to pass while restricting anions. Therefore, shales are considered to be ion-selective membranes which selectively allow cations to move through while restricting anions. Since the diffusion potential is a measure of the ability of a shale to restrict anion movement, it can be used to deduce the shale membrane efficiency.

This chapter deals with measuring the ion selectivity (diffusion potential) of shales when interacting with water-based muds. The idea is to establish a relationship between the shale's membrane efficiency and ion selectivity so that the simpler and quicker electrochemical test can be used for shale and drilling fluid evaluation. Section 4.2 presents a background and literature review regarding the diffusion potential of shale and prior electrochemical testing. In Section 4.3, a complete description of the electrochemical test is given. Section 4.4 discusses the results obtained from this test and establishes a relationship between the membrane efficiency and ion selectivity of shales. Finally, Section 4.5 presents some conclusions and makes recommendations.

4.2 BACKGROUND & LITERATURE REVIEW

Ion-selective membranes yield a modified diffusion potential whereas membranes yield a diffusion potential. If the ion-selective membrane completely blocks the passage of the co-ions, the charge transport is entirely due to the counter ions. This type of membrane is referred as a perfect ion-selective membrane. The maximum possible potential difference, which can be generated by a perfect ion-selective membrane, is given by the Nernst expression as follows,

$$E = (RT/F) \ln (a_2/a_1) \quad \ldots\ldots\ldots\

membrane efficiency. They showed that the composition of the interstitial pore fluid in shales plays a determining role on the establishment of the electrochemical potential and, that in some cases, the behavior of the shale is close to the expected behavior of a perfect cation-selective membrane. They developed mathematical models which estimate shale membrane efficiencies and modified diffusion potentials based on physical parameters of the shale and the drilling fluid. It is important to note that the membrane efficiency calculated by Lomba et al (2000) was based on comparing the actual diffusion potential of shale to the maximum expected diffusion potential. In other words, the membrane efficiency calculated by them is not the same as the hydraulic membrane efficiency as discussed in Chapter 3.

While the above studies measured the diffusion potential of shale, no attempts were made to relate the measured diffusion potential to the membrane efficiency. In addition, the factors that control the diffusion potential (ion selectivity) of shale were not thoroughly investigated.

In this work, we measured diffusion potential (ion selectivity) of shales following the same test matrix used for the membrane efficiency test. This is done in order to correlate the ion selectivity of shale to its membrane efficiency so that our electrochemical test can be used to infer shale membrane efficiency. Moreover, we have studied the dependence of the ion selectivity of shale on ion type and concentration, shale permeability and shale cation exchange capacity. We believe that these are the most important factors, which control the ion selectivity and membrane efficiency of shale.

4.3 ION SELECTIVITY TEST DESCRIPTION

4.3.1 Test Definition and Objectives

The ion selectivity test measures the voltage drop across shale samples that are in contact with fluids of different salinities. The difference in salinity produces an electrical gradient, which is measured using a voltage device. The measured voltage drop is used to calculate the ion selectivity for the shale sample. The ion selectivity reflects the ability of shales to restricts anion from passing through. The ion selectivity is defined as follows:

$$\text{Ion Selectivity \%} = \{[V_m - V_{LJ}] / [V_{PM} - V_{LJ}]\}*100 \quad \text{(4-3)}$$

In equation (4-3), V_m refers to the actual measured voltage drop, V_{LJ} refers to the voltage drop that would be created in a liquid junction and V_{PM} refers to the voltage drop that would be created if a perfect ion-selective membrane separated the two solutions (the Nernst Potential). An ion selectivity value of one indicates that the shale behaves as a perfect cation-selective membrane. Namely, it allows only the positive charges (cations) to pass through and restricts all negative charges (anions). An ion selectivity value of between 0 and 1 indicates that the shale behaves as a non-perfect cation-selective membrane (leaky membrane). An ion selectivity value of 0 means that the shale behaves as a non-selective membrane where it allows all ions to pass through.

Equation (4-3) only applies to salt solutions made up of a single salt where we can estimate the maximum and minimum voltages under perfect membrane and liquid junction scenarios. We cannot directly apply this equation to voltage measurements for water-based muds that may have many different ionic species. The objectives of the experimental tests are as follows:

- Perform electrochemical potential tests on different shale samples using different salt solutions and measure the shale's ion selectivity (resultant voltage drop).
- Study the impact of salt type and concentration on the shale's ion selectivity.
- Study the influence of different cations and anions on the ion selectivity of shales (resultant voltage drop).
- Study the impact of shale's permeability and CEC on its ion selectivity.
- Establish a relationship between the ion selectivity of shale and its membrane efficiency.

4.3.2 Test Equipment

Figure 4-1 shows the experimental set-up and the components that were used in this test. The electrochemical cell consists of two compartments separated by a shale wafer. Two sleeve-type Ag/AgCl reference electrodes (ORION Model 90-01 Single Junction Reference Electrode), filled with 4 M KCl solution (saturated with AgCl) is placed in each compartment. A high-impedance auto-range digital multimeter

MICRONTA 22-186 was connected to the reference electrode in order to measure the electrical potential difference. Figure 4-2 shows an actual photograph of the equipment.

4.3.3 Test Procedure

The following procedure was adopted for our electrochemical potential tests.

- The shale wafer (prepared as described in Chapter 2) is placed between the two compartments. The two compartments are squeezed and tightened using clamps in order to prevent compartment leakage.
- Fill each compartment with the solutions to be tested at the same time in order to avoid the generation of streaming potentials due to convection.
- Connect the reference electrodes to the voltage device.
- Place the two electrodes in the compartments containing the solutions.
- The voltage devices will start displaying the voltage across the shale wafer.
- Record the voltage reading as a function of time.

Before the start of these experiments, the electrodes were checked by measuring the diffusion potential in three different cases. The first case was the diffusion potential when a sandstone sample separated two sodium chloride solutions of concentration of 0.1M and 1M. The resultant diffusion potential after 5 minutes was +9 mV. This is a very reasonable value since it is very close to the expected Liquid junction value of +13 mV. In the second case, the sandstone sample was replaced with a highly porous ceramic disc. The resultant diffusion potential after five minutes was +0.1 mV. This is extremely reasonable since the two sodium chloride solutions were mixed after five minutes and one would expect the voltage drop to vanish. In the third case, we used a piece of shale to separate the two sodium chloride solutions. After five minutes, a voltage drop of –47

mV was obtained. This is quite reasonable since shale is supposed to induce a higher voltage than a sandstone or ceramic disc. The obtained diffusion potential values in all three cases were consistent with our expectations which confirmed that our electrodes were functioning properly. Figure 4-3 shows the diffusion potential development in all three cases.

Our electrochemical experiment time interval was chosen to be 5 minutes as recommended by Lomba et al (2000). In their recommendation, they argue that the diffusion potential reaches 80 % of its final value after 5 minutes of performing the electrochemical test. All tests were conducted according to the procedure mentioned above. While all tests follow the same trend, it is a good idea to show what a typical test looks like. Figure 4-4 shows the voltage measurement when C1-shale was exposed to NaCl solutions of water activities of 0.93 and 0.98.

4.3.4 Test Matrix

We evaluated the ion selectivity of four different shales samples as a result of their interaction with different aqueous solutions at different concentrations. The effects of shale permeability and cation exchange capacity on shales ion selectivity was investigated using four different shales. In addition, this study aimed to investigate the effects that different cations and anions have on the ion selectivity of shales. We also aimed at studying the influence of concentration changes (water activity changes) of these cations and anions on ion selectivity. Tables 4-1 and 4-2 show the test matrix designed to study the effects of cation and anion type and concentration on ion selectivity. The effects of shale permeability and cation exchange capacity are incorporated in Tables 1 and 2 by using different shale types.

4.4 RESULTS & DISCUSSION

4.4.1 Ion Selectivity of Shales During Interaction with Water-Based Muds

The experimental results for C1, C2, Pierre and Arco-China shales are shown in Tables 4-3, 4-4, 4-5 and 4-6 respectively. These Tables display both the measured voltage drop and the calculated ion selectivity in response to a concentration gradient across the shale for different salt solutions at different water activities. These results clearly show that the Arco-China shale has the highest ion selectivity followed by C2, C1 and Pierre shale respectively. This means that Arco-China shale's ability to act as cation-selective membrane is stronger than the other shales. In order to better explain the ability of these shales to act as cation-selective membranes, we have compared their measured voltage drop to the maximum voltage drop that would be generated by a perfect cation-selective membrane. Using equation (4-2), we calculated the maximum voltage drop that would be generated for each test and compared our measured voltage to that theoretical maximum voltage. Tables 4-7, 4-8, 4-9 and 4-10 show the results for C1, C2 , Pierre and Arco-China shales. Again, it is clearly seen that the Arco-China shale was the closet to a perfect cation-selective membrane. Our ion selectivity results show that all shales are not perfect cation-selective membranes and that the Arco-China shale was a better cation-selective membrane than the other shales.

4.4.2 Effects of Ion Type and Concentration on the Ion Selectivity of Shale

Our experimental results showed that the estimated ion selectivity of shales changes with external solution (salt solution) ion type as shown in Figures 4-5, 4-6, 4-7 and 4-8. These Figures show that for each shale type, the ion selectivity changes with the ions that make up the external fluid. Changes in the type of cation and anion that make up the external solution seem to greatly affect the shale ion selectivity as can clearly be

seen from Figures 4-9, 4-10, 4-11 and 4-12. This is attributed to the different mobilities these ions have during their interactions with the shales. Small ions move faster than big ions and mono-valent ions are faster than multi-valent ions. The external solution concentration (water activity) did not seem to strongly affect the measured voltage drop or the estimated ion selectivity as shown in Figures 4-5, 4-6 and 4-7. Changing the external fluid water activity (ions concentration) from 0.93 to 0.85 had little effect on the measured voltage drop or shale ion selectivity.

4.4.3 Effect of Permeability (k) on The Ion Selectivity of Shale

The influence of shale permeability on the shale ion selectivity was investigated with different shales with different permeabilities. Figures 4-13, 4-14, 4-15 and 4-16 show the shale ion selectivity dependence on shale permeability when different shales (with different permeabilities) interacted with salt solutions of different water activities. The general trends shown in these graphs are the same; the ion selectivity of shales increases when the shale permeability decreases. As the shale permeability (pore size) decreases due to burial and compaction, their ability to restrict solutes increases and their ion selectivity increases. In other words, it is the ratio of solute size to pore size that determines their ability to restrict solutes from entering their pore space and thus gives them the ability to behave as ion-selective membrane. Figures 4-17, 4-18, 4-19 and 4-20 show the measured voltage drop dependence on shale permeability.

4.4.4 Effect of Cation Exchange Capacity (CEC) on The Ion Selectivity of Shale

It is argued that shales exhibit membrane behavior because of the charge on the pore walls. The cation exchange capacity of shales is a measure of the intensity of the negative charge environment between clay platelets. Therefore, the cation exchange capacity should influence the shale ion selectivity and measured voltage drop. Figures 4-

21, 4-22, 4-23 and 4-24 show the ion selectivity dependence on shale cation exchange capacity when shales with different cation exchange capacities interacted with salt solutions of different water activities. The general trends shown in these graphs are the same; the ion selectivity of shales increases when the shale cation exchange capacity increases. This is expected since the shale negative charge, indicated by the shale cation exchange capacity, will prevent anions from passing through and only allow cations to pass. In doing so, an electrical potential, indicated by the voltage drop, is created which directly indicates the shale's ability to screen out anions. The higher the electrical potential, the better the shale's ability to screen out anions. When shales are able to completely screen out anions, they are referred to as perfect ion-selective membranes. Figures 4-25, 4-26, 4-27 and 4-28 show the voltage drop dependence on shale cation exchange capacity.

4.4.5 Effect of Cation Exchange Capacity (CEC) and Shale Permeability (k) Ratio on The Ion Selectivity of Shale

In order to show the combined effect of both the cation exchange capacity and permeability of shales on the ion selectivity of shales, we plotted the ratio of the cation exchange capacity to permeability of shales versus the estimated ion selectivity of shales. Figures 4-29, 4-30, 4-31 and 4-32 show the ion selectivity dependence on the ratio of cation exchange capacity and permeability (CEC/k) when shales interacted with different solutions (NaCl, KCl, $CaCl_2$ and KCOOH) at two different water activities (0.93 and 0.85). It is clearly seen from these graphs that the ion selectivity is proportional to the ratio of the cation exchange capacity and permeability of shales. A higher value of cation exchange capacity to permeability ratio (CEC/k) correlates very well with higher ion selectivity. The same argument and conclusion applies to the dependence of voltage drop

on the ratio of the cation exchange capacity and permeability of shales. Figures 4-33, 4-34, 4-35 and 4-36 show the corresponding voltage drop dependence on the ratio of cation exchange capacity and permeability (CEC/k). From these graphs, one can see that the voltage drop increases as the ratio of the cation exchange capacity and permeability (CEC/k) increases.

4.4.6 Effect of Pore Fluid on The Ion Selectivity of Shale

Lomba et al, (2000), argued that the properties of the interstitial pore fluid in the shale plays a determining role on the establishment of the electric potential difference and thus the behavior of shales as ion-selective membranes. These properties may include pore fluid composition, water activity, and water content. Figures 4-9 and 4-10 show the ion selectivity, as a function of cation hydrated diameter, of different shales when exposed to different salt solutions of 0.93 and 0.85 water activities. Also, Figures 4-11 and 4-12 show the ion selectivity, as a function of anion hydrated diameter, of different shales when exposed to different salt solutions of 0.93 and 0.85 water activities.

It is clearly shown that each shale exhibited different ion selectivity when exposed to the same cations and anions. While we believe that this is primarily attributed to differences in shale permeability and cation exchange capacity, we also believe that the shale's pore fluid could play a role in this.

4.4.7 Ion Selectivity and Membrane Efficiency: Correlations and Applications

The membrane efficiency is usually measured in the laboratory using pressure transmission techniques similar to the one we used in our research. These tests are time and space consuming, which might make them impractical at the rig site. In addition, these tests are hard to assemble and handle and a trained engineer is required to troubleshoot the problems and analyze the results. The ultimate goal was to find a

qualitative correlation between the membrane efficiency and ion selectivity of shales so that our electrochemical test may be used on the rig floor to help engineers understand and prepare for shale sections they encounter during normal drilling operations.

We have measured the membrane efficiency and the ion selectivity of shales using pressure transmission and electrochemical tests. In our work, we used the same test matrix for both tests in order to establish qualitative correlations between the membrane efficiency and ion selectivity of shales. We have used 4 different shales types with different properties. Figure 4-37 shows the membrane efficiency versus the ion selectively measurements for all shales. Figures 4-38, 4-39, 4-40 and 4-41 show the membrane efficiency and ion selectivity relationship for C1, C2, Pierre and Arco-China shales respectively when exposed to different salt solutions of different water activities. As shown from the graphs, the membrane efficiency and ion selectivity relationship follow the same trend for all shales. The membrane efficiency is directly proportional to the ion selectivity. This is expected since higher membrane efficiencies are attributed to higher cation exchange capacity of shales (electrical repletion property), which is responsible for co-ion movement restriction, which leads to higher ion selectivity of shale. It is fair to state, based on our experimental results, that the ion selectivity of shales correlate well with membrane efficiency of shales. In addition, one would expect that shales which have high ion selectivities to exhibit high membrane efficiencies. Having established this qualitative relationship between the ion selectivity and membrane efficiency of shales validate the use of our simple electrochemical test on the rig floor to qualitatively evaluate the membrane efficiency of shale through ion selectivity measurements. This will make shale evaluation much easier for the average engineer since the electrochemical test is a faster and easier test to run. In fact the electrochemical test takes about 10 minutes to administer. This is not the case for the pressure

transmission test where an average test runs for about 72 hours. Also, unlike the pressure transmission test, the electrochemical test does not take up much space at the rig floor. In addition, this test is mobile and does not require an electricity source since its components are battery powered. This is not the case for the pressure transmission test where several AC outlets are needed to run many of equipments and that limits the equipment mobility. More importantly, unlike the pressure transmission test, the electrochemical test does not require an engineer to run due to its ease and simplicity. In fact, any of the rig-floor personnel can run the test and collect the data in about 10 minutes.

The main purpose of using the electrochemical test was to qualitatively estimate the shale's membrane efficiency by correlating it to the measured ion selectivity. Knowing the membrane efficiency for shales can help to minimize water movement into shales and thus prevent borehole collapse. As stated earlier, the most common ways for shale stability control are permeability modification, drilling fluid viscosity reduction and strength enhancement by osmotic backflow. Therefore, for shales with high membrane efficiencies, osmotic backflow allows us to strengthen the shales. On the other hand, if the membrane efficiency of the shale is low, using osmosis as a means to avoid shale failure might not be the best approach. In fact, it may be a waste of time and resources, especially if the drilling fluids employed contain high concentrations of special additives to induce osmotic flow. In this case, focusing on other methods for shale stability control would be most beneficial.

In the field, the spontaneous potential (SP) curves measure the electrochemical potential of the formation being drilled using the same principles employed in our electrochemical test. Therefore, it may be possible to use these SP measurements to

qualitatively predict the membrane efficiency of shales. This extension requires additional study.

4.5 CONCLUSIONS

Using electrochemical measurements, we have investigated ion flow when shales interacted with salt solutions. We have reached the following conclusions based on our results and observations.

- The ion selectivity of shales increases when the shale permeability decreases.
- The ion selectivity of shales increases when the shale cation exchange capacity increases.
- The ion selectivity is directly proportional to the ratio of the cation exchange capacity and permeability of shales. Higher cation exchange capacity and permeability (CEC/k) ratio correlates very well with higher ion selectivity.
- The ion selectivity of shale depends on the type and concentration of the cation and anion that make up the external solution.
- Membrane efficiency is directly proportional to ion selectivity.
- The electrochemical test can be used on the rig site to qualitatively predict the membrane efficiency of shales through ion selectivity measurements.

- SP measurements may be used to qualitatively predict the membrane efficiency of shales since they measure the same basic property as our electrochemical cell.

Table 4-1: Test matrix to study the effects cation type and concentration on shales ion selectivity.

Salt Solution (Test Fluid)	Water Activity	Shale to be tested	Temperature
NaCl	0.93	C1, C2, Pierre & Arco-China Shales	70 F
	0.85	C1, C2, Pierre & Arco-China Shales	70 F
KCl	0.93	C1, C2, Pierre & Arco-China Shales	70 F
	0.85	C1, C2, Pierre & Arco-China Shales	70 F
CaCl2	0.93	C1, C2, Pierre & Arco-China Shales	70 F
	0.85	C1, C2, Pierre & Arco-China Shales	70 F

Table 4-2: Test matrix to study the effects of anion type and concentration on shales ion selectivity.

Salt Solution (Test Fluid)	Water Activity	Shale to be tested	Temperature
KCOOH	0.93 0.85	C1, C2, Pierre & Arco-China Shales	70 F
KCl	0.93 0.85	C1, C2, Pierre & Arco-China Shales	70 F
K2CO3	0.93 0.85	C1, C2, Pierre & Arco-China Shales	70 F

Table 4-3: The electrochemical test results for C1-shale during interaction with different salt solutions of different water activities

Salt Solution (Test Fluid)	Water Activity	Measured Voltage Drop (mV)	Ion Selectivity %
NaCl	0.93	-7.9	43.36
	0.85	-11.2	39.41
KCl	0.93	-2.9	13.92
	0.85	-5.6	15
CaCl2	0.93	-1.5	9.63
	0.85	-1.9	7.71
KCOOH	0.93	-8.7	29.63
	0.85	-11.3	25.51

Table 4-4: The electrochemical test results for C2-shale during interaction with different salt solutions of different water activities.

Salt Solution (Test Fluid)	Water Activity	Measured Voltage Drop (mV)	Ion Selectivity %
NaCl	0.93	-18.6	77.63
	0.85	-22.9	61.62
KCl	0.93	-8.5	36.95
	0.85	-9.1	23.11
CaCl2	0.93	-5.8	31.5
	0.85	-6.1	20.33
KCOOH	0.93	-10.2	34.4
	0.85	-30.1	64.62

Table 4-5: The electrochemical test results for Pierre-shale during interaction with different salt solutions of different water activities.

Salt Solution (Test Fluid)	Water Activity	Measured Voltage Drop (mV)	Ion Selectivity %
NaCl	0.93	-7.9	43.36
	0.85	-10.5	38.03
KCl	0.93	-2.7	13.1
	0.85	-3	8.96
CaCl2	0.93	-3.7	20.82
	0.85	-5.2	17.63
KCOOH	0.93	-3.5	13.11
	0.85	-3.8	9.9

Table 4-6: The electrochemical test results for Arco-China shale during interaction with different salt solutions of 0.93 water activity

Salt Solution (Test Fluid)	Water Activity	Measured Voltage Drop (mV)	Ion selectivity %
NaCl	0.93	-14	83.65
KCl	0.93	-7.6	42.48
CaCl2	0.93	-5	38.73
KCOOH	0.93	-7.2	45.41

Table 4-7: The measured voltage drop comparison to the maximum voltage drop for C1-shale and salt solutions interactions.

Salt Solution (Test Fluid)	aw	Measured Voltage Drop, mV	Maximum Voltage Drop, mV	Vmeasured / Vmaximim %
NaCl	0.93	-7.9	-25.58	30.89
	0.85	-11.2	-43	26.05
KCl	0.93	-2.9	-23.83	12.17
	0.85	-5.6	-42.23	13.26
CaCl2	0.93	-1.5	-19.26	7.79
	0.85	-1.9	-32.6	5.83
KCOOH	0.93	-8.7	-30.85	28.2
	0.85	-11.3	-47.1	24

Table 4-8: The measured voltage drop comparison to the maximum voltage drop for C2-shale and salt solutions interactions.

Salt Solution (Test Fluid)	aw	Measured Voltage Drop, mV	Maximum Voltage Drop, mV	Vmeasured / Vmaximim %
NaCl	0.93	-18.6	-25.58	72.71
	0.85	-22.9	-43	53.26
KCl	0.93	-8.5	-23.83	35.67
	0.85	-9.1	-42.23	21.55
CaCl2	0.93	-5.8	-19.26	30.11
	0.85	-6.1	-32.6	18.71
KCOOH	0.93	-10.2	-30.85	33.06
	0.85	-30.1	-47.1	63.91

Table 4-9: The measured voltage drop comparison to the maximum voltage drop for Pierre-shale and salt solutions interactions.

Salt Solution (Test Fluid)	aw	Measured Voltage Drop, mV	Maximum Voltage Drop, mV	Vmeasured / Vmaximim %
NaCl	0.93	-7.9	-25.58	30.88
	0.85	-10.5	-43	24.4
KCl	0.93	-2.7	-23.83	11.33
	0.85	-3	-42.23	7.1
CaCl2	0.93	-3.7	-19.26	19.21
	0.85	-5.2	-32.6	15.95
KCOOH	0.93	-3.5	-30.85	11.34
	0.85	-3.8	-47.1	8.08

Table 4-10: The measured voltage drop comparison to the maximum voltage drop for Arco-China shale and salt solutions interactions.

Salt Solution (Test Fluid)	aw	Measured Voltage Drop, mV	Maximum Voltage Drop, mV	Vmeasured / Vmaximim %
NaCl	0.93	-14	-17.49	80
KCl	0.93	-7.6	-18.4	41.3
CaCl2	0.93	-5	-13.34	37.48
KCOOH	0.93	-7.2	-16.25	44.29

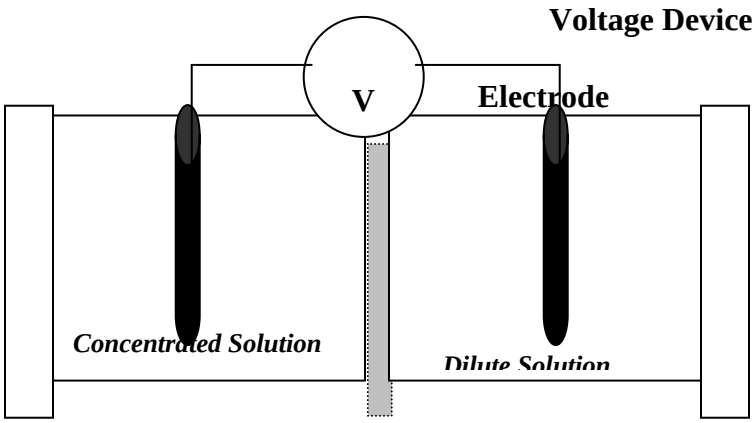

Figure 4-1: Schematic of the electrochemical potential test equipment

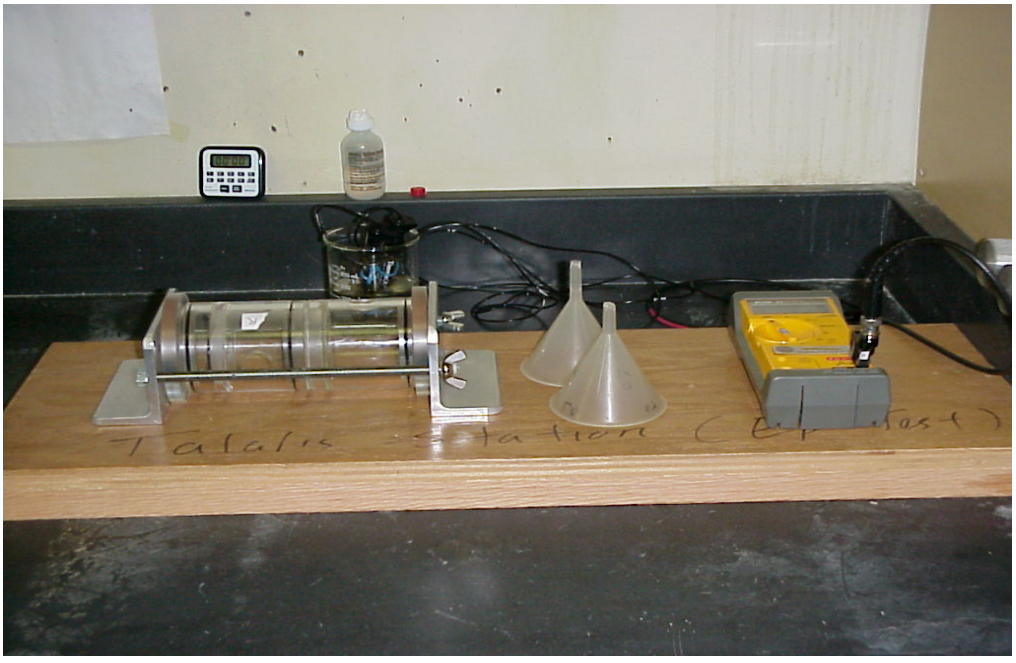

Figure 4-2: Photo of the electrochemical potential test equipment

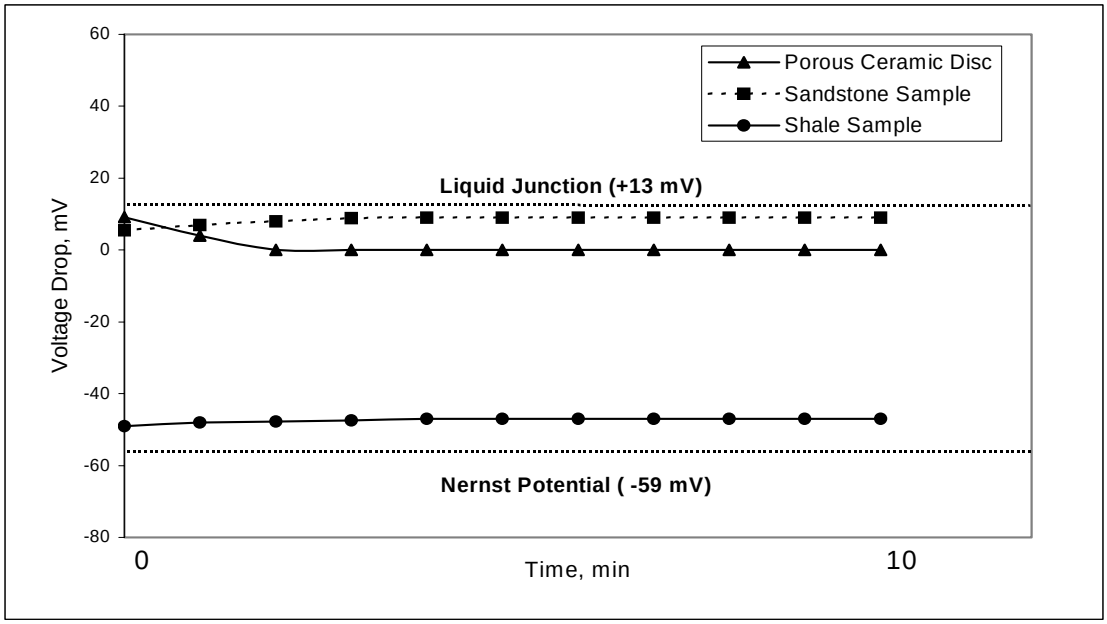

Figure 4-3: Diffusion potential development when porous ceramic disc, sandstone sample and shale sample separated two NaCl solutions of concentrations 0.1M and 1M

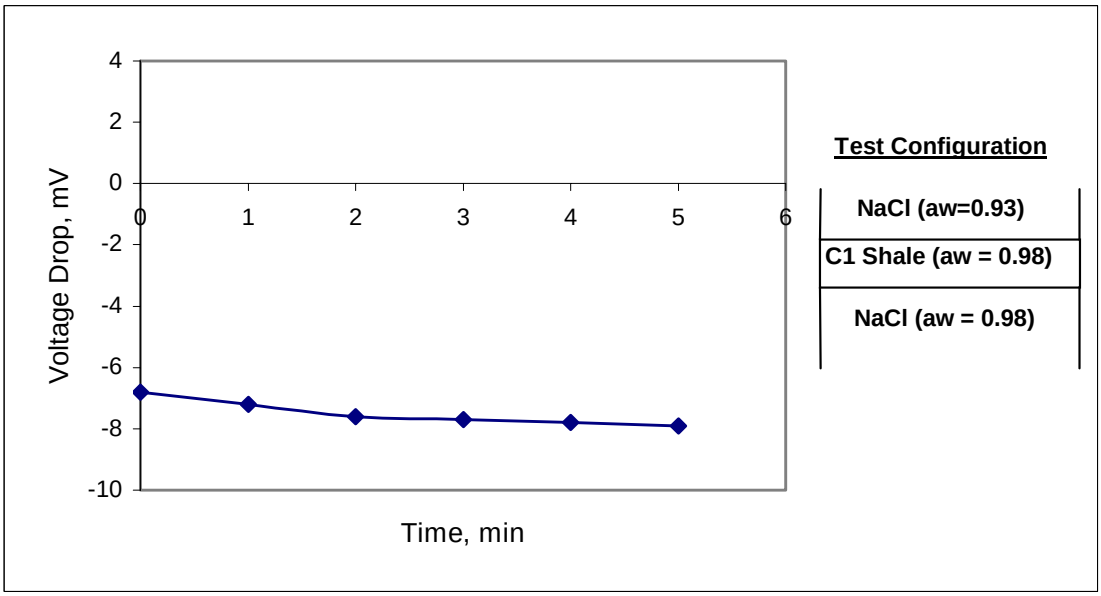

Figure 4-4: Voltage drop measurement for C1-shale (a_w = 0.98) during interaction with NaCl solutions of water activities of 0.93 and 0.98

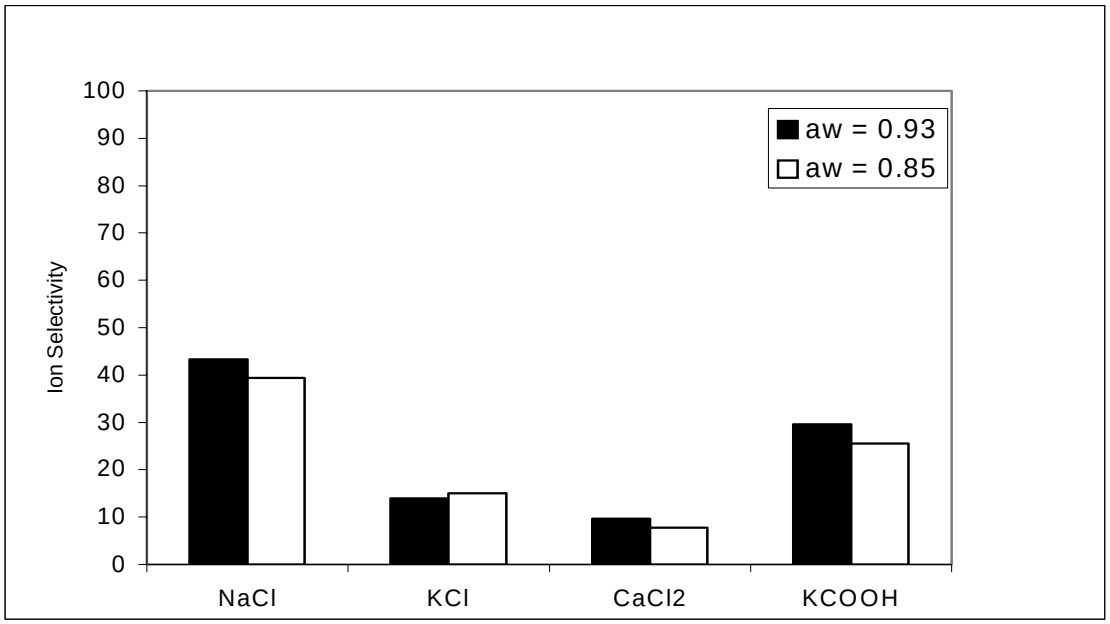

Figure 4-5: Ion selectivity for C1-shale during interaction with different salt solutions of different water activities.

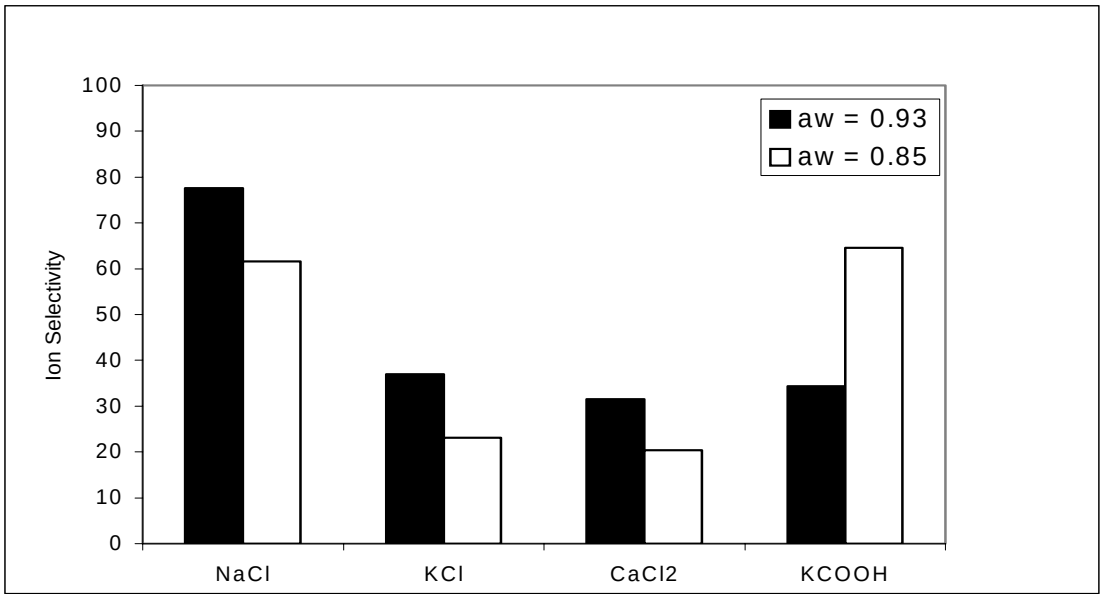

Figure 4-6: Ion selectivity for C2-shale during interaction with different salt solutions of different water activities.

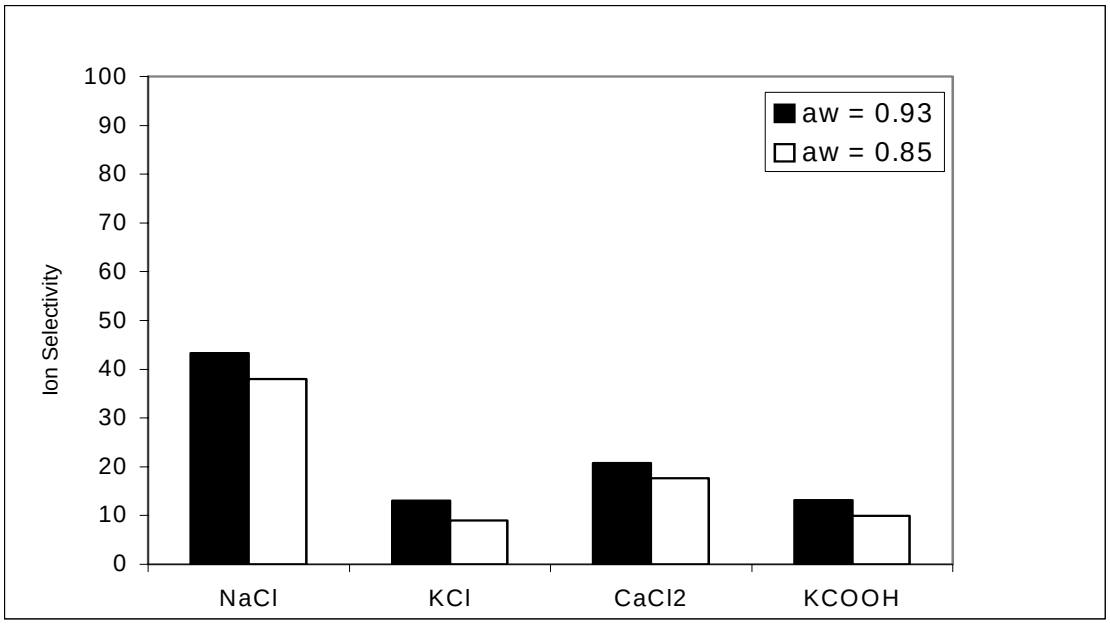

Figure 4-7: Ion selectivity for Pierre shale during interaction with different salt solutions of different water activities.

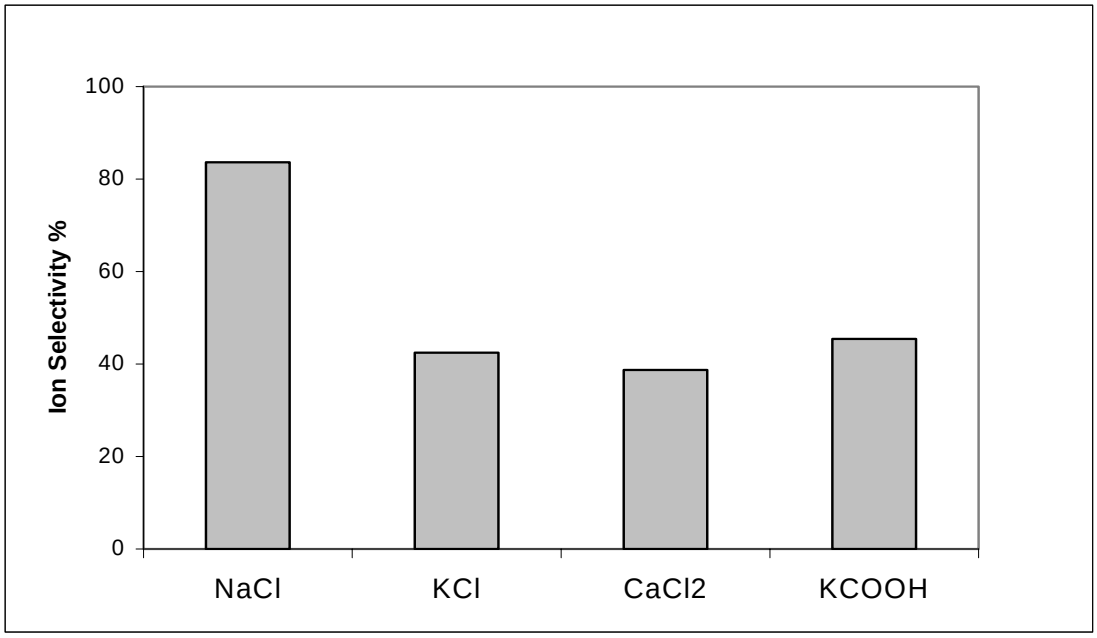

Figure 4-8: Ion selectivity for Arco-China shale during interaction with different salt solutions of different water activities.

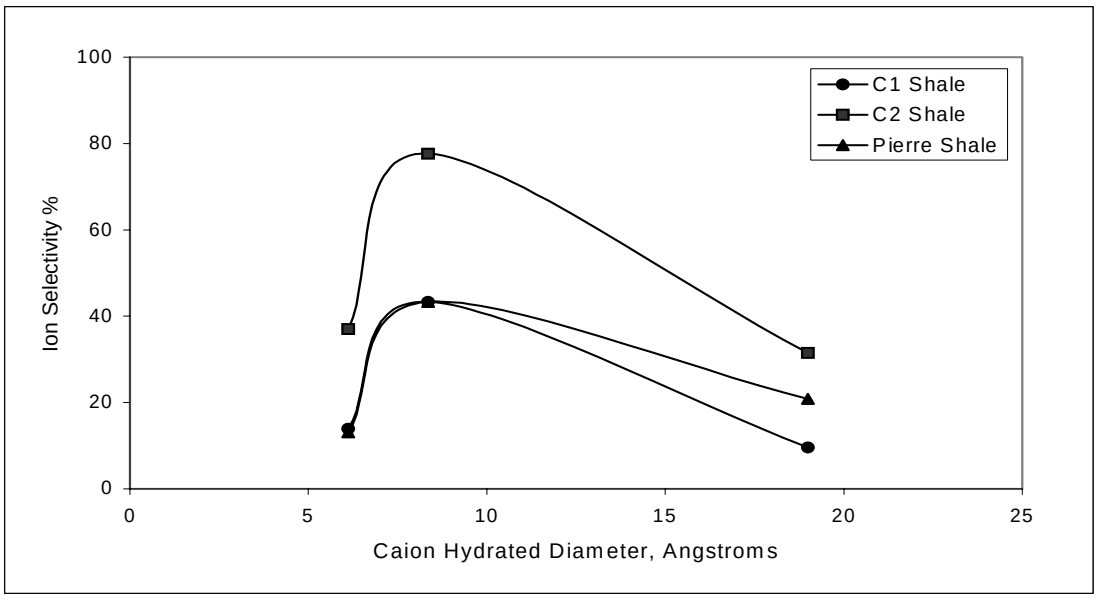

Figure 4-9: Ion selectivity of different shales when exposed to different cations of 0.93 water activity.

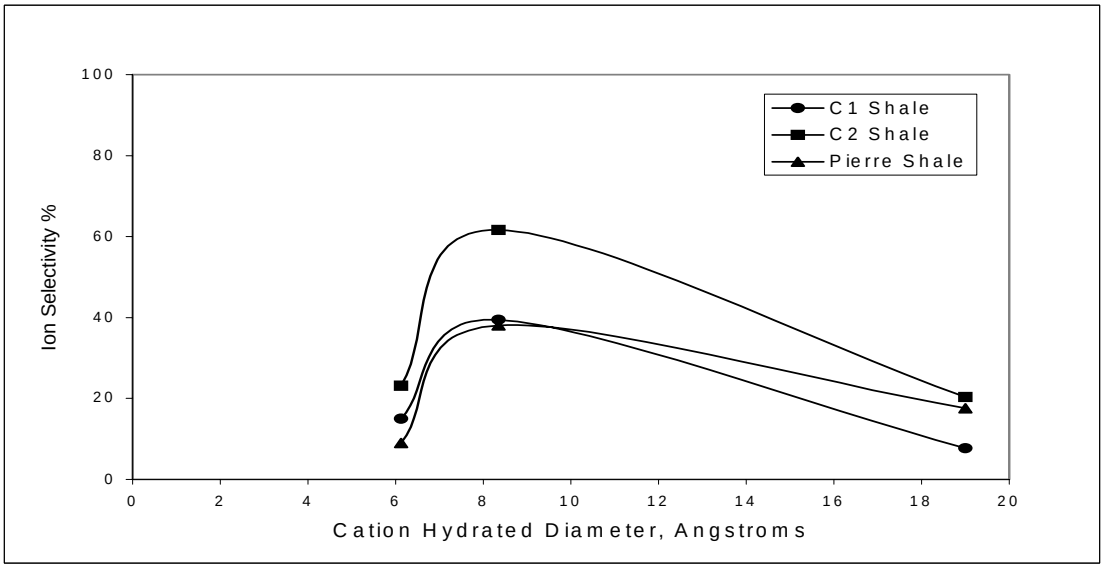

Figure 4-10: Ion selectivity of different shales when exposed to different cations of 0.85 water activity

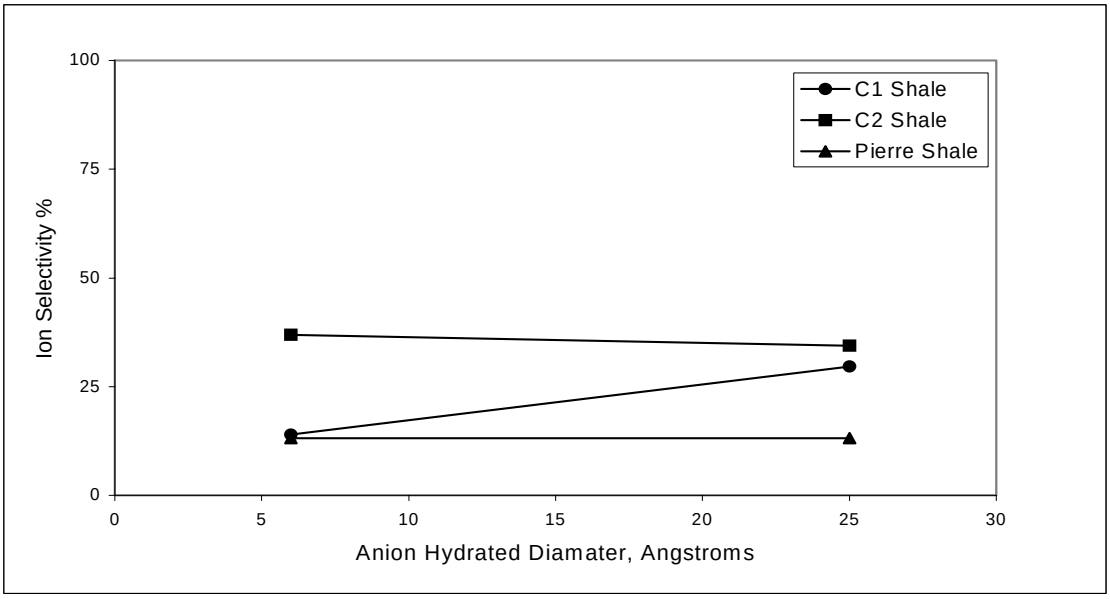

Figure 4-11: Ion selectivity of different shales when exposed to different anions of 0.93 water activity

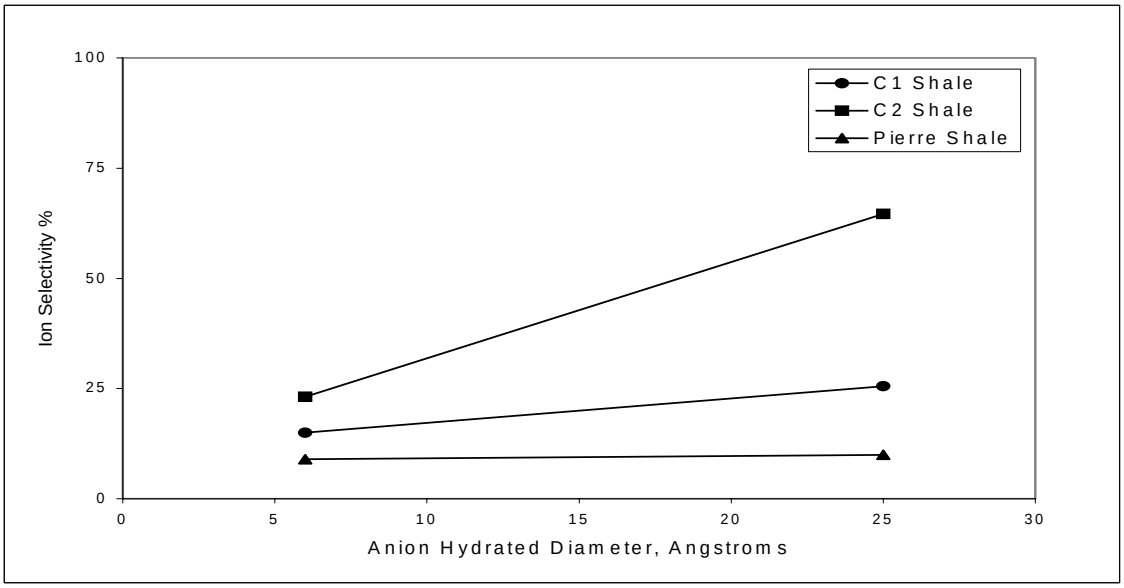

Figure 4-12: Ion selectivity of different shales when exposed to different anions of 0.85 water activity

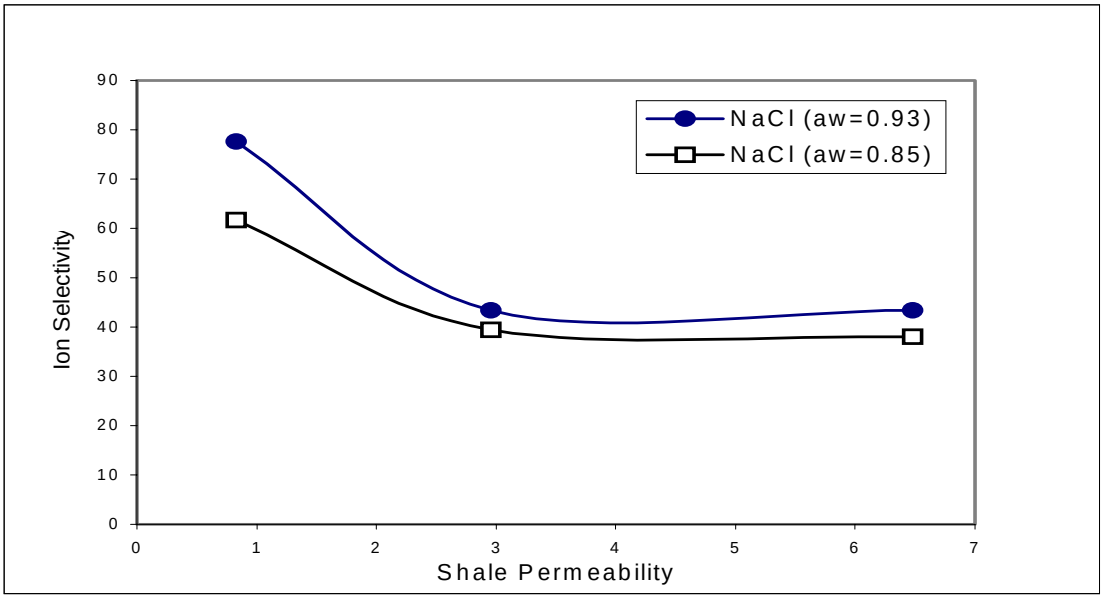

Figure 4-13: Ion selectivity as a function of shale permeability when shales interacted with NaCl solutions of different water activities

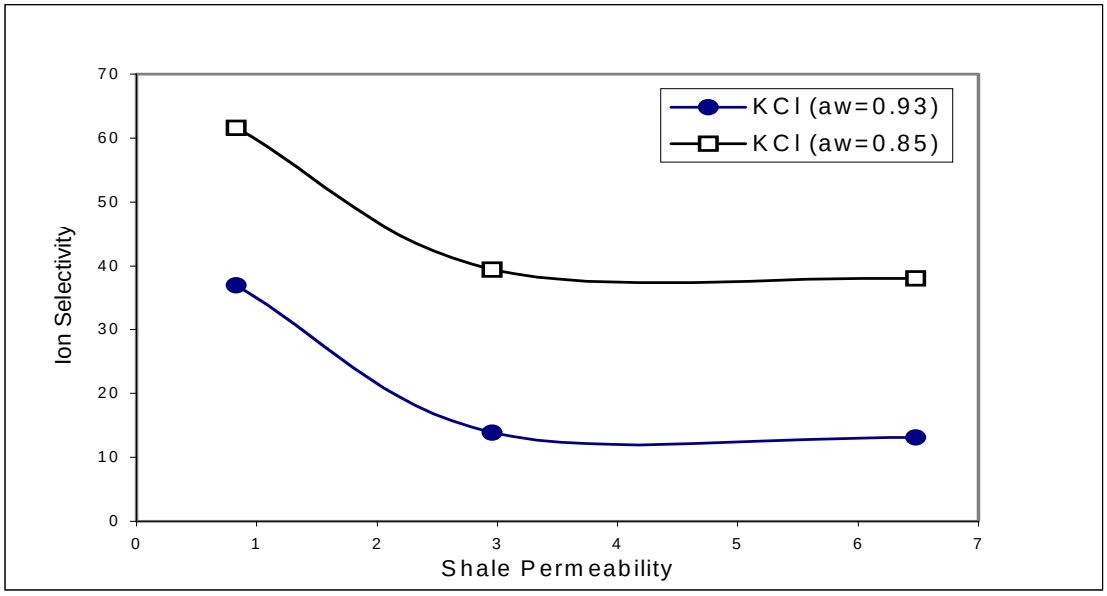

Figure 4-14: Ion selectivity as a function of shale permeability when shales interacted with KCl solutions of different water activities

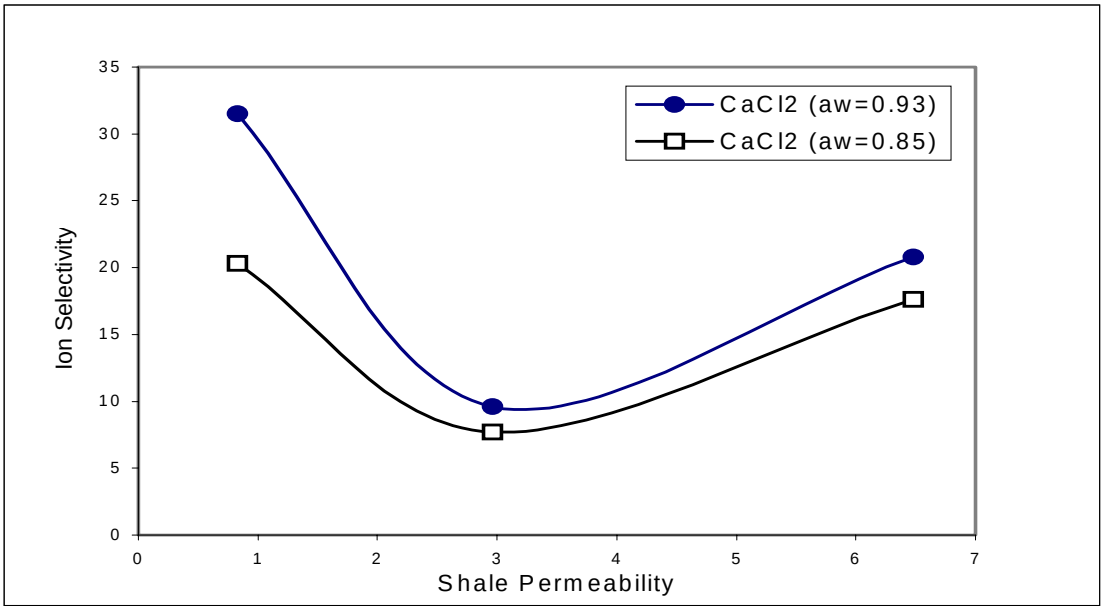

Figure 4-15: Ion selectivity as a function of shale permeability when shales interacted with $CaCl_2$ solutions of different water activities

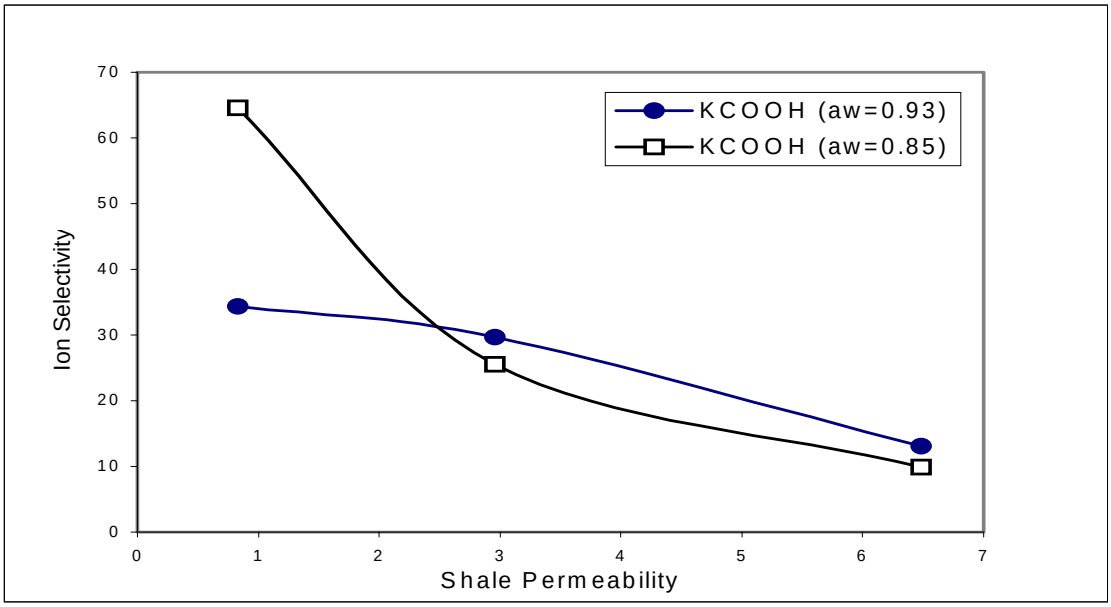

Figure 4-16: Ion selectivity as a function of shale permeability when shales interacted with KCOOH solutions of different water activities

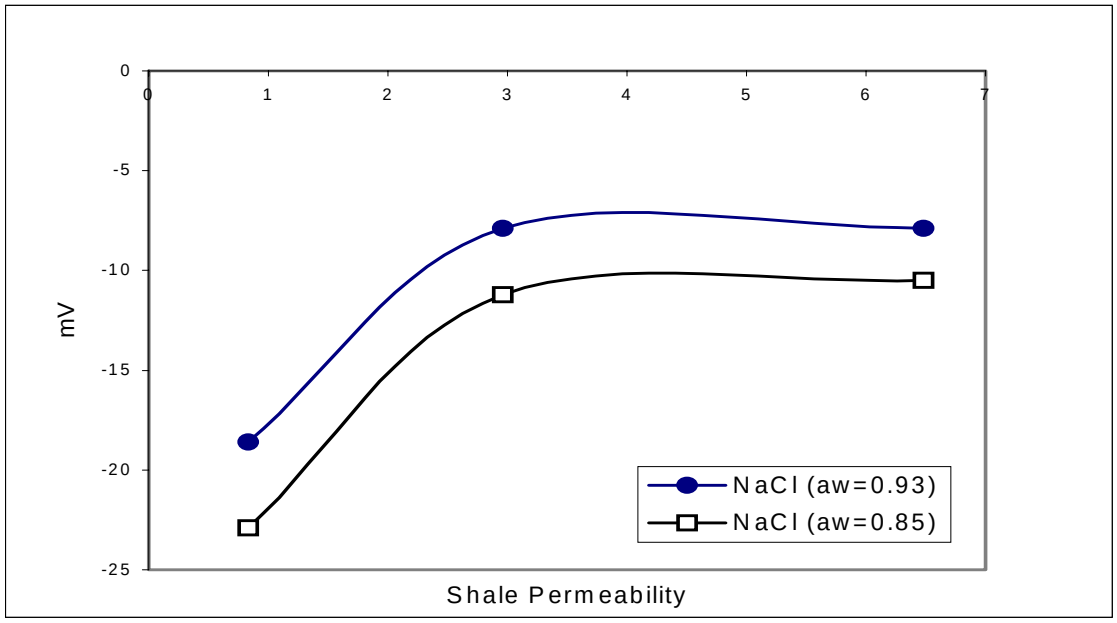

Figure 4-17: Voltage as a function of shale permeability when shales interacted with NaCl solutions of different water activities

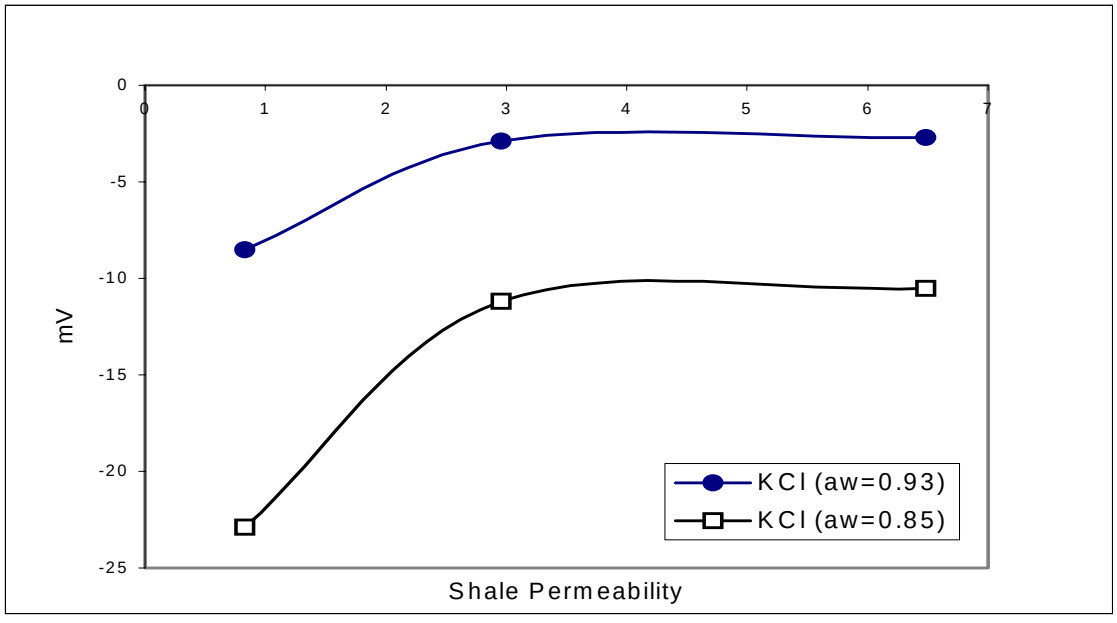

Figure 4-18: Voltage as a function of shale permeability when shales interacted with KCl solutions of different water activities

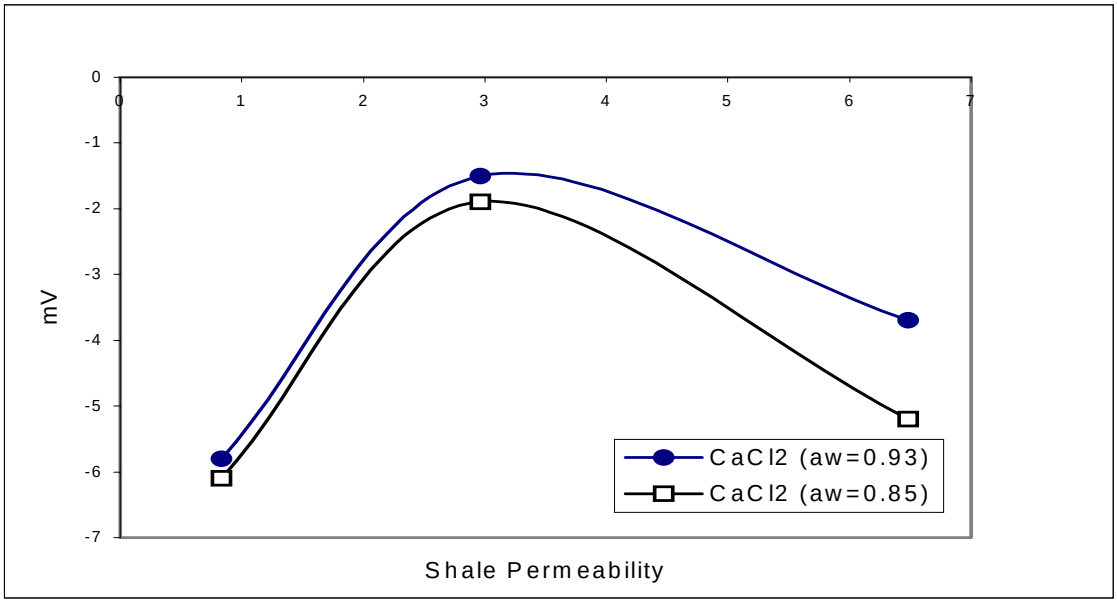

Figure 4-19: Voltage as a function of shale permeability when shales interacted with $CaCl_2$ solutions of different water activities

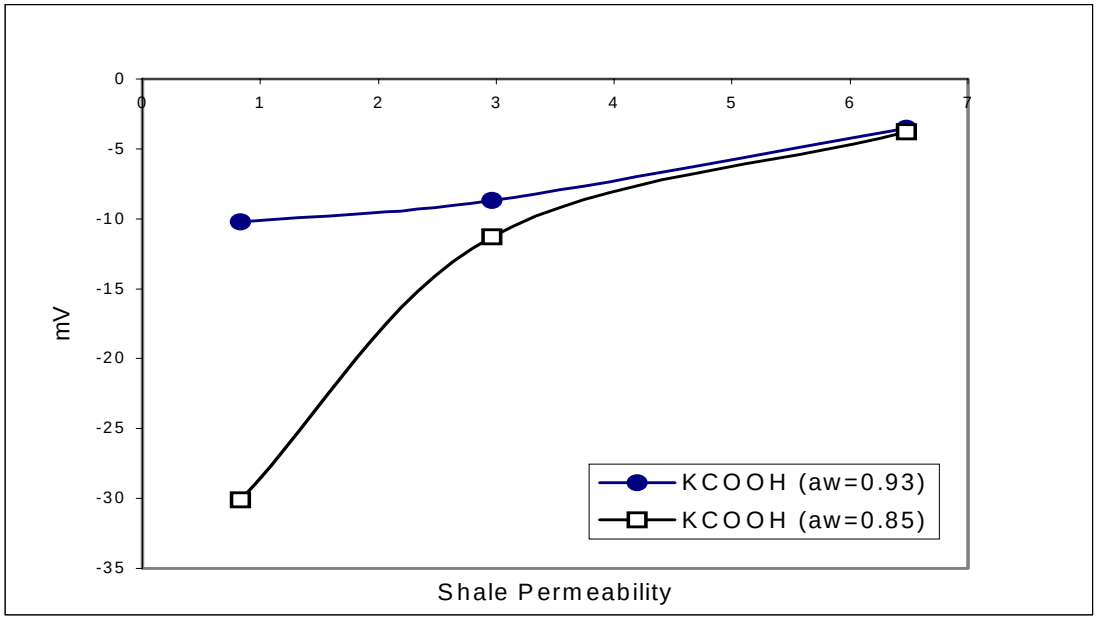

Figure 4-20: Voltage as a function of shale permeability when shales interacted with KCOOH solutions of different water activities

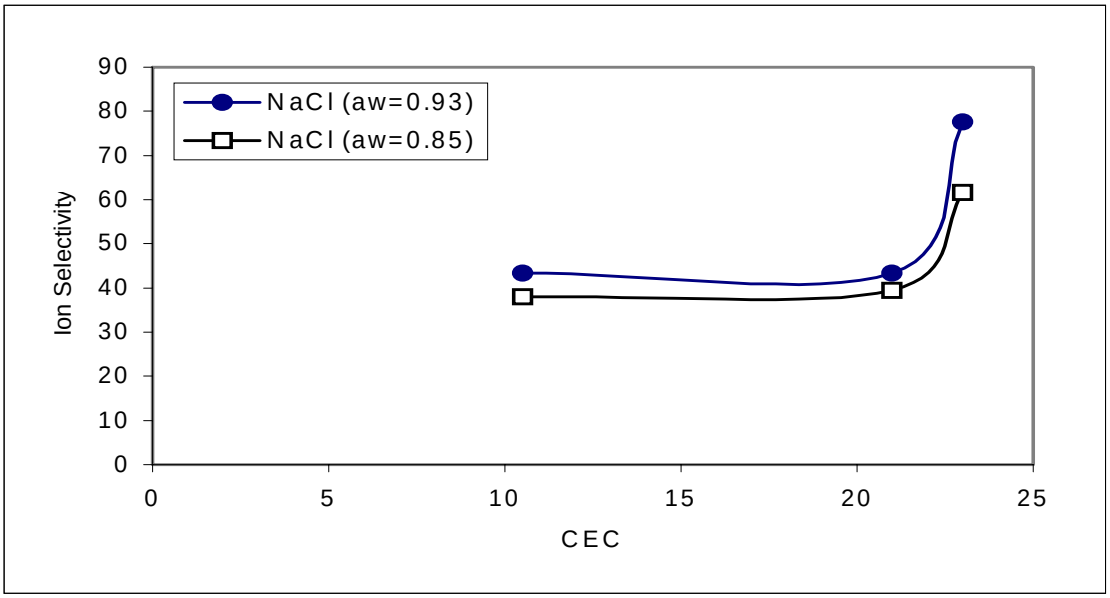

Figure 4-21: Ion selectivity as a function of shale cation exchange capacity when shales interacted with NaCl solutions of different water activities

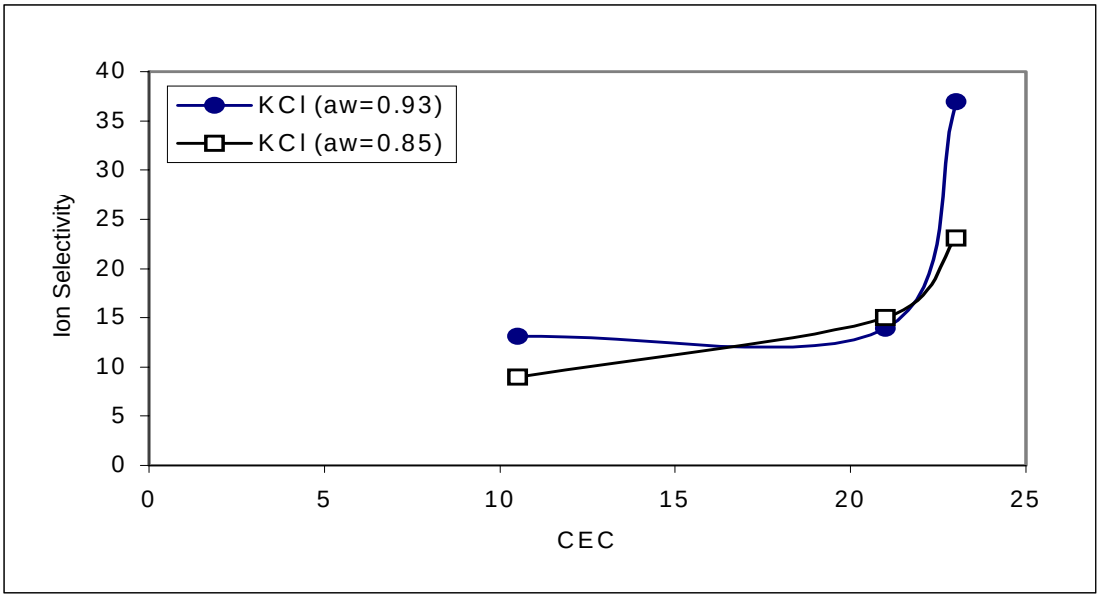

Figure 4-22: Ion selectivity as a function of shale cation exchange capacity when shales interacted with KCl solutions of different water activities.

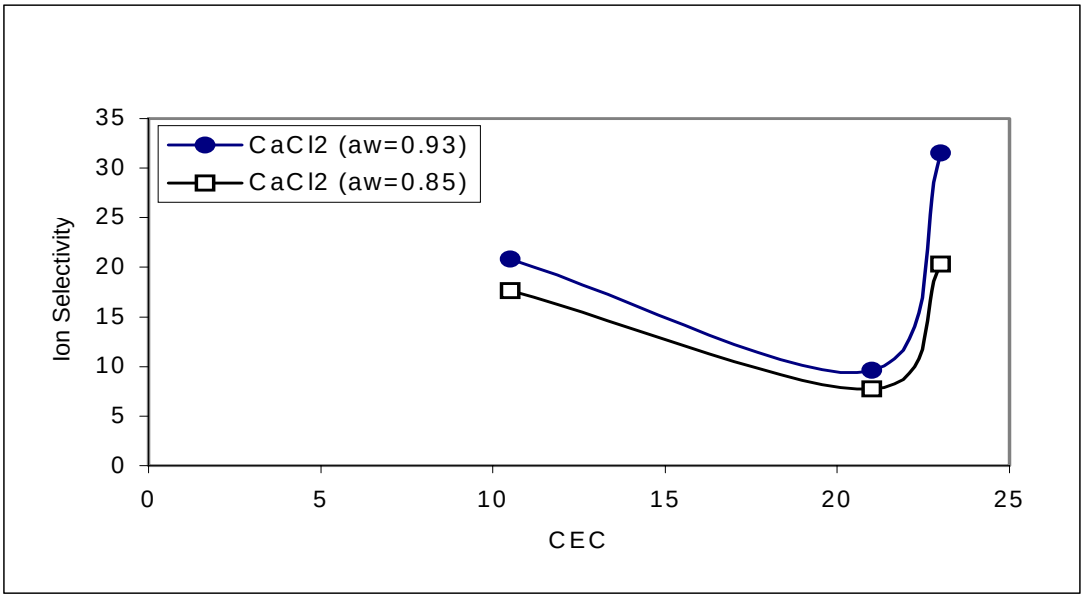

Figure 4-23: Ion selectivity as a function of shale cation exchange capacity when shales interacted with $CaCl_2$ solutions of different water activities

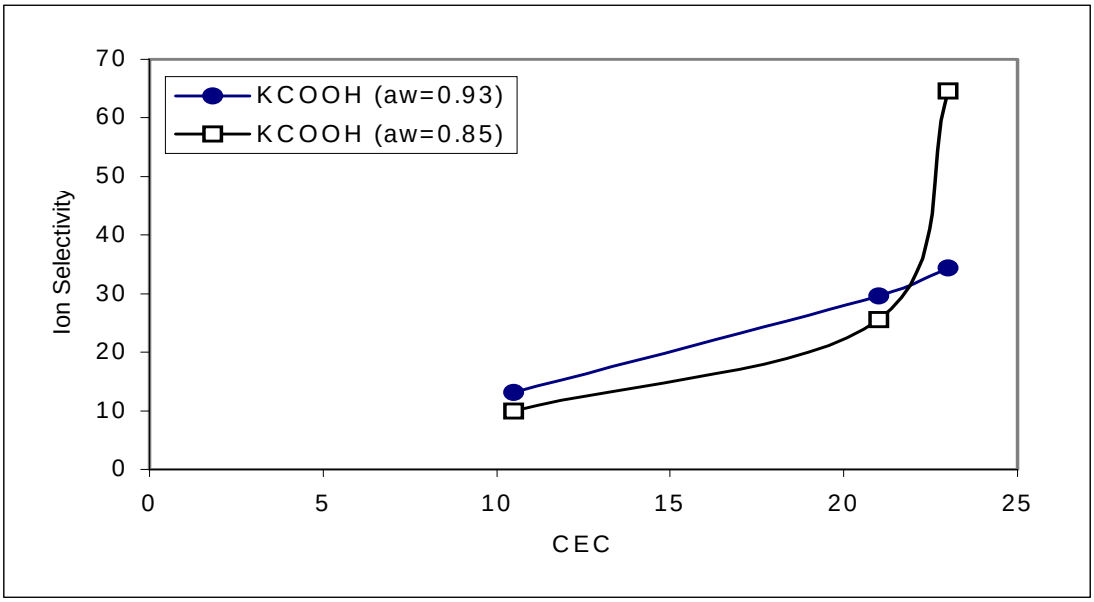

Figure 4-24: Ion selectivity as a function of shale cation exchange capacity when shales interacted with KCOOH solutions of different water activities.

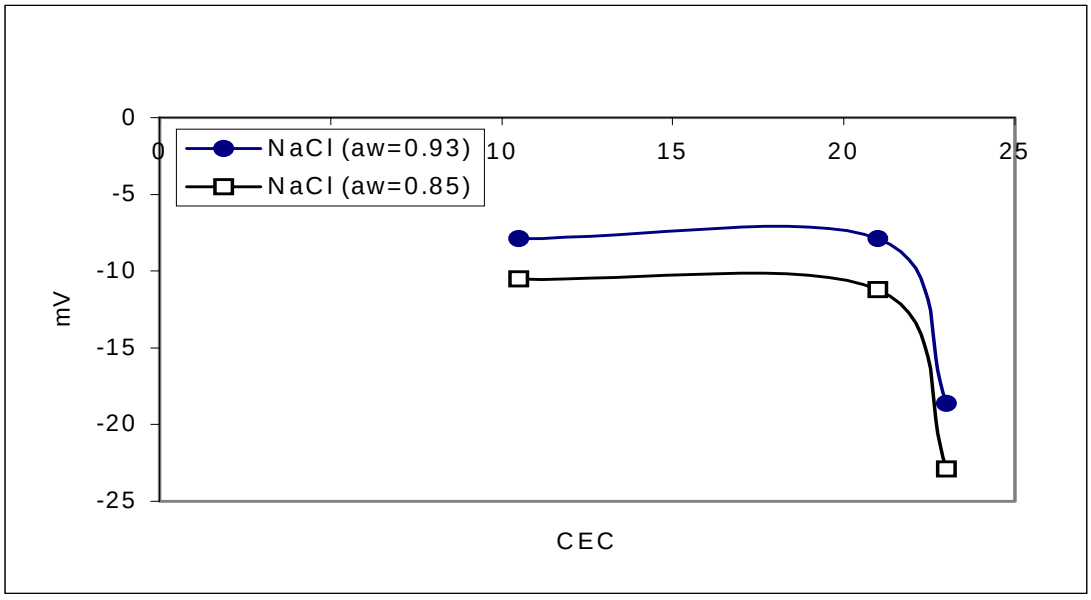

Figure 4-25: Voltage drop as a function of shale cation exchange capacity when shales interacted with NaCl solutions of different water activities.

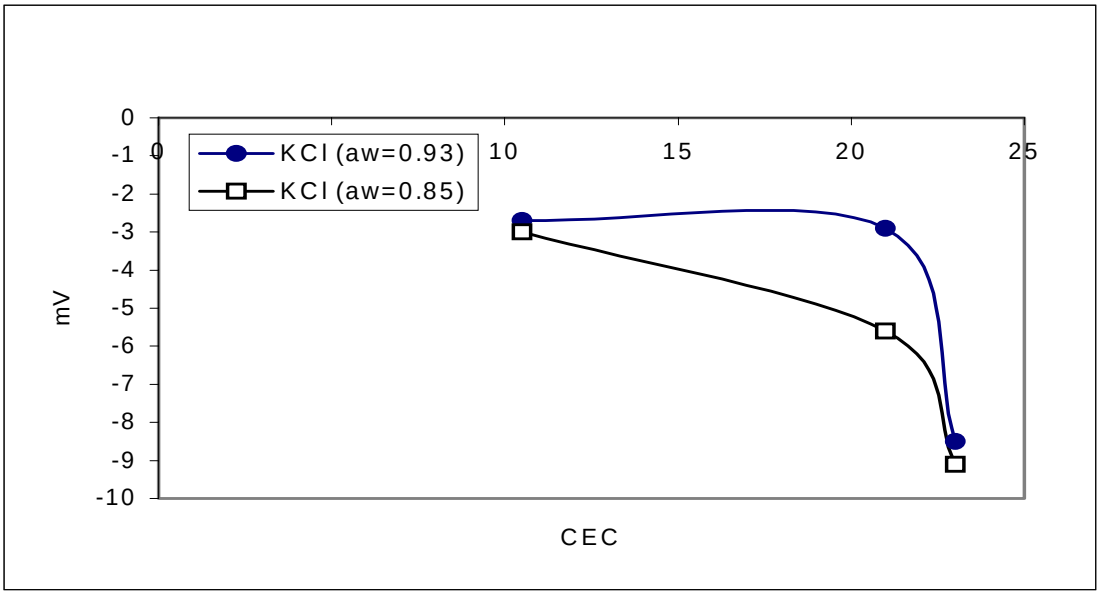

Figure 4-26: Voltage drop as a function of shale cation exchange capacity when shales interacted with KCl solutions of different water activities

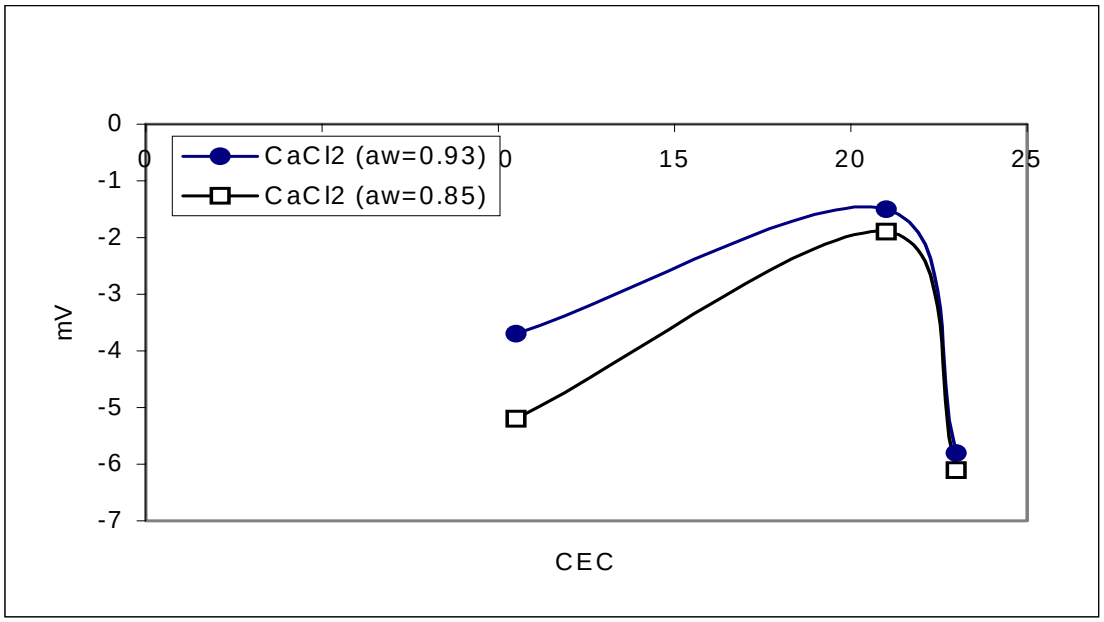

Figure 4-27: Voltage drop as a function of shale cation exchange capacity when shales interacted with $CaCl_2$ solutions of different water activities

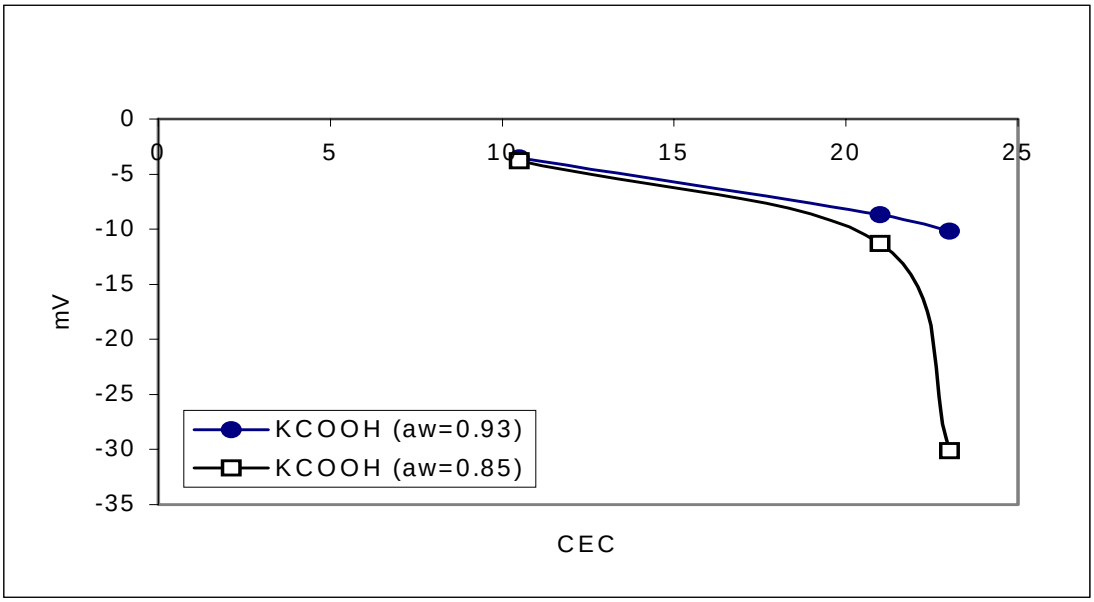

Figure 4-28: Voltage drop as a function of shale cation exchange capacity when shales interacted with KCOOH solutions of different water activities

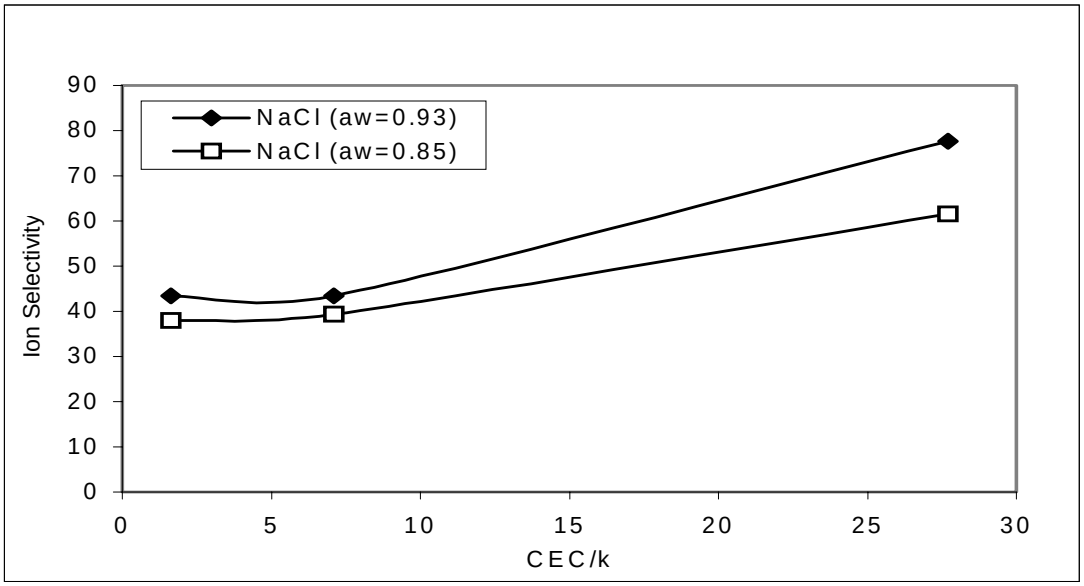

Figure 4-29: Ion selectivity as a function of the ratio of shale cation exchange capacity to shale permeability when shales interacted with NaCl solutions of different water activities.

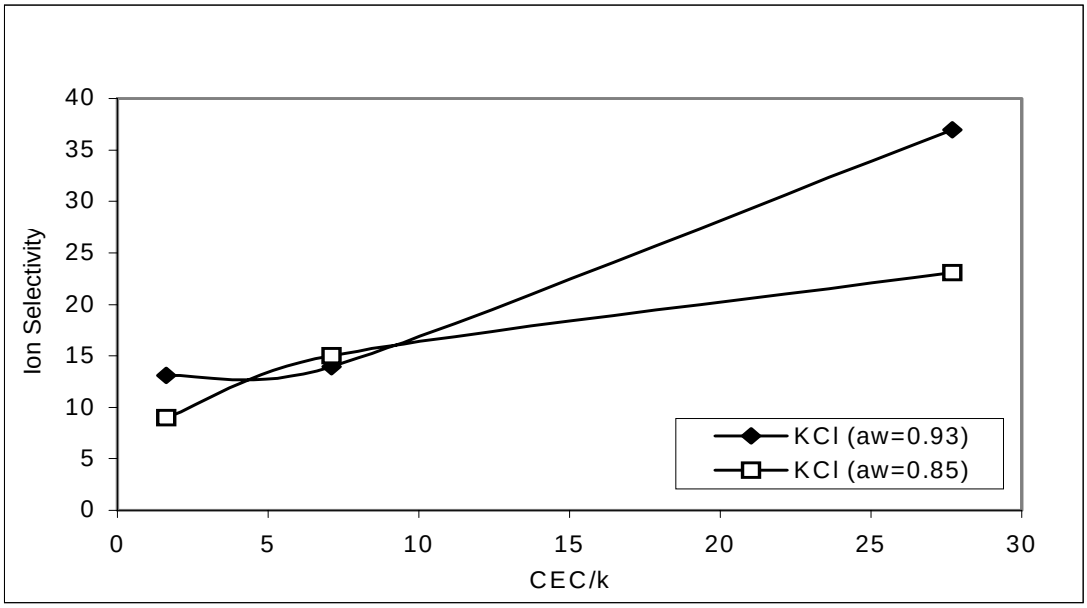

Figure 4-30: Ion selectivity as a function of the ratio of shale cation exchange capacity to shale permeability when shales interacted with KCl solutions of different water activities.

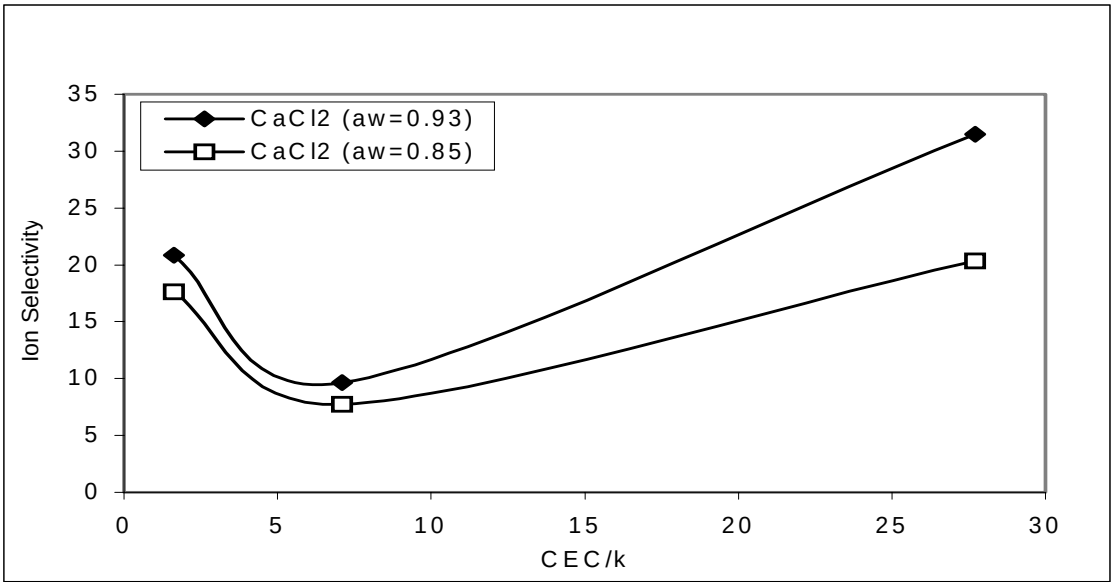

Figure 4-31: Ion selectivity as a function of the ratio of shale cation exchange capacity to shale permeability when shales interacted with $CaCl_2$ solutions of different water activities.

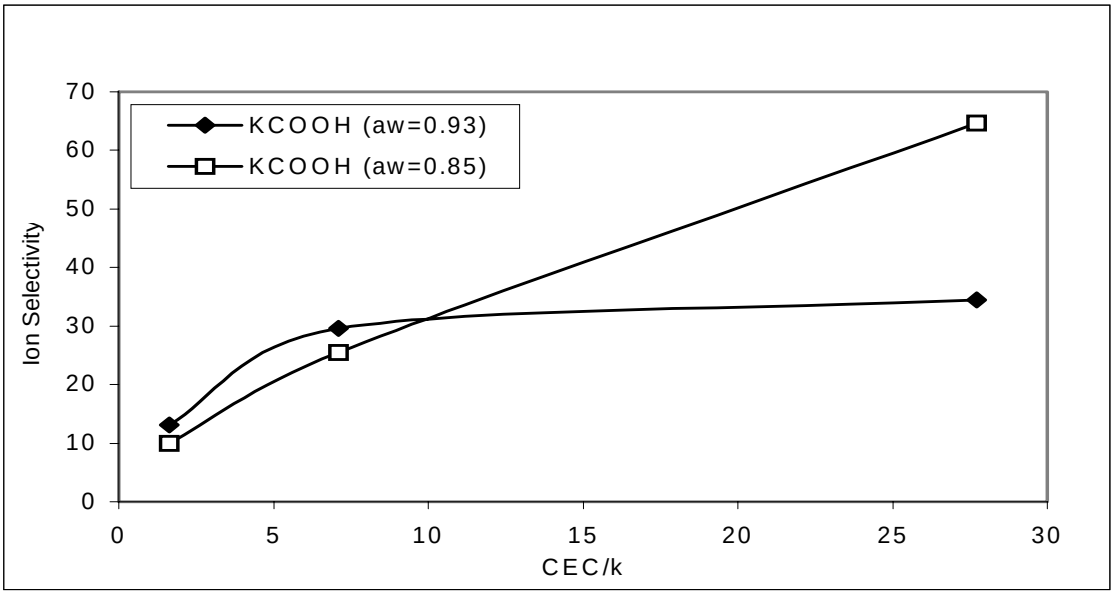

Figure 4-32: Ion selectivity as a function of the ratio of shale cation exchange capacity to shale permeability when shales interacted with KCOOH solutions of different water activities.

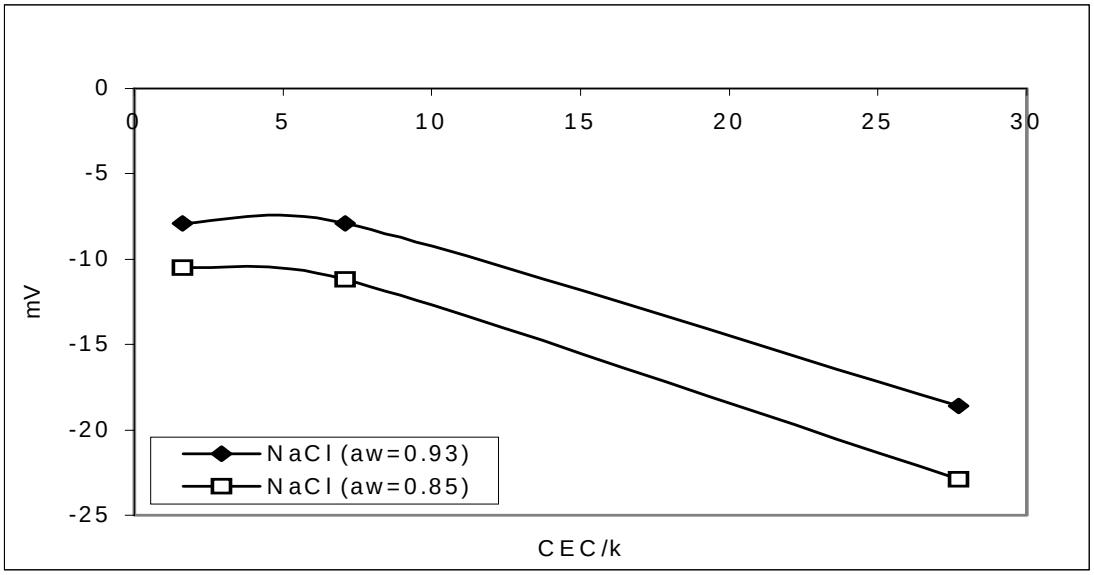

Figure 4-33: Voltage drop as a function of the ratio of shale cation exchange capacity to shale permeability when shales interacted with NaCl solutions of different water activities.

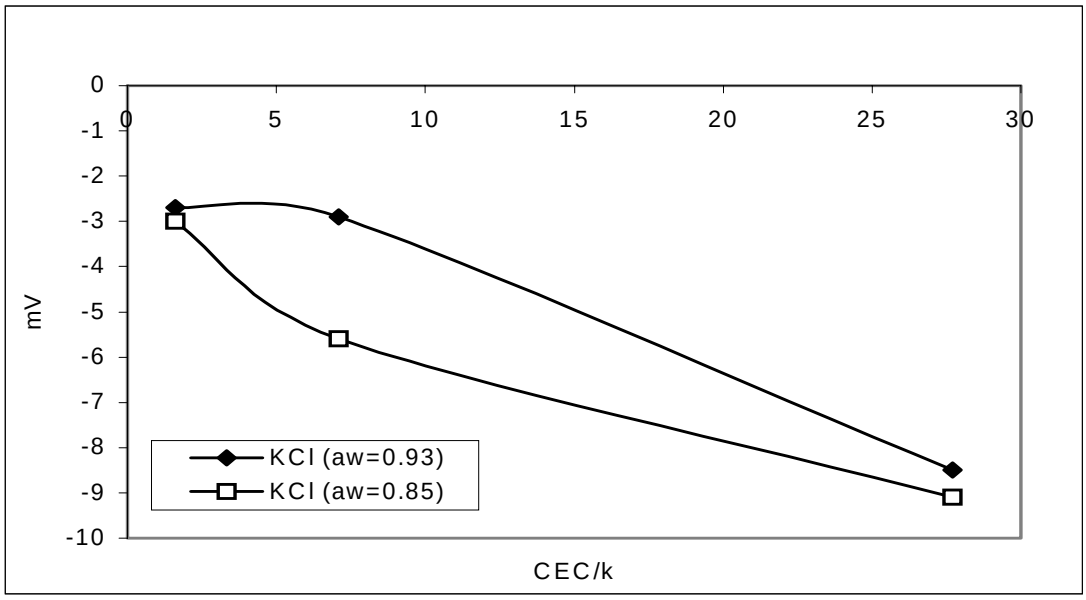

Figure 4-34: Voltage drop as a function of the ratio of shale cation exchange capacity to shale permeability when shales interacted wit KCl solutions of different water activities.

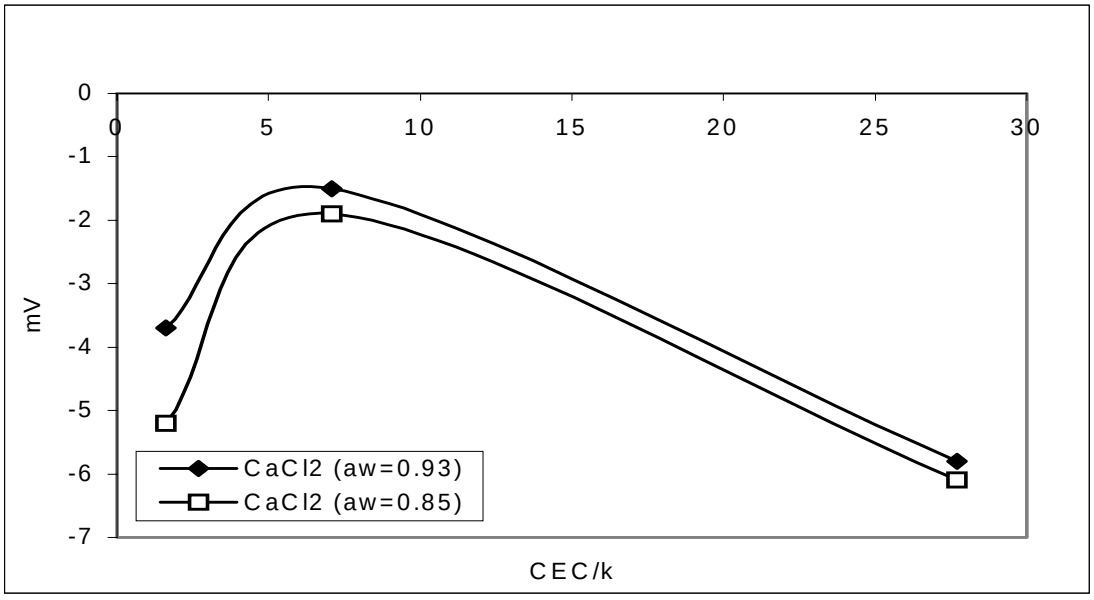

Figure 4-35: Voltage drop as a function of the ratio of shale cation exchange capacity to shale permeability when shales interacted with $CaCl_2$ solutions of different water activities.

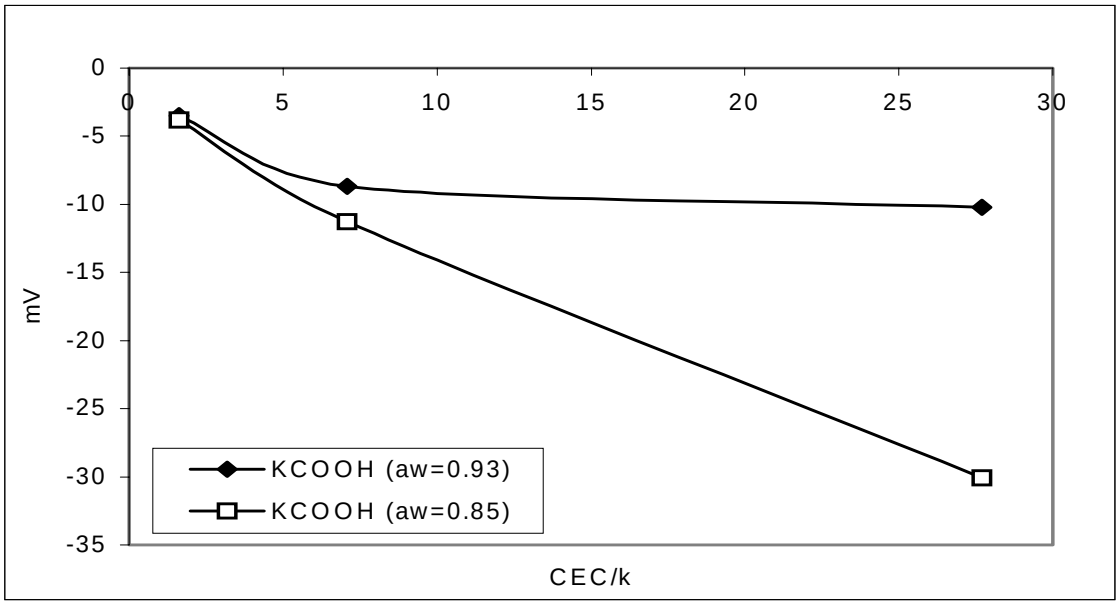

Figure 4-36: Voltage drop as a function of the ratio of shale cation exchange capacity to shale permeability when shales interacted with KCOOH solutions of different water activities.

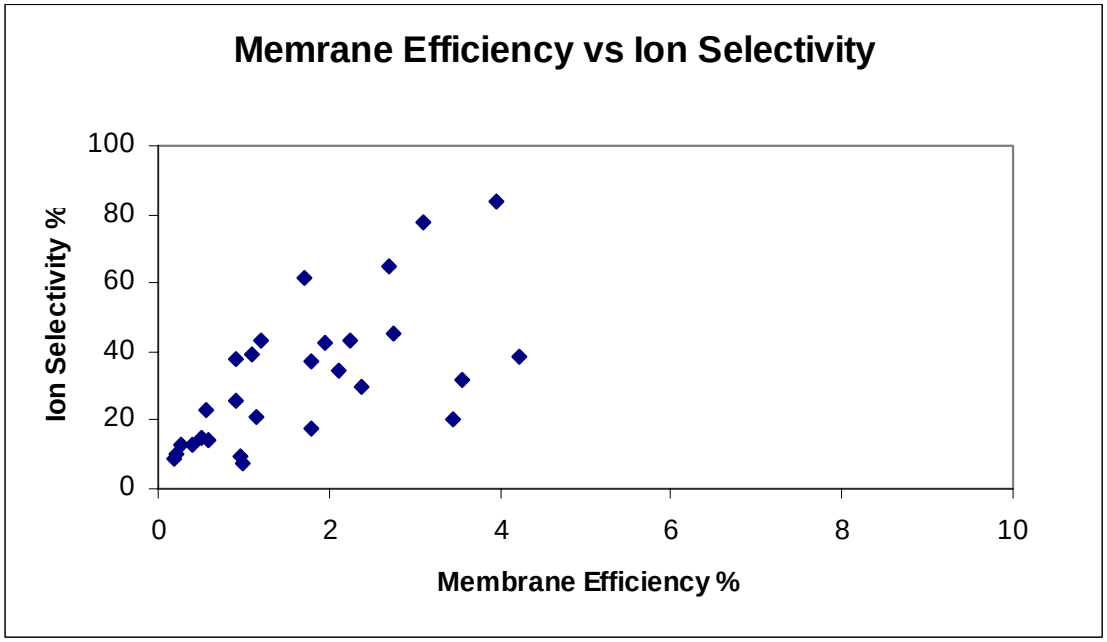

Figure 4-37: Measured ion selectivity versus measured membrane efficiency for all shales.

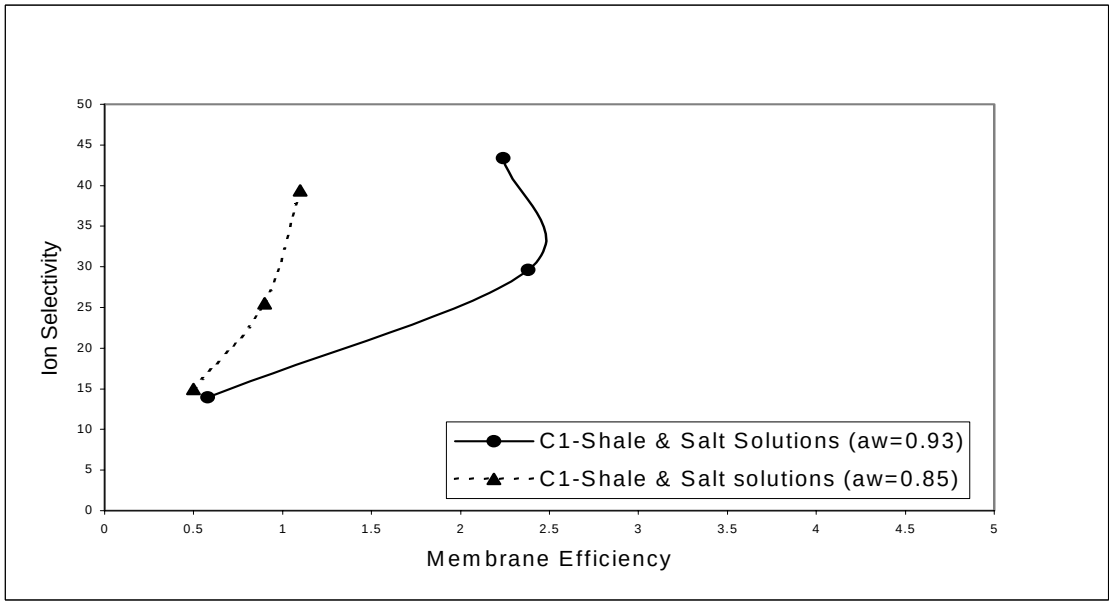

Figure 4-38: The membrane efficiency and ion selectivity relationship when C1-shale interacted with different salt solutions of different water activities

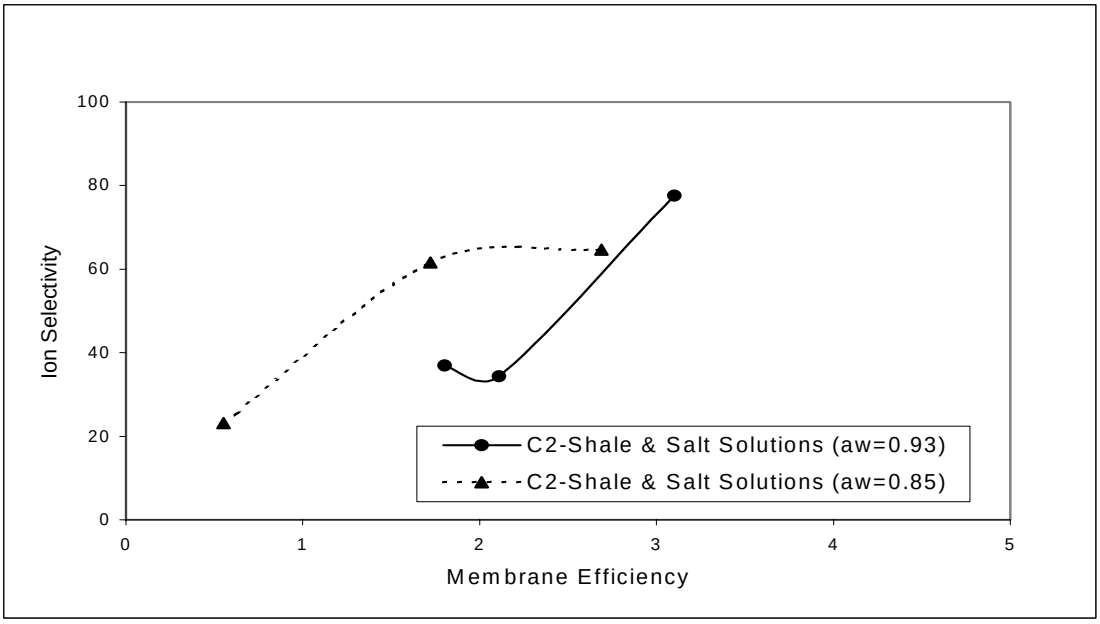

Figure 4-39: The membrane efficiency and ion selectivity relationship when C2-shale interacted with different salt solutions of different water activities

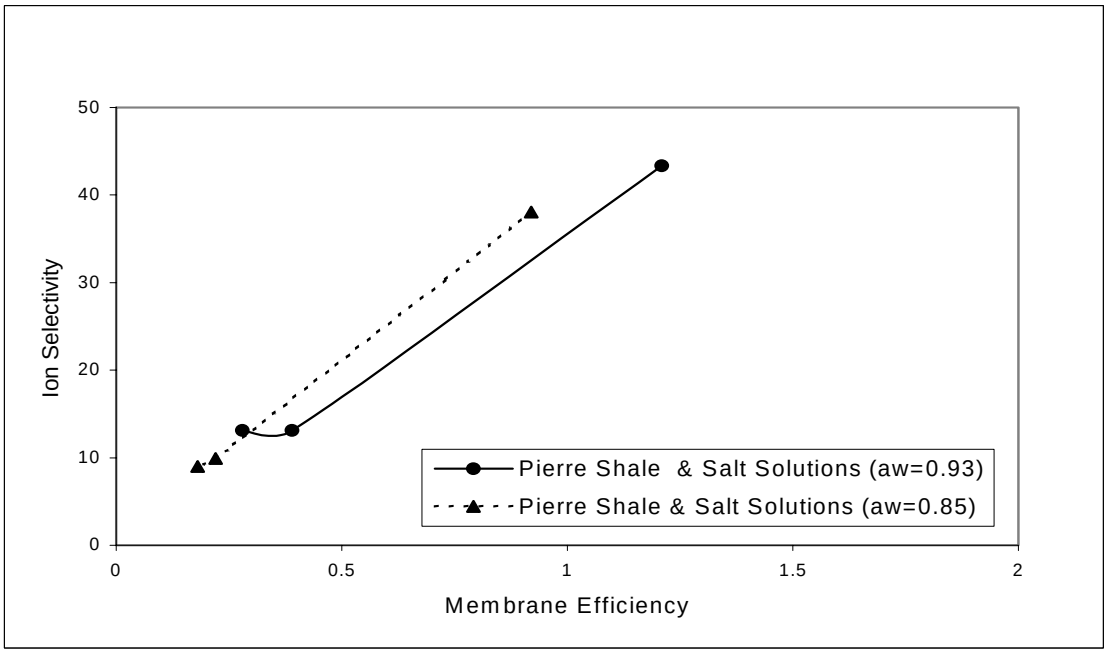

Figure 4-40: The membrane efficiency and ion selectivity relationship when Pierre shale interacted with different salt solutions of different water activities

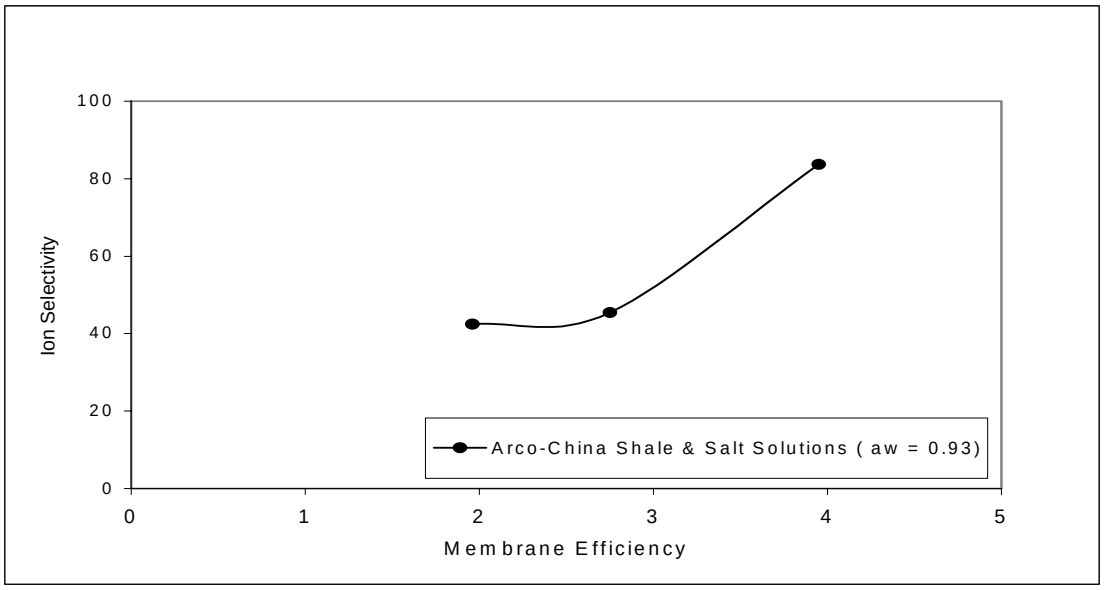

Figure 4-41: The membrane efficiency and ion selectivity relationship when Arco-China shale interacted with different salt solutions of 0.93 water activities

CHAPTER 5

Evaluation of Swelling Behavior and Water and ions Uptake during the Interaction of Shales with Drilling Fluids through Immersion Tests

5.1 INTRODUCTION

When shales interact with water-based muds, both water and ions are allowed to pass through since shales act as leaky semi-permeable membranes. In the absence of a hydraulic pressure gradient, water transport occurs due to osmosis while ion flow takes place due to ionic diffusion. The flow of water into shales results in shale swelling, pore pressure increase and strength reduction, (Mody and Hale, 1993). The flux of ions into shale may change the ionic concentration and composition of the shale pore fluid which could affect the shale matrix mechanical properties and result in shale expansion (swelling), cohesion degradation, weakening of cementing bonds and overall rock strength reduction, (Fam and Dusseault, 1998). It is widely believed that osmotically extracting water out of shales (dehydration of shales) could lead to an increase in shale strength and thus avoid wellbore failure.

The adverse effects of water and ion fluxes on shale have generated a lot of attention and research. Although both effects were well accepted and recognized, shale swelling due to water adsorption received the most attention. Shale swelling measurements were employed since the 1970's in order to study shale and drilling fluid compatibility. The effect of ion flux on shale was not thoroughly investigated despite its importance.

This chapter addresses shale swelling and water and ion uptake when shale interacts with water-based and oil-based muds using immersion and gravimetric techniques. Section 5.2 discusses the background and presents a literature review on shale swelling. In Section 5.3, a full description of the immersion test is given. More specifically, the test definition, objectives, experimental procedure and test matrix are addressed. Section 5.4 analyzes the experimental results for shale interaction with both water-based and oil-based muds. Finally, Section 5.5 draws conclusions and makes recommendations based on the experimental results.

5.2 BACKGROUND AND LITERATURE REVIEW

Shale swelling has long been considered as a direct measure of shale reactivity to drilling fluids. Chenevert (1970) points out that reactive shales tend to adsorb water from drilling fluid if their chemical potential (water activity) is less than that of the drilling fluid and this leads to shale expansion (swelling). This concept has led Chenevert to develop the balanced activity theory in 1970. The balanced activity theory was successfully exploited using oil-based muds. Shales drilled with oil-based muds that have the same or smaller water activity remained stable during drilling. However, this theory did not prove as successful with water-based muds. This is due to the flux of ions into or out of shale due to concentration imbalances.

At first, shale failure was mainly attributed to shale swelling resulting from water adsorption. Many researchers have focused on shale swelling due to water adsorption in order to understand and combat shale failure. Chenevert (1970) studied the effects of water adsorption on shale samples. He found that all the shale samples tested were

altered as a result of water adsorption, especially montmorillonitic shales. He concluded that adsorption by confined shale samples generated internal stresses, which led to compressive strength reduction and ultimately shale failure by either hydrational spalling or vertical fracturing. Building on Chenevert's approach, Bird (1984) conducted some swelling tests on clay minerals. He claimed that the adsorption of water on reactive clay minerals such as smectite provoked a reversible volume increase of the mineralogical structure, which may exceed 80% as demonstrated by measures of the spacing between adjacent clay platelets, which may vary between 10 and 18 Angstrom. This increase occurred in a stepwise manner whilst the weight gain due to water adsorption was monotonous as the water molecules are adsorbed on the surface of the platelets in an ordered way. Low (1987) took a microscopic approach to understanding shale swelling. He directly measured the swelling pressure versus clay platelet distance. The following points can be summarized from his work: (1) DLVO theory predicts a much lower disjoining (or swelling) pressure than the test data, and it is not valid for very close clay platelets. (2) As the clay platelets get closer, the disjoining pressure increases non-linearly. (3) He proposed a model in which the swelling pressure is proportional to the distance in logarithm; but it will predict an infinite pressure when the distance between clays completely vanishes. (4) There is still no theory that can successfully predict the disjoining pressure based on scientific principles. Recently, Steiger (1993) investigated the hydrational behavior of shale by measuring the swelling pressures and strains, which result when shale samples are exposed to different drilling fluids with different water activities. In his test, he placed shale samples within a triaxial load apparatus. The shale samples were exposed to a test fluid in a single stage test or to several test fluids in a multi-stage test. His multi-stage tests showed that the swelling pressures could be controlled by the addition of potassium to the test fluids contacting the shale samples. In

fact, his tests further showed that increasing the concentration of potassium chloride in the test fluid could reduce the swelling pressures to zero. This is in line with field observations, which indicates that the presence of potassium in the drilling fluid helps in controlling wellbore stability problems in shales. Pernot (1999) investigated the phenomena that control shale-swelling pressures. His work attempted to quantify the swelling pressure effect of various fluids in contact with a cretaceous age shale named "Speeton" and a Pleistocene age type of shale named "Gumbo". In his study, he tried to understand the driving mechanisms behind the swelling phenomena. He concluded that methylglucoside stops the swelling of Gumbo shale by possibly creating a barrier, which blocks the flow of ions and water in and out of the shale. He further concluded that lowering the water activity of Speeton shale by adding salt could greatly reduce the swelling pressure.

The above-mentioned studies all agreed that shale swelling occurred when the shale adsorbed water and this happened when the shale had a lower water activity than the test fluid. As a result, all these studies recommended using concentrated drilling fluids in order to prevent shale hydration. Other researchers came to the same conclusions and made similar recommendations.

While these studies provided evidence that shale swells due to water adsorption as a result of a chemical potential difference, other studies doubt these findings. Some researches believe that mishandling of shale could induce capillary effect that could be mistaken for swelling. Forsans and Schmitt (1994) criticized osmotic theories based on laboratory experiments. They stated that capillary effects could greatly alter the shale samples being tested, which in turn lead to misleading data, and possibly wrong interpretations. They introduced a procedure on how to handle shale samples in laboratory testing. They cautioned that improper handling of shale samples could lead to

biased theories, which could have serious consequences if used for field purposes. Similarly, Chenevert and Amanullah (1997*)* showed that shales must be preserved at their native water content if accurate physical measurements are to be made. Their swelling data showed that shales that were altered during handling (hydrated or dehydrated) did not respond properly even when restored to their native hydration conditions. They further argued that the altered shales tend to experience excessive swelling compared to shales that were kept at their native water content.

Santarelli and Carminati (1995) conducted a two-year critical review on all publications that studied swelling and expansion when shale comes in contact with aqueous solutions. Their review revealed that most experimental observations performed in the laboratory were not representative of downhole conditions as air or water vapor had been introduced in the samples, leading to capillary phenomena which have been mistaken for swelling. According to their study, true swelling is unlikely to be an issue downhole. Horsud et al (1998) investigated swelling pressure phenomenon in shale formations. They concluded that the presence of capillary pressure is the main driving mechanism for shale swelling. They stated that osmosis did not play a role in the development of swelling pressure. Santos and Perez (2001) conducted some immersion tests to investigate the behavior of preserved shale samples when immersed in different solutions, trying to identify the importance and relevance of osmosis as well as the effect of other components in the mud, such as mud emulsifiers. Their results showed that the mud salinity was not the only important parameter that controls osmosis. They also showed that shale swelling did not follow the osmotic theory, which led them to believe that other phenomena could play a role in shale swelling.

While the effect of water flux on shale swelling and failure has gained considerable interest, the flux of ions have been generally ignored. Ignoring the effect of

ion flux on shale stability led to the concept of using concentrated salt solutions for shale drilling. While this approach may have worked for some salts such as KCl, it did not work for other salts. In fact, many argue that the flux of ions into shale could have a detrimental impact on shale strength (Ghassemi et al, 2001 and Fam and Dusseault, 1998). Chenevert (1989) argued that sufficient addition of salts to the drilling fluid could eliminate the net movement of free water into the shale, but in doing so another problem is created; the hydrated cations now have a potential to move into the shale because of their activity imbalance relative to the activity of the cations in the shale.

We believe that there exists a need to better understand the effects f both water and ions fluxes on shale swelling and stability. In this work, we measured shale swelling during interaction with water-based and oil-based muds using a newly developed immersion technique. Furthermore, we introduced a simple technique that would account for capillary effects and thus make the swelling data more accurate. In addition, we employed a newly developed gravimetric test that would separately quantify the amount of water and ion uptake during the interaction of shales with drilling fluids.

Another important fact is that most swelling tests were conducted under atmospheric conditions, which do not represent downhole conditions. Therefore, results from these tests should only be used as a starting point for designing drilling fluids. Also, there does not exist a simple test that can be used on rig floors to quickly check shale and drilling fluid compatibility. Most swelling tests are either complex or require specific shale sample size and shape that require special coring and handling procedures.

In this work, we studied the influence of water and ion uptake on membrane efficiency and ion selectivity of shale so that a useful and meaningful relationship between water and ion uptake and membrane efficiency can be obtained. Also, we

propose using our immersion and gravimetric techniques at the rig floor (due to their simplicity) to check drilling fluid compatibility with shales.

5.3 IMMERSION TEST DESCRIPTION

5.3.1 Test Definition and Objectives

The immersion test is a test where shale samples are immersed in drilling fluids (water-based or oil-based muds) over 24 hours. During this time, both the immersed and air weights are taken periodically and converted into shale volume using Archimedes principle in order to investigate their swelling behavior as a result of interacting with these drilling fluids. In addition to analyzing shale-swelling response when immersed in different drilling fluids, this test is designed to measure the amount of water and ions gained or lost during shale and drilling fluid (water-based or oil-based muds) interaction. The test objectives are as follows.

- Perform immersion tests to investigate the swelling behavior of shales when interacting with water-based and or oil-based mud of different water activities.
- Measure the amount of water and ion uptake as a result of shale and drilling fluid interactions utilizing immersion and gravimetric techniques.
- Investigate the effect of shale permeability on shale swelling and water and ion uptake during shale and drilling fluid interactions.
- Investigate the effect of shale cation exchange capacity on shale swelling and water and ion uptake during shale and drilling fluid interaction.

- Investigate the simultaneous impact of osmosis and ion diffusion on shale swelling behavior during shale and drilling fluid interactions.
- Study the influence of water and ion uptake on the membrane efficiency and ion selectivity of shale.

This test has many advantages over other swelling tests and procedures. One of the big advantages of this test is that it is easy to conduct since it requires familiar materials and devices that are readily available. More importantly, this test does not require shale samples to be of certain sizes or dimension like other tests. In fact, this test can be run with shale cuttings (provided they are large enough), which can usually be obtained from the shale shakers at the rig.

5.3.2 Test Equipment

Figure 5-1 shows the experimental set-up and equipment that was used in this test. A high-resolution (0.0001g resolution) weight-balance was used to take weight measurements by suspending the shale sample from the bottom of the weight-balance using a very thin plastic wire as shown. The weight-balance is placed on top of a sealed wooden box. Just below the weight-balance, there is a very small opening where the plastic wire is passed through the top of the box to the inside. It is extremely important to maintain a good seal in order to prevent air currents from affecting the weight measurements. Inside the sealed box, a beaker that is full of the drilling fluid to be tested sits on top of a jack-up metal tray. This jack-up metal tray allows us to raise and lower the drilling fluid as desired. The shale sample is always tied gently to the plastic wire. A hair drier is used in this test for drying purposes and a stopwatch is needed for time management.

5.3.3 Test procedure

The following procedure was adopted for performing the immersion test during shale interaction with water-based muds and oil-based muds. The plastic wire is suspended from the paper clip, which is attached to the bottom of the weight balance. The weight balance is zeroed in order to eliminate the inclusion of the plastic wire and the paper clip weights into the immersion test measurements. The shale sample is gently tied to the plastic wire and left suspended in air until the weight balance reading is stable. The weight of the shale sample in air is taken. The shale sample is then momentarily dipped into the beaker, which is full of the drilling fluid to be tested, and immediately raised out of the fluid. The purpose of this step is to measure the amount of drilling fluid that would wet the shale sample. This amount needs to be subtracted from each air weight measurement when conducting the immersion test. During the test, the wetted shale air weight is subtracted from the original air weight in order to obtain the correction factor for all our measurements. We have obtained different correction factors for our tests ranging between 1.5% to 2.5% depending on the size of the shale sample and the type of the drilling fluid. After determining the correction factor, the test is ready to proceed. The following steps are adopted for our tests:

- Obtain a fresh shale sample from the storage can and clean it using hexane in order to remove any surface oil.
- Suspend the shale sample in air using the plastic wire and measure its dry weight. This weight represents the shale's initial dry weight.
- Immerse the shale sample in the test fluid and immediately measure its immersed weight. This weight represents the shale initial immersed weight.

- Repeat the last two steps in order to obtain the shale's dry and immersed weights for different time intervals which are always taken to be 5 minutes, 10 minutes, 20 minutes, 30 minutes, 1 hour, 2 hours, 3 hours, 4 hours and 24 hours. For each time, you need to correct the dry weight measurement using the measured correction factor as mentioned above.
- Calculate the volume of the shale at each time using Archimedes principle:

$$\text{Volume} = (W_{Dry} - W_{Immersed}) / \rho_{Mud} \quad \ldots\ldots\ldots\ldots\ldots\ldots\ldots\ldots\ldots\ldots \quad (6.1)$$

  Figures 5-2 and 5-3 show the weights (dry and immersed) and volume curves when Pierre shale was exposed to NaCl solution of 0.93 water activity.
- At the end of 24 hours, the shale sample is dried out and then heated at 200 F in an oven. After 24 hours, the shale sample is taken out of the oven and weighted again. This is done in order to utilize a newly developed gravimetric technique for measuring the water and ion uptake in the shale sample during the test. The following gives an outline of this technique.

5.3.3.1 Gravimetric Technique

The purpose of this test is to measure the amount of water and ion gained or lost from shales when interacting with drilling fluids. The following describes the procedure employed in this test. A more detailed description of this test can be found in an SPE publication by Zhang et. al. (2004). For this test to be conducted properly, we need to obtain two shale samples.

For the first sample:

- Weigh Sample in air (W_1)

- Dry sample in oven at 200 F for 24 hours and weigh it (W_2)
- The original amount of water present in the sample can be calculated as follows:

  $W_{w0} = (W_1 - W_2)$. …….. (6.2)
- The water content of the sample is:

  $WC = W_{w0}/W_1$. ……..(6.3)

For the second sample:

- Weigh sample in air (W_1).
- Put sample in a plastic bag, which contains the test fluid, for 24 hours. And weigh it (W_2).
- The weight of ions & water added/lost during this interaction can be estimated as follows:

  $W_3 = W_2 - W_1$ ……..(6.4)
- Dry the sample out in an oven for 24 hours at 200 F and weigh it (W_4). In this process, all water (both original and added) will be removed.
- The amount of water removed during the drying process:

  $W_5 = W_2 - W_4$ …….(6.5)
- The amount of water added/lost during the interaction with the test fluid is:

  $W_w = W_5 - WC*W_1$ ……(6.6)
- The weight of ions added/lost during the interaction with the test fluid is:

  $W_i = W_3 - W_w$ ……..(6.7)

Before we can rely upon our immersion tests results, we needed to validate the immersion technique in order to make sure that the test is valid and can be used for shales and drilling fluids as described above.

5.3.3.2 Immersion Test Validation

It is essential to check the validity of our test against other established techniques. Therefore, we proceeded to check the validity of our test against the technique used for linear swelling measurements. In the linear swelling technique, we employed a digimatic indicator, model (ID-E) with measuring range of 10 mm and a resolution of 0.001 mm. In this test, a shale sample is placed in a small bag and then positioned between a movable and a stationary anvil. To ensure a shrinkage indication, the indicator was preloaded by compressing the spring to (0.05 inch) and then zeroed before pouring the test fluid inside the plastic bag. The indicator displays the displacement of the shale over time and this displacement is converted into a swelling or shrinkage measurement by dividing it by the original shale length. A swelling profile for the shale sample is obtained over a given time. It is important to note that in this test, the swelling behaviour is measured in one direction only.

We have performed both linear swelling measurements and bulk volume swelling measurements using our newly developed immersion test on Pierre shale and NaCl, KCl, and $CaCl_2$ solution in order to see if our immersion test shows the same general trend obtained by the standard linear swelling test. While the linear swelling test is mainly concerned with swelling in one direction, our immersion test is a bulk volume swelling measurement where the shale is allowed to swell in all directions. Therefore, the bulk volume swelling percentage should be higher than the linear swelling percentage. It is typically assumed that the bulk volume swelling percentage should be 2.5 to 3 times

higher than the linear swelling percentage for the same shale and drilling fluid.

Figures 5-4, 5-5 and 5-6 show the bulk volume swelling, obtained from our immersion test, and linear swelling of Pierre shale when exposed to NaCl, KCl, and $CaCl_2$ solution respectively. From these graphs, it is seen that swelling profile obtained from both techniques is very similar. It is also seen that the magnitude of the swelling obtained from the immersion test is about 2 to 3 times higher than the linear swelling. Since the swelling trend and magnitude obtained from our immersion tests are reasonable and they correlate very well with the linear swelling test, we believe that our immersion test is valid for shale and drilling fluid interaction studies.

At the end of each test, we employed the newly developed gravimetric technique to estimate the amount of water and ions exchanged during the interaction of Pierre shale with these salt solutions. Figures 5-7, 5-8 and 5-9 show the water and ions exchanged during linear and bulk volume swelling tests when Pierre shale interacted with NaCl, KCl, and $CaCl_2$ solution respectively. These graphs show that the amount of water and ions exchanged during both tests are almost the same, which validates our immersion test technique and procedure.

5.3.4 Test Matrix

In designing the test matrix, we followed the same membrane efficiency and ion selectivity test matrix in order to correlate shale swelling and water and ions uptake data with the measured membrane efficiency and ion selectivity data. Table 5-1 shows the test matrix designed to study the effects of cation type and concentration on shale swelling behavior and water and ion uptake. Table 5-2 shows the test matrix designed to study the effects of anion type and concentration on shale swelling behavior and water and ion uptake. In addition to water-based muds, we performed shale swelling and water and ion uptake measurements during using oil-based muds.

5.4 RESULTS & DISCUSSION

5.4.1 Impact of Surface Hydration (Capillary Effect) on Shale Swelling During Shale Interaction with Water-Based Muds

In laboratory testing, surface hydration affects shale swelling during shale and drilling fluid interactions even if the two systems were at hydraulic and chemical equilibrium. This surface hydration, often mistaken for osmotic swelling, is caused by capillary effects when shales become dehydrated (desaturated) by operational methods such as poor handling after coring, exposure to air and equilibrating in desiccators for humidity control purposes. In addition, shales can become desaturated due to geologic reasons. According to Fam and Dusseault (1998), shale samples are usually obtained from cores taken at depth (1500-4500 m) or from near surface quarries (5-20 m). In the case of deep cores, the reduction of total stress from about 30 MPa to zero leads to large negative pressure in the shale pore fluid and this can lead to desaturation through cavitation. When the desaturated shale gets exposed to aqueous solutions, water adsorption takes place in response to the negative pressure in the shale. This water adsorption due to surface hydration is often mistaken for shale swelling even if the shale water activity is higher than the drilling fluid water activity.

We investigated the surface hydration phenomenon in order to better analyze and interpret swelling data obtained from our immersion test. We performed linear and bulk volume swelling tests on Pierre shale using NaCl, KCl and $CaCl_2$ solutions that have the same water activity as Pierre shale. Figures 5-10 and 5-11 show the linear swelling curves and bulk volume swelling curves respectively. It is clear from these Figures that significant shale hydration took place even when the water activity of the shale matched the water activity of the salt solution. Since there were no chemical or hydraulic forces to

account for the water adsorption and resulting shale hydration, we believe that this hydration was mainly due to surface hydration. Therefore, it is extremely important to account for surface hydration phenomenon when analyzing shale swelling measurements.

We have developed a technique, which allows us to account for surface hydration during shale and drilling fluid immersion tests. First, the immersion test should be performed using a simulated pore fluid, which should have the same composition and water activity as that of the shale in order to eliminate any osmotic interaction. The swelling response, obtained from this test, represents the surface hydration effect. This surface hydration effect should be subtracted from the actual bulk volume swelling data.

In making up the simulated pore fluid, we assumed that C1, C2 and Pierre shales had NaCl as the most dominant component in their pore fluids. Figures 5-12 and 5-13 show respectively the linear and semi-log plots of surface hydration curves for C1, C2, Pierre and Arco-China shales during interaction with NaCl solution of 0.98 water activity. It is important to state that C1 and C2 shales were equilibrated in desiccators of 0.98 water activities prior to conducting immersion tests in different salt solution while Pierre shale samples were kept in oil at all time prior to testing. Keeping Pierre shale in oil at all times seemed to lessen the surface hydration effect appreciably. This was made clear to us when we compared the surface hydration curve for Pierre shale, when it was kept in a 0.98 activity desiccator for two weeks, with the surface hydration curve when the Pierre sample was kept in oil at all times. The result was significant as shown in Figure 5-14. It is shown that the surface hydration effect is smaller when the shale sample was taken out the oil can and tested immediately as opposed to equilibrating it in a desiccator for two weeks. We believe that keeping shales in desiccators dehydrates them and induces surface hydration effects when they are contacted by aqueous fluids.

After accounting for surface hydration effect, we performed our immersion tests in order to study shale swelling and the amount of water and ion uptake as a result of the interaction with different water-based muds. At the end of the immersion test, we constructed the actual bulk volume swelling curve and then subtracted the surface hydration curve from it. This left us with the true bulk volume swelling curve as a function of the physcio-chemical interaction between the shale and the drilling fluid only. Figure 5-15 shows a sample of this method.

Figures 5-16, 5-17, 5-18 and 5-19 show the true bulk volume swelling of C1-shale when contacted by NaCl, KCl, $CaCl_2$ and KCOOH solutions of different water activities. Figure 5-20 shows water and ion uptake during the interaction of C1-shale with different salt solutions of different water activities. Figures 5-21, 5-22, 5-23 and 5-24 show the true bulk volume swelling of C2-shale when contacted by NaCl, KCl, $CaCl_2$ and KCOOH solutions of different water activities. Figure 5-25 show water and ion uptake during the interaction of C2-shale with different salt solutions of different water activities. Figures 5-26, 5-27, 5-28 and 5-29 show the true bulk volume swelling of Pierre shale when contacted by NaCl, KCl, $CaCl_2$ and KCOOH solutions of different water activities. Figure 5-30 shows water and ion uptake during the interaction of Pierre shale with different salt solutions of different water activities. Figure 5-31 shows the true bulk volume swelling of Arco-China shale when contacted by NaCl, KCl, $CaCl_2$ and KCOOH solutions of 0.93 water activities. Figure 5-32 shows water and ion uptake during the interaction of Arco-China shale with different salt solutions of 0.93 water activities.

5.4.2 Impact of Ion Concentration on Shale Swelling and Water and Ion Uptake

The swelling behavior of shales and the water and ion uptake is related to the concentration of solutes in the drilling fluid. Figures 5-33, 5-35 and 5-37 show the bulk

volume swelling response of C1, C2 and Pierre shales when exposed to NaCl, KCl, $CaCl_2$ and KCOOH solution of 0.93 water activities. These Figures show that after 24 hours all shales experienced swelling when exposed to salt solution that had lower water activities (a_w = 0.93) than the shales (a_w = 0.98). This is counter intuitive since one would expect that shales would lose water and thus shrink, especially when the shale's water activity is higher than that of the salt solution. So what does this swelling tell us? I believe that this swelling is a direct result of ionic diffusion into shales. Since the ionic concentration is higher in the salt solution than in the shales, ions invaded the shales in order to equilibrate the ionic concentration imbalance in the shales. The invasion of ions into the shales might have changed the pore fluid composition and mechanical properties of the shale, which could have lead to weakening of cementing bonds and cohesion degradation and thus matrix expansion and swelling. It is important to mention that while ions are flowing into the shale due to the imposed concentration gradient, water is osmotically flowing out of the shale due to the chemical potential gradient. While water extraction out of the shale due to osmosis leads to shale shrinkage, ion diffusion into the shale causes shale expansion and swelling. These two forces, osmosis and ion diffusion, can operate simultaneously. The net flux is what actually determines the swelling state of the shale. If the ion diffusion into the shale has a stronger effect than the water extraction out of the shale due to osmosis, then the shale should swell. On the other hand, if the osmotic force that extracts water out of the shale has a stronger effect than ionic diffusion into the shale, then the shale should shrink. This is supported by the fact that when all shales were exposed to salt solution of a much lower water activity (a_w =0.85), all shales experienced shrinkage. This effect can be seen in Figures 5-34, 5-36 and 5-38.

Therefore, it is fair to state, based on our experimental results, that during shale and water-based mud interactions, we believe that osmosis becomes more dominant in

concentrated solutions while ion diffusion is more dominant in dilute solutions. Figure 5-31 shows the true bulk volume swelling of Arco-China shale when exposed to salt solution of 0.93 water activity. Arco-China shale experienced swelling in all cases. This is expected since the salt solution water activities are higher than that of Arco-China shale. Due to the chemical potential imbalance, water osmotically flowed into Arco-China shale, which resulted in the swelling of the shale. Thus, it is fair to say that osmosis played a bigger role than ion diffusion in this case.

The amount of water and ion uptake into shales as a result of exposure to salt solution was estimated using the gravimetric technique. Figures 5-20, 5-25, 5-30 and 5-32 show the amount of water and ion uptake during the interaction of C1, C2, Pierre and Arco-China shales with NaCl, KCl, $CaCl_2$ and KCOOH solutions respectively. It is clearly shown from these Figures that water was extracted from the shales, and ions flowed into the shales when the water activity of the shale was higher than that of the salt solution as in the case of C1, C2 and Pierre shales. On the other hand, water flowed into the shale and ions flowed out of the shale when the water activity of the shale was less than that of the salt solution as in the case of the Arco-China shale. Additionally, it can be seen that the amount of water and ion uptake increases when the solute concentration in the salt solution increases. It is clear from these Figures that Pierre shale showed the highest uptake of water and ions due to its high permeability.

5.4.3 Impact of Shale Permeability on Shale Swelling and Water and Ion Uptake

The relative solute size to shale pore throat size plays an important role in shale swelling and controls the amount of water and ion uptake during shale and aqueous solution interaction. As stated before, shale swelling is directly related to the amount of water and ion uptake. Whenever ion diffusion into shales becomes more dominant than water flow out of shales, swelling occurs. Swelling also occurs when shale adsorbs

water. On the other hand, when water extraction out of shales overtakes ion diffusion into shale, shrinkage occurs.

Shale permeability is a direct measure of shale pore size. It is widely accepted that higher permeabilities translate into bigger shale pore throat sizes. According to Tan et al (1996), shale is not an ideal semi-permeable membrane to water-based solutions because it has a range of pore size including wide pore throats, which result in significant permeability to solutes. As the pore size decreases the solute interacts more strongly with the pore walls, which reduces the permeability of the membrane to the solute. This will result in an increase in the reflection coefficient of the shale.

The amount of water and ion uptake into shales is directly proportional to shale permeability. Figures 5-39, 5-40, 5-41 and 5-42 show the amount of water and ion uptake versus shale permeability when shales with different permeabilities interacted with NaCl, KCl, CaCl2 and KCOOH solutions of 0.93 and 0.85 water activities. It is clearly seen from these Figures that when shale permeability increases, the amount of water and ion uptake increases. This is expected since higher permeabilities translate into bigger pore throat sizes through which water and ions can flow.

Different solutes diffuse into shales differently based on their relative size to the shale pore throat size. Figures 5-43 and 5-44 show the amount of ion uptake for different solutes (ion) as a function of shale permeability. It is clearly shown that NaCl solution uptake into shale is less than KCl and KCOOH solution. This is attributed to the fact that the hydrated diameter of Na^+ is bigger than the hydrated diameter of K^+ and as the solute size relative to shale permeability increases, the amount of ionic diffusion decreases. It can also be seen from our experimental results that there does not seem to be a clear relationship between anion size and invasion into shales. Our results show that Cl^- uptake was lower than $COOH^-$ uptake when KCl and KCOOH of 0.93 water activities

interacted with shales. This is not expected since the hydrated diameter of Cl^- is much smaller than that of $COOH^-$. However, when KCl and KCOOH solution of 0.85 water activities were exposed to shales, Cl^- uptake was higher than $COOH^-$ uptake and that is expected to happen due to hydrated diameter effect.

It is important to note that the amount of water and ion uptake increases as the salt solution water activity decreases (solutes concentration increases). This is expected since the decrease in water activity promotes more water and ion exchange due to the chemical potential and concentration gradients imposed between the shales and the salt solution.

5.4.4 Impact of Cation Exchange Capacity (CEC) on Shale Swelling and Water and Ion Uptake

It is argued that shale can prevent ion movement on the basis of electrical repulsion due to the presence of negative charges on shale surfaces. The cation exchange capacity of shale is a measure of the intensity of the negative charge environment between clay platelets and hence will determine the shale's ion selective property. Therefore, the cation exchange capacity should influence the amount of water and ion uptake and thus affect shale swelling when interacting with drilling fluids. Figures 5-45, 5-46, 5-47 and 5-48 show the amount of water and ion uptake as a function of the shale cation exchange capacity with different solutions (NaCl, KCl, $CaCl_2$ and KCOOH) of 0.93 and 0.85 water activities. The general trends shown in these graphs are the same; the ion uptake decreases when the shale cation exchange capacity increases. This is expected since the shale negative charge, indicated by the shale cation exchange capacity, will prevent the co-ion from passing through, thus decreasing the total ion uptake by the shale.

5.4.5 Impact of Cation Exchange Capacity (CEC) and Shale Permeability (k) Ratio on Shale Swelling and Water and Ion Uptake

In order to show the combined effect of both the cation exchange capacity and permeability of shales on the amount of water and ion uptake and thus shale swelling, we plotted the ratio of the cation exchange capacity to permeability of shales versus the water and ions uptake. Figures 5-49, 5-50, 5-51 and 5-52 show the amount of ion and water dependence on the ratio of cation exchange capacity and permeability (CEC/k) when shales interacted with NaCl, KCl, $CaCl_2$ and KCOOH at different water activities (0.93 and 0.85). It is clearly shown from these graphs that the water and ion uptake is inversely proportional to the ratio of the cation exchange capacity and permeability of shales. Higher cation exchange capacity and permeability (CEC/k) ratio correlates very well with lower water and ion uptake. This is expected since higher CEC/k ratio yielded higher membrane efficiencies and ion selectivities during shales and salt solution interaction. Therefore, it is clear from the above discussion that as amount of ion uptake into shales decreases, the membrane efficiency and ion selectivity of the shale should increase.

5.4.6 Shale Swelling and Water and Ion Uptake during Shale Interaction with Oil-Based Muds

The interaction of shale and oil-based muds is much simpler than shale and water-based muds interaction due to the presence of a threshold capillary pressure and the fact that oil-based muds behave as semi-permeable membranes where they more efficiently prevent ion movement. Figures 5-53, 5-54, 5-55, 5-56, 5-57 and 5-58 show the bulk volume swelling and linear swelling curves for C1, Pierre and Arco-China shales during exposure to oil-based muds of varying water activities. Also, Figures 5-59, 5-60 and 5-

61 show the amount of water and ion uptake during C1, Pierre and Arco-China shales interaction with oil-based muds of varying water activities.

It is clear from Figures 5-53 through 5-58 that oil-based muds exhibit better membrane efficiency behavior than salt solutions. For all shales, oil-based muds were able to extract water out of shales when the water activity of the oil-based muds was lower than that of the shale. On the other hand, water flowed into shales when the water activity of the oil-based muds was higher than that of the shale. This shows that oil-based muds do behave as semi-preamble membranes but it does not show if they behave as perfect semi-permeable membranes where they completely stop ion movement.

In order to better clarify this point, we ran a gravimetric test after each oil-based mud and shale interaction. The results were surprising as shown in Figures 5-59 through 5-61. In these graphs, it is shown that some ions were exchanged. This leads us to believe that our oil-based muds were not perfect semi-permeable membranes. We reached the same conclusion when we conducted pressure transmission tests and found that the membrane efficiency of these oil-based muds was not 100%. We attributed the non-ideal membrane behavior of these muds to the emulsifier used and or the emulsion stability of the oil-based mud.

During oil-based muds interaction with shales, it is obvious that osmosis is the dominant force that is responsible for regulating water flow in or out of shales. The higher the water activity difference between the oil-based mud and the shale, the higher the amount of water flow becomes. When C1 and Pierre shales were exposed to oil-based muds of 0.85 water activities, they shrank considerably especially when compared to their interaction with other oil-based muds of higher water activities. Therefore, it is fair to say that osmosis is the main mechanism for regulating water flow when shales Interacted with oil-based muds.

5.4.7 Impact of Water and Ions Uptake on the Membrane Efficiency of Shale

Our experimental results showed that low shale membrane efficiencies are attributed to the exchange of ions. More specifically, the experimental results clearly showed that the measured low membrane efficiencies were actually accompanied by ion exchange between the salt solutions and the shales. Figures 5-62, 5-63 and 5-64 show the membrane efficiency dependence on water and ions uptake for C1, C2 and Pierre shales respectively when they interacted with different salt solutions of 0.93 water activities. Figures 5-65, 5-66 and 5-67 show the membrane efficiency dependence on water and ions uptake for C1, C2 and Pierre shales respectively when they interacted with different salt solutions of 0.85 water activities.

Although the experimental results showed that the membrane efficiency generally decreased with increasing ionic exchange, there did not seem to be a clear-cut inverse relationship between the membrane efficiency and the water and ions exchange. This could be due to the fact that the membrane efficiency test was done under pressure while the water and ions uptake test was done under atmospheric conditions.

5.4.8 Impact of Water and Ions Uptake and on the Ion Selectivity of shale

The ion selectivity and water and ions uptake relationship during shale and salt solutions interaction is more defined than the membrane efficiency and water and ion uptake relationship. This could be due to the fact that both the ion selectivity and water and ion uptake tests were both done under atmospheric conditions.

Figures 5-68, 5-69 and 5-70 show the ion selectivity dependence on water and ion uptake for C1, C2 and Pierre shales respectively when they interacted with different salt solutions of 0.93 water activities. Figures 5-71, 5-72 and 5-73 show the ion selectivity dependence on water and ion uptake for C1, C2 and Pierre shales respectively when they interacted with different salt solution of 0.85 water activities. It is clearly shown from

these graphs that the ion selectivity increases when the ion uptake decreases. This is expected since the ion selectivity measures the ability of shale to exclude the co-ion from passing through. Thus, the lower the amount of ion uptake, the higher the ion selectivity should be. So, it is fair to argue, based on our experimental results, that there exists a strong relationship between the shale ion selectivity and its ability to exchange ions. The ion selectivity of shales increases as the amount of ion uptake into shales decreases. This validates our concept of ion selectivity since we related it to the shale's ability to exclude ions. This is evident from the strong relationship between the ion uptake and the estimated ion selectivity of shales. Low ion uptake was correlated with high ion selectivity of shales under the same conditions.

5.5 CONCLUSIONS

From the above study, the following conclusions were reached.

- The immersion test presented herein is a valid and reliable tool for studying shale and drilling fluids interaction.
- The immersion test results show good correlation with the more popular linear swelling test.
- The immersion test is a great rig-site tool because it is easy to conduct and it requires familiar materials and devices that are readily available.
- More importantly, the immersion test does not require shale samples to be of certain sizes or dimension like other tests. In fact, this test can be run with large shale cuttings, which can be easily obtained from the shale shakers at the rig.

- The amount of water and ion uptake into shales as a result of exposure to drilling fluids can be estimated using a gravimetric technique.
- It is extremely important to account for surface hydration (capillary effects) phenomenon when conducting shale swelling measurements.
- Among other geologic and operational factors, we believe that keeping shales in desiccators dehydrates them and induces surface hydration (capillary) effects when they are contacted by aqueous fluids.
- It is recommended that shales be stored in oil jars at all times prior to testing. The oil jars should be completely sealed in order to prevent exposure to the atmosphere.
- The invasion of ions into the shales may change the pore fluid composition and the mechanical properties of the shale (cohesion degradation and matrix expansion and swelling).
- Osmosis and ion diffusion, operate simultaneously during the interaction of shales with drilling fluids. The net force is what actually determines the swelling state of the shale.
- When shales interact with water-based muds, osmosis becomes more dominant in concentrated solution while ion diffusion is more dominant in dilute solutions.
- The amount of water and ion uptake increases when the solute concentration in the solution increases.
- The relative solute-size to shale pore-size plays an important role in shale swelling and controls the amount of water and ion uptake.

- The amount of water and ion uptake into shales is directly proportional to shale permeability.
- The invasion of cation into shales is inversely proportional to their hydrated diameters. On the hand, there does not seem to be a clear relationship between anion hydrated radii and their invasion into shales.
- Water and ion uptake decreases when the shale cation exchange capacity increases.
- The water and ion uptake is inversely proportional to the ratio of the cation exchange capacity and permeability of shales.
- Osmosis is the main mechanism for regulating water flow when shales interact with and oil-based muds.
- Oil-based muds did not behave as perfect semi-permeable membranes. This may be due to the emulsifier used and emulsion instability.
- Based on our experimental data, low membrane efficiencies are actually related to ion exchange between the salt solution and the shales. However, there does not seem to be a clear-cut inverse relationship between the membrane efficiency and the water and ions exchange from our graphs.

Table 5-1: Test matrix to study the effects cation type and concentration on shales swelling behavior and water and ion uptake during shales and salt solution interaction

Test Fluid	Water Activity	**Shale tested**	**Temperature**
NaCl	0.93	C1, C2, Pierre & Arco-China Shales	70 F
	0.85	C1, C2, Pierre & Arco-China Shales	70 F
KCl	0.93	C1, C2, Pierre & Arco-China Shales	70 F
	0.85	C1, C2, Pierre & Arco-China Shales	70 F
CaCl2	0.93	C1, C2, Pierre & Arco-China Shales	70 F
	0.85	C1, C2, Pierre & Arco-China Shales	70 F

Table 5-2: Test matrix to study the effects of anion type and concentration on shales swelling behavior and water and ion uptake during shales and salt solution interaction.

Test Fluid	**Water Activity**	**Shale tested**	**Temperature**
KCOOH	0.93 0.85	C1, C2, Pierre & Arco-China Shales	70 F
KCl	0.93 0.85	C1, C2, Pierre & Arco-China Shales	70 F

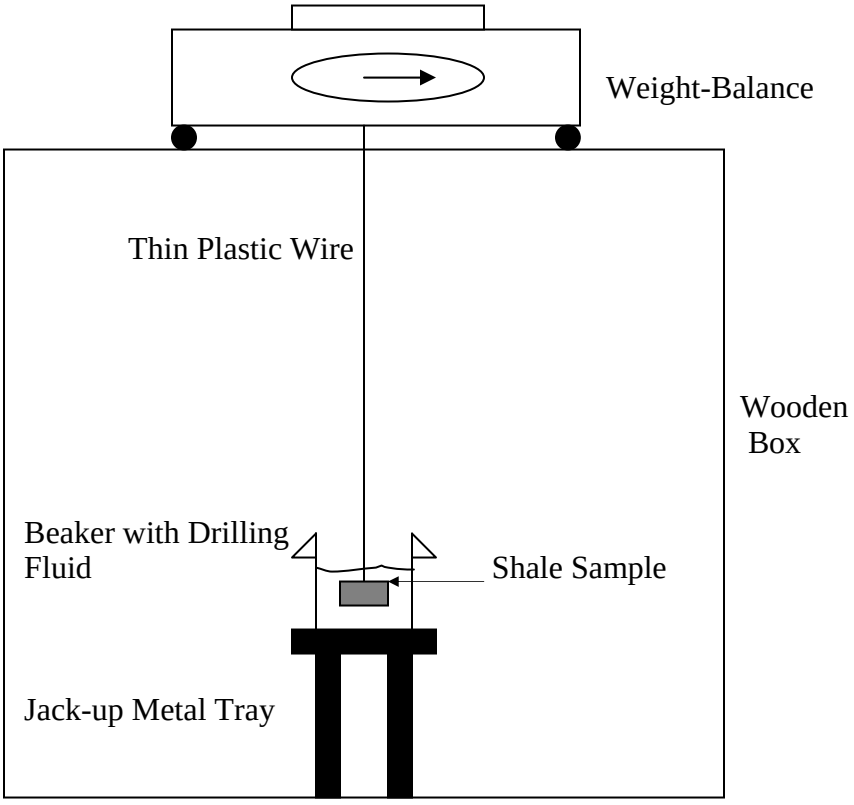

Figure 5-1: The experimental equipment and set-up for the immersion test.

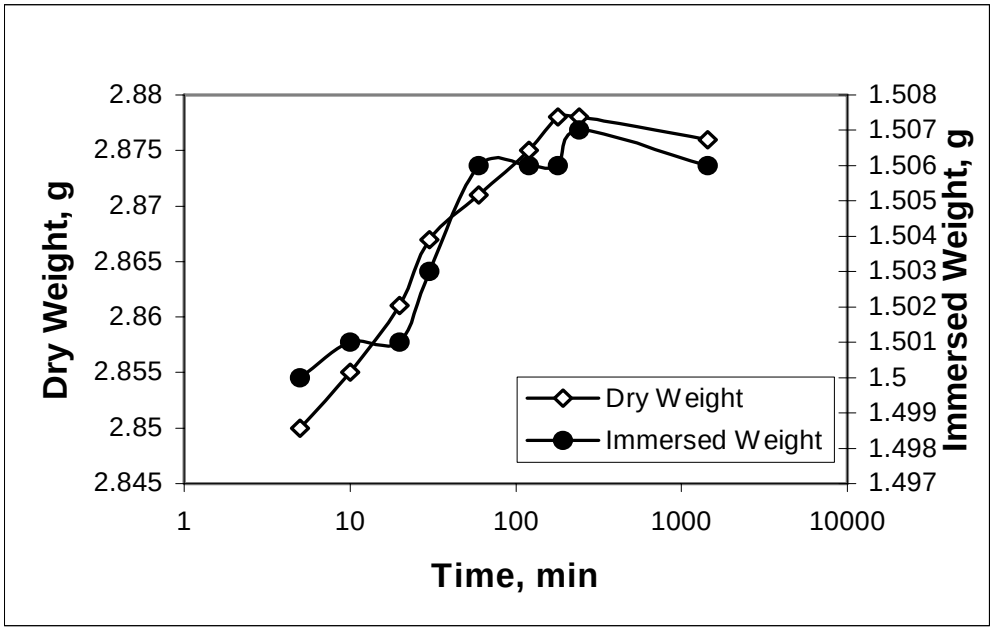

Figure 5-2: Measured dry and immersed weights of Pierre shale when exposed to 0.93 NaCl solution

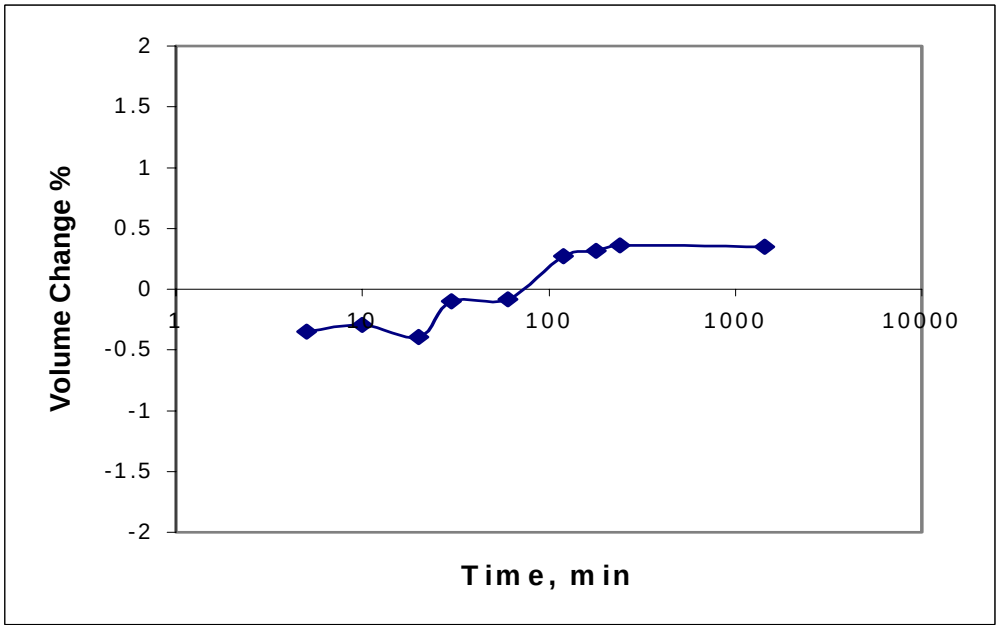

Figure 5-3: Calculated volume change % (bulk volume swelling) of Pierre shale when exposed to 0.93 NaCl solution

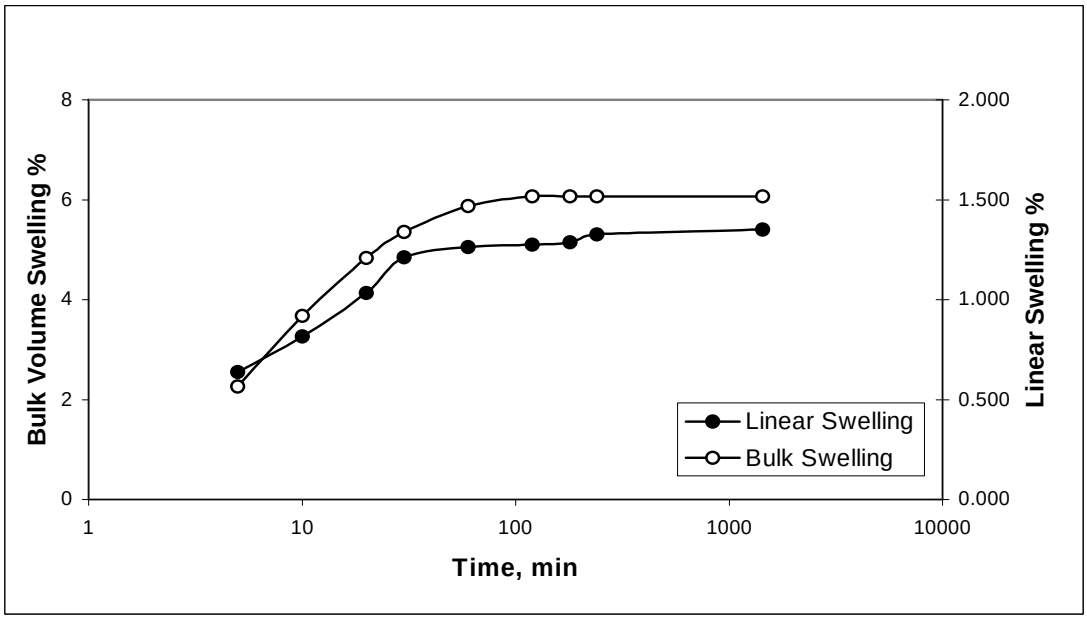

Figure 5-4: Bulk volume and linear swelling comparison when Pierre shale interacted with NaCl (a_w = 0.98) solution.

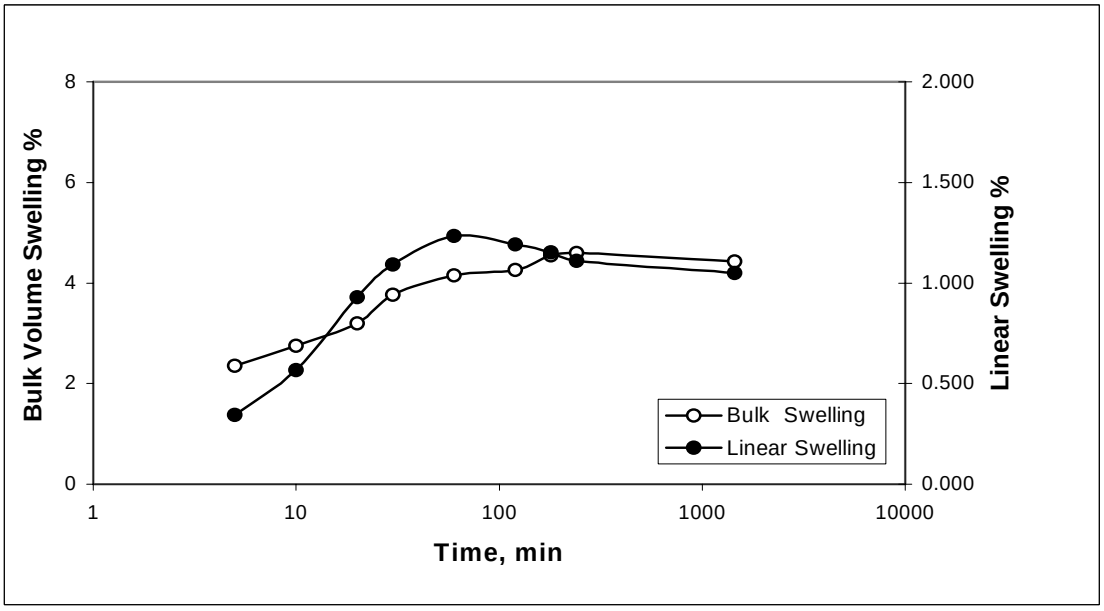

Figure 5-5: Bulk volume and linear swelling comparison when Pierre shale interacted with KCl (a_w = 0.98) solution.

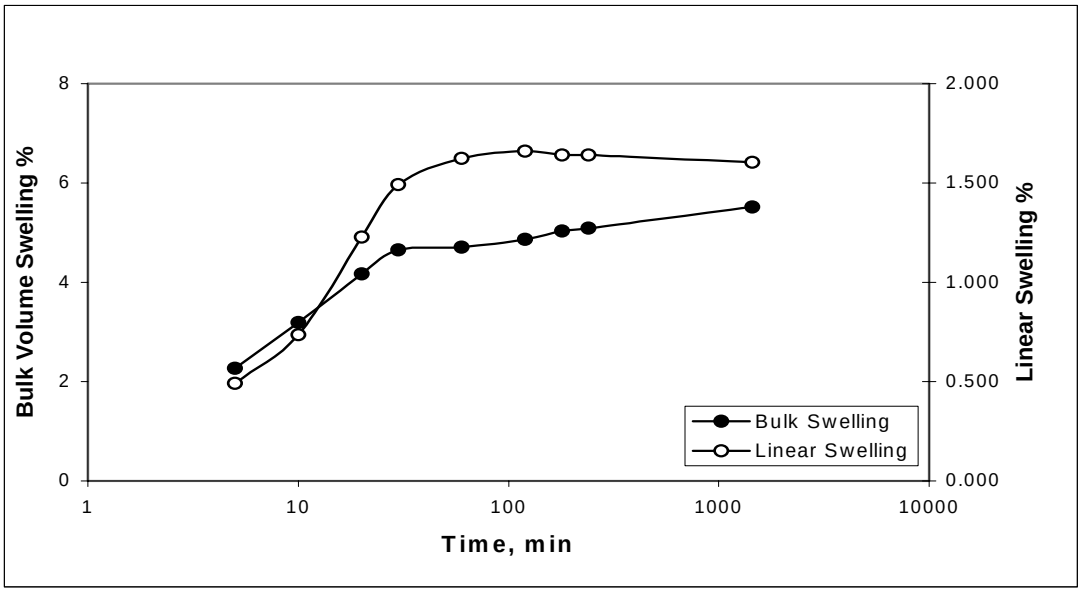

Figure 5-6: Bulk volume and linear swelling comparison when Pierre shale is immersed in $CaCl_2$ (a_w = 0.98) solution.

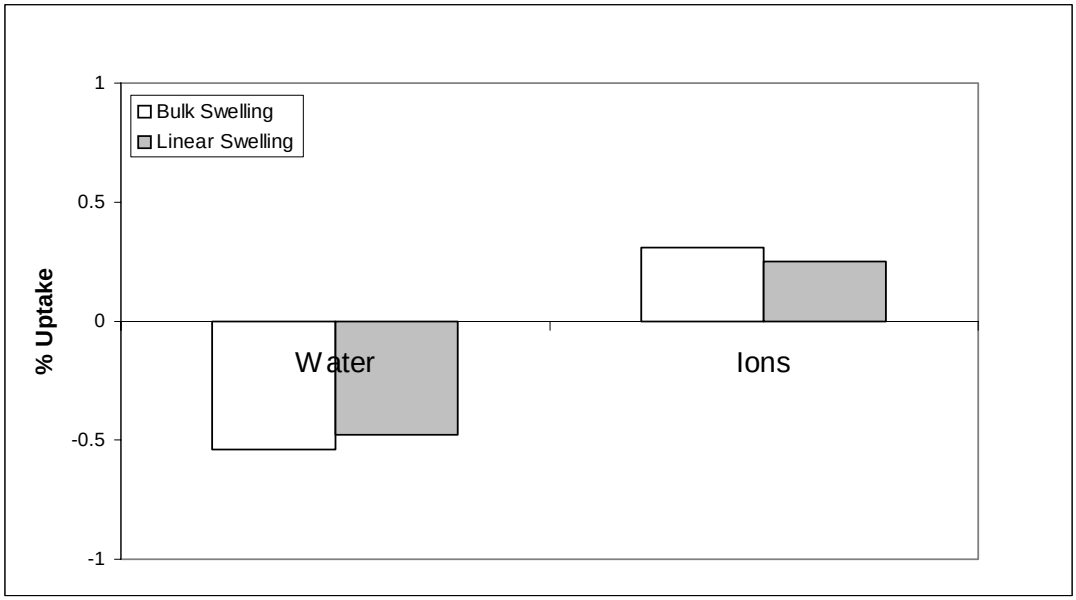

Figure 5-7: Water and ion exchange during bulk volume and linear welling tests for Pierre shale when immersed in NaCl (a_w = 0.98) solution.

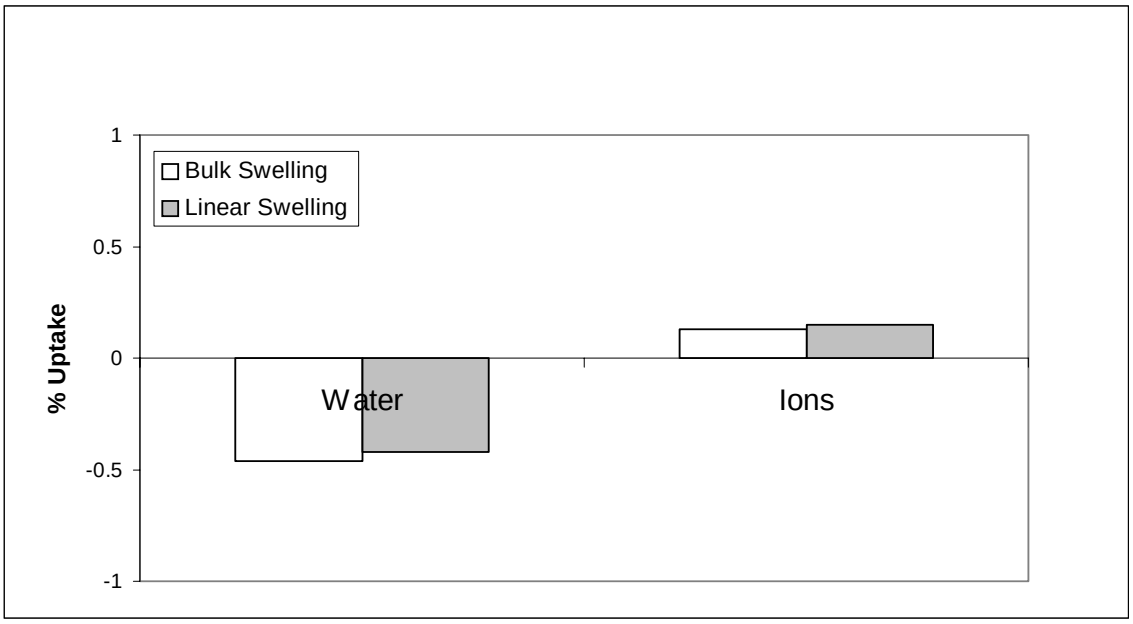

Figure 5-8: Water and ion exchange during bulk volume and linear swelling tests for Pierre shale when interacted with KCl (a_w = 0.98) solution

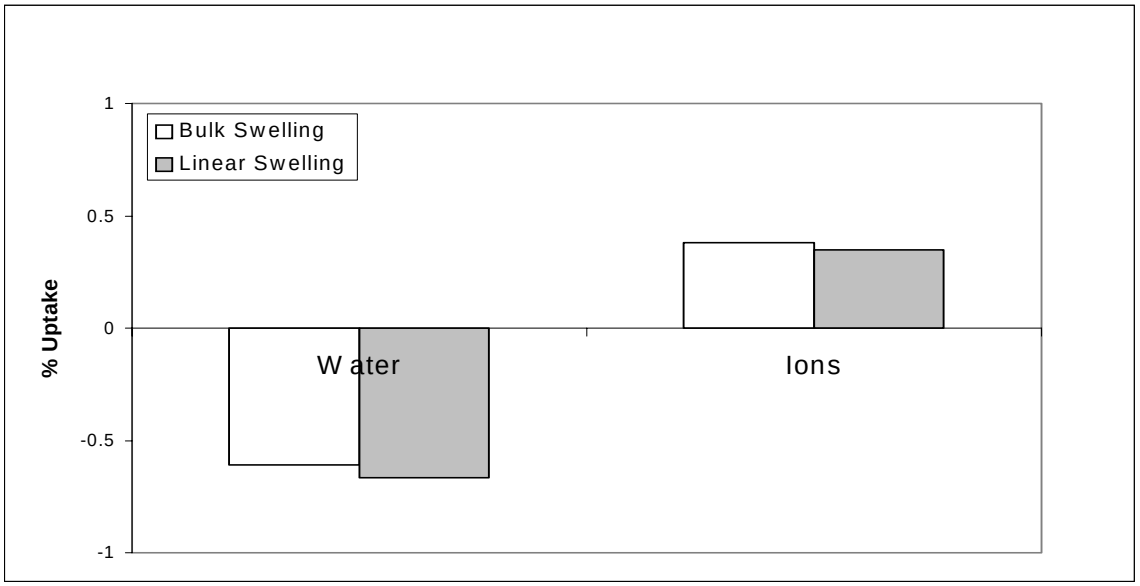

Figure 5-9: Water and ion exchange during bulk volume and linear swelling tests for Pierre shale when interacted with $CaCl_2$ (a_w = 0.98) solution

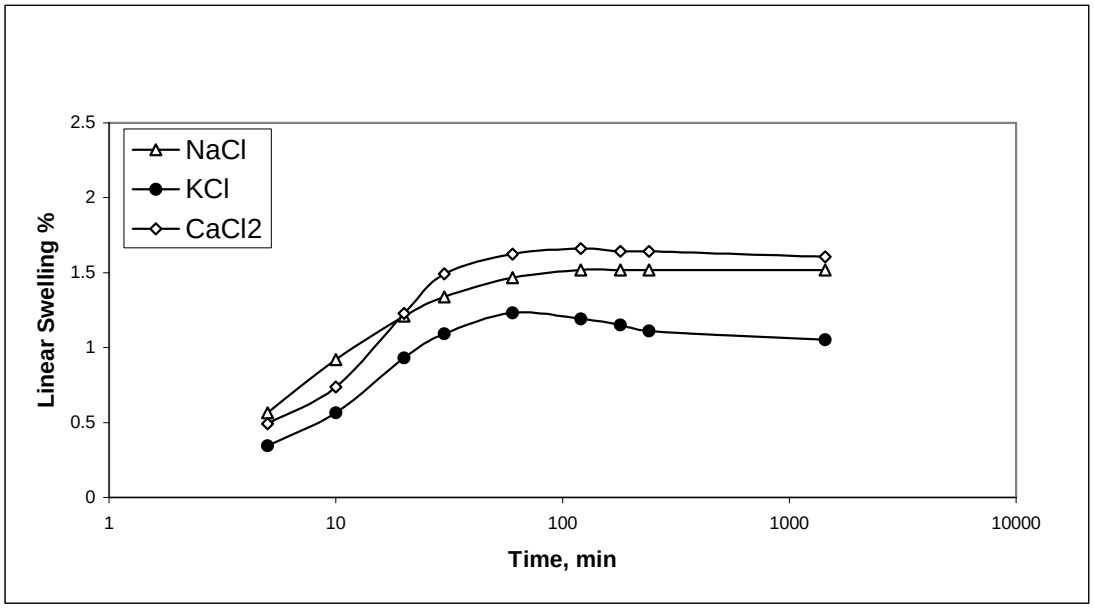

Figure 5-10: Linear swelling curves when Pierre shale (a_w =0.98) was immersed in different salt solutions (a_w = 0.98).

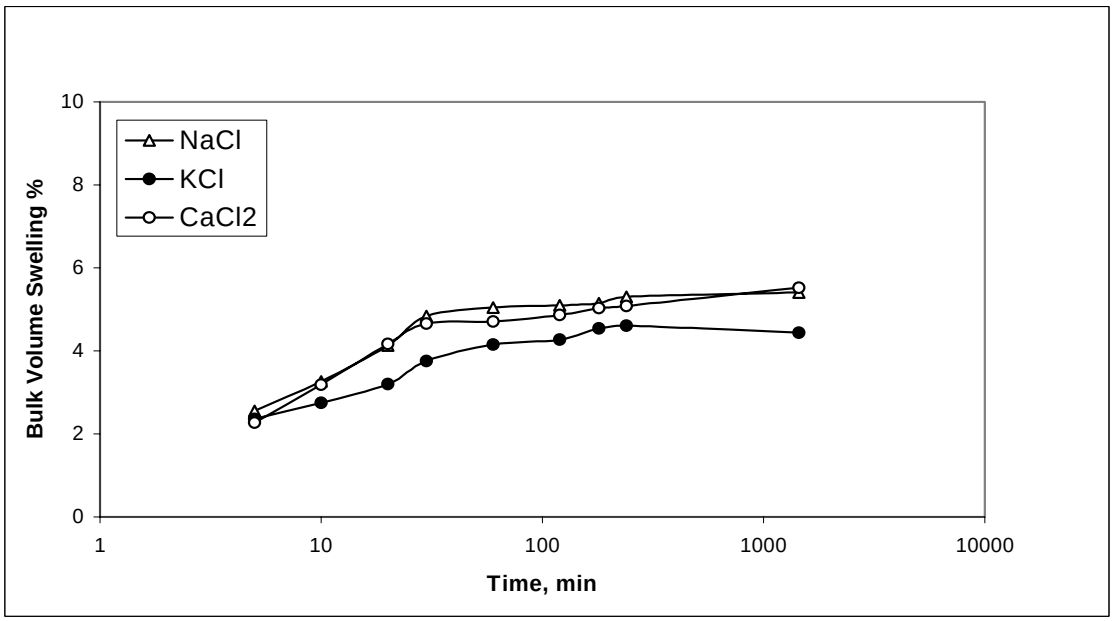

Figure 5-11: Bulk volume swelling curves when Pierre shale (a_w =0.98) was immersed in different salt solutions (a_w = 0.98).

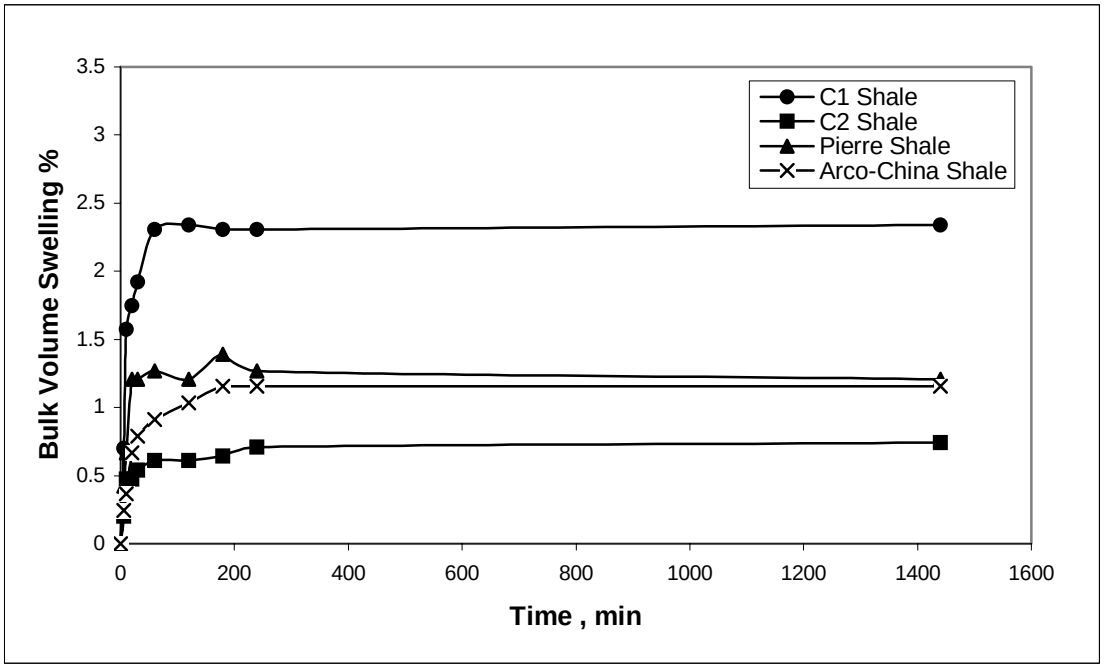

Figure 5-12: Linear plot of surface hydration curve for all shales tested.

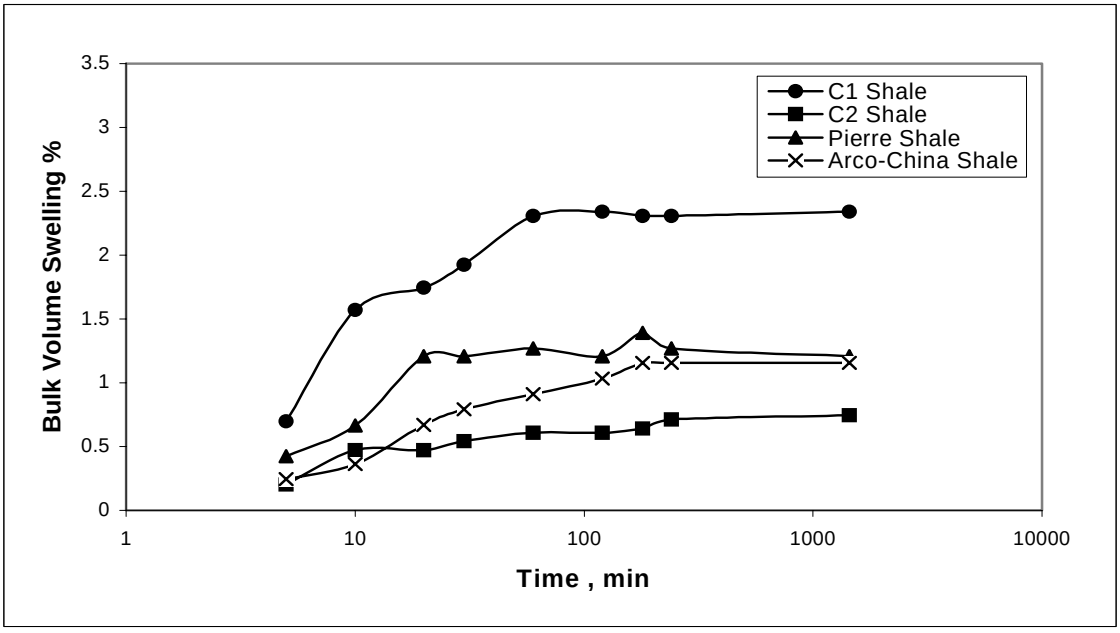

Figure 5-13: Semi-log plot of surface hydration curve for all shales tested.

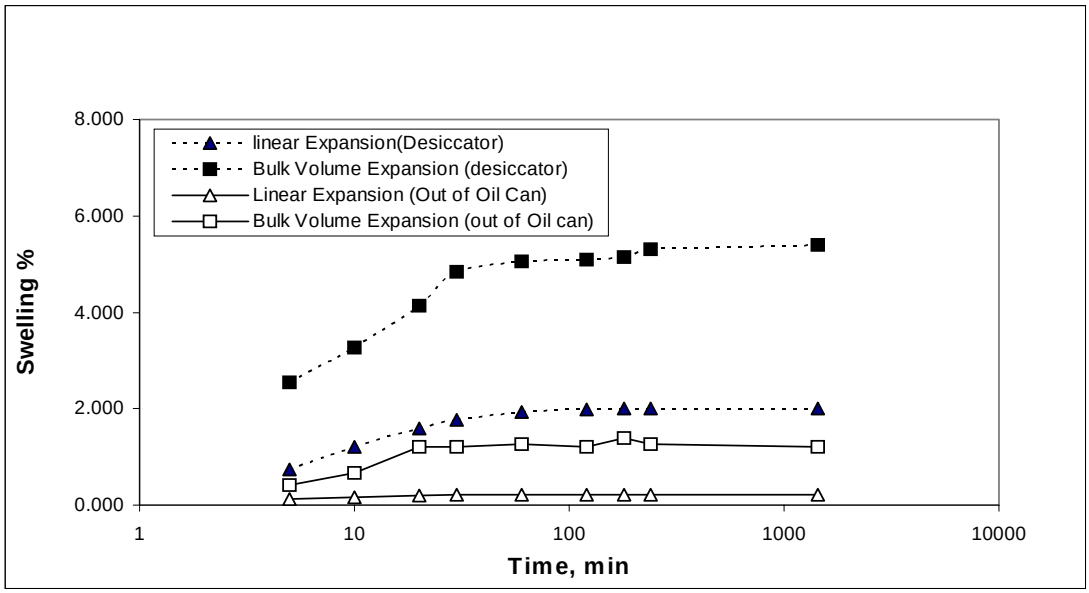

Figure 5-14: Surface hydration effect comparison between keeping Pierre shale in desiccator or in oil.

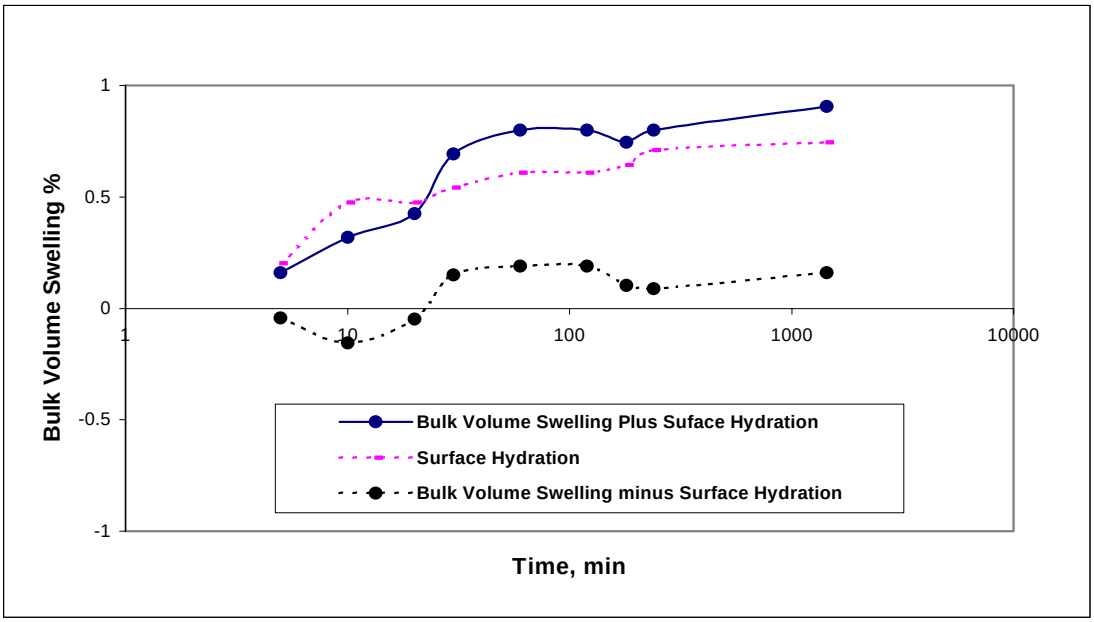

Figure 5-15: Subtracting surface hydration curve from actual bulk volume swelling curve to yield true bulk volume swelling curve for C2-shale when interacted with NaCl (a_w = 0.93) solution.

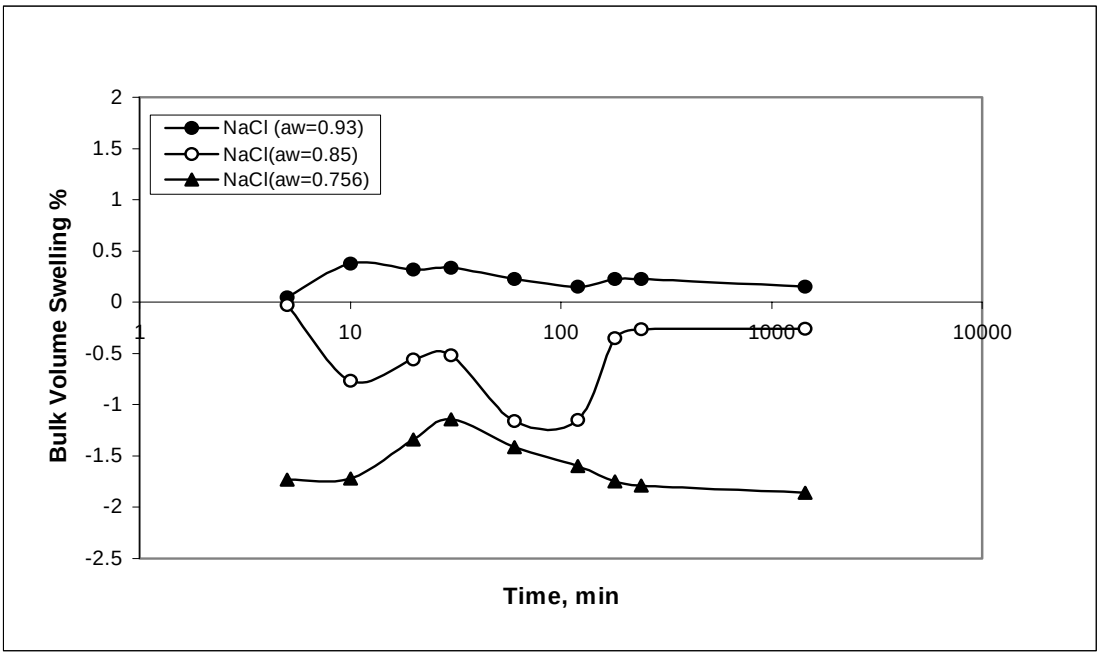

Figure 5-16: True bulk volume swelling for C1-shale during interaction with NaCl solution of different water activities.

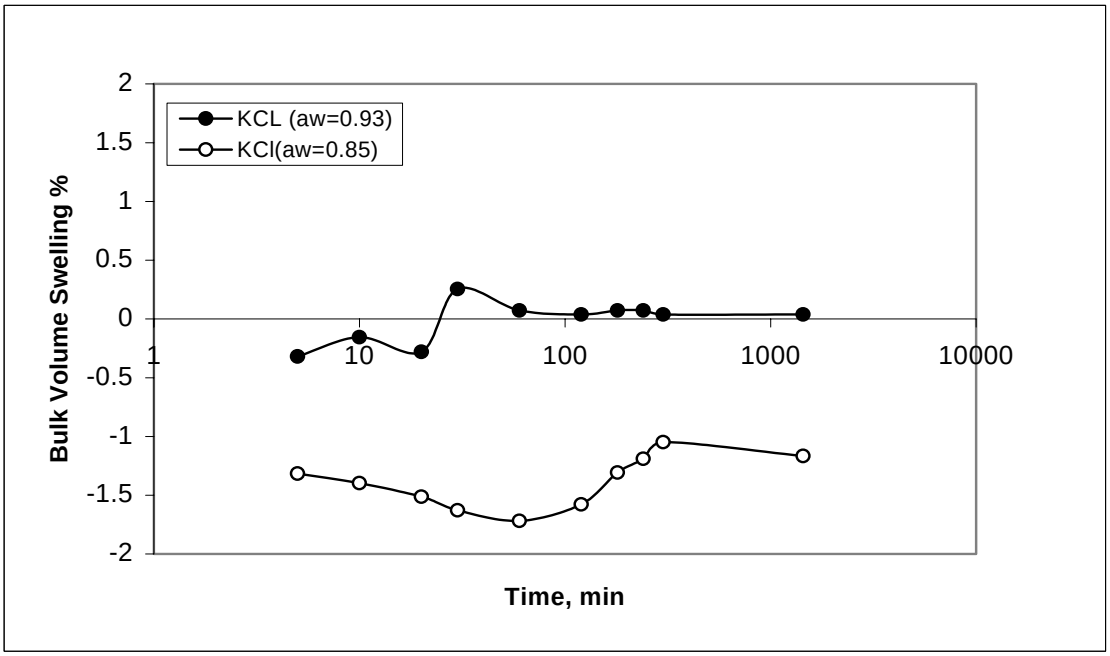

Figure 5-17: True bulk volume swelling for C1-shale during interaction with KCl solution of different water activities.

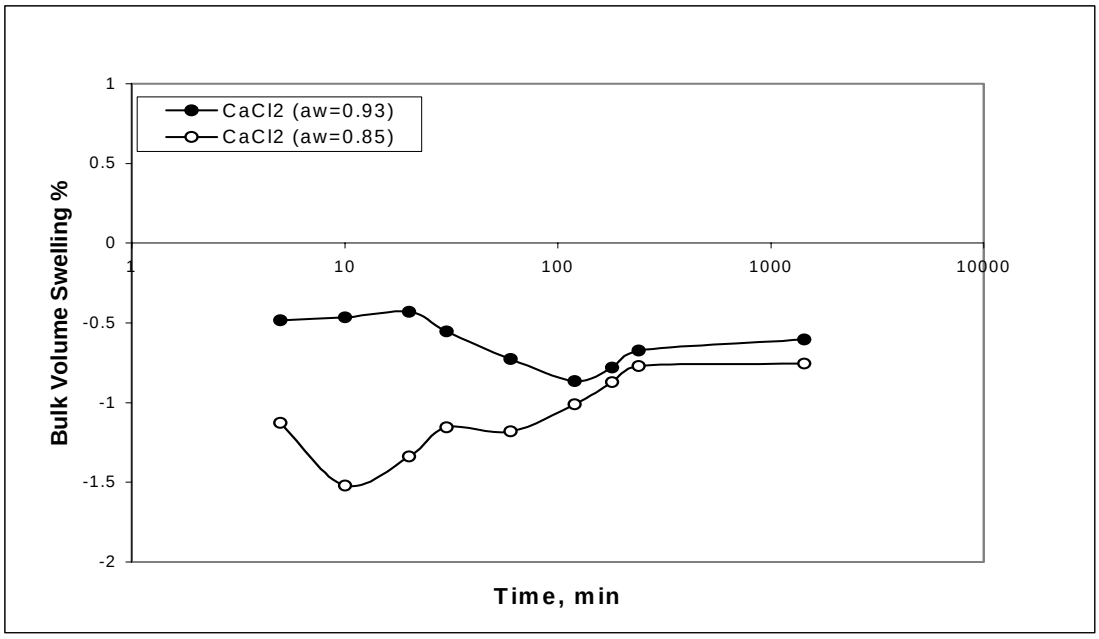

Figure 5-18: True bulk volume swelling for C1-shale during interaction with $CaCl_2$ solution of different water activities.

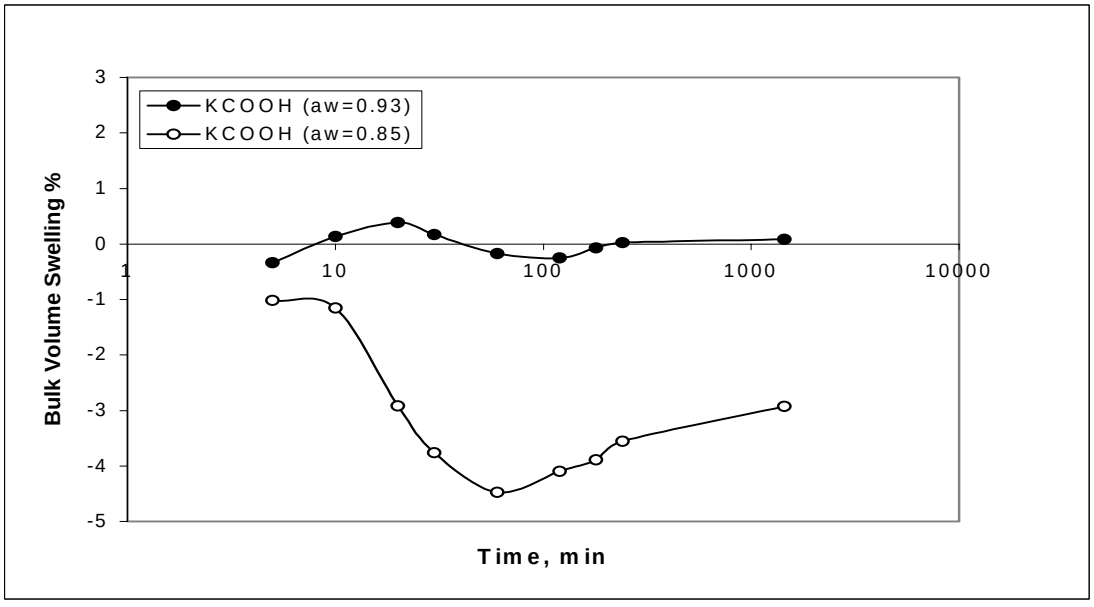

Figure 5-19: True bulk volume swelling for C1-shale during interaction with KCOOH solution of different water activities.

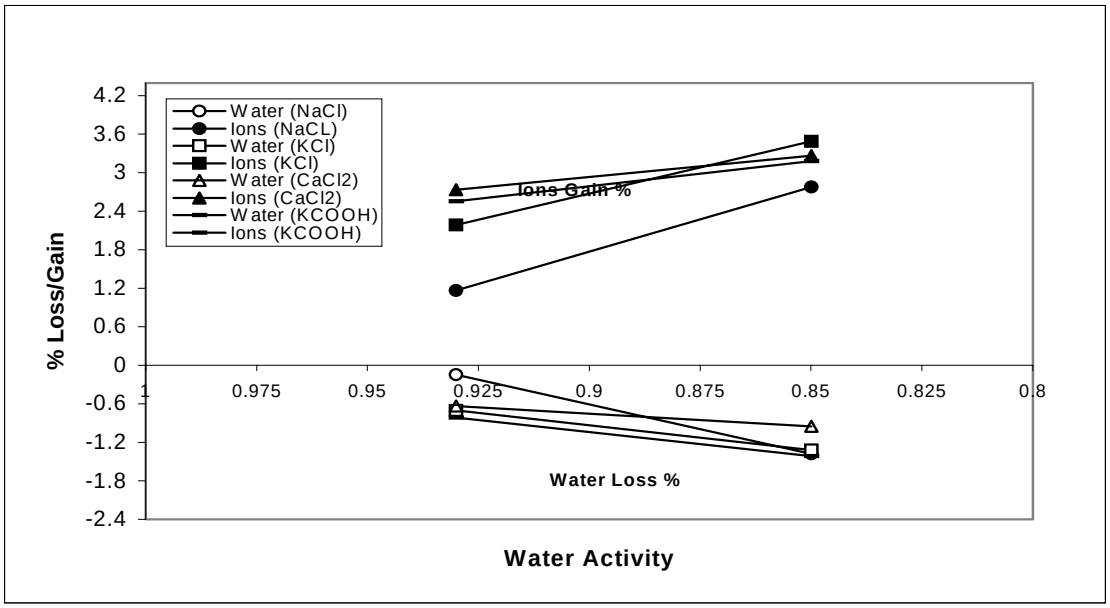

Figure 5-20: Water and ion uptake during C1-shale interaction with different salt solutions of different water activities.

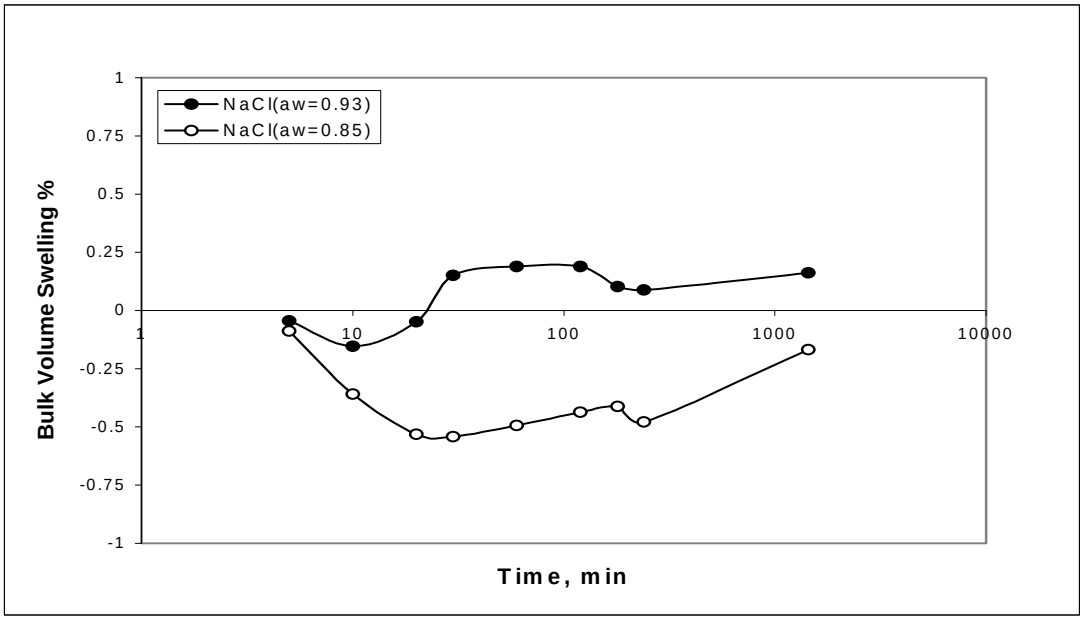

Figure 5-21: True bulk volume swelling for C2-shale during interaction with NaCl solution of different water activities.

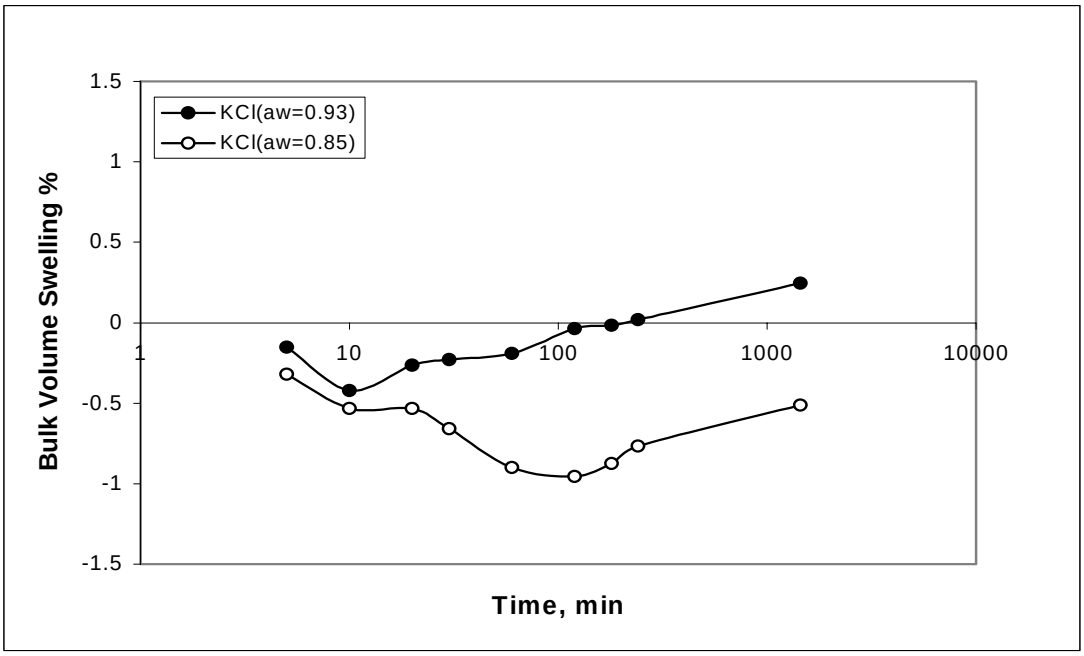

Figure 5-22: True bulk volume swelling for C2-shale during interaction with KCl solution of different water activities.

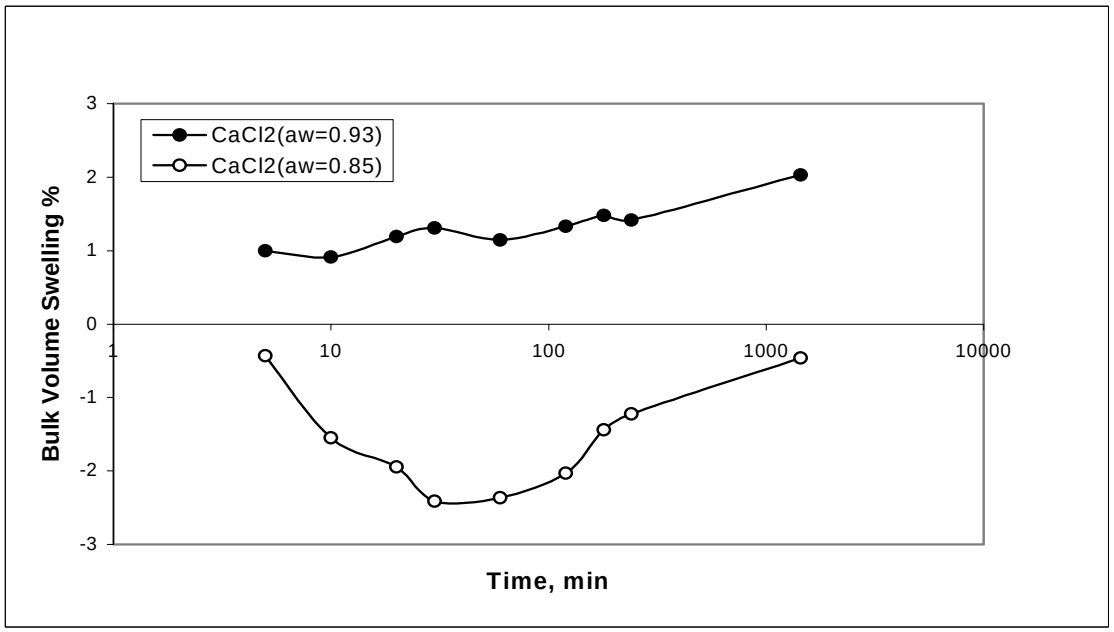

Figure 5-23: True bulk volume swelling for C2-shale during interaction with $CaCl_2$ solution of different water activities.

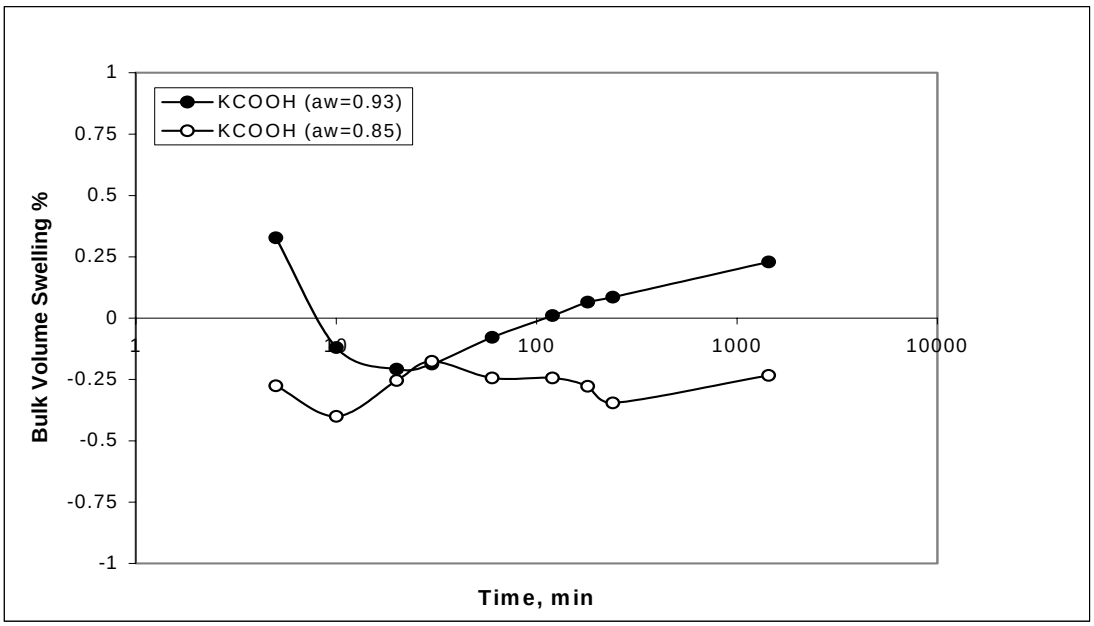

Figure 5-24: True bulk volume swelling for C2-shale during interaction with KCOOH solutions of different water activities.

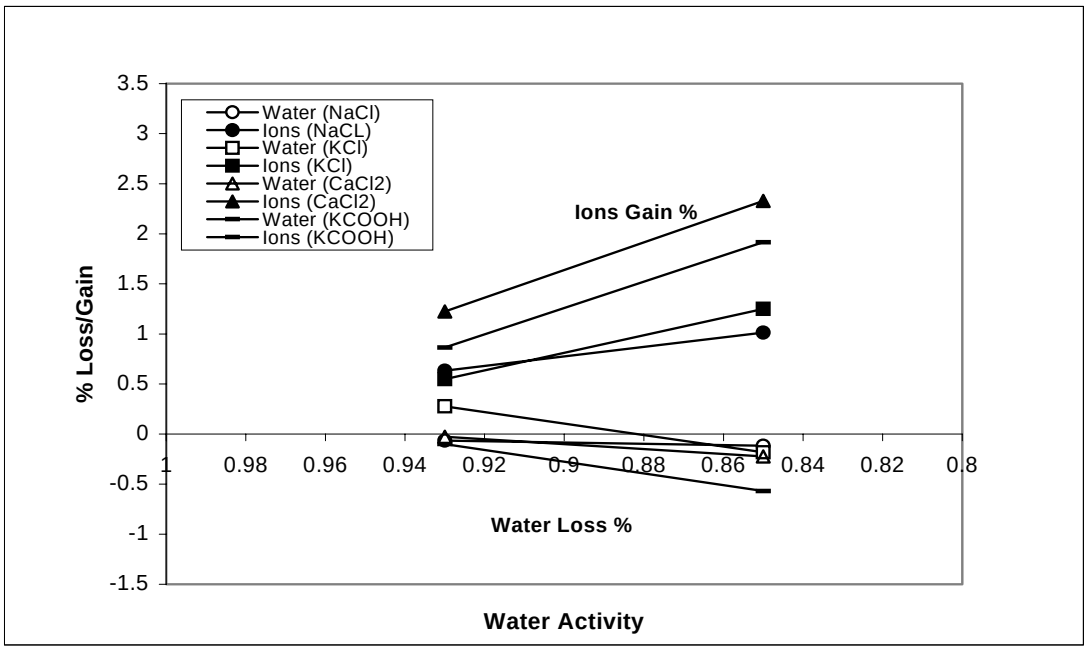

Figure 5-25: Water and ion uptake during C2-shale interaction with different salt solutions of different water activities.

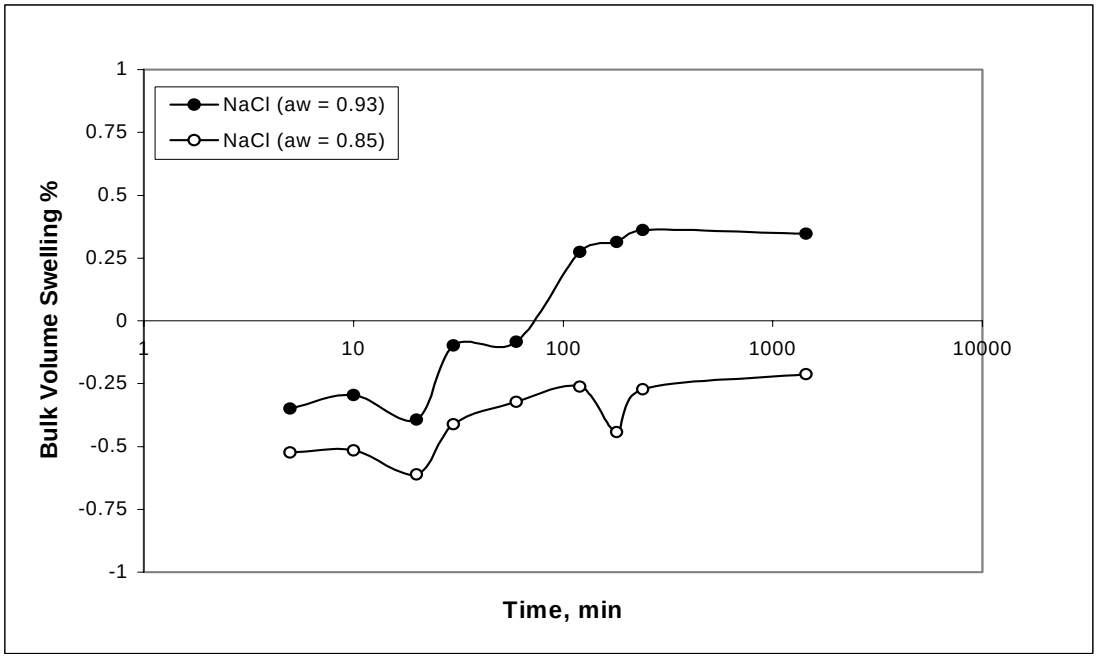

Figure 5-26: True bulk volume swelling for Pierre shale during interaction with NaCl solutions of different water activities.

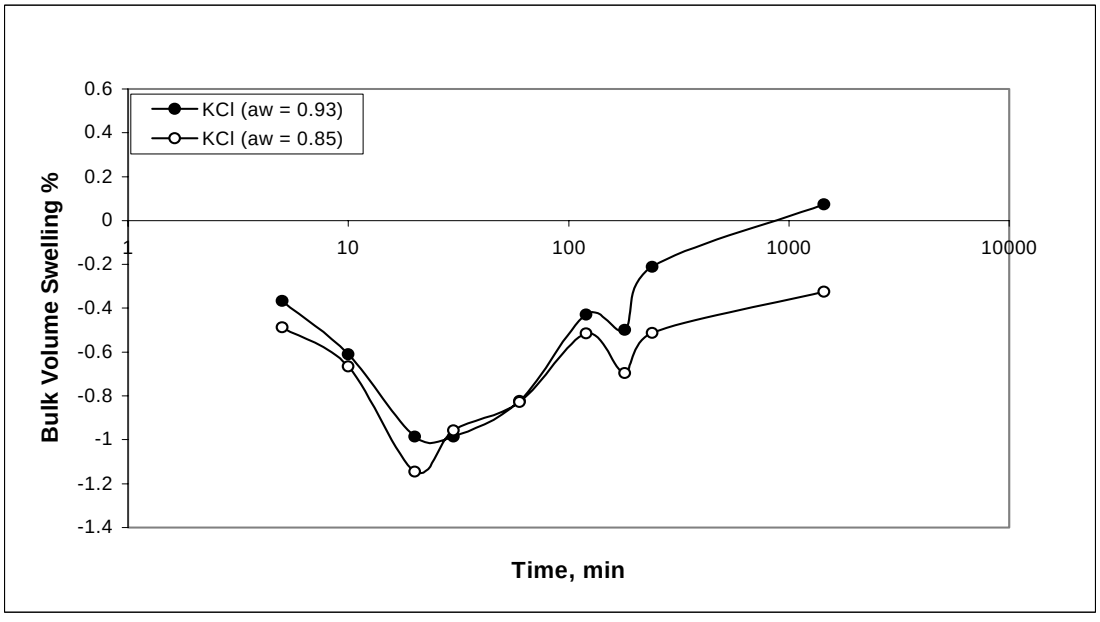

Figure 5-27: True bulk volume swelling for Pierre shale during interaction with KCl solution of different water activities.

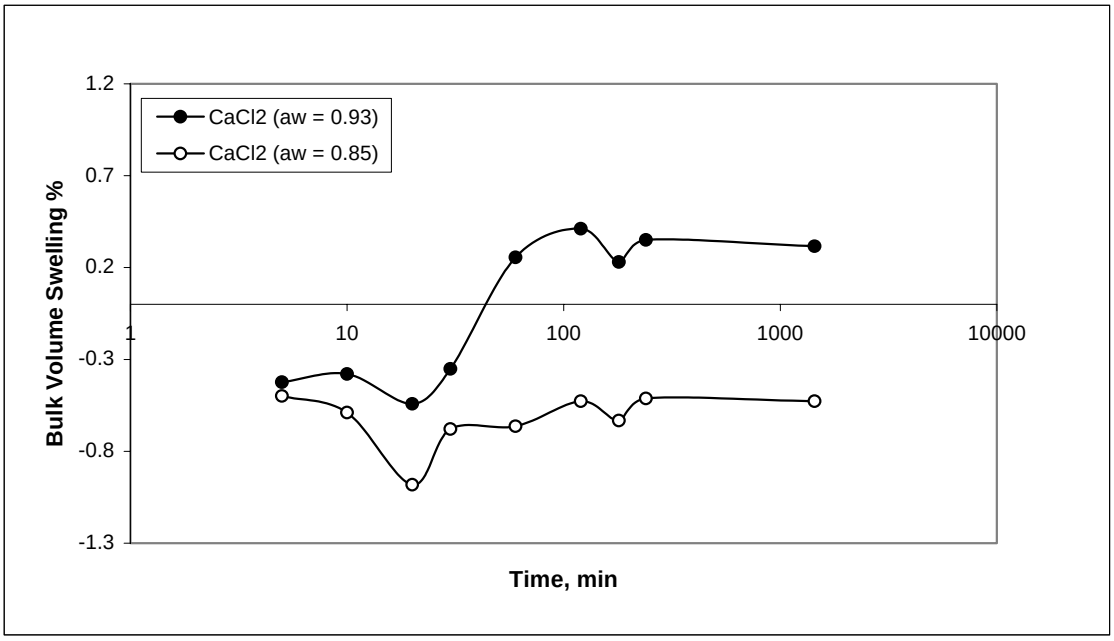

Figure 5-28: True bulk volume swelling for Pierre shale during interaction with CaCl2 solutions of different water activities.

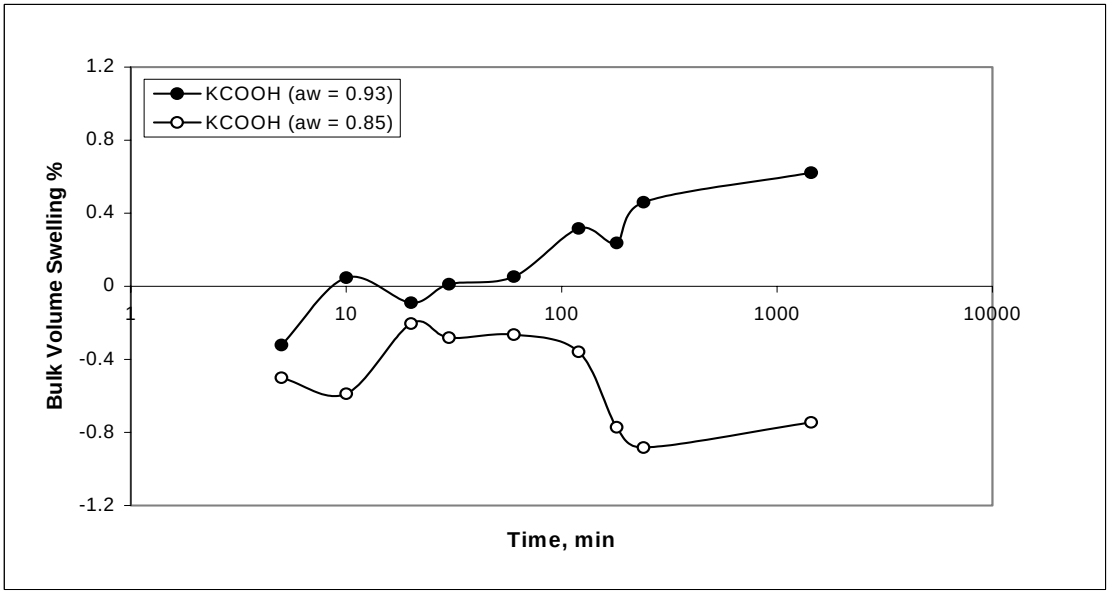

Figure 5-29: True bulk volume swelling for Pierre shale during interaction with KCOOH solutions of different water activities.

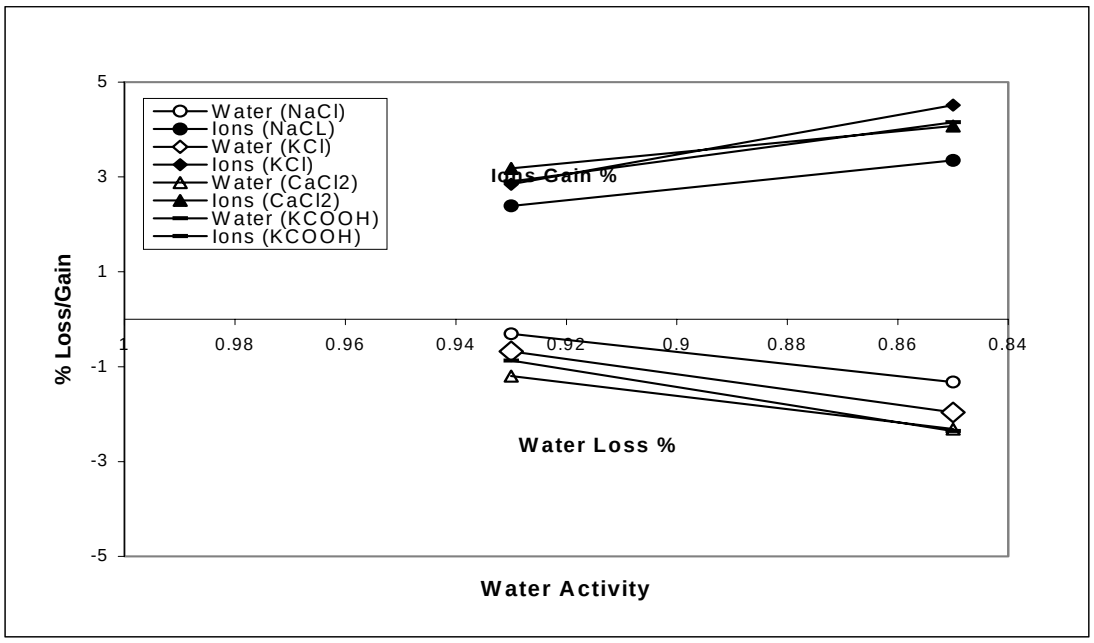

Figure 5-30: Water and ions uptake during Pierre shale interaction with different salt solutions of different water activities.

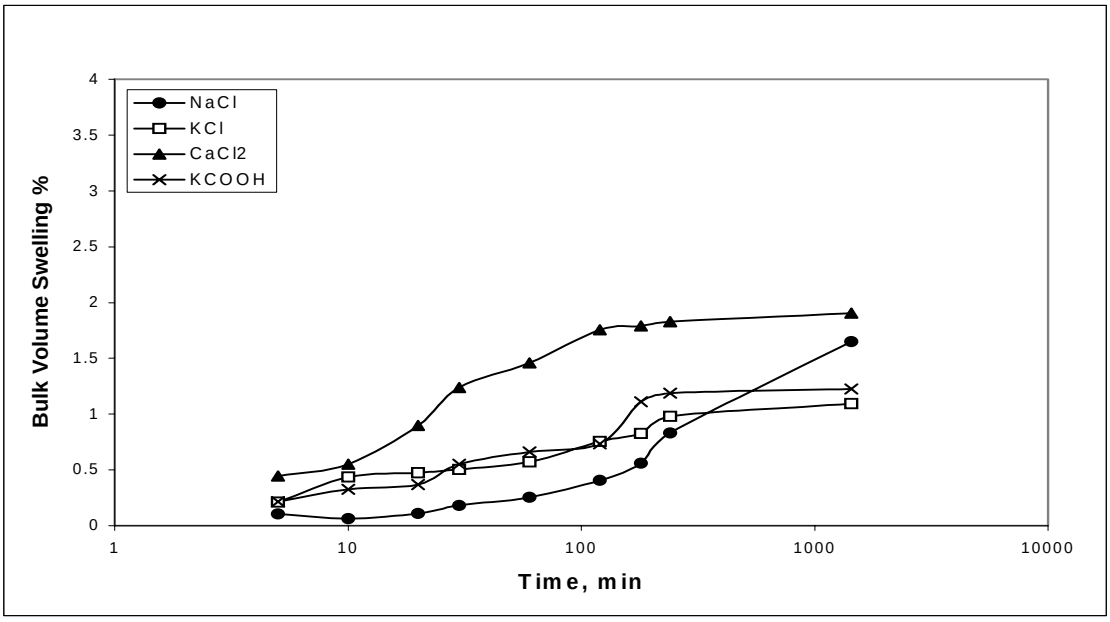

Figure 5-31: Bulk volume swelling response of Arco-China shale during interaction with different salt solutions of 0.93 water activity.

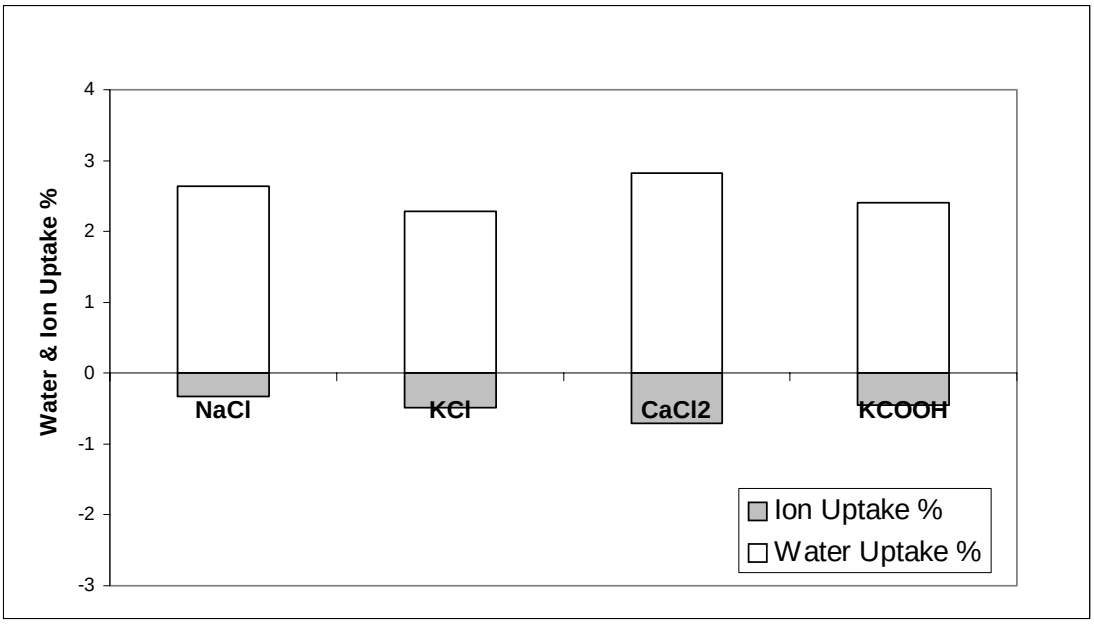

Figure 5-32: Water and ion uptake during Arco-China shale interaction with different salt solutions of different water activities.

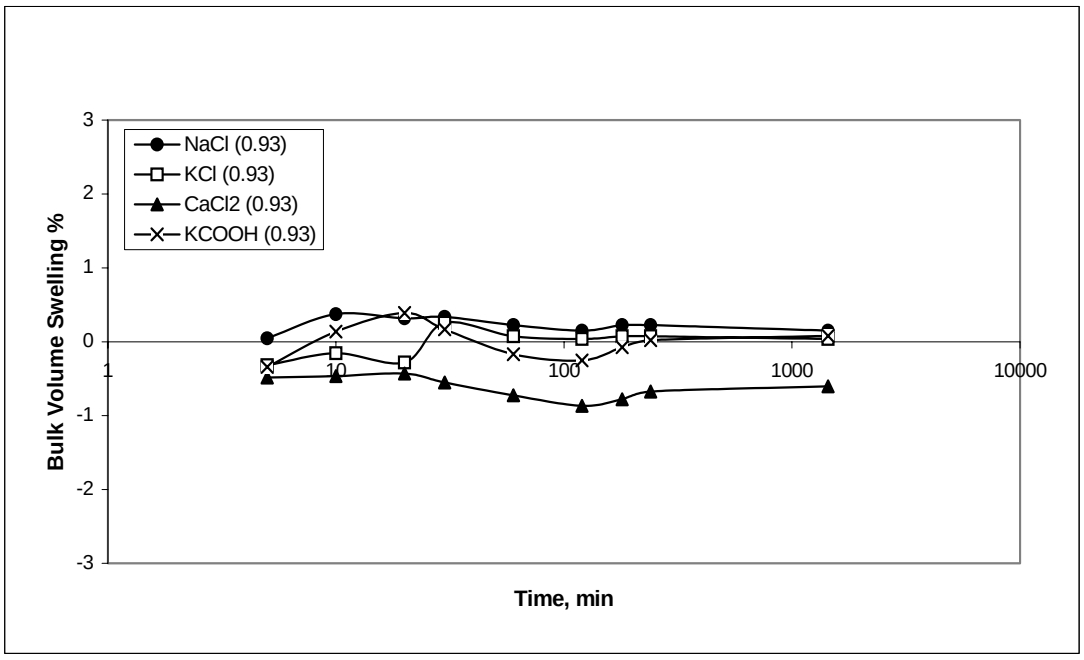

Figure 5-33: Bulk volume swelling response of C1 shale during interaction with different salt solutions of 0.93 water activity.

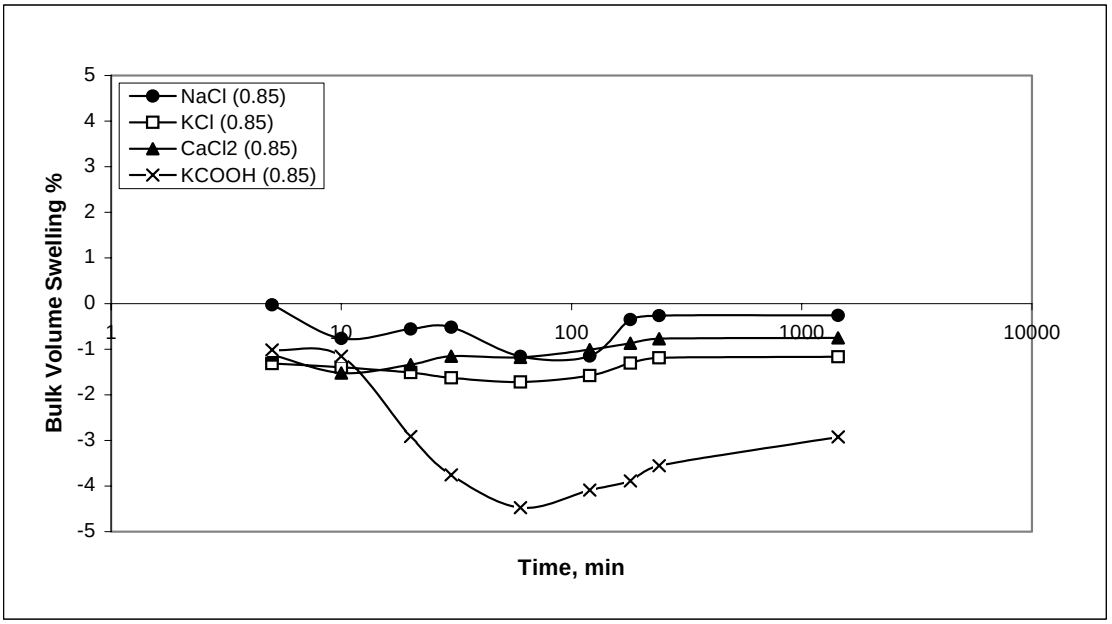

Figure 5-34: Bulk volume swelling response of C1 shale during interaction with different salt solutions of 0.85 water activity.

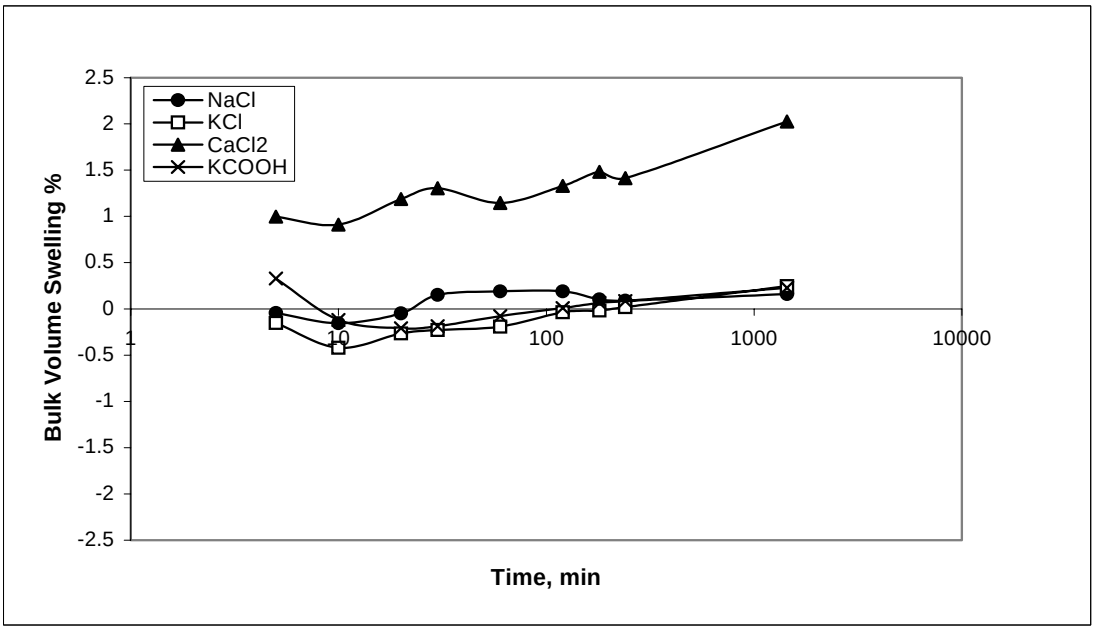

Figure 5-35: Bulk volume swelling response of C2 shale during interaction with different salt solutions of 0.93 water activity.

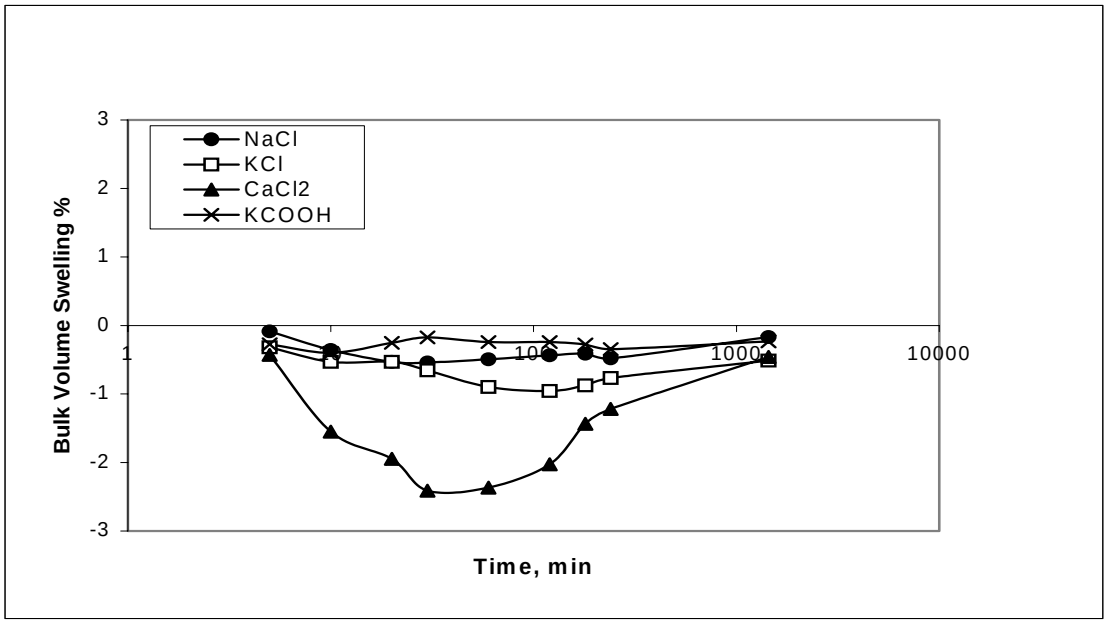

Figure 5-36: Bulk volume swelling response of C2 shale during interaction with different salt solutions of 0.85 water activity.

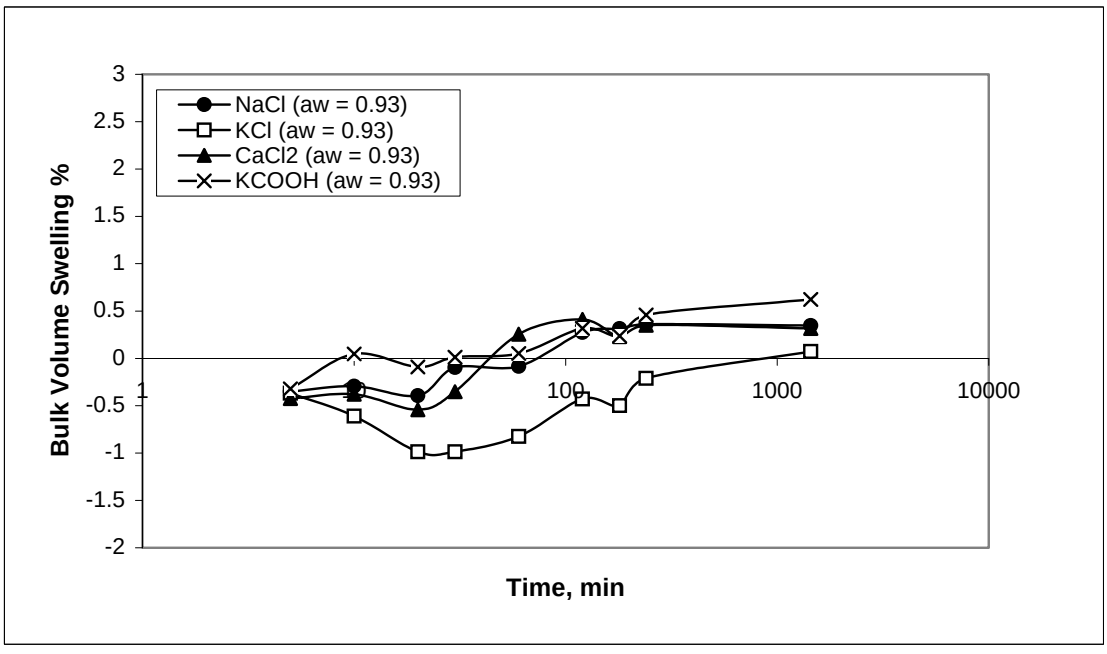

Figure 5-37: Bulk volume swelling response of Pierre shale during interaction with different salt solutions of 0.93 water activity.

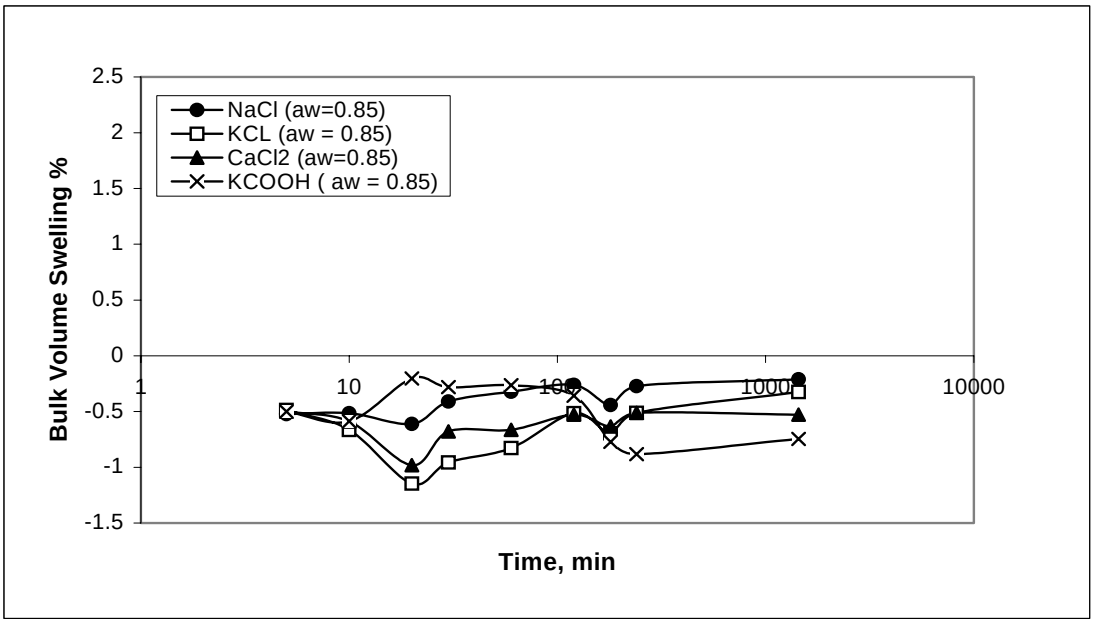

Figure 5-38: Bulk volume swelling response of Pierre shale during interaction with different salt solutions of 0.85 water activity.

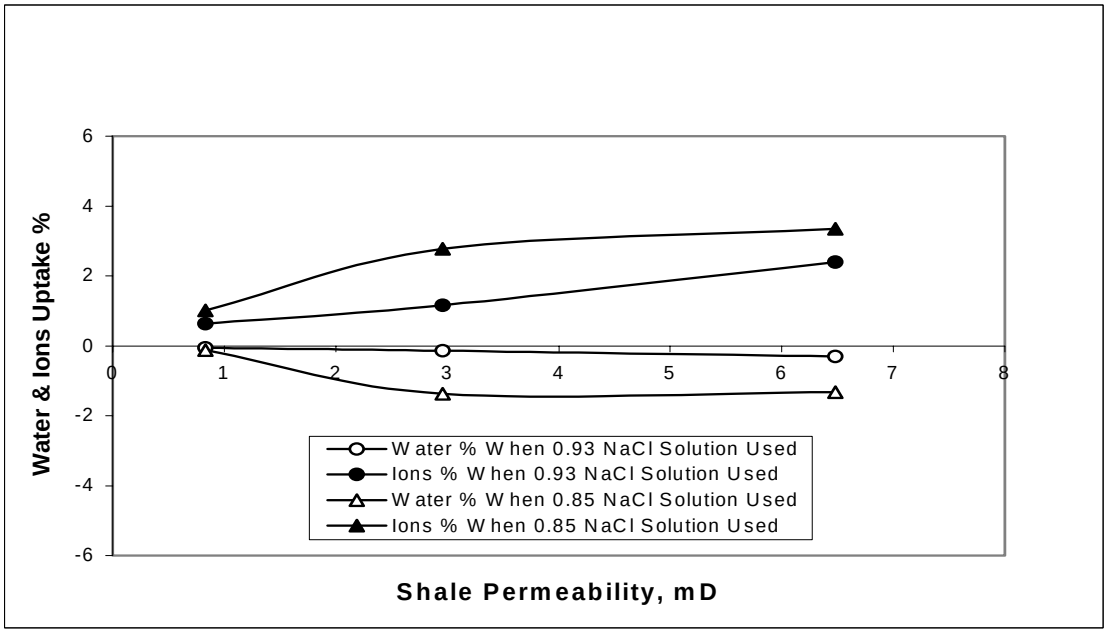

Figure 5-39: Water and ion uptake versus shale permeability (NaCl solution).

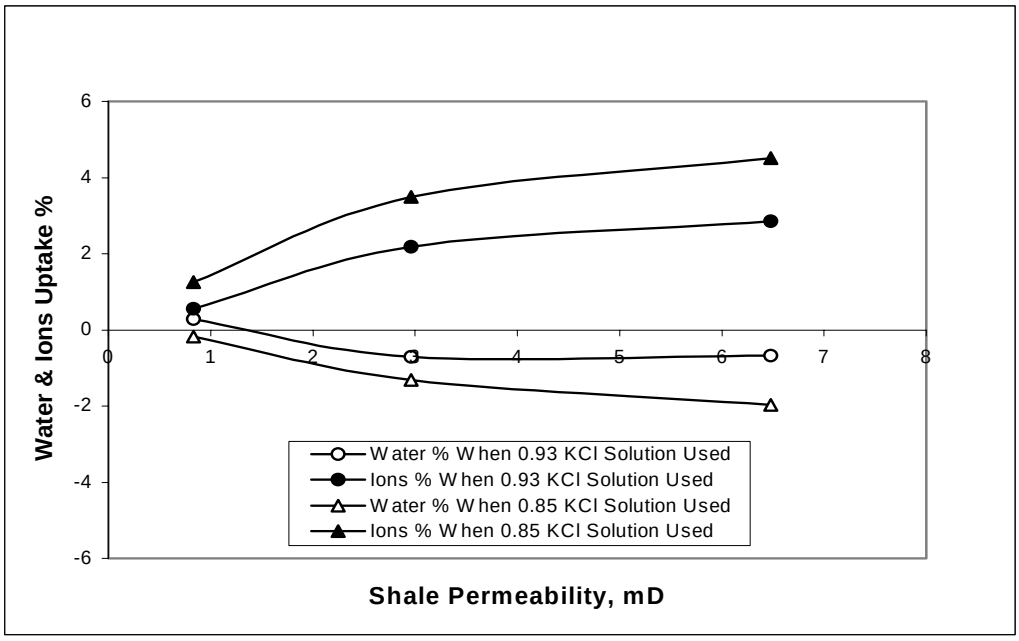

Figure 5-40: Water and ion uptake versus shale permeability (KCl solution).

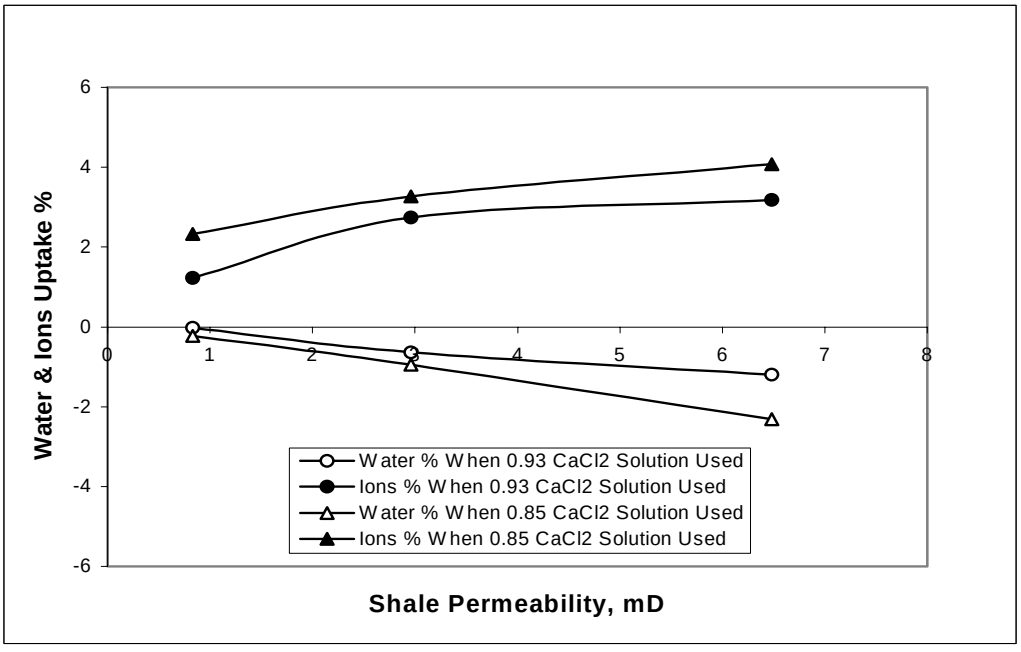

Figure 5-41: Water and ion uptake versus shale permeability ($CaCl_2$ solution).

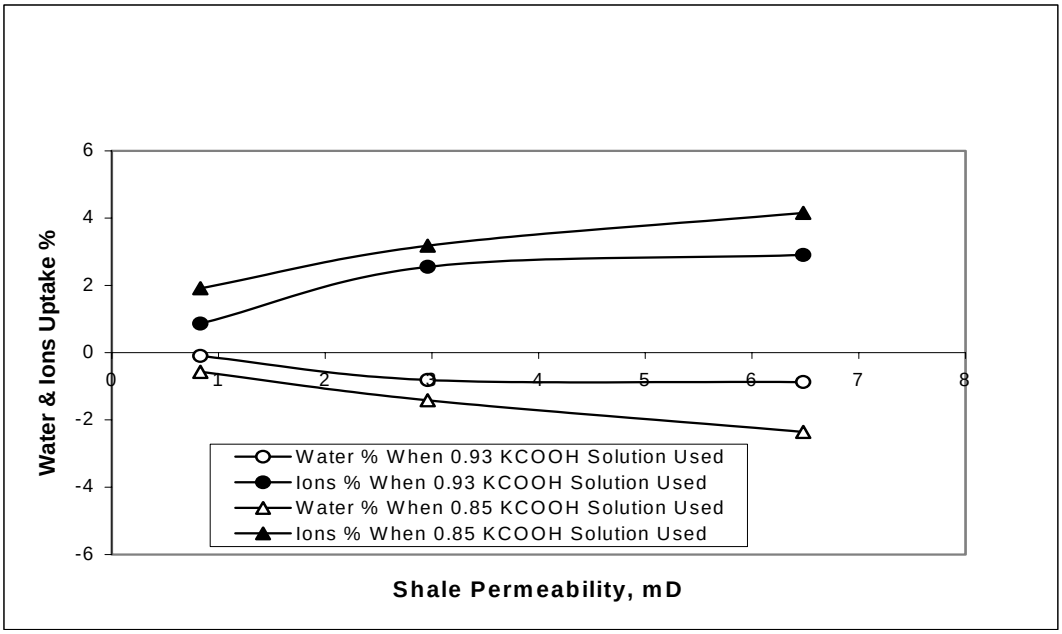

Figure 5-42: Water and ions uptake versus shale permeability (KCOOH solution).

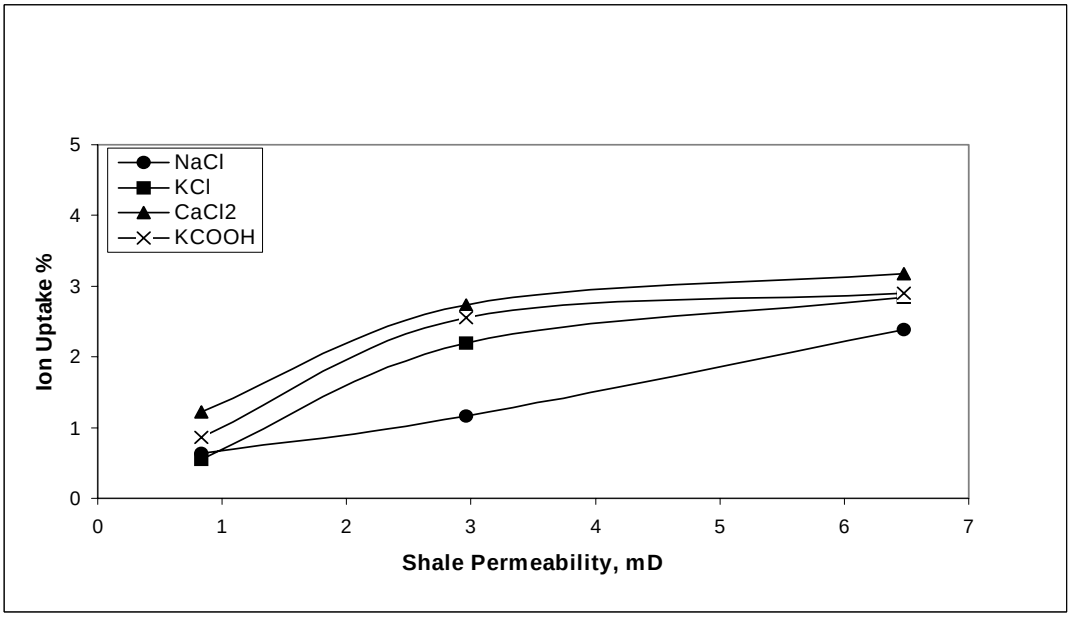

Figure 5-43: Ion uptake versus shale permeability when different salt solutions of 0.93 water activity interacted with shales of different permeabilities.

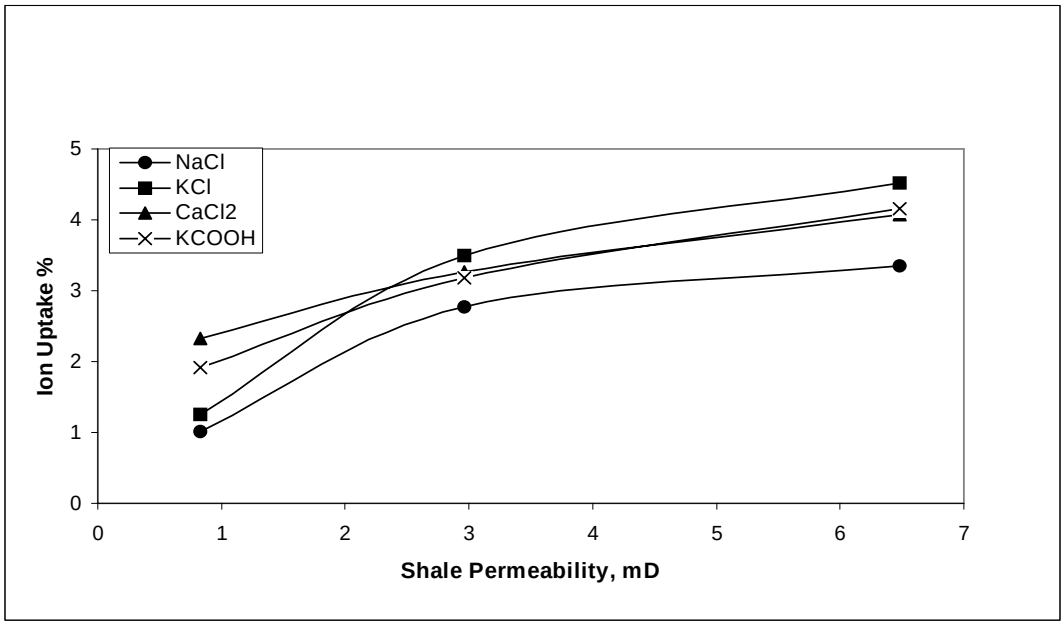

Figure 5-44: Ion uptake versus shale permeability when different salt solution of 0.85 water activities interacted with shales of different permeabilities.

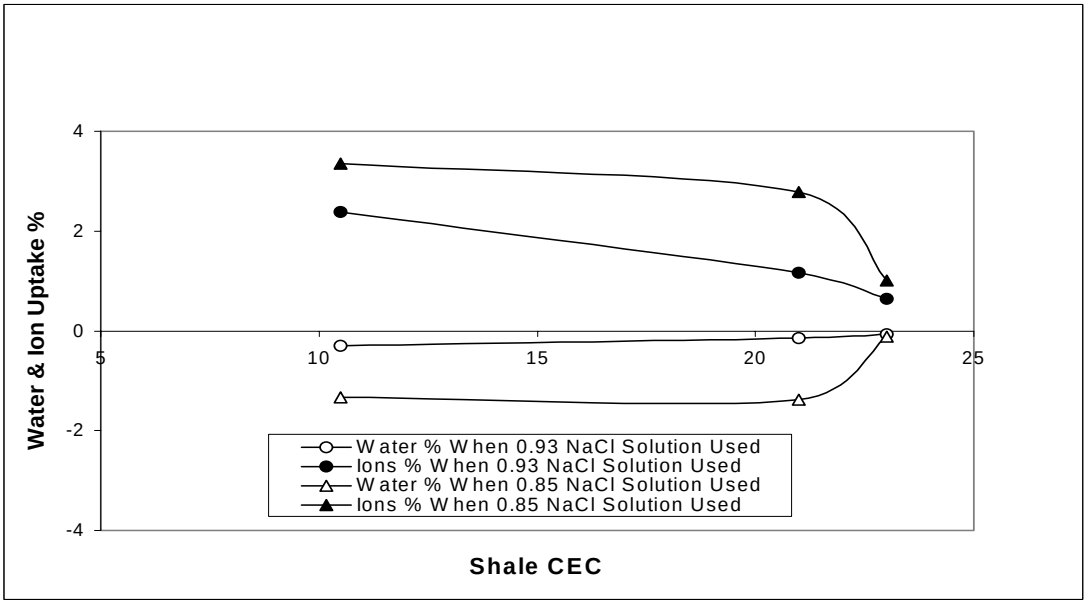

Figure 5-45: Water and ion uptake versus shale CEC (NaCl solution).

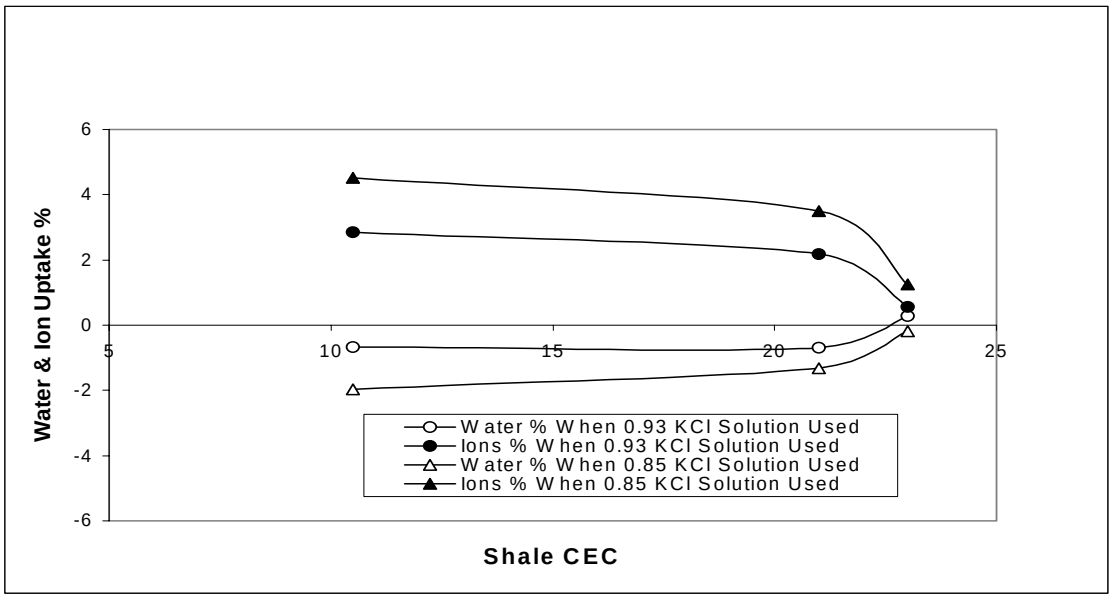

Figure 5-46: Water and ion uptake versus shale CEC (KCl solution).

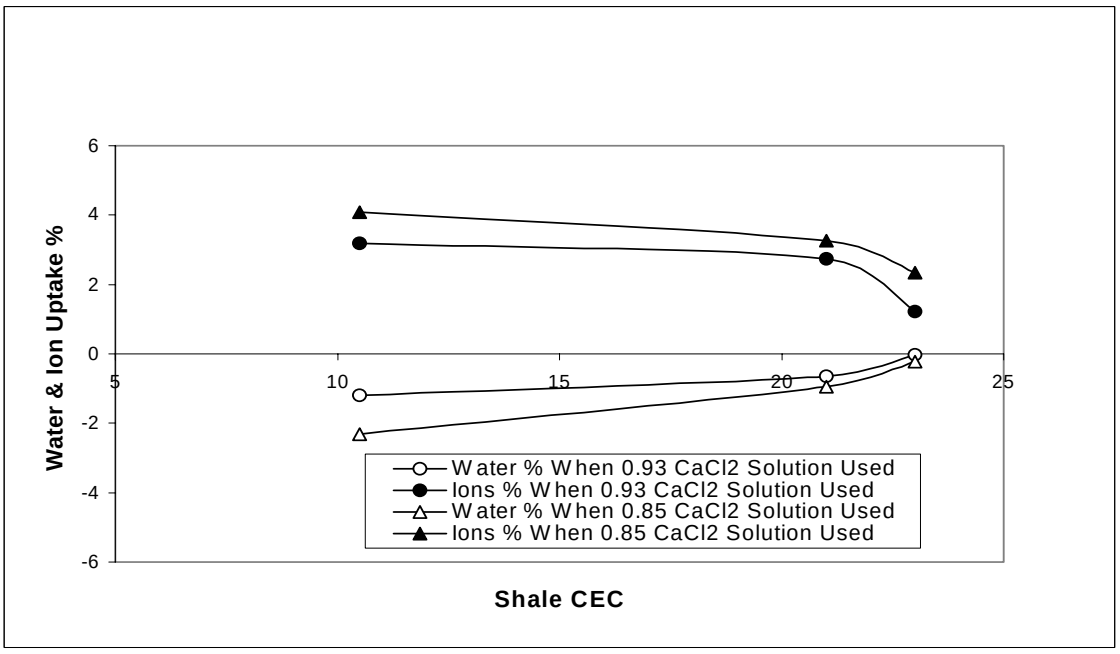

Figure 5-47: Water and ion uptake versus shale CEC ($CaCl_2$ solution).

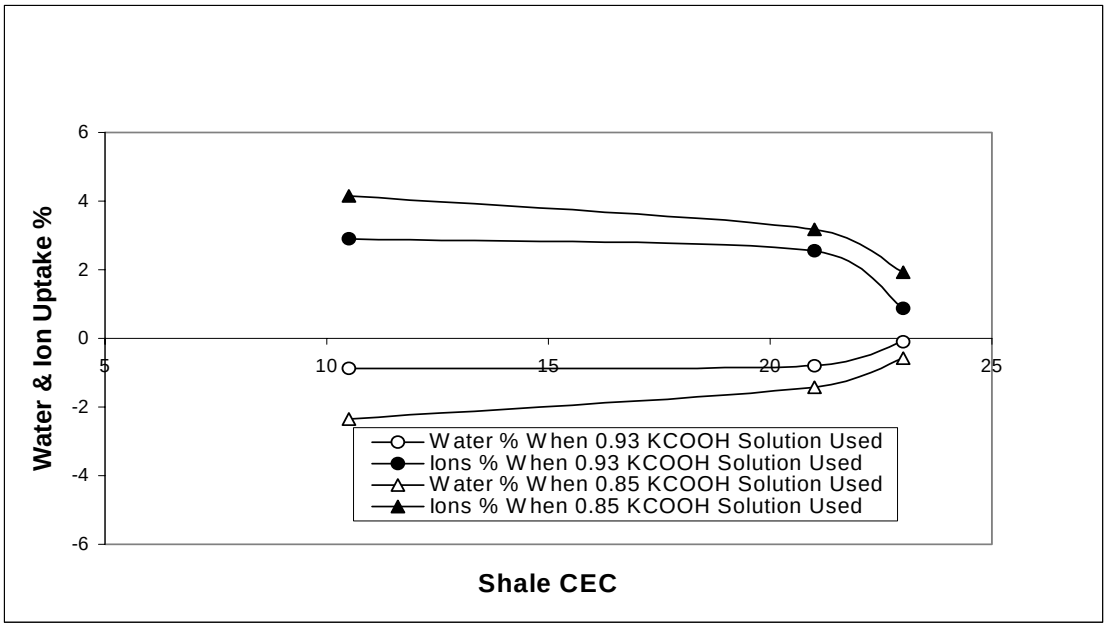

Figure 5-48: Water and ion uptake versus shale CEC (KCOOH solution).

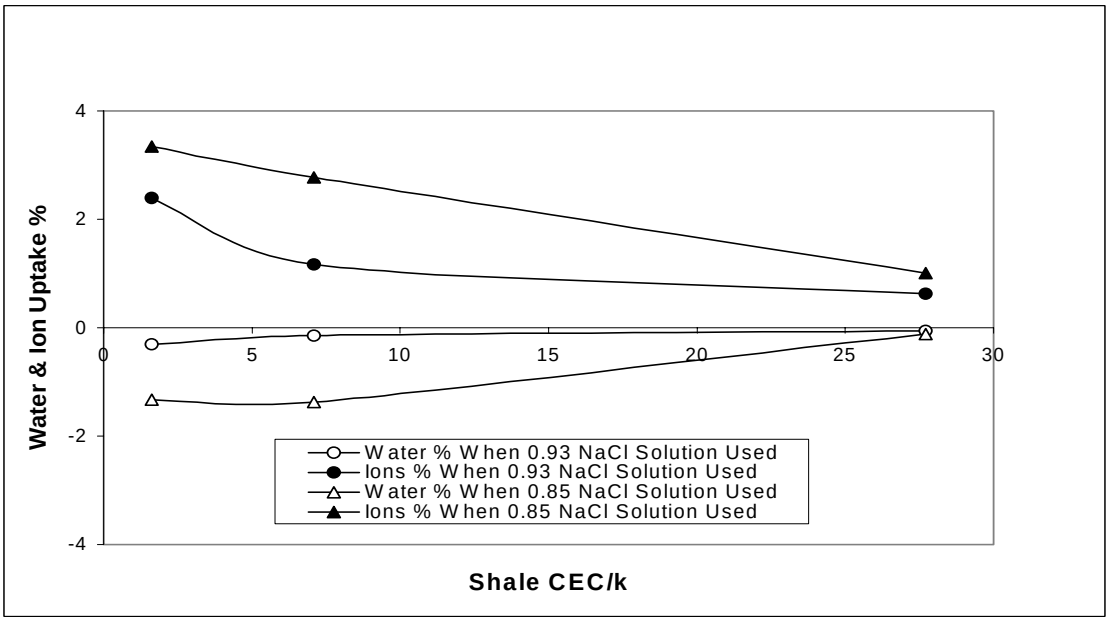

Figure 5-49: Water and ion uptake versus shale CEC/k (NaCl solution).

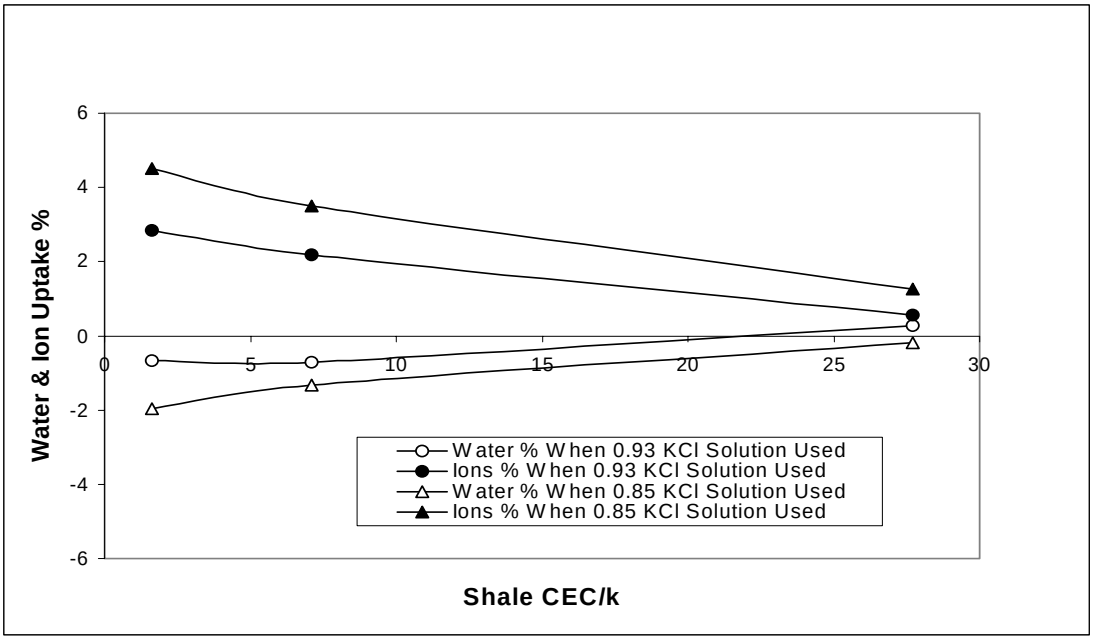

Figure 5-50: Water and ion uptake versus shale CEC/k (KCl solution).

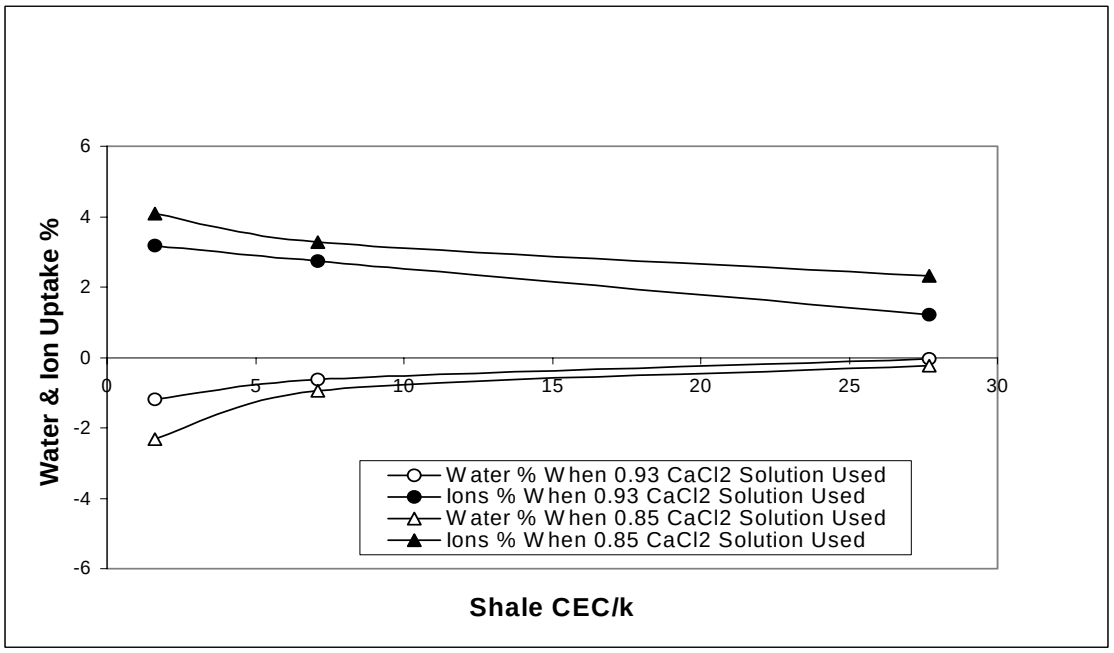

Figure 5-51: Water and ion uptake versus shale CEC/k ($CaCl_2$ solution)

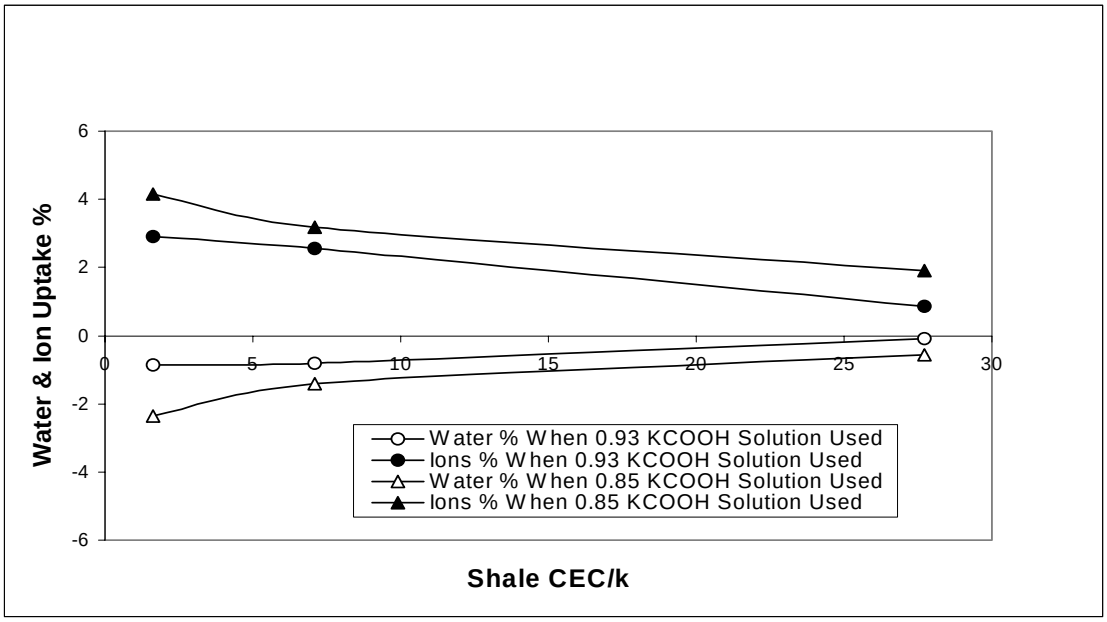

Figure 5-52: Water and ion uptake versus shale CEC/k (KCOOH solution).

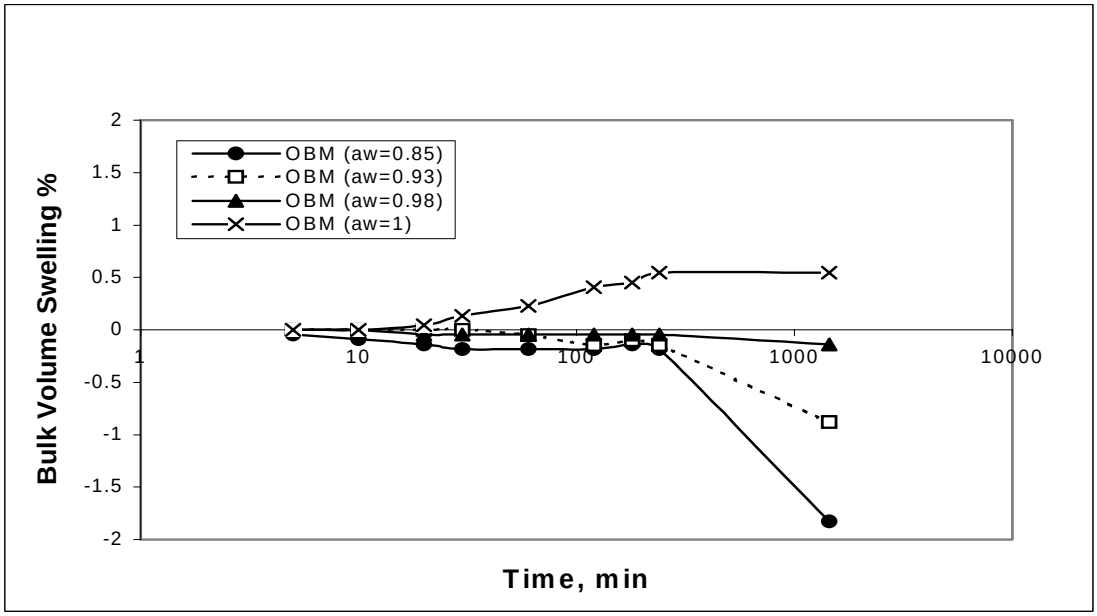

Figure 5-53: Bulk volume swelling curves for C1-shale (a_w = 0.98) during interaction with oil-based muds of different water activities.

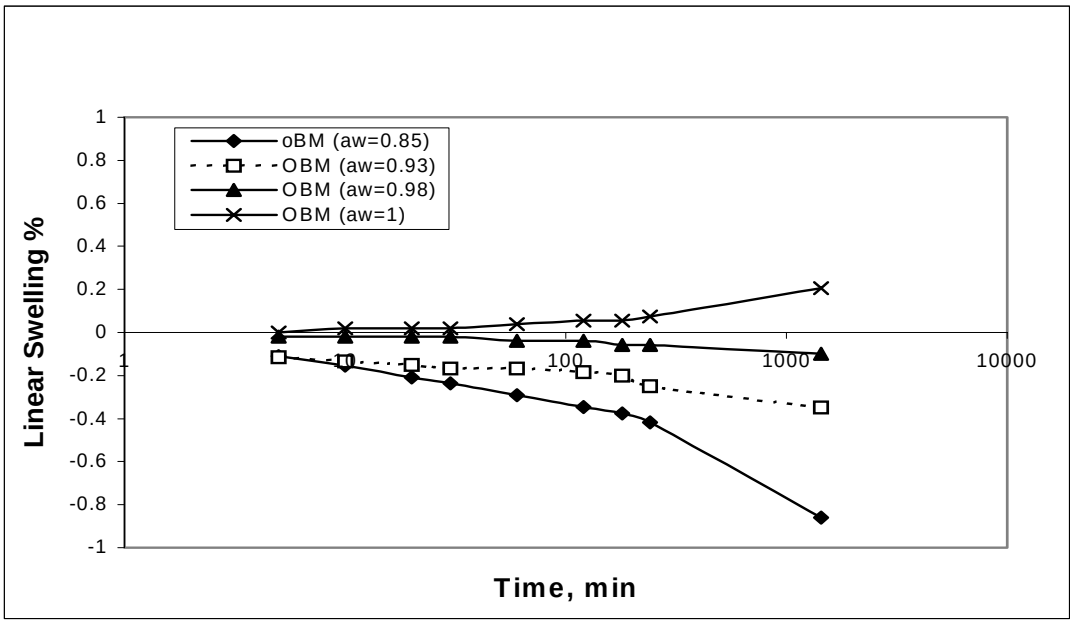

Figure 5-54: Linear swelling curves for C1-shale during interaction with oil-based muds of different water activities.

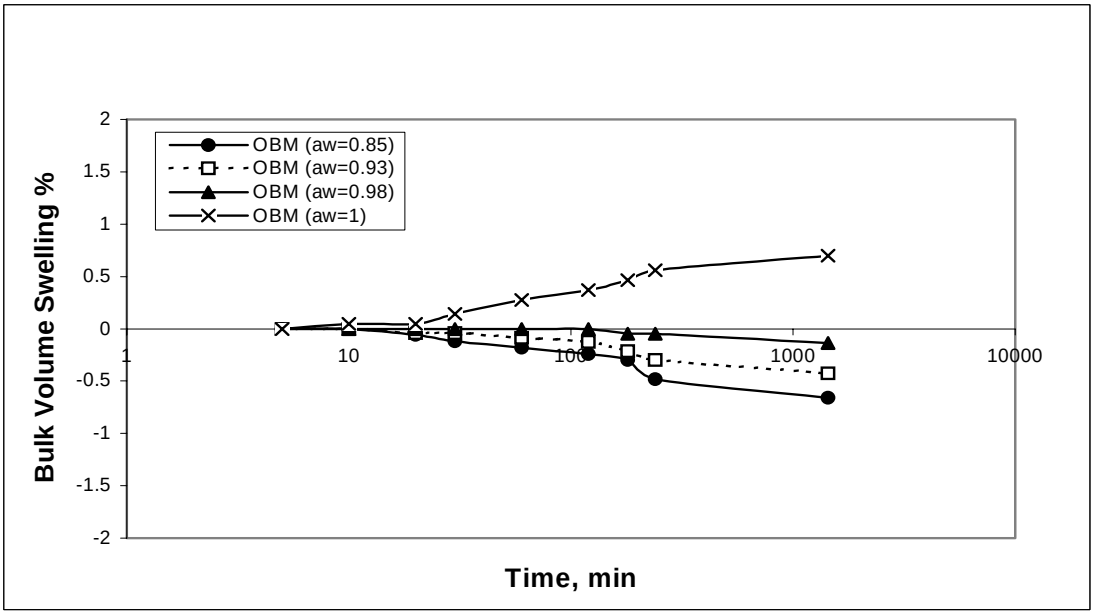

Figure 5-55: Bulk volume swelling curves for Pierre shale during interaction with oil-based muds of different water activities.

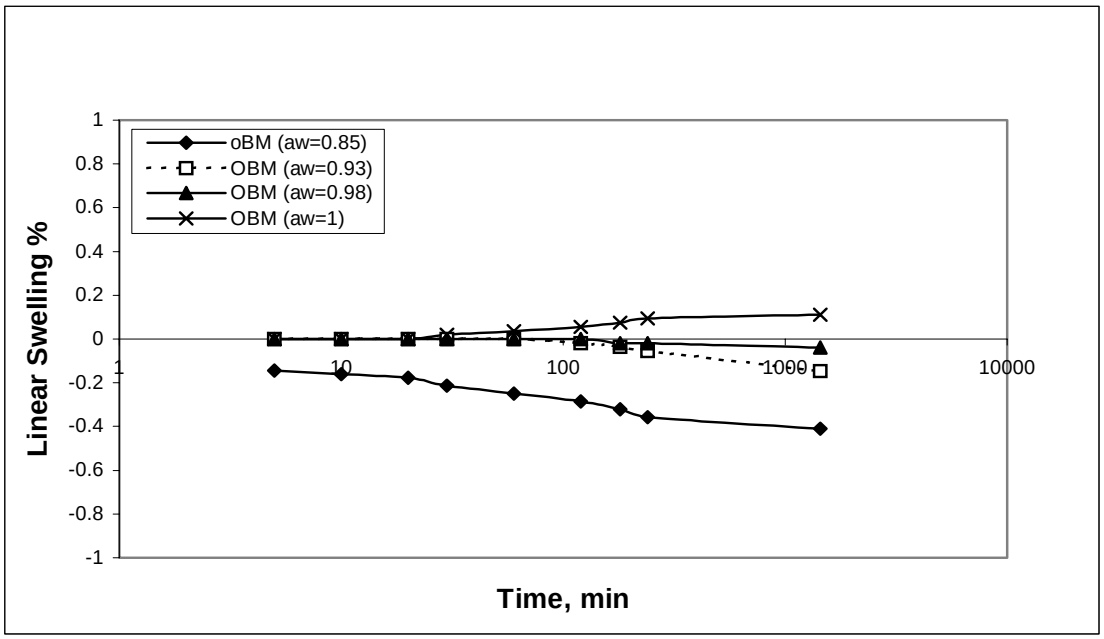

Figure 5-56: Linear swelling curves for Pierre shale during interaction with oil-based muds of different water activities.

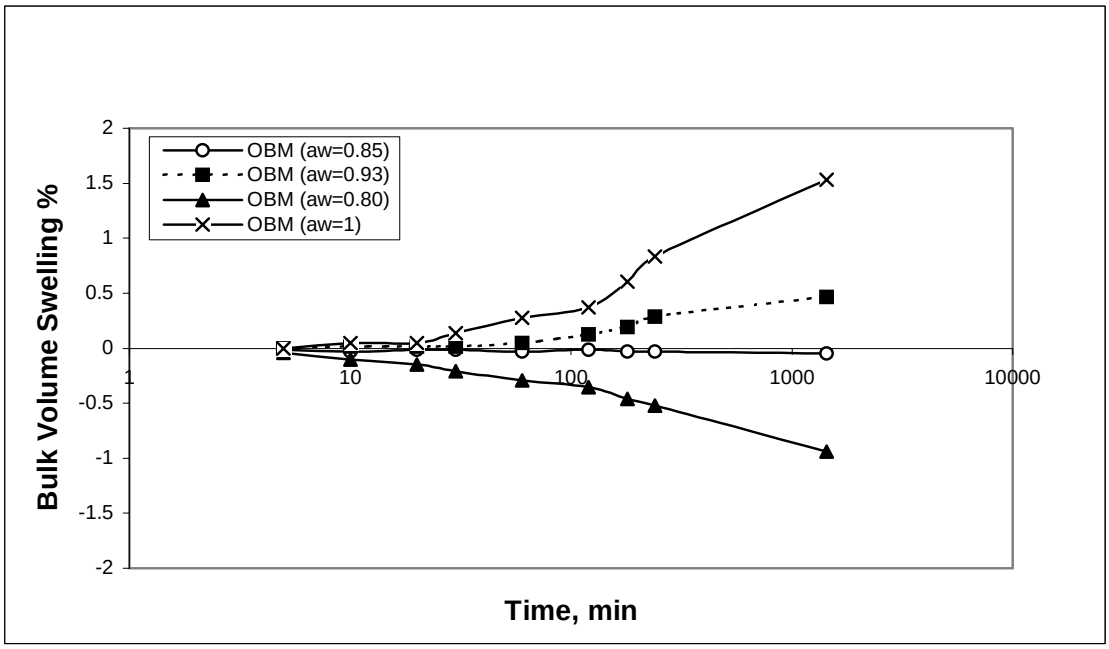

Figure 5-57: Bulk volume swelling curves for Arco-China shale during interaction with oil-based muds of different water activities.

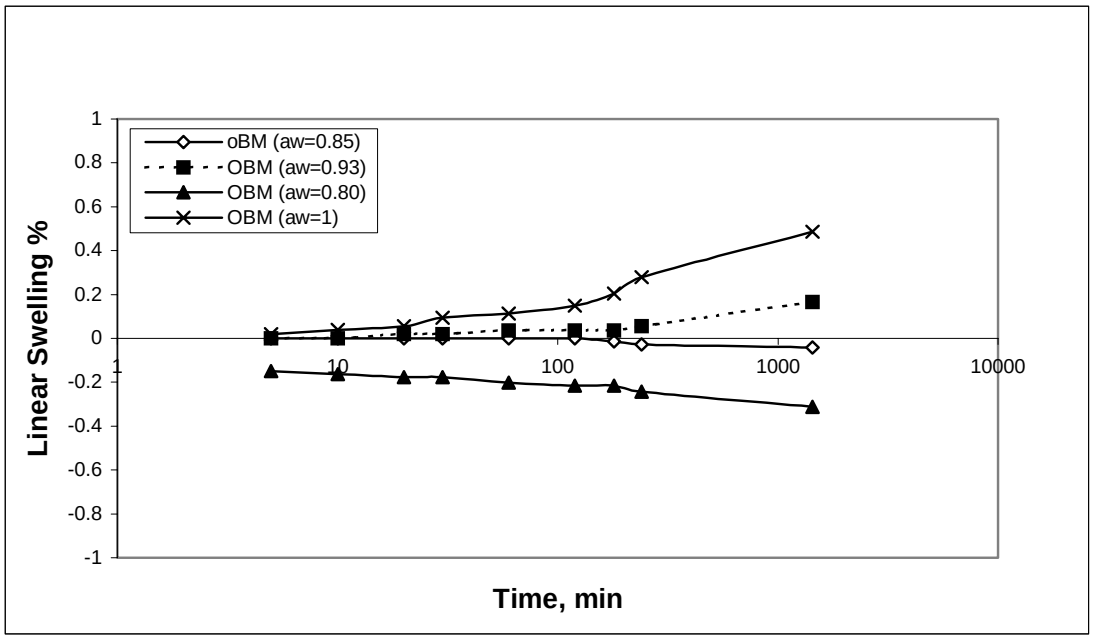

Figure 5-58: Linear swelling curves for Arco-China shale during interaction with oil-based muds of different water activities.

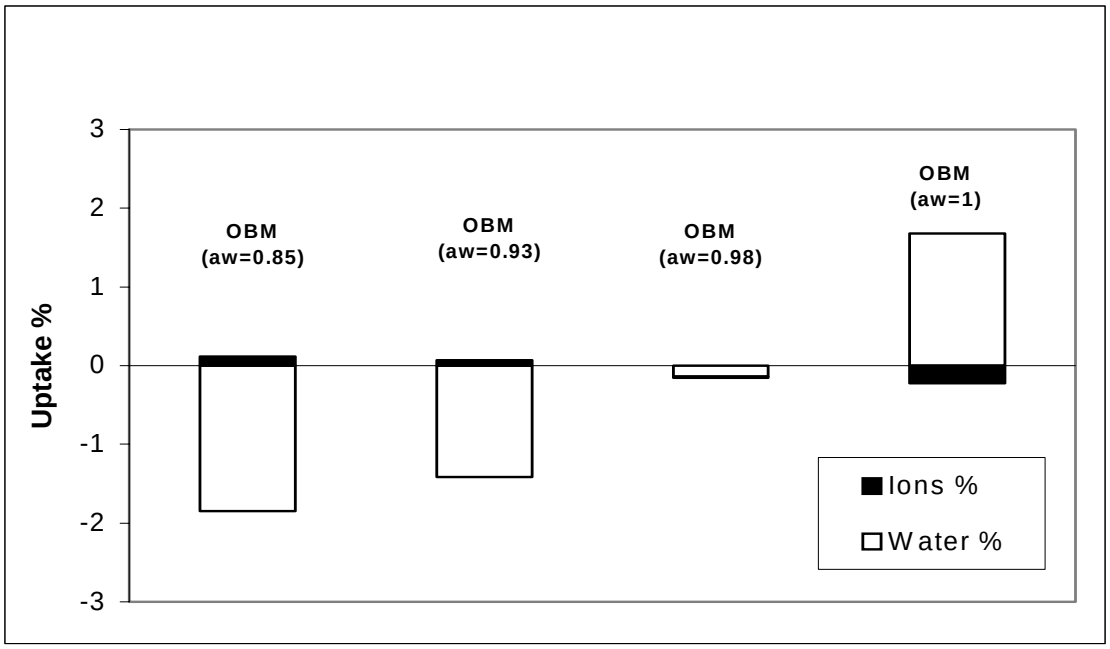

Figure 5-59: Water and ion uptake during C1-shale interaction with oil-based muds of different water activities.

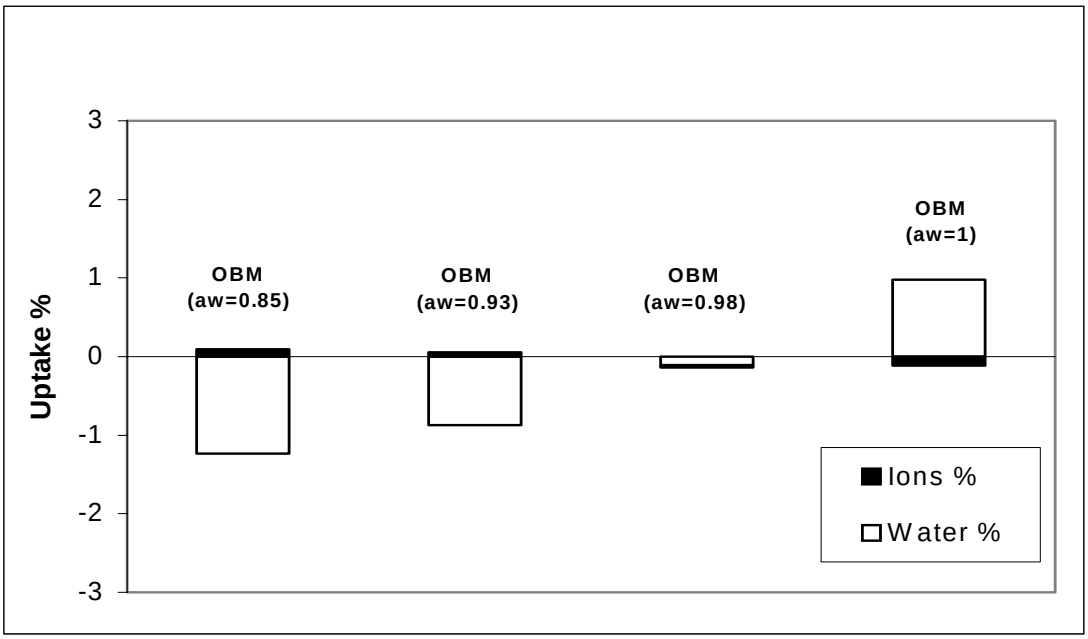

Figure 5-60: Water and ion uptake during Pierre shale interaction with oil-based muds of different water activities.

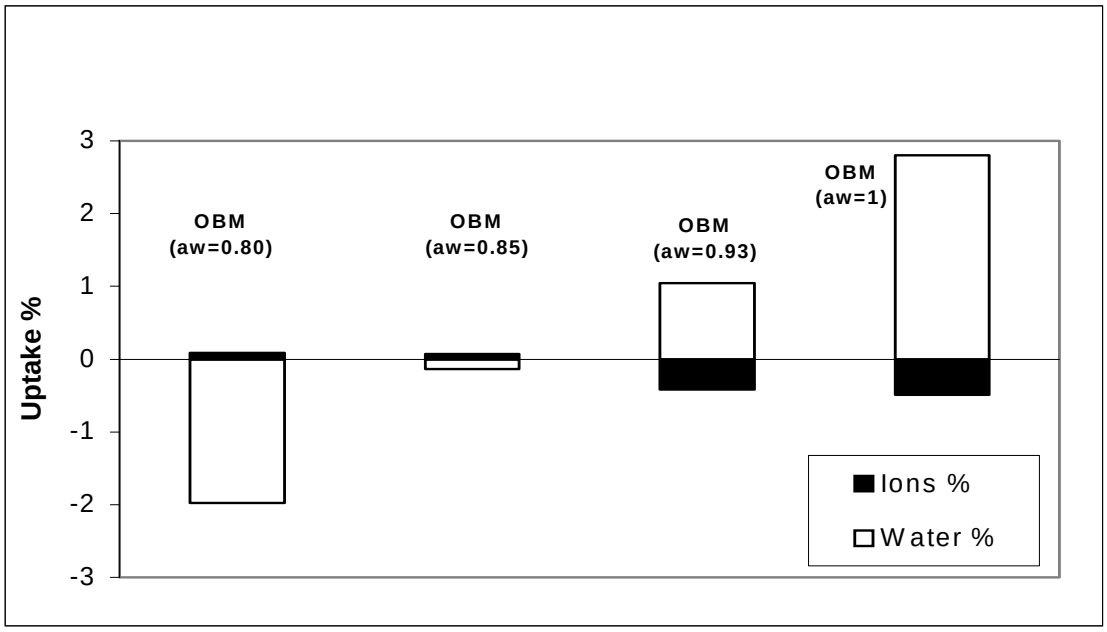

Figure 5-61: Water and ion uptake during Arco-China shale interaction with oil-based muds of different water activities.

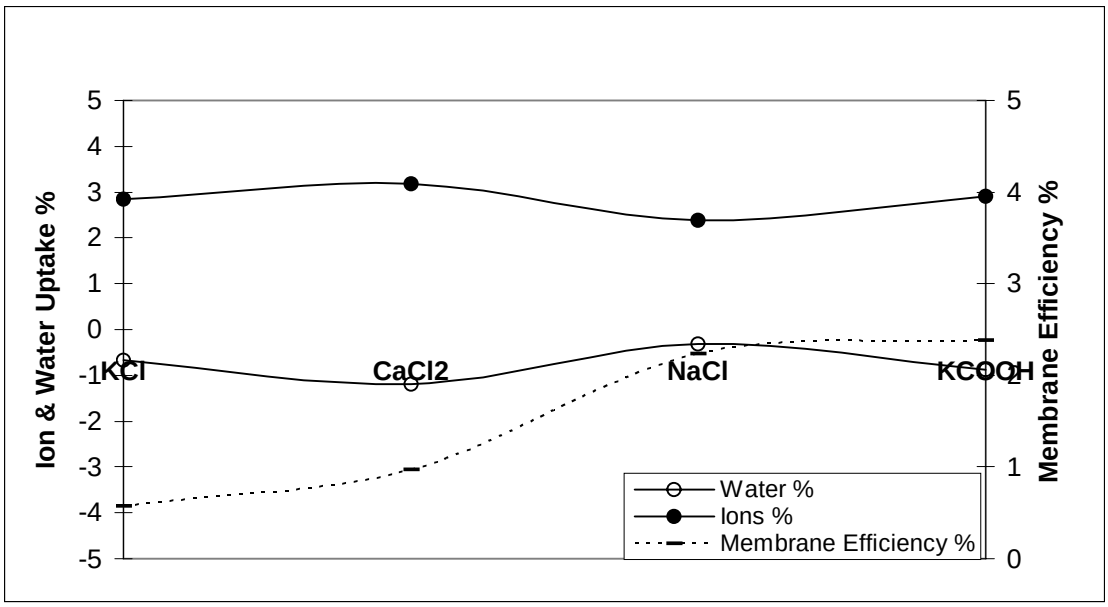

Figure 5-62: The membrane efficiency dependence on water and ion uptake for C1 shale when interacted with different salt solutions of 0.93 water activity.

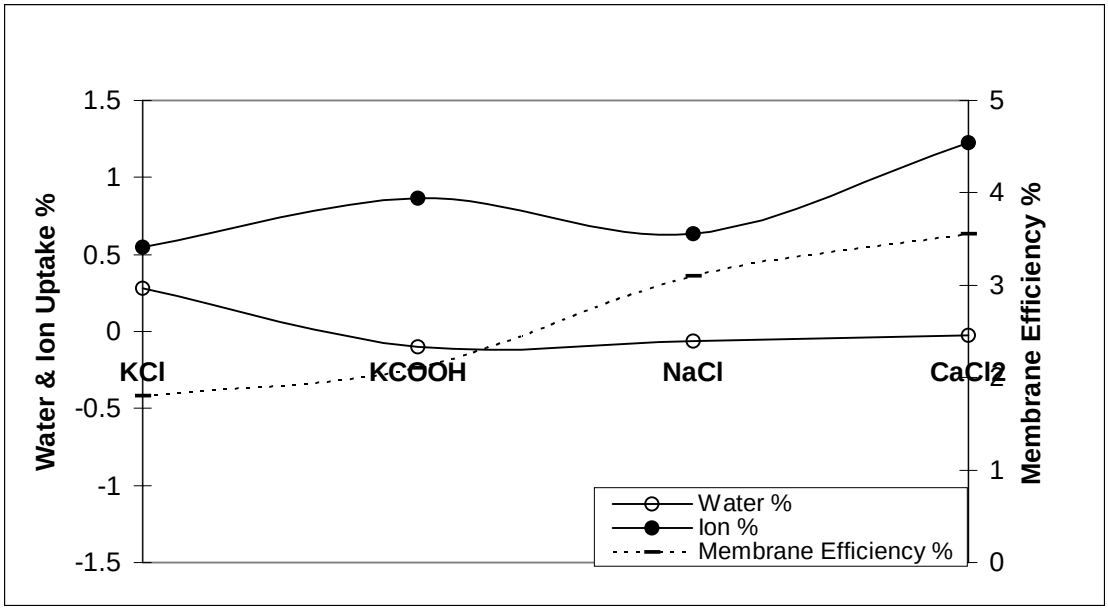

Figure 5-63: The membrane efficiency dependence on water and ion uptake for C2 shale when interacted with different salt solutions of 0.93 water activity.

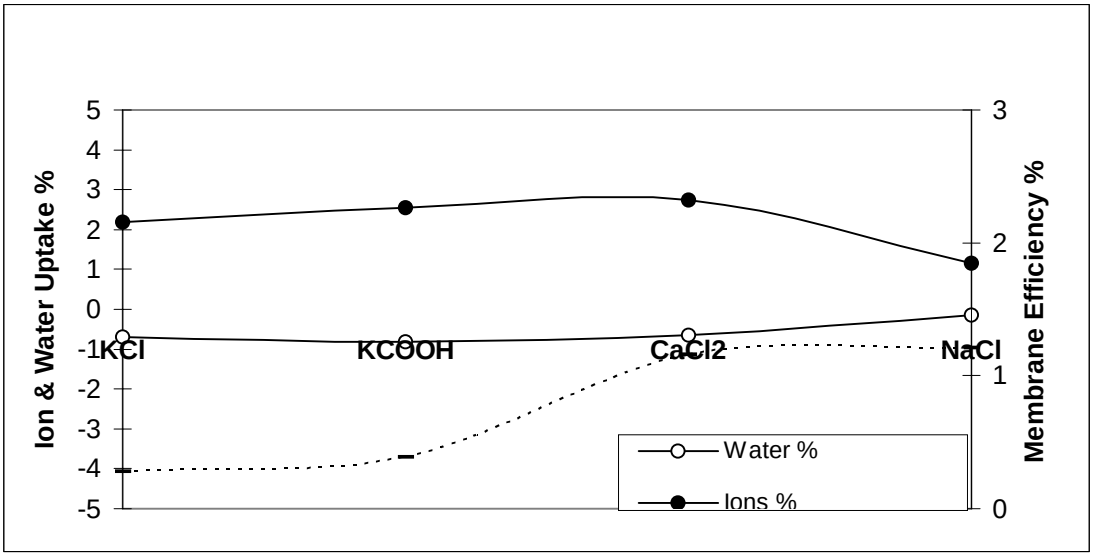

Figure 5-64: The membrane efficiency dependence on water and ion uptake for Pierre shale when interacted with different salt solutions of 0.93 water activity.

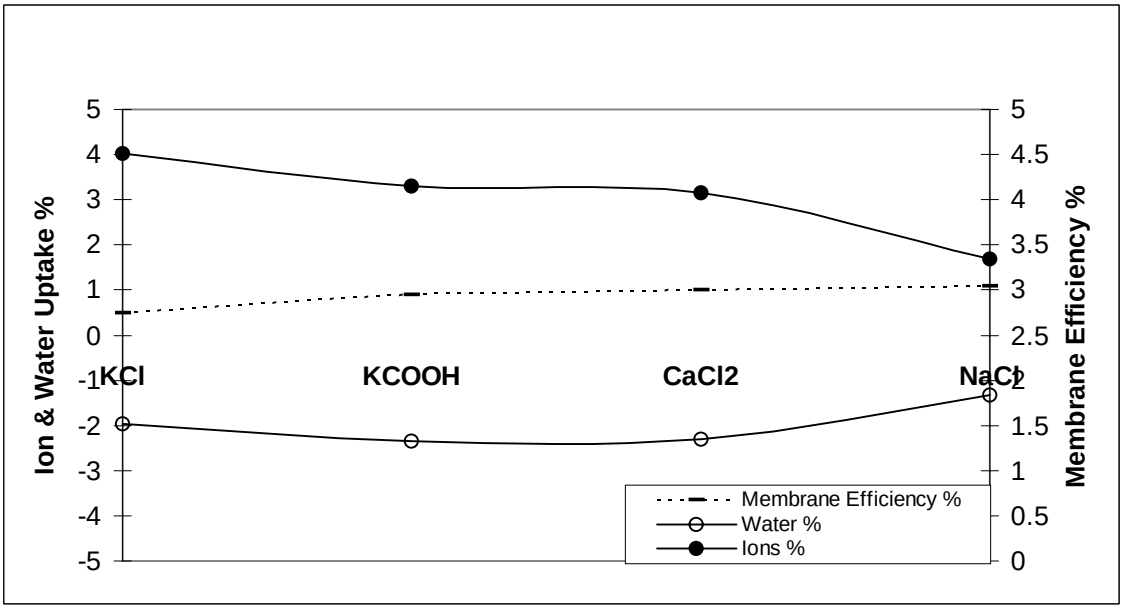

Figure 5-65: The membrane efficiency dependence on water and ion uptake for C1-shale when interacted with different salt solutions of 0.85 water activity.

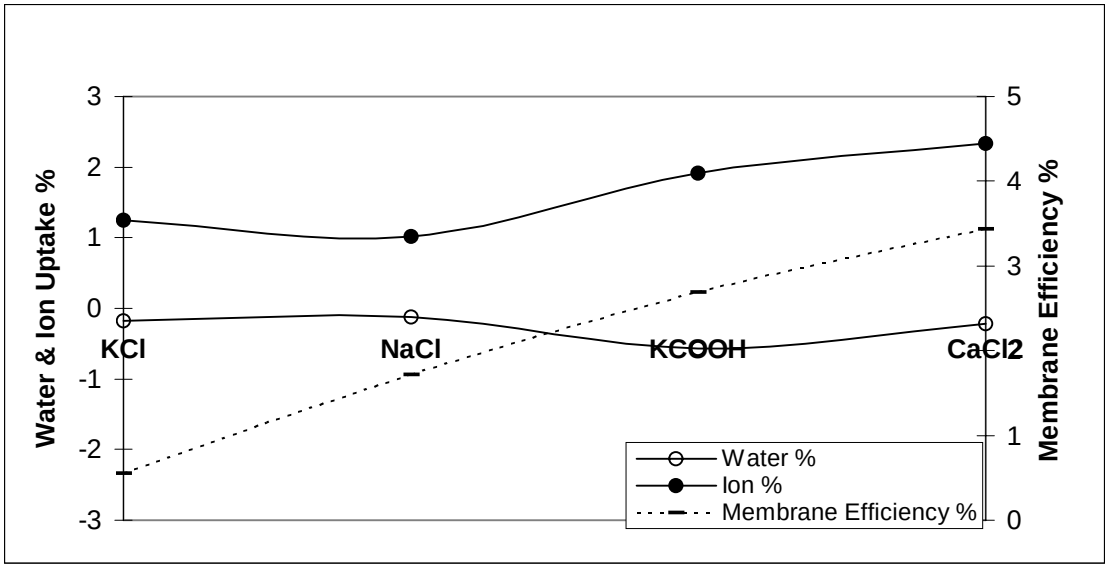

Figure 5-66: The membrane efficiency dependence on water and ion uptake for C2-shale when interacted with different salt solutions of 0.85 water activity.

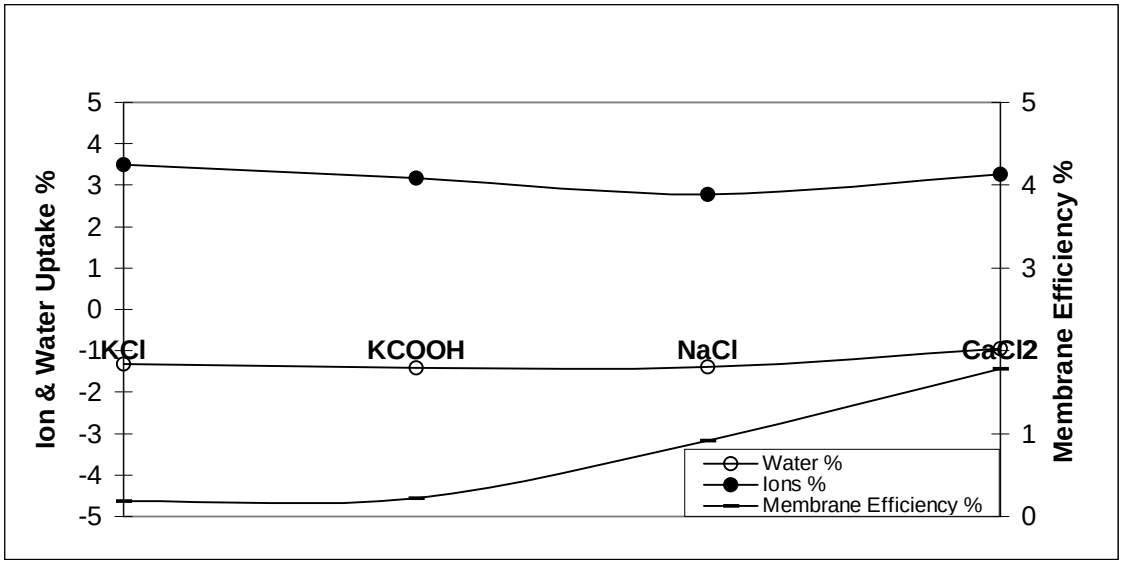

Figure 5-67: The membrane efficiency dependence on water and ion uptake for Pierre shale when interacted with different salt solutions of 0.85 water activity.

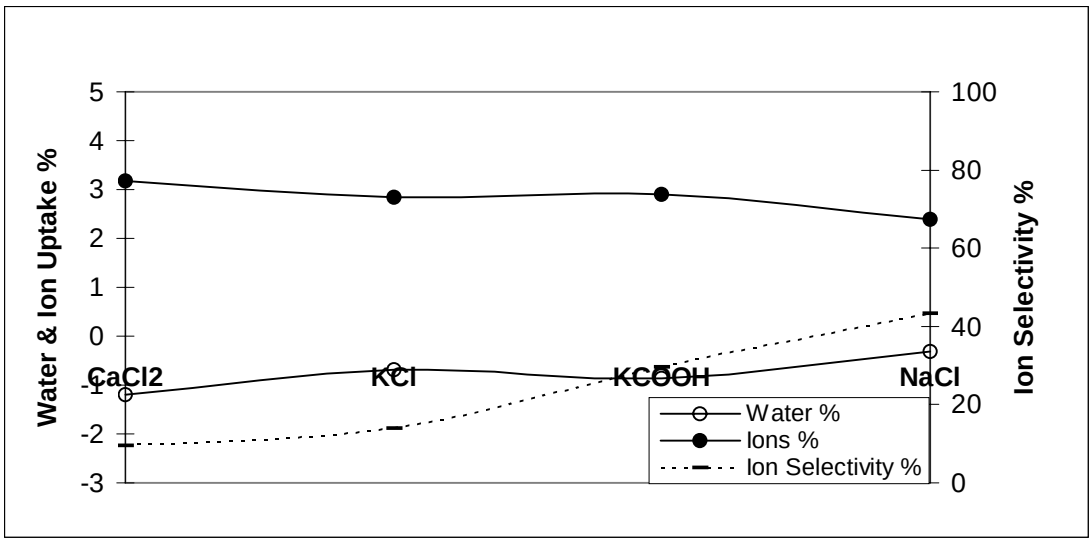

Figure 5-68: The ion selectivity dependence on water and ion uptake for C1 shale when interacted with different salt solutions of 0.93 water activity.

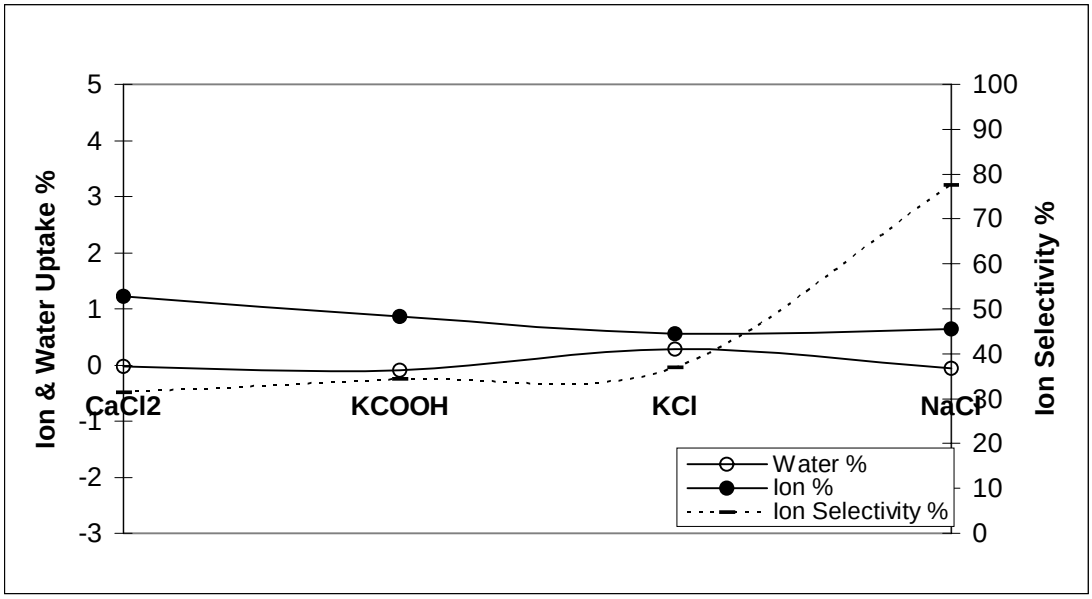

Figure 5-69: The ion selectivity dependence on water and ion uptake for C2 shale when interacted with different salt solutions of 0.93 water activity.

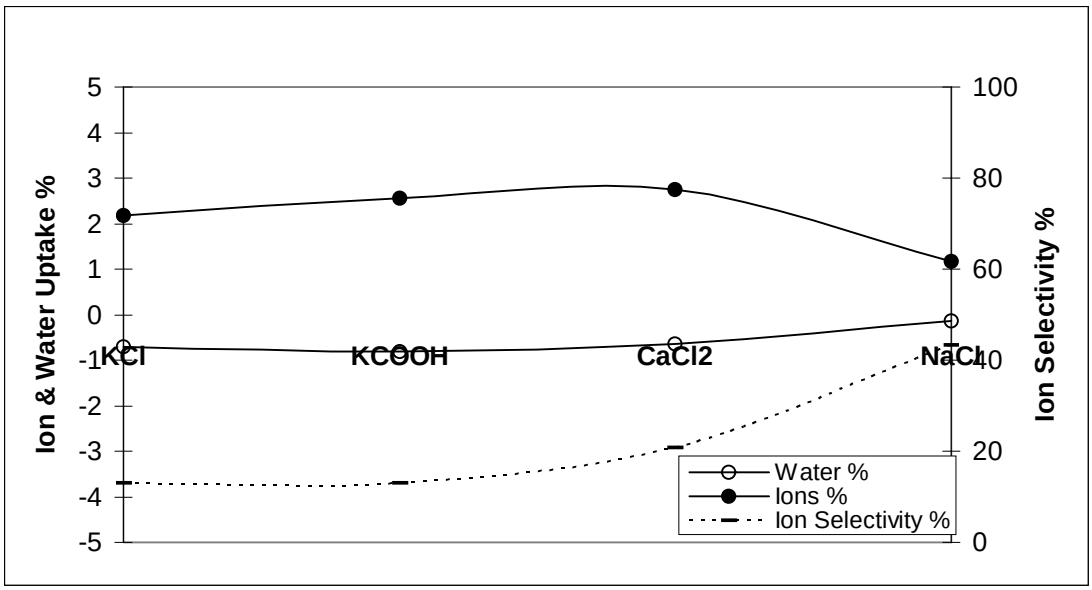

Figure 5-70: The ion selectivity dependence on water and ion uptake for Pierre shale when interacted with different salt solutions of 0.93 water activity.

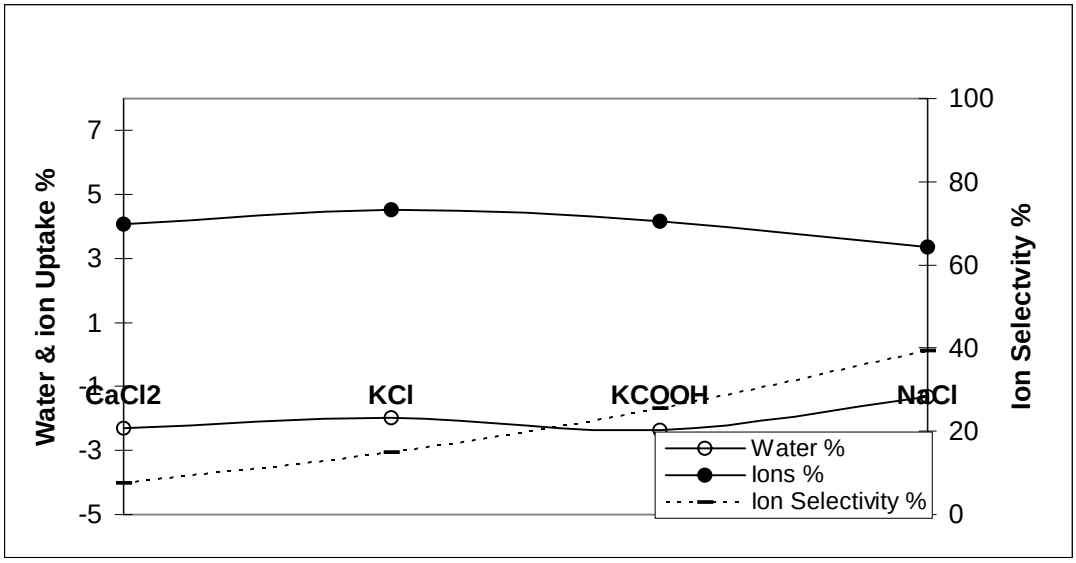

Figure 5-71: The ion selectivity dependence on water and ion uptake for C1 shale when interacted with different salt solutions of 0.85 water activity.

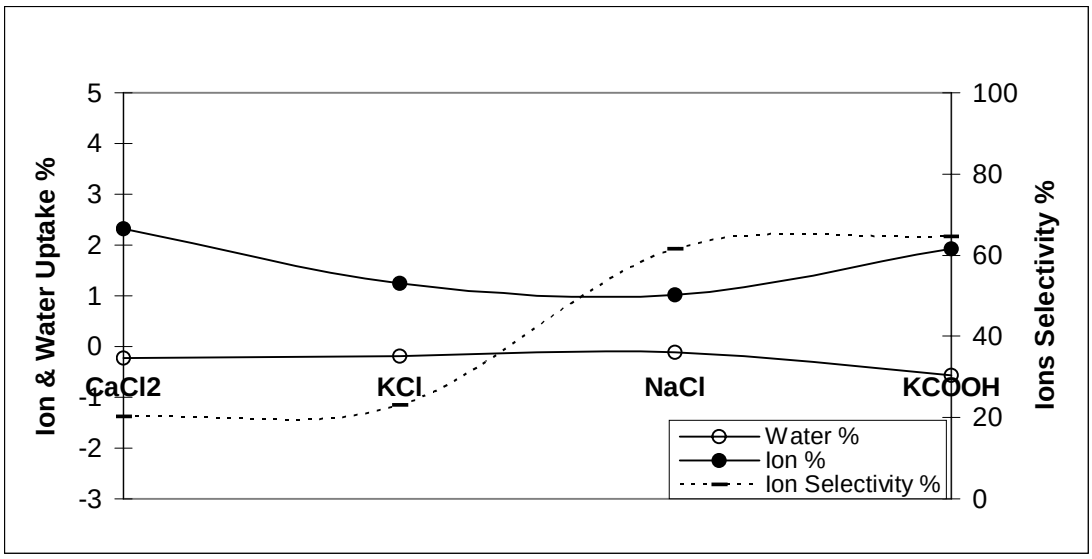

Figure 5-72: The ion selectivity dependence on water and ion uptake for C2 shale when interacted with different salt solutions of 0.85 water activity.

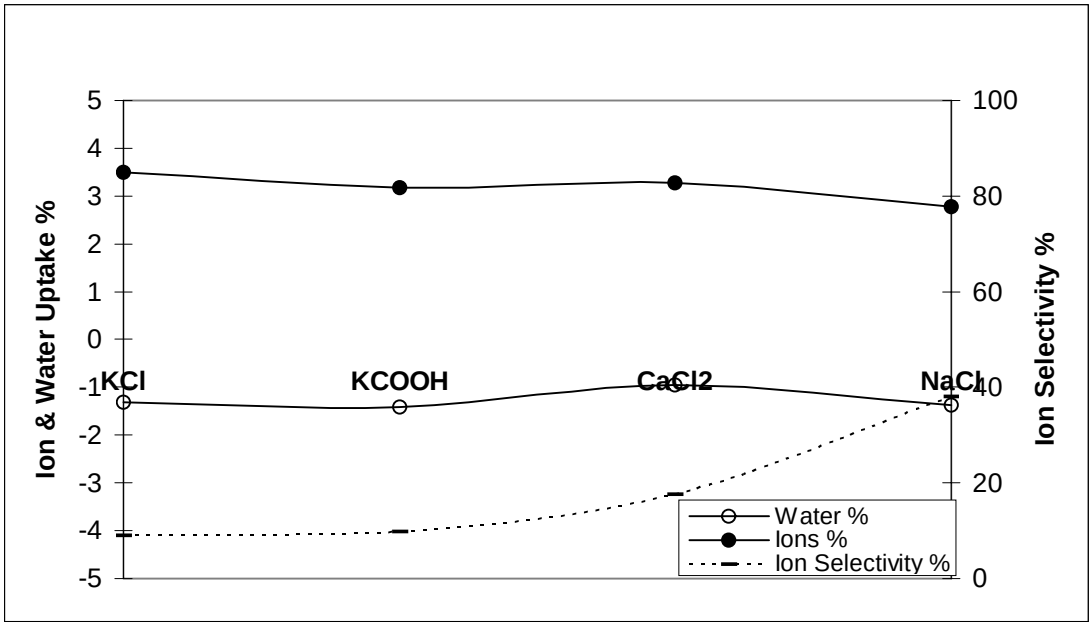

Figure 5-73: The ion selectivity dependence on water and ion uptake for Pierre shale when interacted with different salt solutions of 0.85 water activity.

CHAPTER 6

Impact of Temperature on the Membrane Efficiency of Shale

6.1 INTRODUCTION

The chemical and physical properties of both shale and drilling fluid are highly influenced by temperature (van Oort, 1997). Such physicochemical effects of temperature on interactions with drilling fluids have been mostly ignored due to the fact that these interactions become more complicated under high temperature conditions. Many authors have conducted shale membrane efficiency experiments at ambient temperature. The results obtained were used to guide in the formulation of drilling fluids that are aimed at solving shale problems downhole where the temperature is much higher. This approach ignores the effect of temperature and could lead to inaccurate wellbore instability diagnosis and remediation**.**

Chenevert and Strassner (1975) showed that the swelling behavior of shales when coming in contact with aqueous solutions is influenced by temperature. They attributed this to the fact that the water activities of the shale and the drilling fluid change as the temperature changes, though not by the same magnitude. They added that the difference in water activities between the shale and the drilling fluid changes the chemical potential gradient and thus leads to more or less water adsorption by the shale. While changes in temperature certainly affect the chemical potential and thus the adsorptive pressure of shales, we believe, that higher temperature could affect the mechanical and physico-chemical properties of a shale and could indeed impact its membrane efficiency.

Besides the effect of temperature on a shales' adsorptive pressure and membrane efficiency, the existence of a temperature gradient across the shale could also have an effect on the transport of water in or out of shales. It is well accepted that fluid flow through a membrane is accompanied by the flow of solute, heat and current. According to Ghassemi et al (2001), the presence of a temperature gradient can trigger thermal osmosis. This concept could be used to thermally induce an osmotic back flow out of the shale in order to enhance its strength.

This chapter addresses the influence of temperature on shales' interactions with aqueous solutions. Membrane efficiency measurements were conducted under high pressure and high temperature conditions in order to best simulate downhole conditions. In addition, experiments were run to show the influence of thermal osmosis on a shales' interactions with aqueous solutions.

6.2 HIGH TEMPERATURE MEMBRANE EFFICIENCY TEST DESCRIPTION

6.2.1 Test Definition and Objectives

The high temperature membrane efficiency test makes use of a pressure transmission technique where shale samples are subjected to both hydraulic and osmotic gradients during exposure to water-based muds. This test makes use of an oven in order to vary the test temperature as desired. The pressure drop across the shale sample at different temperatures is measured in response to both hydraulic and osmotic pressure gradients. The pressure drop at different temperatures is converted to membrane efficiency in order to analyze the temperature effect on shale membrane efficiencies.

The thermal osmosis test also makes use of a pressure transmission technique where shale samples are subjected to both hydraulic and osmotic gradients during exposure to water-based muds. However, in this test, the temperature of the upstream fluid, flowing across the shale, is raised from 70^{o}F to 200^{o}F while the shale and downstream fluid is kept at 70^{o}F. This is done in order to create a temperature gradient across the shale so as to study the significance of thermal osmosis. The pressure drop across the shale sample before and after imposing a temperature gradient is measured and converted to a membrane efficiency of the shale. The membrane efficiency before and after imposing a temperature gradient is analyzed in order to see the effect of thermal osmosis in our test. The following describes the objectives of these tests.

- Perform pressure transmission tests on shale samples at different temperatures in order to estimate the shale membrane efficiency and resultant osmotic pressure.
- Study the impact of elevated temperatures on the membrane efficiency of shale and the resultant osmotic pressure.
- Study the influence of thermal osmosis, in response to temperature gradient, on the membrane efficiency of shales.

6.2.2 Test Equipment and Procedure

In order to evaluate temperature effects on interactions of shales with drilling fluids, we have used the same equipment and experimental set up that was used in Chapter 3. The only difference is that the cell and flow lines were kept inside an oven. The oven allowed us to vary the temperature in order to study its effect on the membrane

efficiency of shale and induced osmotic pressure. In this test, we exposed the shale to a salt solution of different water activity at room temperature (70^{o}F). After the test has reached equilibrium, we raised the temperature of the oven that hosts the shale and the salt solutions to 200^{o}F. We waited until the test reached equilibrium again and then dropped the temperature of the oven to 70^{o}F. This test was done in this sequence in order to have a direct comparison between the shale membrane efficiencies at different temperatures. This made analyzing the results much easier since the only differing factor was temperature.

For thermal osmosis experiments, we also employed the same equipment and experimental set up used in Chapter 3. However, we used a heating wire to wrap only the upstream flow lines in order to increase its temperature as desired. It is important to note that the upstream flow lines were wrap-heated while the shale and downstream chamber were kept at room temperature in order to create a temperature gradient across the shale. In these experiments, we imposed hydraulic and osmotic gradients across the shale at room temperature (70^{o}F). After the test reached equilibrium, the upstream flow lines (fluid) temperature was raised and kept at 200^{o}F while the downstream fluid temperature was maintained at 70^{o}F. After equilibrium was again reached, we dropped the upstream flow lines and fluid temperature to 70^{o}F. Note that we only varied the upstream temperature in this test so that we can verify and measure thermal osmosis effects on the membrane efficiency of shale.

6.3 RESULTS & DISCUSSION

As stated previously, we conducted two types of experiments in order to investigate the effects of temperature on shale interactions with aqueous solutions. The following discusses the results obtained from these experiments.

6.3.1 Membrane Efficiency of Shale at High Temperature

In this test, we have measured the membrane efficiency for the same shale (C1 shale) and drilling fluid at both 70^{o}F and 200^{o}F temperatures in order to study the effect of temperature on the membrane efficiency of shale. Figures 6-1, 6-2, 6-3 and 6-4 show C1 shale interactions with NaCl, KCl, $CaCl_2$ and KCOOH at different temperatures where the test temperature was increased from 70^{o}F to 200^{o}F and then returned to 70^{o}F. From these figures, it is clearly seen that the pressure drop and the membrane efficiency of C1 shale were affected by temperature changes. For example, in the case where C1 shale was exposed to NaCl solution at room temperature, the estimated membrane efficiency and pressure drop were 1.97% and 20.3 psi respectively. When the temperature of the system was raised to 200^{o}F, the membrane efficiency and pressure drop increased to 2.74% and 28.2 psi. When the temperature was dropped again to 70^{o}F, the membrane efficiency and induced pressured drop decreased to 1.6% and 16.5 psi respectively. It is clearly seen that both the membrane efficiency and pressure drop were influenced by temperature. This trend was also observed when C1 shale interacted with KCl, $CaCl_2$ and KCOOH solutions.

6.3.2 Impact of Temperature on the Physico-Chemical Properties of Shale

Two phenomena are observed in these tests. The first phenomenon is that the pressure drop and membrane efficiency of C1 shale increased when the temperature increased from 70^{o}F to 200^{o}F. Figures 6-5 and 6-6 show the pressure drop and membrane efficiency behavior of C1 shale for NaCl, KCl, CaCl2 and KCOOH solutions as the temperature is changed from 70^{o}F to 200^{o}F. It is clearly shown that the pressure drop and membrane efficiency increased for all solutions when the temperature was raised from 70^{o}F to 200^{o}F. It is important to state that the membrane efficiency at 200^{o}F was calculated assuming that the water activities of the shale and aqueous fluids did not change as the temperature increased. This assumption may not be valid since we know that the water activity of fluids changes with temperature. Chenevert and Strassner (1975) showed that the water activity of shale and oil muds increased when the temperature increased from 25^{o}C to 100^{o}C. More specifically, they showed that the shale's water activity increased with temperature more rapidly than the salt solution's water activity. In other words, the water activity (chemical potential) gradient increased as the temperature increased. In our tests, we started with a 0.98 shale water activity and 0.93 salt solution water activity. As we increased the temperature from 70^{o}F to 200^{o}F, we believe that both the shale and salt solution water activities increased though not by the same magnitude. We believe that the shale water activity increased more than the salt solution water activity and this in turn increased the chemical potential gradient, which was manifested in a bigger pressure drop. While we believe that the chemical potential gradient increase is a valid explanation for the higher pressure drop and membrane efficiency as the temperature increased from 70^{o}F to 200^{o}F, this may not tell the whole story. The increase in temperature may have affected the physical and electrochemical properties of the clay. The diffuse double layer that occurs at the interface between the

clay surface and the bulk solution is comprised of the permanent negative charges on the clay and the cations (counter-ions) in the solution that balance the negative charge. At equilibrium, the counter-ions are subjected to two equal but opposing forces; the electrical force that attracts the cations to the negative surface, and the diffusive force which tends to move the cations away from the region of high concentration. The balance between these two gives rise to a distribution of cations in water adjacent to the clay surface and determines the thickness of the diffuse double layer. An increase in temperature will increase the kinetic energy of the cations in the diffuse double layer between the clay platelets. This increase in kinetic energy of cations could overcome the attractive forces between them and the shale negative surface and this indeed could allow them to diffuse away from the shale surface. This expansion of the double layer increases the clays (or shales) ability to screen out co-ions and thus improves its membrane efficiency.

In addition to the shale's negative surface charge, the shale's membrane efficiency is also a strong function of the shale's pore throat size. We believe that if the shale is confined and not allowed to expand, an increase in temperature could reduce the shale's pore throat size which could increase the shale's ability to block ions from moving in based on size restrictions. In our experiments, the shale could not expand in the radial and vertical directions since it was physically confined. When the shale's temperature increased, the solids in the shale could have expanded differentially and this could have reduced the shale pore throat size, which in turn could have improved the shale's membrane efficiency.

The second phenomenon that is observed from our high temperature experiments is that when the temperature was returned back to 70^{o}F, there is a clear a hysteresis effect (i.e. the membrane efficiency of the shale after cooling it to 70^{o}F from 200^{o}F was lower

than the originally estimated membrane efficiency at the same temperature (70^{o}F)). Figure 6-7 shows the membrane efficiency hysteresis effect for C1 shale when exposed to NaCl, KCl, CaCl2 and KCOOH solutions. Chenevert and Strassner (1975) showed that the shale's water activity and oil mud's water activity decreased when the temperature decreased though not by the same magnitude. They claimed that the shale's water activity decreased more rapidly than the oil mud's water activity. This explanation fits our data very well. We believe that as the temperature decreased from 200^{o}F to 70^{o}F, the shale's water activity decreased more than the salt solution's water activity. We also believe that the original water activity gradient was not restored. Namely, we believe that the water activity gradient is less than that originally available at 70F before heating the shale and aqueous solution and this lead to a lower pressure drop and membrane efficiency.

Besides the water activity gradient effect, we believe that heating the shale to such elevated temperature and then cooling it may have caused irreversible changes in the shale's chemical and mechanical (plastic effects) make up. The irreversible changes could have affected the shale's pore throat size and diffuse double layer configuration. All of these effects may have lead to a decrease in the shale's ability to screen out ions and thus lowered the shale's membrane efficiency.

6.3.3 Impact of Thermal Osmosis on Shale Interaction with Water-Based Muds

A second set of experiments were conducted in order to verify the impact of thermal osmosis on water transport in or out of shale. Figures 6-8, 6-9 and 6-10 show how C1 shale membrane efficiency changed in response to imposing a temperature gradient across it during interaction with NaCl, KCl and KCOOH solutions respectively. These graphs show three membrane efficiency values, which correspond to different

temperature gradients. The first membrane efficiency ($\sigma 1$) corresponds to no temperature gradient across the shale, the second membrane efficiency ($\sigma 2$) corresponds to a 130^{o}F temperature gradient across the shale and the last membrane efficiency ($\sigma 3$) corresponds to no temperature gradient after the shale has been exposed to 130^{o}F temperature gradient. In the absence of a temperature gradient, our experiments resemble those performed in Chapter 3 where the membrane efficiency of the shale is measured in response to both hydraulic and osmotic gradients.

Let's examine the part of the graph that deals with shale behavior after imposing a temperature gradient across it. It can be seen that the equilibrium membrane efficiency of C1 shale when interacted with NaCl, KCl and KCOOH solutions increased after imposing a temperature gradient across it. However, there were two distinct effects that took place when we imposed a temperature gradient across the shale. Namely, there was a sudden increase in the downstream pressure followed by a gradual decline until equilibrium was reached. The sudden downstream pressure increase is caused by the water flux from the upstream flow line and into the downstream chamber since the temperature of the upstream flow line was raised from 70^{o}F to 200^{o}F while the downstream chamber temperature remained at 70^{o}F. This temperature gradient was responsible for the water flux into the downstream chamber and hence the downstream pressure increase. This water flux is referred as thermal osmosis.

After the early downstream pressure increase, a gradual downstream pressure decline is observed until the downstream pressure reached equilibrium. We believe that increasing the temperature of the upstream fluid and the downstream fluid, due to hot water influx, have changed the water activity of both fluids. In addition, the influx of hot water into the downstream chamber have diluted the fluid and thus increased its water activity further. As a result, the water activity gradient across the shale sample has

increased when compared to what it was originally before imposing the temperature gradient. This increase in water activity gradient was indeed responsible for the gradual pressure decline and the higher membrane efficiency at equilibrium.

It is clear from the above discussion that the thermal osmosis effect on water transport in shales is only important during early time after imposing a temperature gradient. Heat and associated water will flow from the hot side to the cooler side. After some time, water transport in shales will be governed by the water activity gradient assuming that the hydraulic gradient does not change. Table 6-1 calculates the % increase in C1 shale's membrane efficiency as a result of imposing a130^{o}F temperature gradient across it. The C1 shale's membrane efficiency improvement ranged from 2.37% when interacting with NaCl solutions to 7.14% when interacting with KCOOH solutions. The temperature effect on shale's membrane efficiency is much higher when KCOOH solution was involved owing to the big size of the formate ion.

In summary, flow induced by the presence of a temperature gradient across shales (thermal osmosis) will regulate water transport during early times. However, the temperature effect on the chemical potential of all species in the shale and wellbore fluid will eventually become the dominant factor in regulating water transport. As a result, the thermal osmosis effect will dissipate. The overall effect of thermal osmosis appears to be small.

6.4 CONCLUSIONS

The following conclusions can be drawn based on the results obtained.

- The membrane efficiency of shales increases substantially with temperature.

- The chemical potential of both the shale and the drilling fluids increase with temperature though not by the same magnitude.
- If the shale is confined and not allowed to expand, an increase in temperature could reduce the shale's pore throat size which could indeed increase the shale ability to block ions from moving in based on size restriction.
- Membrane efficiency hysteresis effects are observed when temperature is cycled.
- Exposing the shale to elevated temperature and then cooling it could cause irreversible changes in the shale chemical and mechanical make up which may affect the shale's pore throat size and diffuse double layer configuration and impact the shale's membrane efficiency.
- In the presence of a temperature gradient across shales, thermal osmosis regulates water transport during the early times. However, the temperature effect on the chemical potential of all species in the shale and wellbore fluid will eventually become the dominant factor in regulating water transport. As a result, thermal osmosis effects will dissipate.

Table 6-1: C1 shale membrane efficiency change due to temperature gradient change

Salt Solution	**σ for (0F) Temp Gradient**	**σ for (130F) Temp Gradient**	**σ Change**
NaCl	1.69%	1.73%	2.37%
KCl	0.7%	0.74%	5.71%
KCOOH	2.52%	2.7%	7.14%

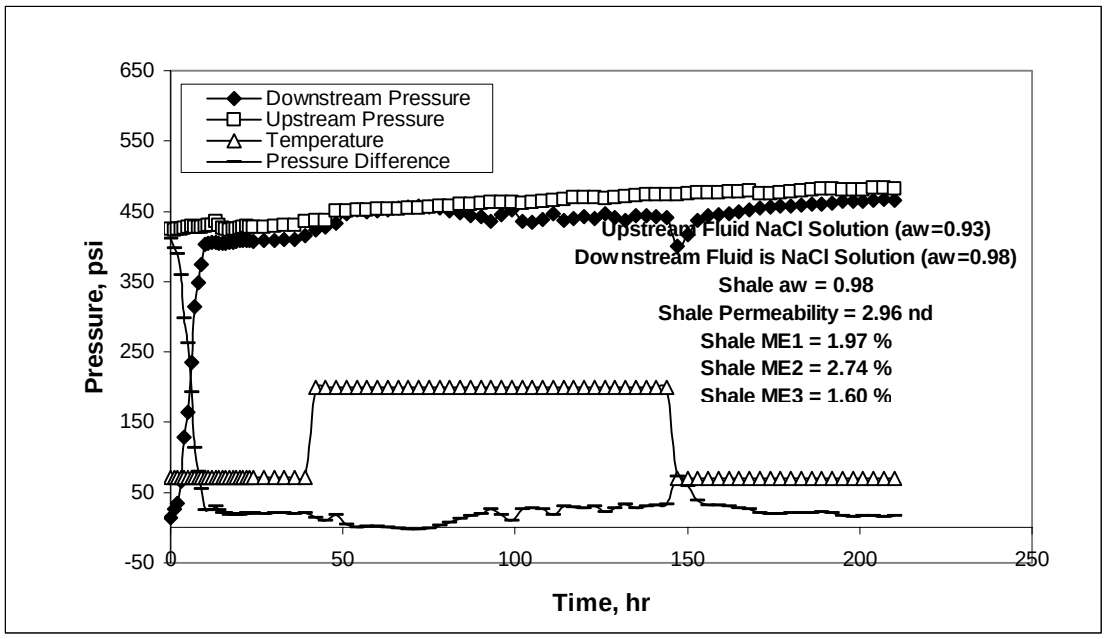

Figure 6-1: Membrane efficiency behavior of C1 shale when exposed to NaCl solutions of different water activity at different temperatures.

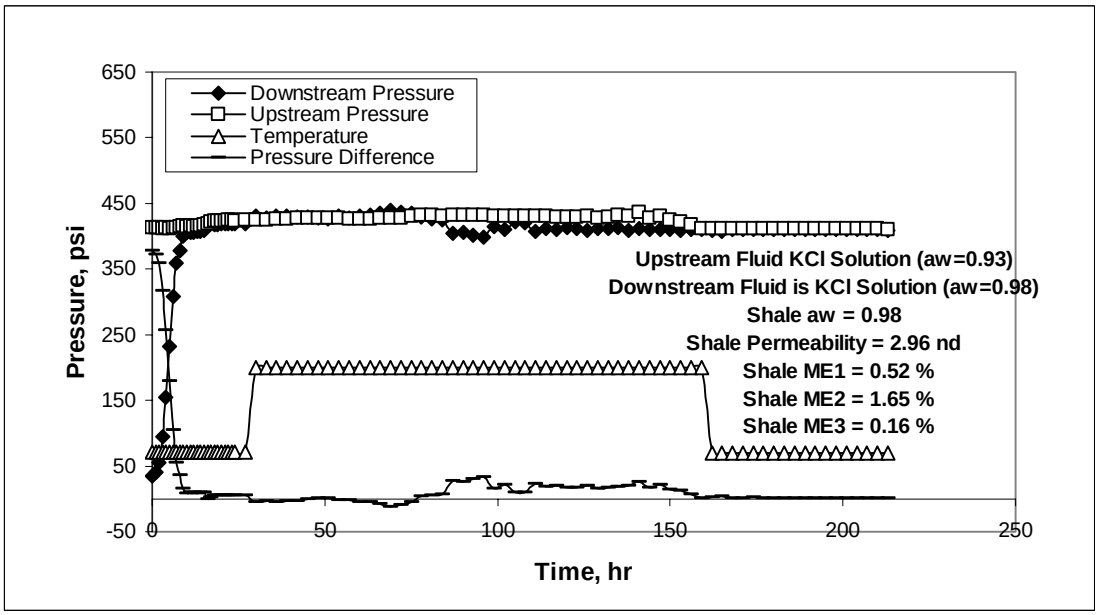

Figure 6-2: Membrane efficiency behavior of C1 shale when exposed to KCl solutions of different water activity at different temperatures.

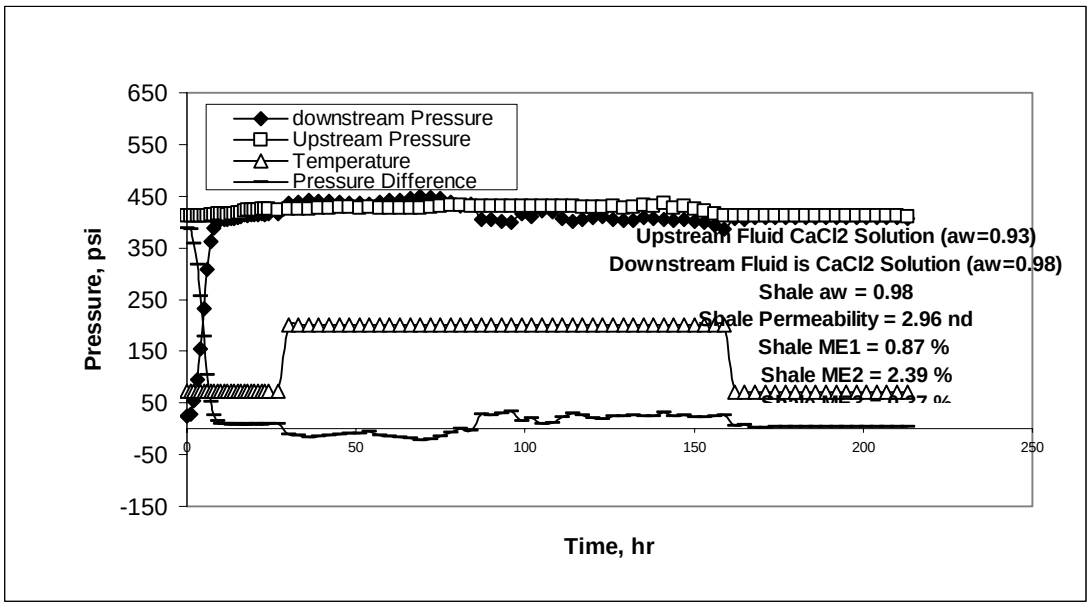

Figure 6-3: Membrane efficiency behavior of C1 shale when exposed to $CaCl_2$ solutions of different water activity at different temperatures.

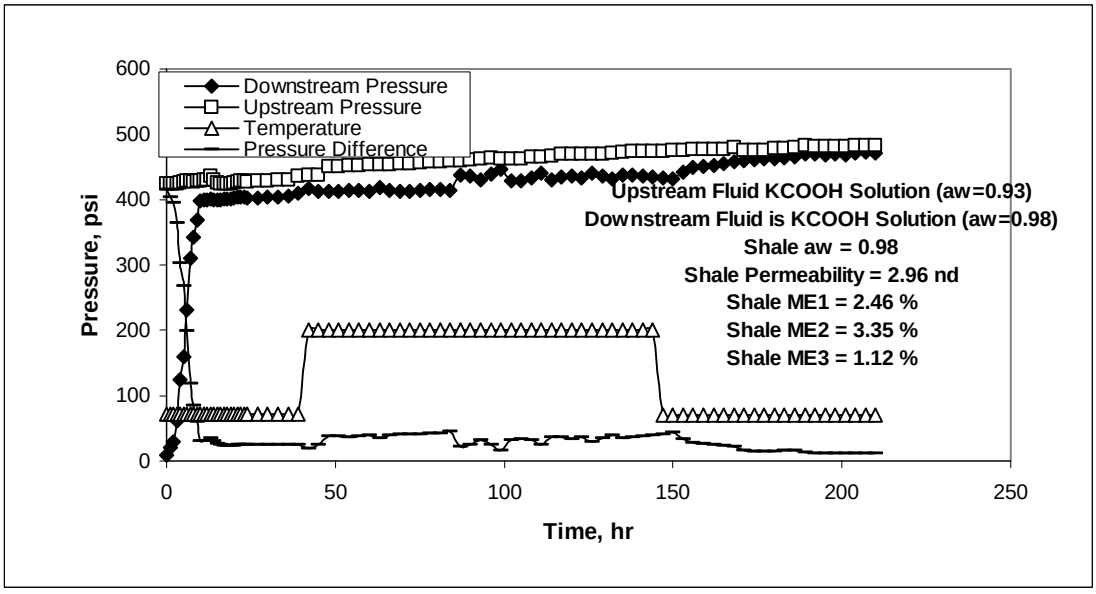

Figure 6-4: Membrane efficiency behavior of C1 shale when exposed to KCOOH solutions of different water activity at different temperatures.

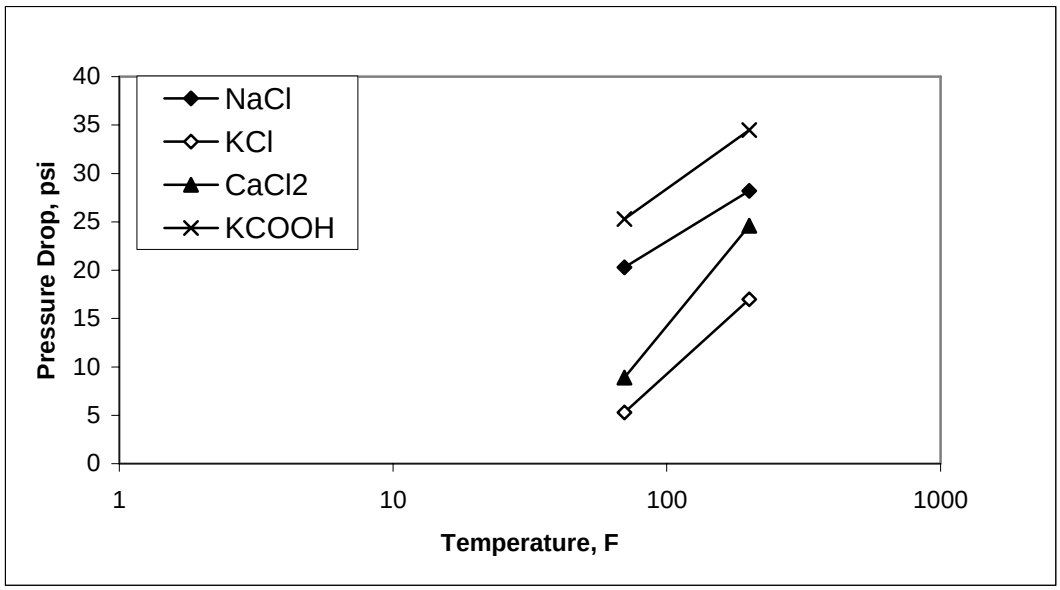

Figure 6-5: Pressure drop behavior with temperature when C1 shale interacted with different aqueous solutions.

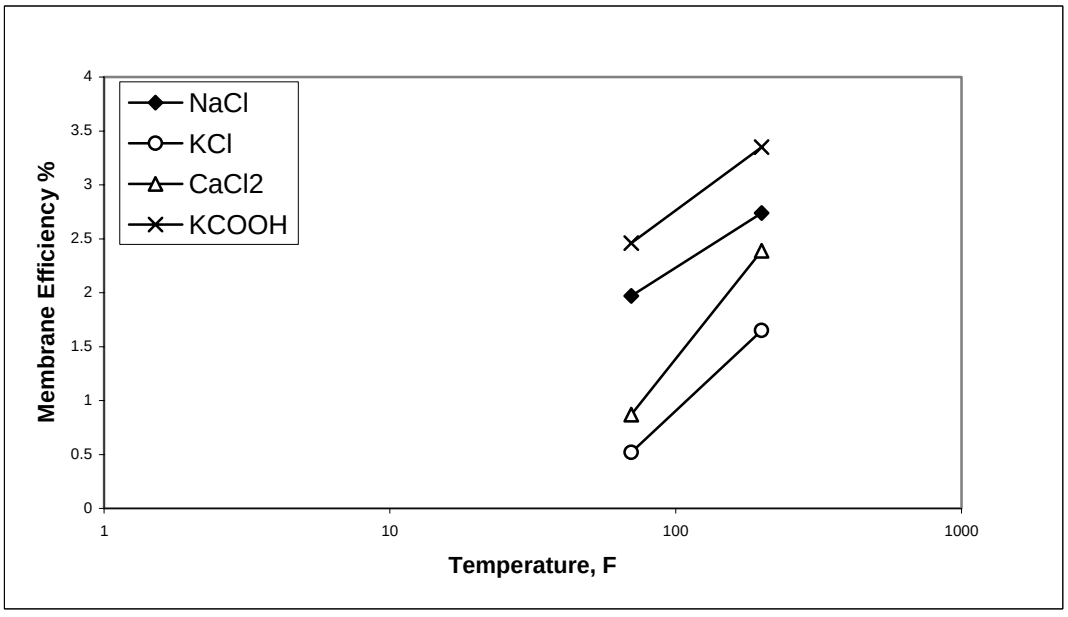

Figure 6-6: Membrane Efficiency dependence on temperature when C1 shale interacted with different aqueous solutions.

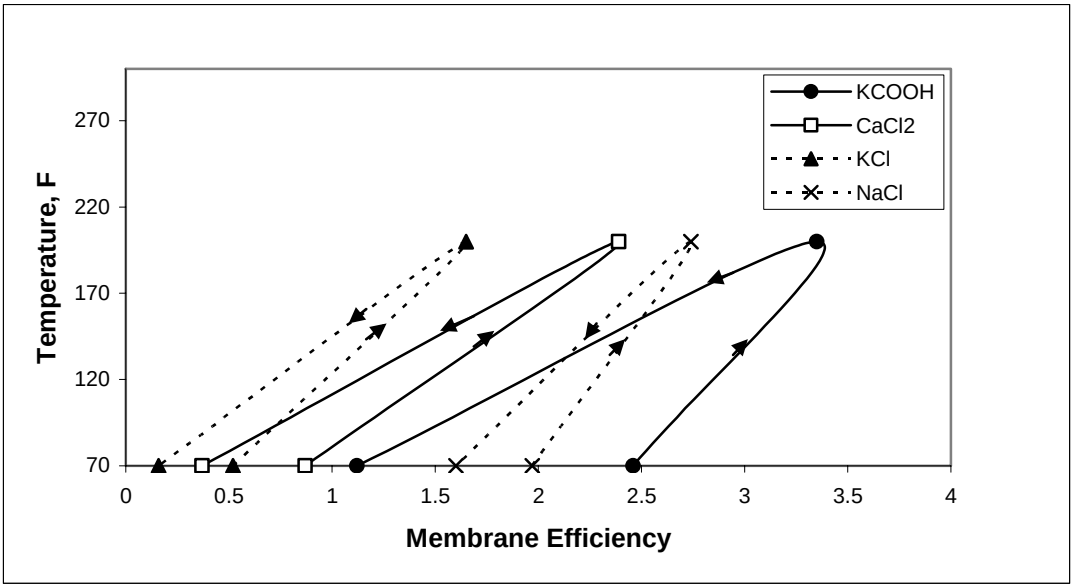

Figure 6-7: Membrane Efficiency hysteresis when C1 shale interacted with different aqueous solutions.

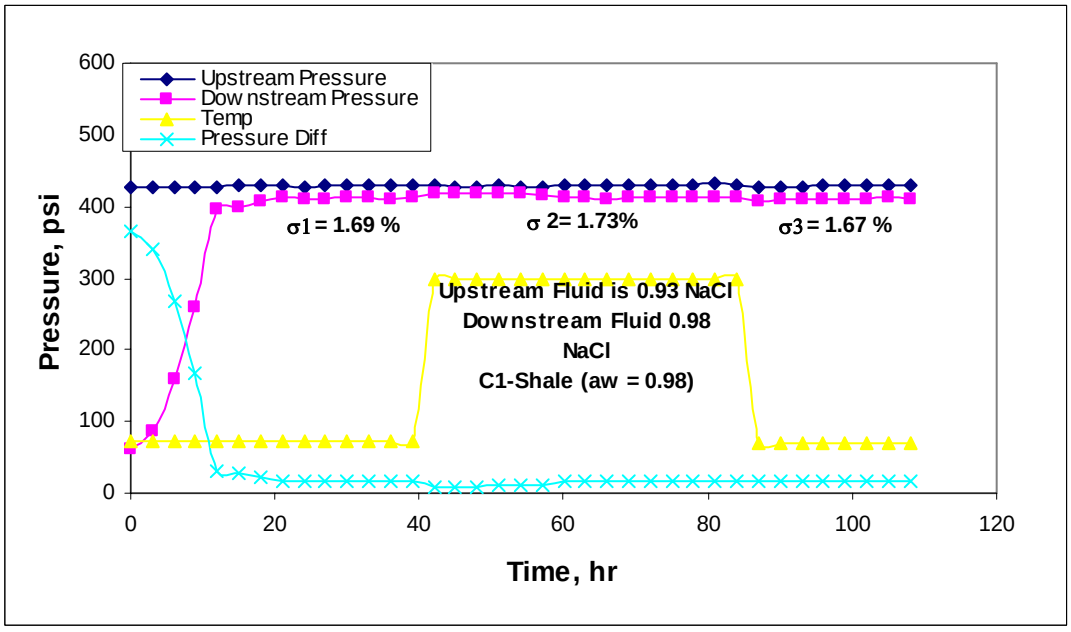

Figure 6-8: Thermal osmosis experiment for C1 shale and NaCl solutions.

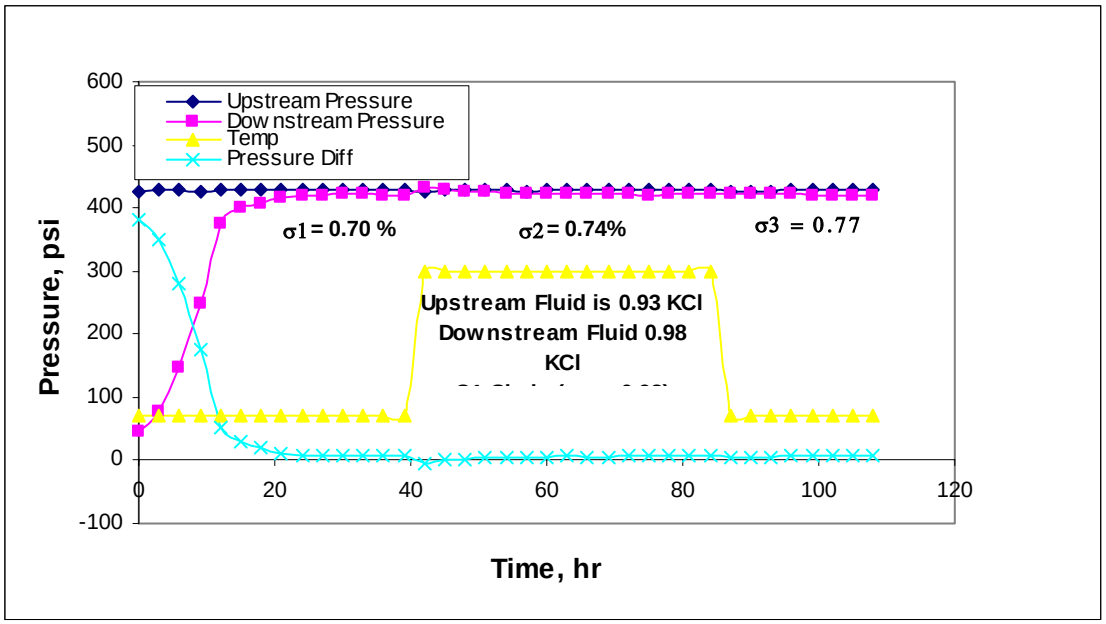

Figure 6-9: Thermal osmosis experiment for C1 shale and KCl solutions.

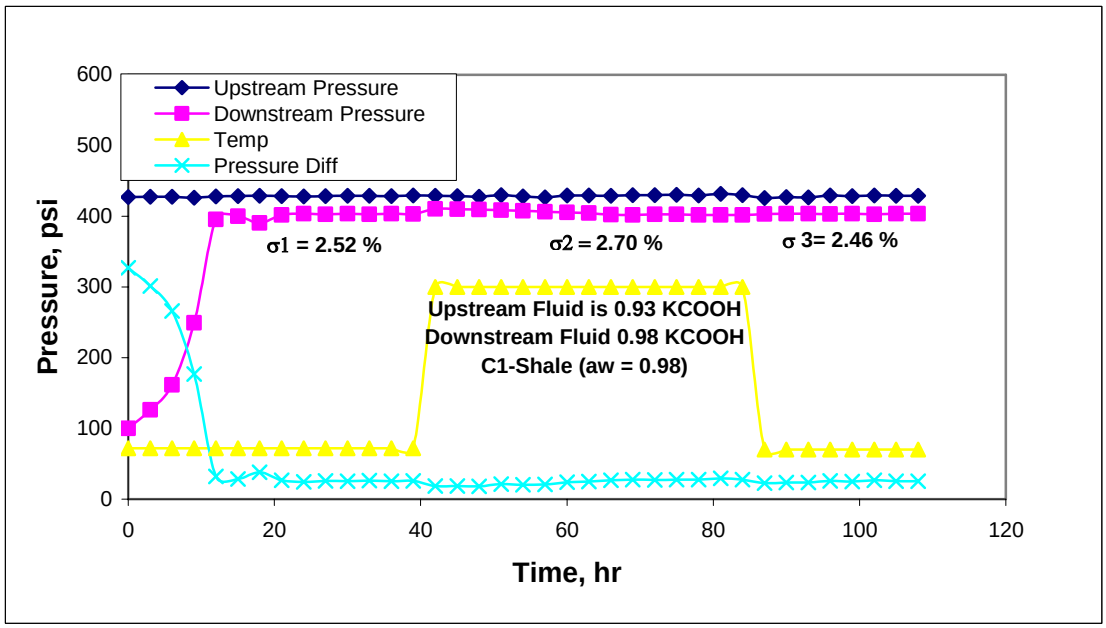

Figure 6-10: Thermal osmosis experiment for C1 shale and KCOOH solutions.

CHAPTER 7

Measurements of Capillary Entry Pressures through Shales

7.1 INTRODUCTION

In order for hydrocarbon accumulations to exist, there must be a source rock to produce the hydrocarbon, a reservoir rock to host the hydrocarbon and a good cap rock to trap it and stop its migration upwards. According to Vavra et al (1992), a seal is generally defined as a sediment, rock or immobile fluid with high capillary entry pressure (also known as capillary breakthrough or capillary entrance pressure) that acts to stop the flow of hydrocarbon. Salts, anhydrites, silty shales and clay mineral-rich shales are some common seal lithologies.

Shale plays a major role in petroleum exploration and production because they are commonly considered to be both source rock and a seal. Their ability to exhibit good sealing characteristics arises from their small, water-wet, pore throat sizes. These small pore throats are responsible for generating high capillary pressures, which excludes hydrocarbon from the water-wet shale. Shales are also used as underground seals for CO_2 sequestration. One of the critical aspects of CO_2 sequestration is the ability of the shale to stop the flux of CO_2 through it. This ability depends on the capillary entry pressure of CO_2 in shales. The capillary pressure is given by the following equation:

$$P_c = 2\sigma\cos\theta / r \quad \text{.....} \quad (7.1)$$

where σ is the interfacial tension between the oil and the water, θ is the contact angle and r is the shale pore throat radius.

In order for hydrocarbons to enter a shale, the differential pressure between the hydrocarbon column and the water must exceed the minimum capillary entry "threshold" pressure of the shale. By definition, the minimum capillary entry pressure is the capillary pressure at which the non-wetting phase, usually oil, starts to displace the wetting phase, usually water, contained in the largest pore throat within a water-wet formation. It can be seen from equation (7.1) that the capillary entry pressure can be significant especially for shales with very small pore throats.

The minimum capillary entry pressure concept is used by reservoir engineers to estimate the height of a hydrocarbon column that is trapped by shale as shown in Figure 7-1. At equilibrium, the height of the hydrocarbon column, also called seal capacity, is give by the following equation:

$$h = Pc / (\rho_w - \rho_o)\, g \quad \ldots\ldots\ldots\

capillary forces between the shale pore fluid and the water-based mud filtrate. This is not the case with oil-based muds since the continuous oil-phase produces capillary effects when contacting water-wet pores.

It is argued by many researchers that oil-based muds will not penetrate water-wet shales unless the pressure differential between oil-based mud and the shale pore fluid exceeds the minimum capillary entry "threshold" pressure of the shale. Therefore, oil-based muds have been used extensively to drill troublesome shales before environmental regulations limited their use.

This chapter presents an experimental study to measure the capillary entry pressure between a shale and non-wetting fluids. In Section 7.2, a background and literature review on capillary entry pressure in shale is presented. Section 7.3 gives a detailed description of the test used for measuring the capillary entry pressure in shale. A complete discussion of the experimental results is presented in Section 7.4. Finally, Section 7.5 draws conclusions and makes recommendations based on the experimental results.

7.2 BACKGROUND AND LITERATURE REVIEW

The concept of capillary pressure has extensively been used in petroleum exploration and production. Capillary pressure data has been used for reservoir properties evaluation, sealing capacity and transition zone thickness determination (Berg, 1957 and Jennings, 1987). Capillary pressure data are obtained from either empirical modeling based on log data or laboratory core measurements. While much effort was

dedicated for the evaluation of reservoir rock properties using capillary pressure data, not much have been done on impact of capillary pressure on the sealing capacity of shale.

Krooss et al (2004) employed a pressure transmission test to measure capillary entry pressures in shale and mud rocks using CO_2, N_2 and NH_4 as the non-wetting fluids. In their study, gas breakthrough experiments were performed by creating an instantaneous high pressure gradient (up to 20 MPa) across the shale sample and monitored the gas flux across the shale by means of a closed pressure chamber downstream of the shale. At the end of the experiment, the difference between the upstream (gas) and downstream pressures was labeled the capillary entry pressure. They measured capillary entry pressures that ranged from 0.1MPa up to 6.7 MPa. We believe that these measured pressures do not represent the capillary entry pressures of these non-wetting fluids due to establishment of gas saturation resulting from the gas flux. Dewhurst et al (2002) presented capillary pressure measurements that indicate that gas columns of 250 m could be sealed by Muderong shale. Also, they showed that column heights of between 550 m and 750 m of CO2 could be trapped by the Muderong shale. Although these studied discussed the ability of shale to act as geologic traps, they did not investigate the impact of shale and non-wetting fluids properties on the sealing capacity of shale.

Oil-based muds have shown great success in preventing borehole instability in shale formations. This is due to the fact that the shale is not weakened by pore pressure penetration by either the oil phase (in most cases) or the emulsified water. The utilization of osmosis to prevent water movement in shales is well documented (Chenevert, 1970), however, very little has been published regarding the factors that control oil penetration in shales.

Hale et al (1993) argue that the hydraulic permeability of shales is extremely low (10^{-7} to 10^{-12} darcies) and also that oil will not enter the shale pores unless the differential pressure exceeds the minimum capillary entry pressure. The presence of a threshold capillary entry pressure between oil-based muds and low permeability water-wet shales is considered to be the main factor in preventing the oil from entering the shale pores. The capillary entry pressure depends on both the water-wet shale and the non-wetting fluid properties. According to equation (7.1), the capillary pressure depends on the interfacial tension between the shale pore fluid and the non-wetting fluid, the contact angle and the shale pore throat radius.

In this work, we measured the capillary entry pressure of various non-wetting fluids through different shales. In addition, we have investigated the dependence of the capillary entry pressure on shale permeability and interfacial tension between shale and non-wetting fluid. We also calculated the shale pore throat radius from the capillary entry pressure data for different shales. This pore throat radius corresponds to the radius of the largest pores in the shale.

7.3 CAPILLARY ENTRY PRESSURE TEST DESCRIPTION

7.3.1 Test Definition and Objectives

The purpose of this test is to analyze the phenomena of capillary forces that prevent non-wetting fluids from entering shales at low to moderate overbalance pressures. It has been argued that the presence of interfacial tension forces between the water-wet shale and oil-based mud are responsible for shale stability since it prevents direct communication between the oil and water phases of the oil-based mud and the

shale pore fluid as long as the capillary entry "threshold" pressure is not exceeded (Hale et al, 1993). Once the applied differential pressure exceeds the minimum capillary entry pressure, oil will flow into the shale, increase its pore pressure, and possibly result in shale instability. The capillary entry pressure is a function of the interfacial tension between the non-wetting fluid and the shale pore fluid, the shale wettability and the shale pore throat radius, which is directly correlated to shale permeability. The objectives of this test are as follows:

- Measure capillary entry "threshold" pressure of non-wetting fluids in shales.
- Investigate the effect of interfacial tension between the non-wetting fluid and shale pore fluid on the capillary entry pressure
- Investigate the effect of shale permeability on the capillary entry pressure

7.3.2 Test Equipment and Procedure

This test is designed to measure the minimum capillary entry pressures of laboratory made oil-based mud, crude oil, nitrogen gas and decane in contact with shales. In order to get a better understanding of this phenomenon, we used three different shales of different permeabilities. It is believed that shale permeability, interfacial tension between the non-wetting fluid and the shale and shale wettability are the dominant factors that control this minimum capillary entry pressure. The equipment used in this study is the same as used for other studies and is shown in Figure (3-5).

In this test, a 0.25" thick shale sample was exposed to non-wetting fluids. During the test, a pressure differential was gradually increased across a shale sample until a pressure increase was detected on the downstream side of the shale. The pressure

differential existing at that time was labeled as the capillary entry pressure and was held constant until pressure had equalized on both sides of the shale. After the pressure equilibrated on both sides, a reverse flow test is run where the upstream pressure is dropped to a value that is below that of the downstream. Figure (7-2) shows a typical capillary entry pressure test. The detailed steps taken during this test are given in the following outline.

- Close V2, V3
- Open V1 (a two-way valve)
- Using a vacuum pump, evacuate the downstream chamber. It is very important that the chamber is as air free as possible. The presence of air will extend the time duration greatly.
- Next, fill the injection pump with the simulated pore fluid. Using the injection pump, pressurize the downstream reservoir with the simulated pore fluid. The applied pressure should be the same as that of the initial upstream pressure.
- Close V1
- Connect the vacuum pump to V2 and evacuate the upstream flow line and main cell. The presence of air in the upstream flow lines and main cell could distort the test outcome.
- Close V2
- Fill the bottom compartment of the pressure vessel with the desired non-wetting fluid.
- Open V3 and pressurize the top compartment of the pressure vessel using nitrogen gas supplied by the gas cylinder.
- The pressure gauge upstream is used to monitor the test fluid pressure to make sure that

it is maintained at the desired level.

- After both the upstream and downstream pressures stabilize, raise the upstream pressure by 100 psi and monitor the downstream pressure for any increase. We decided that waiting for ½ hour is enough.
- If the downstream pressure stays the same (constant), raise the upstream pressure by another 100 psi and watch the downstream pressure gauge for another ½ hour.
- Keep raising the upstream pressure in increments of 100 psi until the downstream pressure starts to increase. When the downstream pressure starts to increase, this means that non-wetting fluid has flowed through the shale and the minimum capillary entry pressure was overcome.
- The difference in the upstream and downstream pressures when the breakthrough occurs is the minimum entry "threshold" pressure for the non-wetting fluid and shale system.

7.3.3 Test Matrix

In our research, we have measured the minimum capillary entry pressure of four non-wetting fluids in contact with three different shales samples. Table 7-1 shows the test matrix designed to study the minimum capillary entry pressure of a laboratory made oil-based mud, crude oil, nitrogen gas and decane during their interaction with C1, Pierre and Arco-China shales. Each non-wetting fluid followed the same matrix set-up as shown in Table 7-1.

7.4 RESULTS & DISCUSSION

7.4.1 Interfacial Tension and Capillary Entry Pressure Data

The interfacial tension between the shale pore fluid and the non-wetting fluids must be determined in order to better analyze our capillary entry pressure experiments. As stated earlier, we have employed four non-wetting fluids in our experiments; laboratory made oil-based mud, crude oil, nitrogen gas and decane. Using these fluids, we have determined the interfacial tension between the non-wetting fluids and simulated pore fluids of shales. For the pore fluid, we prepared a sodium chloride solution of 0.98 water activity. We have used the du Nouy tensiometer that employs the ring method for interfacial tension measurements. Table 7-2 shows the measured interfacial tensions between all non-wetting fluids and simulated pore fluids.

After determining the interfacial tension of the non-wetting fluids, the capillary entry "threshold" pressure test was conduced as per the experimental procedure mentioned previously. The experimental results for the capillary entry pressure varied from 150 psi to 950 psi as shown in Table 7-3. The differences in capillary entry pressures are attributed to variations of the properties of shale and non-wetting fluids. It can be seen that capillary entry pressure for oil-based muds can be high and this explains their ability to stabilize shales. It also shows that shale can exhibit high resistance to non-wetting fluid penetration and that explains why shale is considered to be a good seal.

Figures 7-2, 7-3, 7-4 and 7-5 show the capillary entry pressure test when C1-shale was exposed to oil-based mud, crude oil, nitrogen gas and decane respectively. Figures 7-6, 7-7, 7-8 and 7-9 show the capillary entry pressure test when Pierre shale was exposed to oil-based mud, crude oil, nitrogen gas and decane respectively. Figures 7-10, 7-11, 7-

12 and 7-13 show the capillary entry pressure test when Arco-China shale was exposed to oil-based mud, crude oil, nitrogen gas and decane respectively.

7.4.2 Impact of Interfacial Tension on Capillary Entry Pressure

Interfacial tension arises when two immiscible fluids come in contact with each other. The interfacial tension decreases as the miscibility of the fluids coming in contact with each other increases. Water or brine is almost always considered to be the wetting fluid in porous media such as shales while oil and natural gas are considered to be the non-wetting fluid. It is agreed upon that high pressures are required to initiate non-wetting fluid flow through water-wet shales owing to the presence of interfacial tension between the non-wetting fluid and the shale pore fluid. This pressure is referred to as the minimum capillary entry pressure. Figure 7-14 shows the effect of interfacial tension on the minimum capillary entry pressure for C1, Pierre and Arco-China shales. It can clearly be seen that the capillary entry pressure increased as the interfacial tension increased for all shales.

We conducted a special study that further sheds light on the minimum breakthrough pressure in shales. We flowed decane through the shale before contacting it with crude oil. Figure 7-15 shows the minimum capillary entry pressure when crude oil interacted with un-flushed shales and flushed shales with decane. The minimum capillary entry pressure for crude oil through all shales was lowered when the shales were flushed with decane prior to crude oil contact. An average 33% reduction in the minimum breakthrough pressure for crude oil through all shales was attained as a result of flushing the shales with decane. We believe that after flushing the shale with decane, the shale's large pores were partially filled with decane and that changed the capillary pressure curve (capillary hysteresis).

7.4.3 Impact of Shale Permeability on Capillary Entry Pressures

The minimum capillary entry pressure is the pressure required to flow through the biggest pores within a porous medium. In other words, the non-wetting fluid will first displace the wetting fluid present inside the largest pores. As the non-wetting fluid flows into shale, more pressure is required to displace the pore fluid contained within the small pores. Our objective was to determine the minimum capillary entry pressure, otherwise know as displacement pressure. We have intentionally used three different shales with different permeabilities in order to show the effect of pore size on the development of the minimum capillary entry pressure. Figure 7-16 shows the capillary entry pressure dependence on shale permeability (pore throat size). It is shown that for each non-wetting fluid, the minimum breakthrough pressure decreased as the permeability increased. This is expected since higher permeabilities translate into larger pores through which the non-wetting fluid displaces the wetting fluid. According to equation (7.1), the capillary entry pressure is inversely proportional to the pore radius. It can also be seen from Figure 7-14 that at each interfacial tension, Arco-China shale had the highest entry pressure while Pierre shale had the lowest pressure. These results confirm the belief that lower pore throat sizes increase the minimum entry pressure since Arco-china shale has the lowest permeability while Pierre shale has the highest permeability. From Figure 7-16 it can be seen that nitrogen always yielded the highest required pressure to initiate flow through all shales since it has a high interfacial tension (72 dyne/cm). On the other hand, the laboratory made oil-based mud yielded the lowest capillary entry pressure through all shales. This is expected since this oil-based mud contained an emulsifier that lowered the interfacial tension to 5.8 dyne/cm.

7.4.4 Pore Throat Radius Calculations from Capillary Entry Pressures

Measurements

According to equation (7.1), the shale pore throat radius can be calculated once the minimum capillary entry pressure and the interfacial tension between the non-wetting fluid and the shale pore fluid are known. It is essential to remember that this pore throat radius corresponds to the radius of the largest pore within the shale. Figures 7-17, 7-18 and 7-19 show the calculated pore throat radius for Arco-China, C1 and Pierre shales respectively during interactions with all non-wetting fluids. It is shown in Figure 7-20 that, when excluding the oil-based mud results, the calculated pore throat radii from the breakthrough experiments for each shale are close. The average calculated pore throat radius for Arco-China, C1 and Pierre shales is 20.1 nm, 25.8 nm and 31.8 nm respectively. These calculated pore throat radii correlate very well with the measured permeabilities for these shales.

The smaller pore radius obtained from the oil-based mud measurements may be artificially low because the droplets of water in the oil-based mud may coalesce due to the large overbalance pressures applied. This may cause invasion of the shale by water (not the oil-phase) and hence give a lower value for the capillary entry pressure.

7.4.5 Impact of Shale Cation Exchange Capacity on Capillary Entry Pressures

The cation exchange capacity of shale correlates well with the measured capillary entry pressure as shown in Figure 7-21. The capillary entry pressure increased for all non-wetting fluids when the cation exchange capacity of shale increased. This means that the cation exchange capacity of shale can be used as a means to predict its capillary entry pressure. The electro-chemical potential test, described in Chapter 4, is an easy method for inferring the cation exchange capacity of shale. Therefore, this test may be used for predicting the capillary entry pressure of shale.

7.5 CONCLUSIONS

- Capillary entry pressures in the range of 150 psi to 950 psi were measured for three different shales and four different non-wetting fluids.
- The measured capillary entry pressure increases as the interfacial tension between non-wetting fluid and shale pore fluid increases.
- The measured capillary entry pressure is inversely proportional to the shale permeability.
- The measured capillary entry pressure increases as cation exchange capacity of the shale increases.
- Incorporating surfactant “emulsifiers” in oil-based mud formulations reduces the interfacial tension and thereby reduces the minimum capillary entry pressure.

Table 7-1: Test matrix to study the capillary entry pressure of non-wetting fluids during their interaction with different shales.

Shale Type	Shale Permeability	Downstream Fluid	Test Fluid "Upstream"	Temp
C1 – Shale	2.96 nD	NaCl (aw = 0.98)	OBM (aw = 0.98)	70
Pierre Shale	6.48 nD	NaCl (aw = 0.98)	OBM (aw = 0.98)	70
Arco-China Shale	0.45 nD	NaCl (aw = 0.85)	OBM (aw = 0.85)	70

Table 7-2: Measured interfacial tensions for non-wetting fluids

Non-Wetting Fluid	Interfacial Tension (dynes/cm)
Oil-Based Mud	5.8
Crude Oil	57.8
Nitrogen Gas	72
Decane	24.86

Table 7-3: Measured capillary entry pressure of non-wetting fluids in contact with C1, Pierre and Arco-China shales

	Oil-Based Mud	**Crude Oil**	**Nitrogen Gas**	**Decane**
C1-Shale	250 psi	600 psi	700 psi	365 psi
Pierre Shale	150 psi	470 psi	630 psi	270 psi
Arco-China Shale	300 psi	750 psi	950 psi	450 psi

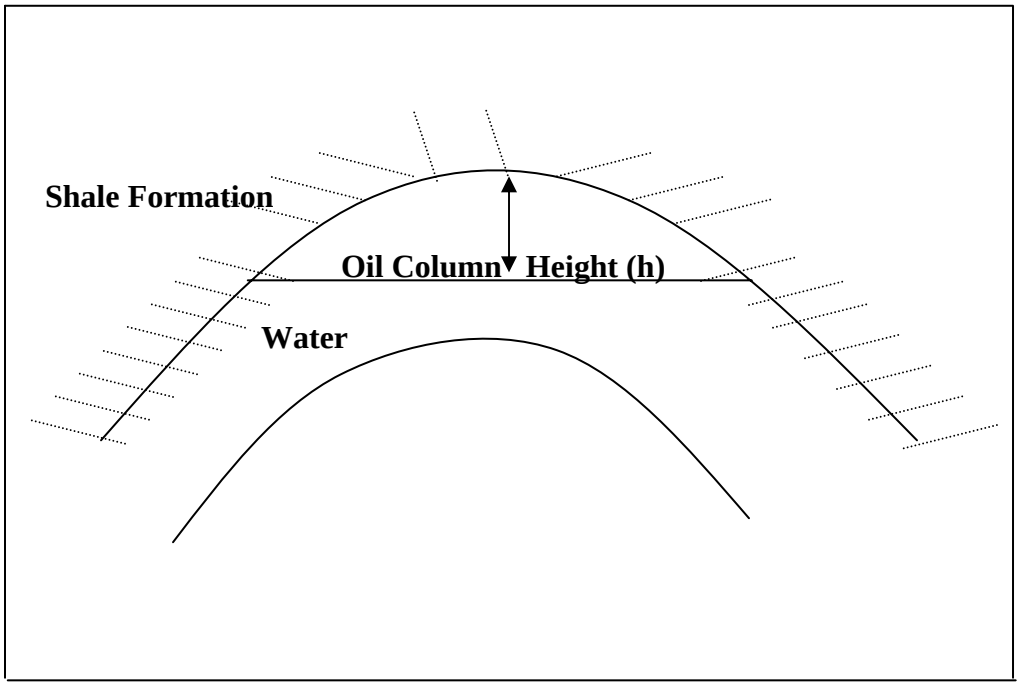

Figure 7-1: Schematic showing an oil column in an anticline.

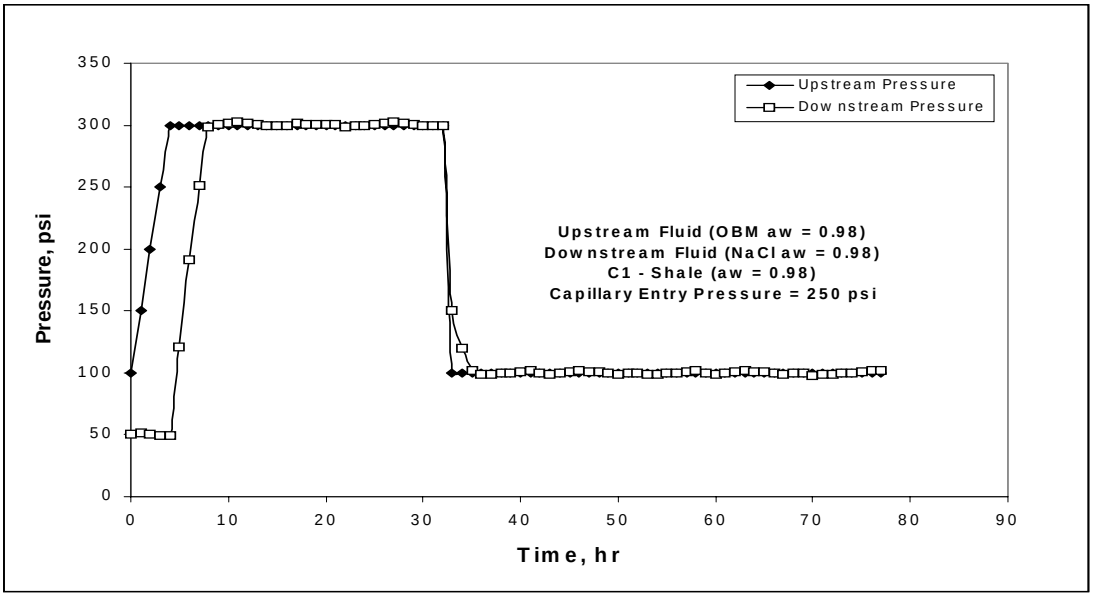

Figure 7-2: Capillary entry pressure test for C1-shale and oil-based mud.

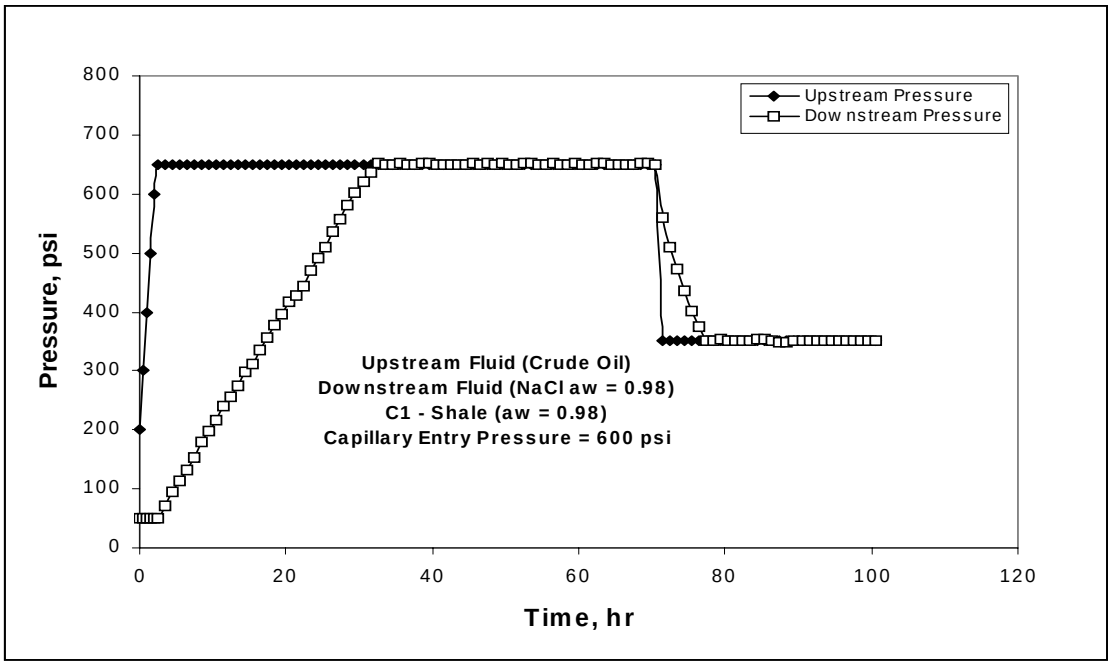

Figure 7-3: Capillary entry pressure test for C1-shale and Crude Oil.

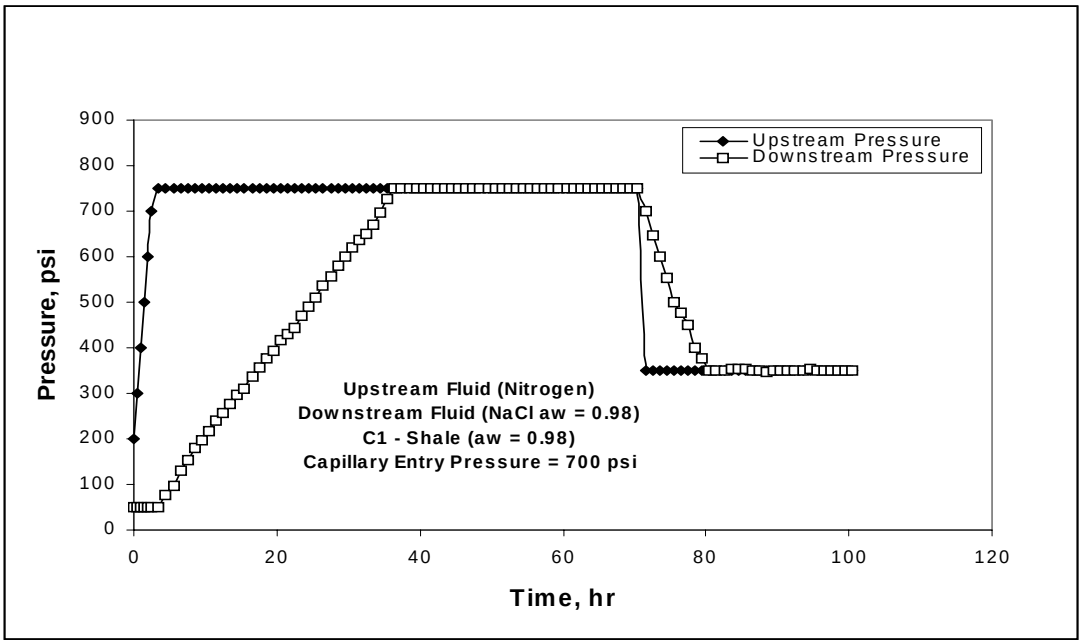

Figure 7-4: Capillary entry pressure test for C1-shale and Nitrogen.

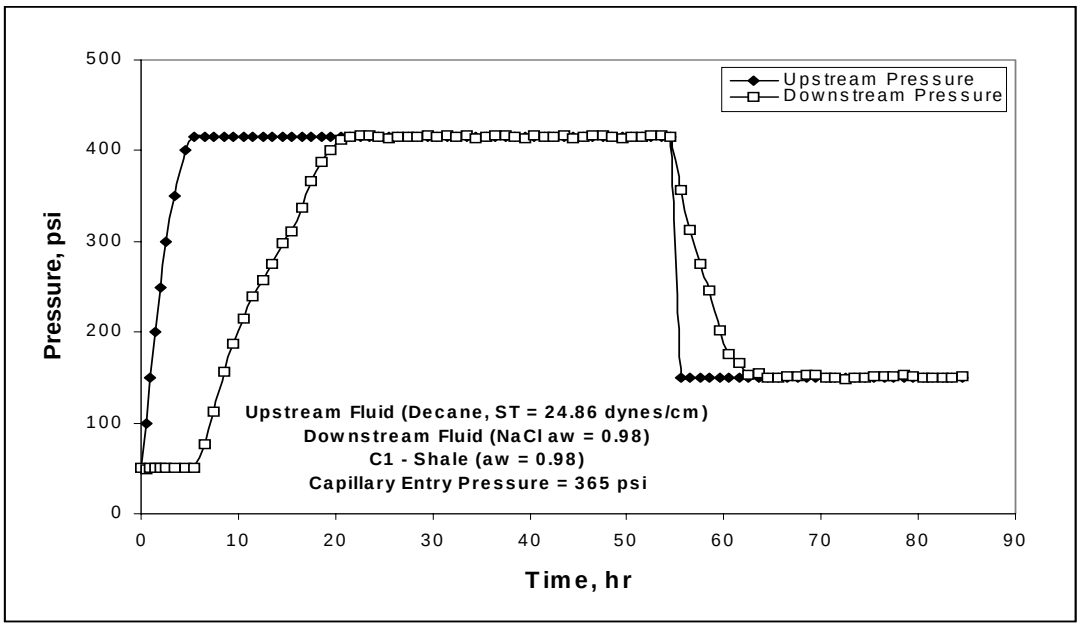

Figure 7-5: Capillary entry pressure test for C1-shale and Decane

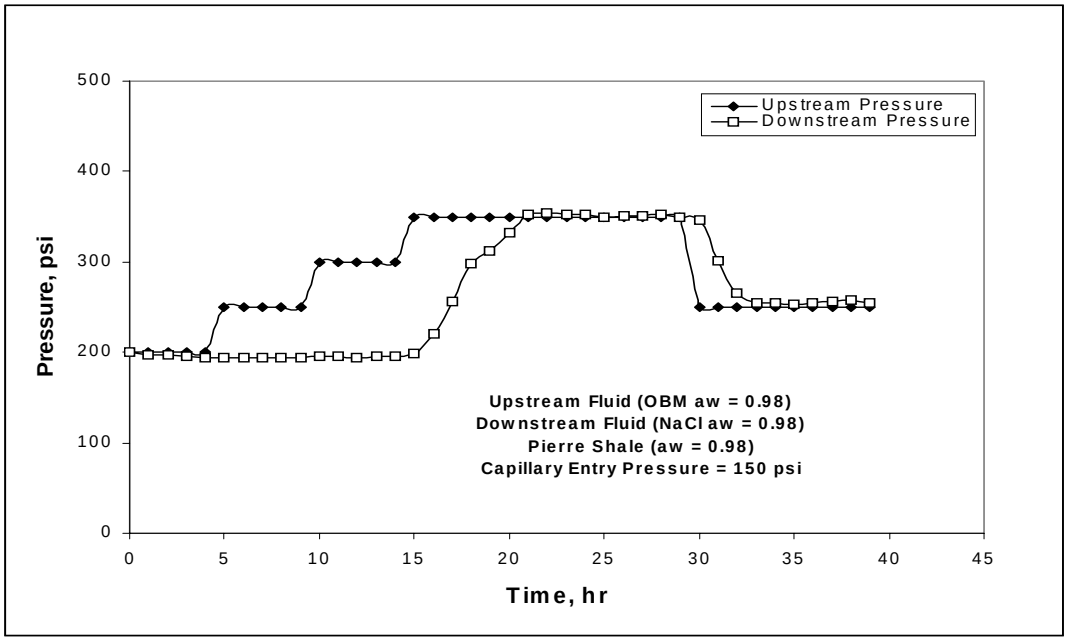

Figure 7-6: Capillary entry pressure test for Pierre shale and oil-based mud.

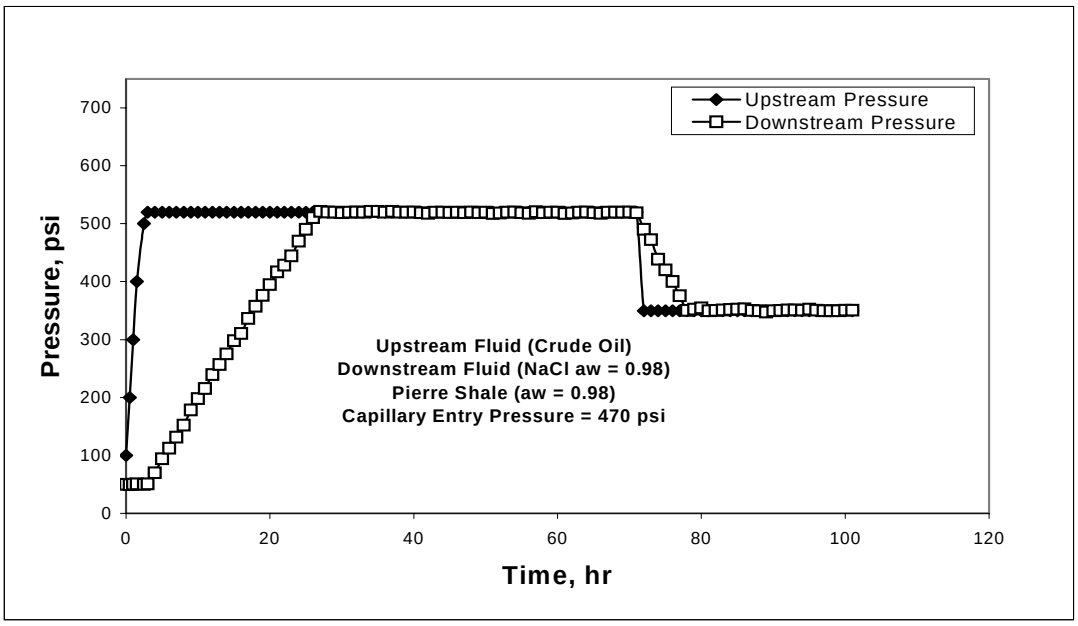

Figure 7-7: Capillary entry pressure test for Pierre shale and crude oil.

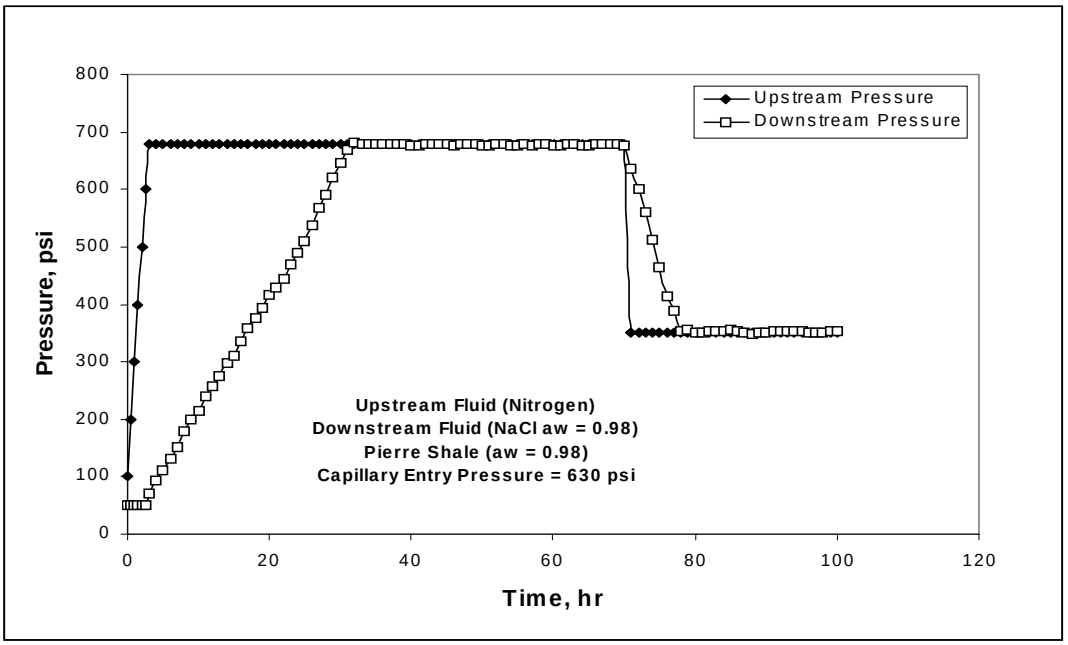

Figure 7-8: Capillary entry pressure test for Pierre shale and Nitrogen.

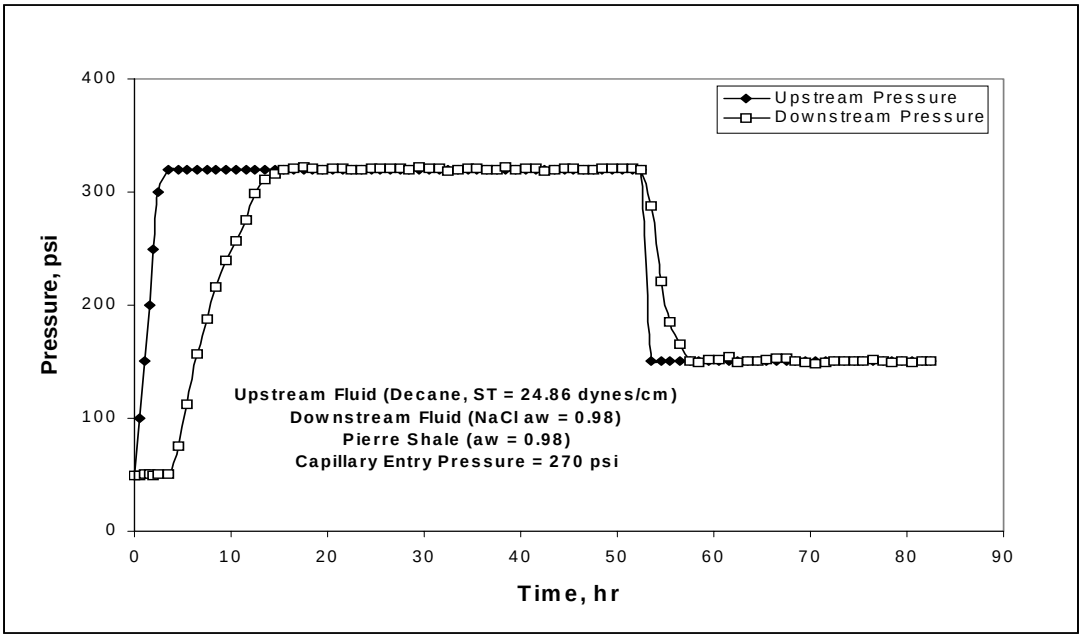

Figure 7-9: Capillary entry pressure test for Pierre shale and Decane.

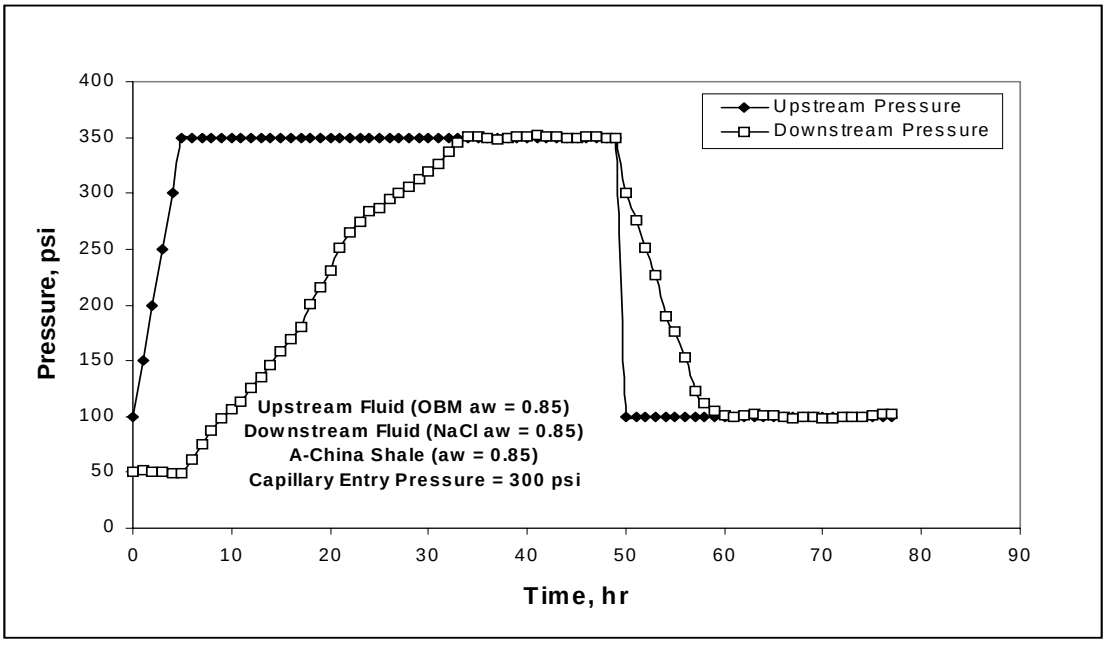

Figure 7-10: Capillary entry pressure test for Arco-China shale and oil-based mud.

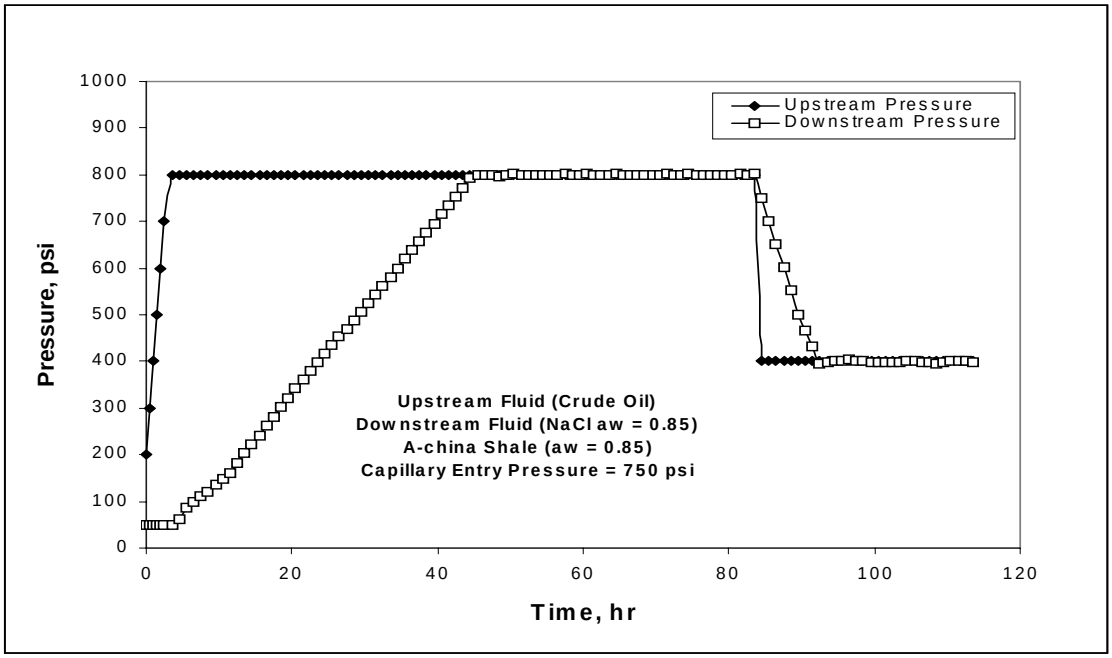

Figure 7-11: Capillary entry pressure test for Arco-China shale and crude oil.

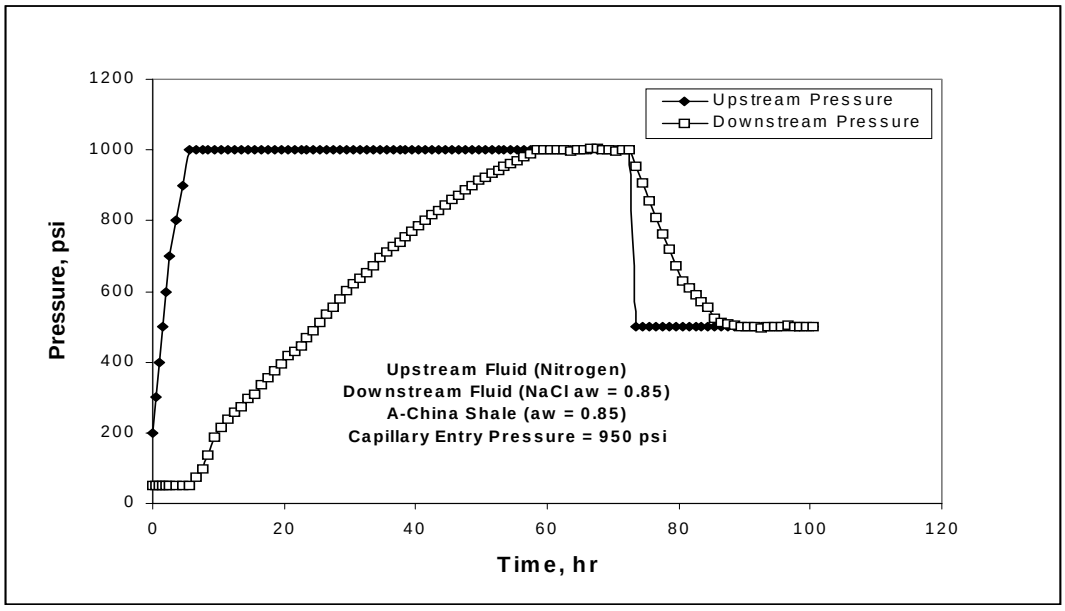

Figure 7-12: Capillary entry pressure test for Arco-China shale and Nitrogen.

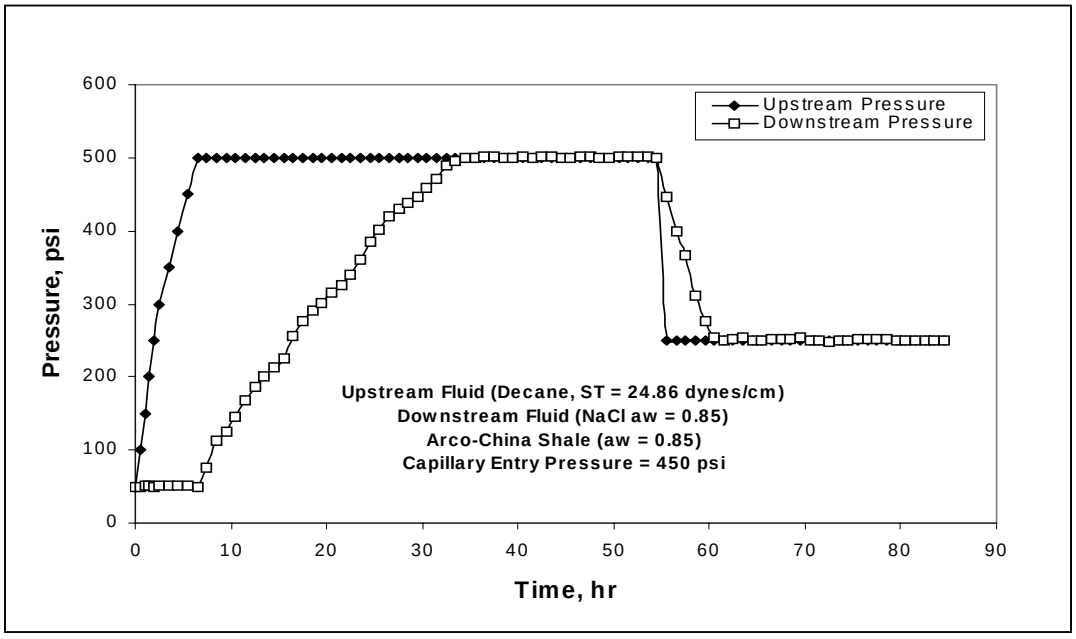

Figure 7-13: Capillary entry pressure test for Arco-China shale and decane.

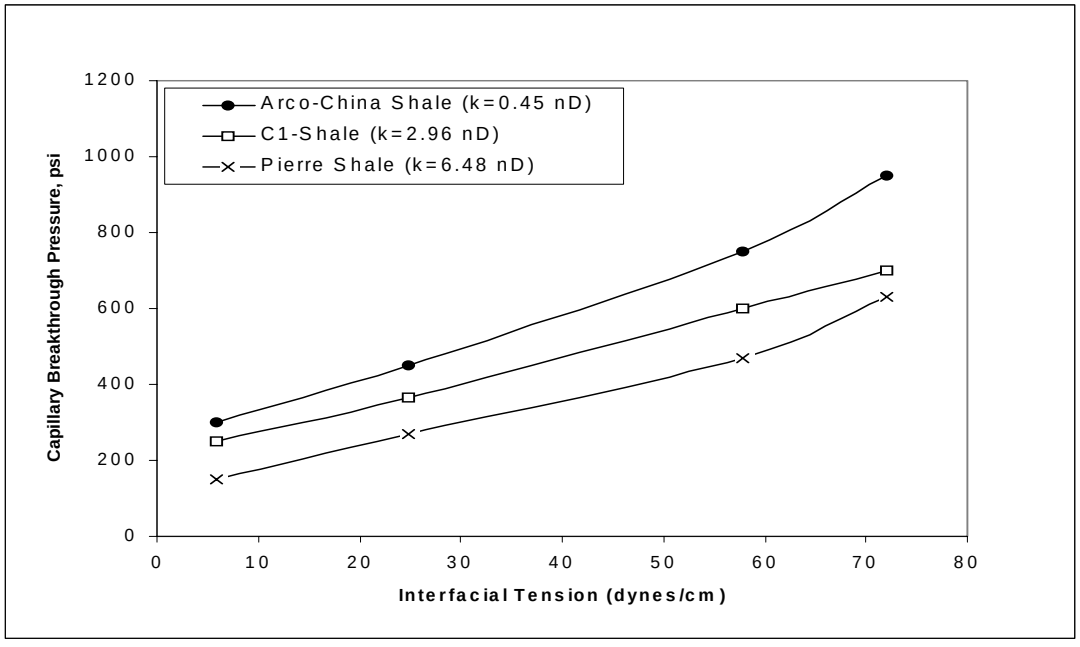

Figure 7-14: The effect of interfacial tension on the minimum capillary entry pressure for C1, Pierre and Arco-China shales.

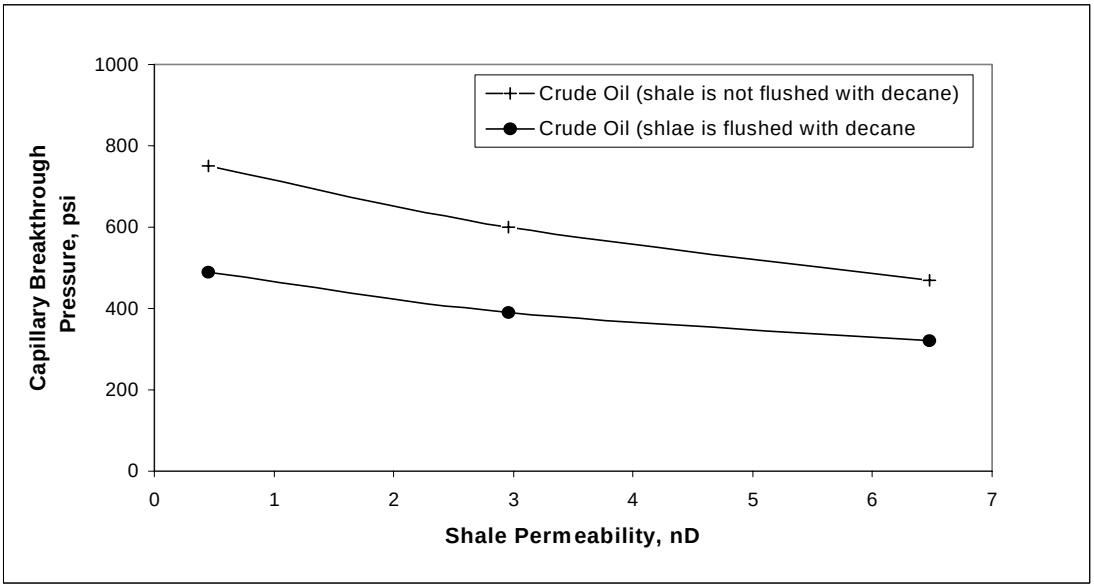

Figure 7-15: The minimum capillary entry pressure when crude oil interacted with un-flushed shales and flushed shales with decane.

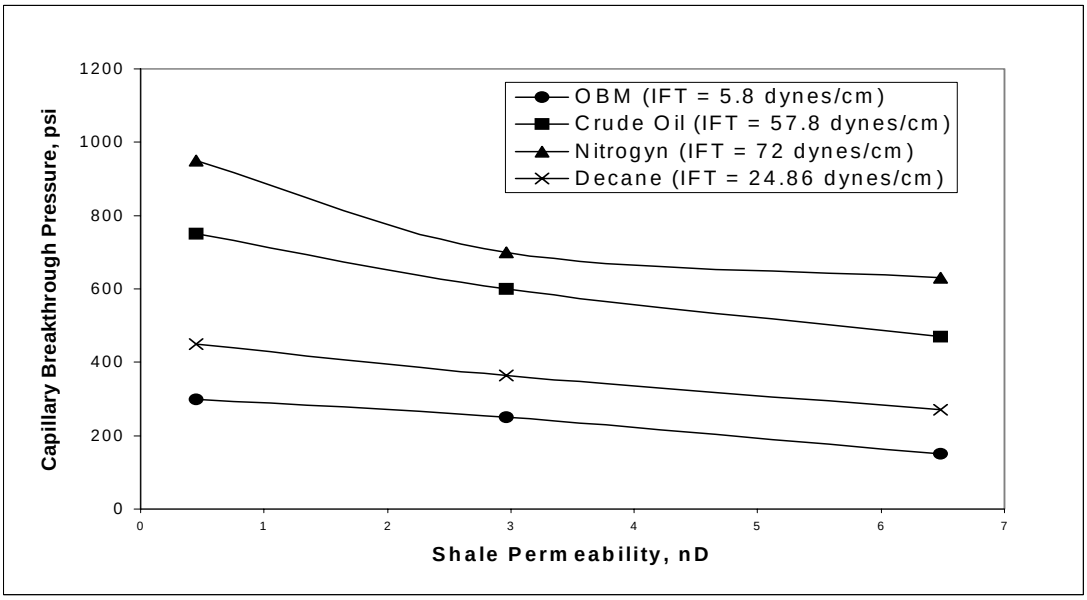

Figure 7-16: The capillary entry pressure dependence on shale permeability (pore throat size).

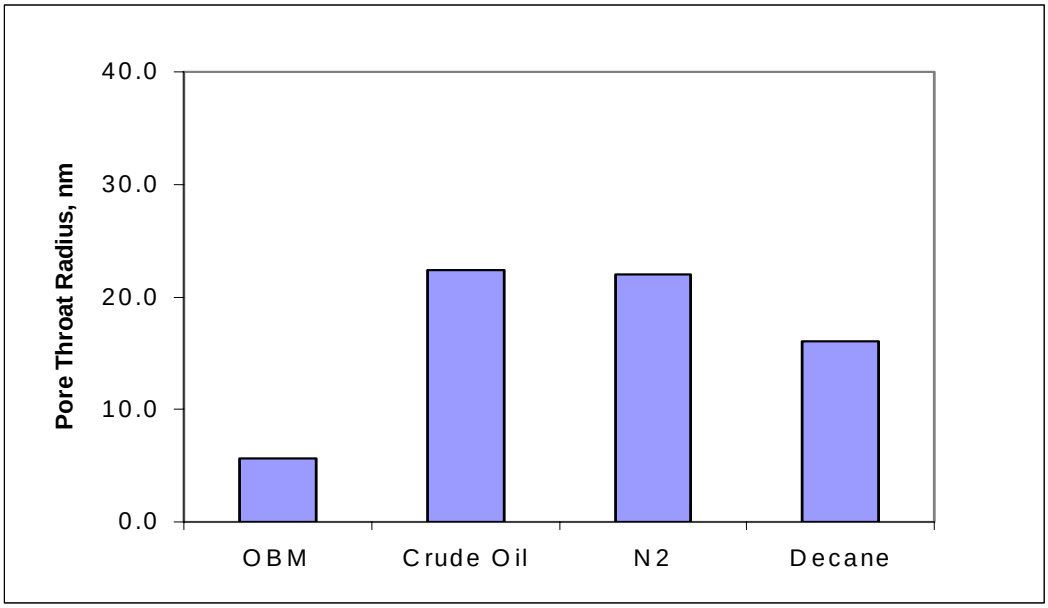

Figure 7-17: The calculated pore throat radius for Arco-China shale for different non-wetting fluids.

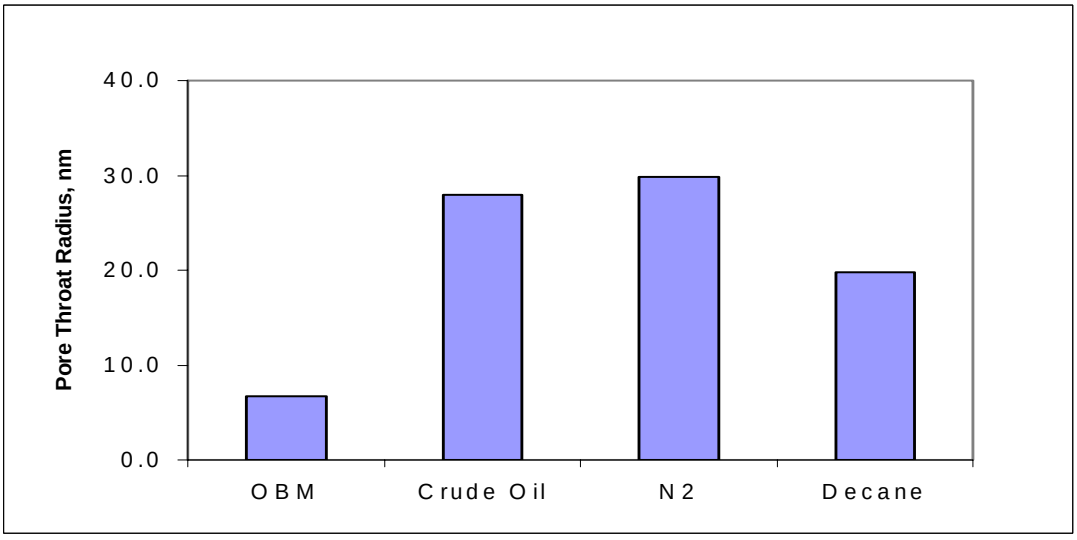

Figure 7-18: The calculated pore throat radius for C1 shale for different non-wetting fluids.

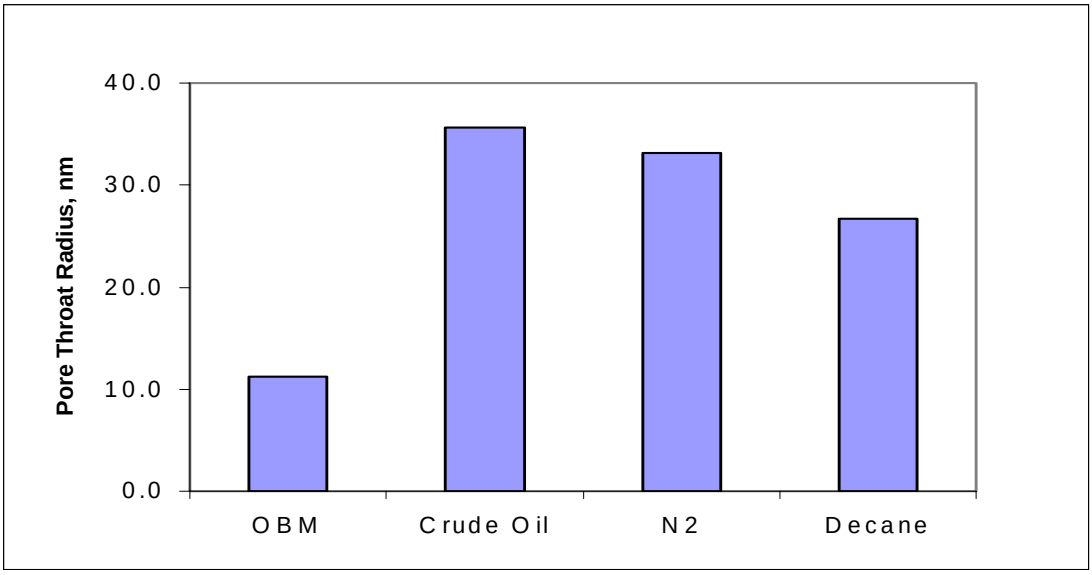

Figure 7-19: The calculated pore throat radius for Pierre shale for different non-wetting fluids.

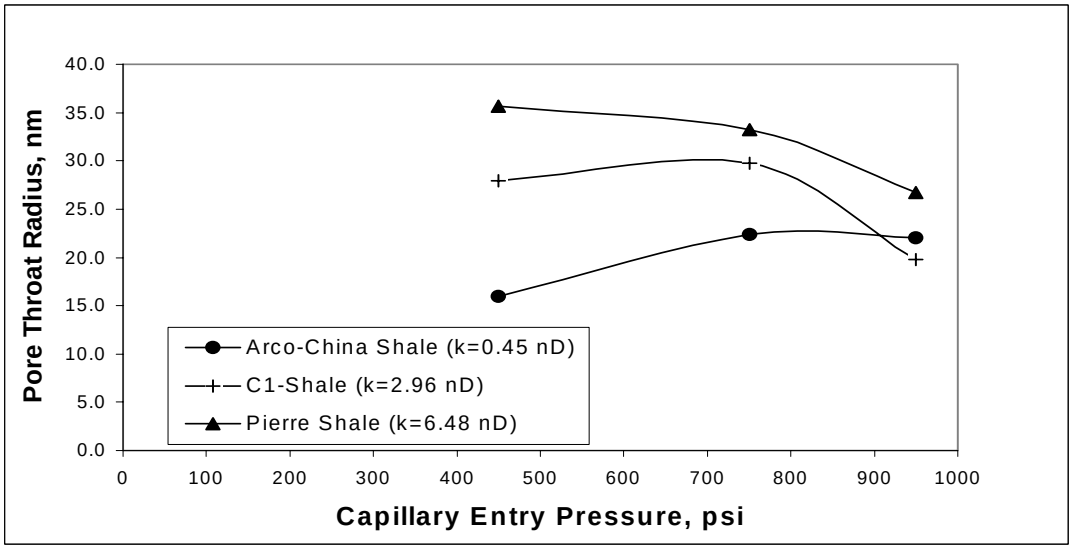

Figure 7-20: Calculated pore throat radius for all shales from capillary entry Pressure measurements.

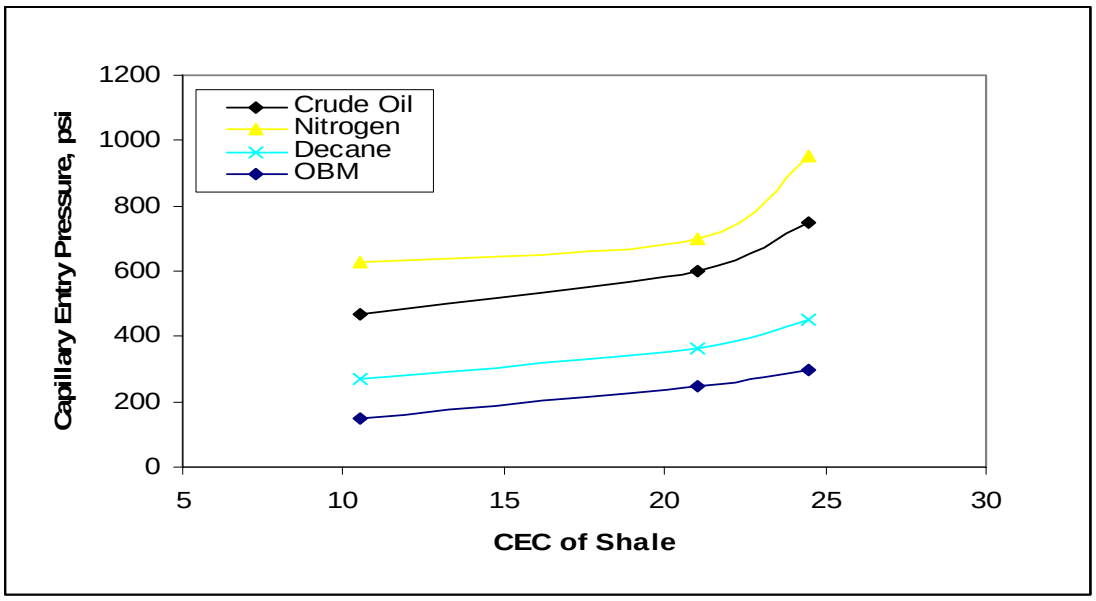

Figure 7-21: The capillary entry pressure dependence on shale cation exchange capacity (CEC).

CHAPTER 8

Conclusions

The flux of water and ions in or out of a shale is one of the most important physico-chemical effects influencing wellbore stability. Osmotically extracting water out of a shale and preventing ion flow into a shale is an effective way of minimizing shale instability problems when drilling with water-based muds. Three important properties of shales were measured in this dissertation: the membrane efficiency, the ion selectivity and the flux of water and ions into or out of a shale.

The measured membrane efficiency of all the shales studied was low and ranged from 0.18% to 4.23%. This means that in order to induce high osmotic backflow out of a shale, salts at high concentration must be incorporated into the design of water-based muds. In doing so, another potential problem may be created, ionic diffusion into the shale. Ionic diffusion can cause shale instability through unfavorable reactions between the ions and the shale matrix. This is manifested in weakening of cementing bonds and fabric deterioration. While osmotic backflow strengthens the shale through pore pressure and water content reduction, ionic diffusion can either weaken or strengthen the shale.

In this study, it was shown that the membrane efficiency of a shale is positively correlated with the cation exchange capacity of the shale and inversely correlated with shale permeability. Furthermore, it was shown that the ratio of solute size to shale pore throat size determines the ability of shales to restrict solutes from entering their pore space and thus provide a shale the ability to behave as a semi-permeable membrane. Cations and anions with large hydrated diameters yielded higher membrane efficiencies

than cations and anions with small hydrated diameters. In addition, it was shown that temperature plays an important role in shale and drilling fluid interactions. More specifically, it was shown that the membrane efficiency of shales increases with temperature. Hysteresis in membrane efficiency is observed when the temperature is cycled. It was shown that in the presence of a temperature gradient across shales, water transport due to thermal osmosis is negligible.

The ion selectivity of shales was measured, through electrochemical potential tests. We showed that shales behave as non-ideal ion-selective membranes that restrict but do not completely block the passage of anions. The ion selectivity of shales was found to correlate positively with the cation exchange capacity of the shale and inversely with the shale permeability. The ion selectivity of shales was found to depend on the type and concentration of the cations and anions that make up the external solution. More importantly, the measured ion selectivity was shown to correlate well with the measured membrane efficiency obtained from the pressure transmission tests. Therefore, we propose using the simpler and quicker electrochemical test, on the rig site, as a semi-quantitative measure of the membrane efficiency of shales.

Experimental results, obtained from our immersion test, show that both osmosis and ionic diffusion take place simultaneously and that the overall effect depends on the properties of both the shale and the invading ion. It was found that, when shales interact with water-based muds, osmosis becomes more dominant in concentrated solutions while ion diffusion is more dominant in dilute solutions. The amount of ion uptake into shales was found to be directly proportional to shale permeability. It was also shown that before interpreting shale swelling data, the surface hydration (capillary) effects must be accounted for, as such effects could be mistaken for shale swelling. In order to eliminate

capillary effects, we recommend storing shales in sealed oil jars at all times prior to testing.

The membrane efficiency of oil-based muds was high compared to that of water-based muds. However, this membrane efficiency was not 100 % as postulated by many researchers. This may be due to emulsion instability. We have also shown that there exists a minimum capillary entry pressure for oil-based muds before they initiate flow into a shale. The minimum capillary entry pressure of oil-based muds was shown to depend on the interfacial tension between the shale pore fluid and the oil-based mud and on the shale permeability. The high membrane efficiency of oil-based muds together with the high capillary entry pressures are the main factors responsible for the success of oil-based muds in drilling shale formations.

Appendix A

A1. PERMEABILITY MODEL

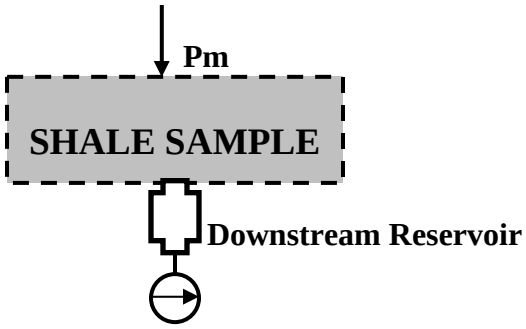

The above system describes our experimental set up. We needed to develop a mathematical model, which describes the shale's permeability. In our experiments, a fluid with constant pressure (P_m) is circulating on top of our shale sample while a reservoir under the shale is initially maintained at a pressure P_o. We assume that initially both the shale and the downstream reservoir have a pressure P_o.

The diffusivity equation, in low permeability rocks, is used to describe our system. The partial differential equation is written as:

$$\partial^2 P / \partial x^2 = (1/K)\partial P / \partial t \quad \text{.....(1)}$$

$$K = k / \phi \mu C$$

where;

K is the shale's conductivity

k is the shale's permeability

ϕ is the porosity of the shale

μ is the fluid viscosity

C is the fluid compressibility

Equation (1) describes our system with the flowing initial and boundary conditions.

Initial Condition:

$P(x, 0) = P_o$ (This means that the initial pressure in the shale and downstream reservoir is P_o)

Boundary Conditions:

$P(0, t) = P_m$

$$\partial P / \partial x(L,t) = q\mu / KA$$

Our system is not equipped to measure the flow rate at x = L. Therefore, a modification to this boundary condition is introduced using the concept of compressibility as follows.

$$C = -(1/V)\partial V / \partial P$$
$$\partial V = -CV\partial P$$

$$q = \partial V / \partial t$$

$$q = -CV\partial P / \partial t$$

Therefore;

$$\partial P / \partial x(L,t) = -(CV\mu / KA)\partial P / \partial t$$

where $\partial P / \partial t$ is the pressure change with time in the downstream reservoir.

We now proceed to solve equation (1) with the given boundary and initial conditions.

We will use the method of Laplace Transform to solve equation (1).

$$\partial^2 P/\partial x^2 = (1/K)\partial P/\partial t$$

$$sP - P(x,0) = K\partial^2 P/\partial x^2$$

$$sP - Po = K\partial^2 P/\partial x^2$$

$$K\partial^2 P/\partial x^2 - sP = -Po$$

$$\partial^2 P/\partial x^2 - sP/K = -Po/K \quad \ldots\ldots(2)$$

Equation (2) is a second order non-homogenous equation. The method of variation of parameter will be used to solve equation (2).

First, a solution for the homogenous part is obtained.

$$\partial^2 P/\partial x^2 - sP/K = 0$$

$$m^2 - s/K = 0$$

$$m = \pm\sqrt{s/K}$$

$$P(x,s) = C_1 e^{\sqrt{s/K}\,x} + C_2 e^{-\sqrt{s/K}\,x}$$

Second, a particular solution (y_p) for the non-homogenous part is obtained.

Let:

$$y_1 = e^{\sqrt{s/K}\,x}$$

$$y_2 = e^{-\sqrt{s/K}\,x}$$

$$y'_1 = \sqrt{s/K}\,e^{\sqrt{s/K}\,x}$$

$$y'_2 = -\sqrt{s/K}\,e^{-\sqrt{s/K}\,x}$$

Finding the worngskin W :

$$W = -2\sqrt{s/K}$$

$$y_p = -Po/2s - Po/2s$$

$$y_p = -Po/s$$

Therefore, the general solution is:

$$P(x,s) = C_1 e^{\sqrt{s/K}x} + C_2 e^{-\sqrt{s/K}x} - Po/s \quad \text{.....(3)}$$

C_1 and C_2 are determined from the boundary conditions. We must transform the boundary condition into a Laplace form in order to solve for C_1 and C_2.

Boundary conditions:

$$P(0,s) = Pm/s \quad \text{.....(BC1)}$$
$$\partial P/\partial x(L,s) = -(CV\mu/KA)(sP - Po)$$
$$let\beta = CV\mu/KA$$
$$\partial P/\partial x(L,s) = -\beta(sP - Po) \quad \text{.....(BC2)}$$

Applying the boundary conditions yields the following equations, which can be solved to obtain C_1 and C_2.

Applying BC1:

$$Pm/s = C_1 + C_2 - Po/s$$
$$C_1 + C_2 = 1/s(Pm + Po)$$
$$C_1 + C_2 = A \quad \text{.....(4)}$$
$$where;$$
$$A = 1/s(Pm + Po)$$

Applying BC2:

$$-\beta(sP - Po) = \alpha C_1 e^{\alpha L} - \alpha C_2 e^{-\alpha L}$$

where;

$\alpha = \sqrt{s/K}$

$E = BC_1 + DC_2$.....(5)

$E = -\beta(sP - Po)$

$B = \alpha e^{\alpha L}$

$D = -\alpha e^{-\alpha L}$

We will solve equation (4) and (5) for C_1 and C_2.

$C_1 = (DA+E)/(D-B)$

$C_2 = (BA-E)/(B-D)$

$P(x,s) = ((DA+E)/(D-B))e^{\sqrt{s/K}x} + ((BA-E)/(B-D))e^{-\sqrt{s/K}x} - Po/s$.....(6)

We now appeal to the literature to find a solution to equation (6). Using Carslaw and Jaeger book titled "Conduction of Heat in Solids" and Van Oort et al (1994), a solution to equation (1) that satisfies the boundary and initial conditions was found.

The solution can be expressed as:

$(P(x,t) - Po)/(Pm - Po) = 1 - 2\sum_{n=1}^{\infty} EXP(-\phi_n{}^2 Kt/L^2)\sin(x\phi_n/L)/(\cos\phi_n \sin\phi_n + \phi_n)$.....(7)

where;

$\phi_n \tan\phi_n = AL\phi/V$

ϕ is the porosity of the shale sample

V is the downstream reservoir volume

L is the length of the shale sample

A is the cross-sectional area of the shale sample

Van Oort et al (1994) states that the parameter ϕ_n depends strongly o the ratio of the sample pore volume to the downstream reservoir volume. He further explain that when this ratio is small, as the case for our experimental system, equation (7) reduces to the following equation at x =L.

$$(P(L,t)-Po)/(Pm-Po)=1-EXP(-Akt/\mu CVL) \quad \text{.....(7)}$$

where *P(L,t)* is the pressure of the downstream reservoir which equals the pressure of the shale sample at x = L.

Taken the natural logarithm of equation (7) yields:

$$\ln[(Pm-P(L,t))/(Pm-Po)]=\lambda t$$

where λ = -Ak/μCVL

$$\lambda=\ln[(Pm-P(L,t))/(Pm-Po)]/t \quad \text{.....(8)}$$

According to equation (8), if we plot ln[*(Pm-P(L,t))/(Pm-Po)*] versus time, the slope of line equals λ

The following procedure is adopted in order to estimate the permeability of the shale sample.

- Pressurize the downstream reservoir up the desired value.
- Allow the downstream pressure to stabilize and let this pressure be Po. The downstream pressure should equal the shale's pore pressure.
- Starts flowing upstream fluid on top of the shale at Pm.
- Record the downstream pressure with time; this is P(L,t).
- Plot ln[*(Pm-P(L,t))/(Pm-Po)*] versus time.

- Determine the slope of the line (λ).
- Calculate the shale permeability as follows:

  $k = (\lambda \mu CVL / (-A))$

References

Ballard, T.J., Beare, S.P., and Lawless T.A., "Fundamentals of Shale Stabilization: Water Transport Through Shales", SPE 24974, Presented at the European Petroleum Conference held in France, 16-18 November, 1992.

Berg, R. R. "Capillary Pressures in Stratigraphic Traps", AAPG Bulleting, vol. 59, p.939-956, 1975.

Bird, P., "Hydration Phase Diagrams and Friction of Montmorillonite Under Laboratory and Geologic Conditions with Implications for Shale Compaction, Slope Satbility and Strength of Fault Gouge", Techonophys., 107, pp. 235-260, 1984.

Bol, G. M., Wong, S.W., Davidson, C. J., and Woodland, D. C., "Borehole Stability in Shale", SPE Paper 24975, Presented at the European Petroleum Conference in Cannes, France, November 16-18, 1992.

Chenevert, M. E., "Shale Alteration by Water Adsorption", Journal of Petroleum Technology, pp. 1141-1148, September 1970.

Chenevert, M. E., "Shale Control With Balanced Activity Oil Continuous Muds", Journal of Petroleum Technology, October 1970.

Chenevert, M. E. and Strassner, J. E., "Temperature Effects on Water Activities of Argillaceous Shales and Oil Mud systems", Presented to the Fifteenth Oil and Gas Conference, Balatonfured, Hungary, September 14, 1975.

Chenevert M. E., “Diffusion of Water and Ions into Shales”, Presented at the International Symposium on Rock Mechanics and Rock Physics, Pau, France, August 28-31, 1989.

Chenevert, M. E., and Amanullah, M., “Shale Preservation and Testing Techniques for Borehole Stability Studies”, SPE/IADC Paper 37672, Presented at the SPE/IADC Drilling Conference in Amsterdam, The Netherlands March 4-6, 1997.

Dewhurst, D. N, Jones, R. M, and Raven M. D “Microstructural and Petrophysical Characterization of Muderong Shale: Application to Top Seal Risk” Petroleum Geoscience, Vol. 8, pp. 371-383, 2002.

Dzialowski A., Hale, A., and Mahajan, S., “Lubricity and Wear of Shale: Effects of Drilling Fluids and Mechanical Parameters”, SPE/IADC Paper 25730, Presented at the SPE/IADC Drilling Conference in Amsterdam, February 23-25,1993.

Edwin A., Hackett R. and Hackett J., “A Laboratory Technique for Screening Shale Swelling Inhibitors” SPE 11117, Presented at the 57th Annual Fall technical Conference and exhibition of the Society of Petroleum engineers of AIME held in New Orleans, LA, September 26-29, 1982.

Ewy, R. T., and Stankovich, R. J., “Pore pressure change due to shale-fluid interactions: Measurements under simulated wellbore conditions”, Proceedings Pacific Rocks 2000, Fourth North American Rock Mechanics Symposium, Seattle. Pages. 147-154, Balkema, Rotterdam, July 31-August 3, 2000.

Fam M. A., and Dusseault M. B., “Borehole Stability in Shales: A Physico-Chemical Perspective” SPE/ISRM 47301, Presented at the SPE/ISRM Eurock 98 held in Trondheim, Norway, 8-10 July 1998.

Forsans, T. M., and Schmitt, L., “Capillary forces: The neglected factor in shale instability studies?” Eurock 94, Belkema, Rotterdam, 1994.

Fritz, S.J., and Marine, I.W., “Experimental Support for a Predictive Osmotic Model of Clay Membranes”, Geochim. Cosmochim., Acta 47, 1515-1522, 1983.

Ghassemi A., Diek A., and Santos H., “Effects of Ion Diffusion and Thermal Osmosis on Shale Deterioration and borehole Instability” AADE 01-NC-HO-40, Presented at the AADE 2001 National Drilling Conference held in Houston, Texas, March 27-29, 2001

Hale, A. H., and Mody, F. K., “Experimental Investigation of the Influence of Chemical Potential on Wellbore Stability”, IADC/SPE Paper 23885, Presented at the SPE/IADC Drilling Conference in New Orleans, Louisiana, February 18-21,1992.

Hale A. H., Mody F. K., and Salisbury D. P., “ The Influence of Chemical Potential on Wellbore Stability” SPE Drilling & Completion, Pages 207-216, September 1993.

Horsud, P., Bostrom, B., Sonstebo, E. F., and Holt, R. M., “Interaction Between Shale and Water-Based Drilling Fluids: Laboratory Exposure Tests Give New Insight Into Mechanisms and Field Consequences of KCl Contents”, Presented at the SPE Annual Technical Conference and Exhibition in New Orleans, LA, September 1998.

Jennings, J. B “Capillary Pressure Techniques: Application to Exploration and Development Geology” AAPG Bulletin, Vol 71, pp 1196-1209, 1987.

Jin M., and Sharma M. M., “Shaly Sand Formation Evaluation Using a Single Membrane Potential Measurement”, Journal of Petroleum Science and Engineering, 99, 1994.

Keijzer J.S., Kleingeld P.J., and Loch J.P.G., “Chemical Osmosis in Compacted Clayey Material and the Prediction of Water Transport” Engineering Geology 53, Pages 151-159, 1999.

Krooss, B. M., Hildenbrand, A., Alles, S., Littke, R. and Pearce, J. “ Assessment of the CO2 Sealing Efficiency of Pelitic Rocks: Two-Phase Flow and Diffusive Transport” 2004.

Lomba, R. F., Chenevert, M. E., and Sharma, M. M., “The ion-selective membrane behavior of native shales”, Journal of Petroleum Science and Engineering, pp. 9-23, 2000.

Low P. F., and Anderson D. M., “Osmotic Pressure equations for Determining Thermodynamic Properties of Soil Water” Soil Science, V 86, Pages 251-258, 1958.

Low, P. F., “Structural Component of the Swelling Pressure of Clays, “ Langmuir 3 (1), pp. 18-25, 1987.

Manohar Lal “Shale Stability: Drilling Fluid Interaction and Shale Strength” SPE 54356, Presented at the 1999 SPE Latin American and Caribbean Petroleum Engineering Conference held in Caracas, Venezuelan, 21-23 April 1999.

Mody, F. K., and Hale, A. H., “A Borehole-Stability Model To Couple the Mechanics and Chemistry of Drilling Fluid Shale Interactions”, SPE/IADC 25728, Presented at the SPE/IADC Drilling conference held in Amsterdam, 23-25 February 1993.

Mody, F. K., Tare, U. A., Tan, C. P., Drummond, C. J., and Wu, B., “Development of Novel Membrane Efficient Water-Based Drilling Fluids Through Fundamental Understanding of Osmotic Membrane Generation in Shales”, SPE Paper 77447,

Presented at the SPE Annual Technical Conference and Exhibition in San Antonio, Texas, October, 2002.

Mondshine, T. C., "A New Potassium Based Mud System", SPE 4516, Presented for the 48th Annual Fall Meeting of The Society of Petroleum Engineers of AIME in Las Vegas, Nev., Sept 30 – Oct 3, 1972.

Pernot, V. F., " Troublesome Shale Control Using Inhibitive Water-Base Muds"', Thesis Presented to the Faculty of the Graduate School of the University of Texas at Austin, May 1999.

Santarelli F., Chenevert M., and Osisanya U., "On the Stability of Shales and Its Consequences in Terms of Swelling and Wellbore Stability" IADC/SPE 22886, Presented at the IADC/SPE Drilling Conference held in New Orleans, Louisiana, February 18-21, 1992.

Santarelli, F. J., and Carminati, S., "Do Shales Swell? A Critical Review of Available Evidence", SPE/IADC Paper 29421, Presented at the SPE/IADC Drilling Conference in Amsterdam, The Netherlands, February 28 - March 2, 1995.

Santos H., and Perez R., "What Have We Been Doing Wrong in Wellbore Stability?" SPE 69493, Presented at the SPE Latin American and Caribbean Petroleum Engineering Conference and Exhibition held in Buenos Aires, Argentina, 25-28 March 2001.

Schlemmer R., Patel A., Friedheim J., Young S., and Bloys, J. B., "Progression of Water-Based Fluids Based on Amine Chemistry: Can the Road Lead to True Oil Mud Replacement", AADE-03NTCE-36, Presented at AADE 2003 National technology Conference, held in Houston, Texas, April 1-3, 2003.

Sherwood J. D., “Ionic Transport in Swelling Shale”, Advances in colloid and Interface science, 61, Pages 51-64, 1995.

Simpson, J. P., Walker, T. O., and Jiang, G. Z., “Environmentally Acceptable Water-Based Mud Can Prevent Shale Hydration and Maintain Borehole Stability”, SPE Drilling & Completion, pp. 242-249, December 1995.

Staverman A. J., Rec. Trav. Chim., 71, 623, 1952

Steiger, R. P., “Advanced Triaxial Swelling Tests on Preserved Shale Cores”, Presented at the 54th U.S Symposium on Rock Mechanics, June 27-30, 1993.

Tan C., Richards B., and Rahman S., “Managing Physico-Chemical Wellbore Instability with the Chemical Potential Mechanism” SPE 36971, Presented at the 1996 Asia Pacific Oil and Gas conference in Adelaide, 28 October, 1996.

van der Zwaag, C. h., “Experimental Studies of Physicochemical Reactions Between Water-Based Drilling Fluids and Argillaceous Rock Formations”, Ph.D. dissertation, Norwegian Institute of Technology, The University of Trondheim, Norway, 1995.

van Oort, E., Hale, A. H., and Mody, F. K., “Critical Parameters in Modeling the Chemical Aspects of Borehole Stability in Shales and in Designing Improved Water-Based Shale Drilling Fluids”, SPE Paper 28309, Presented at the SPE Annual Technical Conference and Exhibition in New Orleans, LA, September 25-28, 1994.

van Oort, E., Hale, A. H., and Mody, F. K., “Transport in Shales and the Design of Improved Water-Based Shale Drilling Fluids”, SPE Drilling & Completion, pp. 137-146, September, 1996.

van Oort, E., “Physico-Chemical Stabilization of Shales”, SPE Paper 37263, Presented at the SPE International Symposium on Oilfield Chemistry in Houston, Texas, February 18-21, 1997.

van Oort, E., “On the Physical and Chemical Stability of Shales”, Journal of Petroleum Science & Engineering 38 (2003), Pages 213-235, 2003.

Vavra L., Kaldi J., Sneider M., “Geological Applications of Capillary Pressure: a Review” American Association Petroleum Geologists, v 76/6, 1992.

Zhang J., Chenevert M. E., AL-Bazali T., and Sharma M., “A New Gravimetric – Swelling Test for Evaluating Water and Ion Uptake in Shales”, SPE Paper 89831, Presented at the SPE Annual Technical Conference and Exhibition in Houston, Texas, 26-29 September 2004.

Vita

Talal Mohammad AL-Bazali was born in Kuwait City, Kuwait on September 3, 1972. After completing his high school in Kuwait, he attended the University of Tulsa where he obtained his B.S degree in Petroleum Engineering on December 1996. He joined Kuwait Petroleum International on February 1997 where he mainly worked as an analyst in different departments. On August 2000, he joined the University of Texas at Austin in order to get his M.S and Ph.D degrees in Petroleum Engineering. Talal is married and has three beautiful children named Rakan, Mohamad and Sara.

Permanent address: P.O. Box 1490
Jahra, Kuwait 01016

This dissertation was typed by the author